N° D'ORDRE

THÈSE DE DOCTORAT

SPECIALITE : PHYSIQUE

Ecole Doctorale « Sciences et Technologies de l'Information des Télécommunications et des Systèmes »

Présentée par : Cristina Ioana CIOCHINĂ

Sujet :

CONCEPTION D'UNE COUCHE PHYSIQUE POUR LA LIAISON MONTANTE DANS DES SYSTÈMES DE RADIOCOMMUNICATIONS MOBILES CELLULAIRES

Soutenue le 02 juillet 2009 devant les membres du jury :

Président du jury :	M. Pierre DUHAMEL	(CNRS, France)
Rapporteurs :	M. Jean-François HÉLARD	(INSA, France)
	M. Michel TERRÉ	(CNAM Paris, France)
Examinateur :	M. Stefan KAISER	(DoCoMo Euro-Labs, Allemagne)
Directeurs de thèse	M. Hikmet SARI	(Supélec, France)
	M. David MOTTIER	(Mitsubishi Electric R&D Centre Europe)

Abstract

Single Carrier FDMA (SC-FDMA) combining multi-carrier-like multiple access with single-carrier-like envelope fluctuations has been chosen to embody the air interface of future wireless communication systems. This scheme is robust to multipath propagation and allows flexible management of the spectral resource, while having low dynamic range. SC-FDMA can be further enhanced by exploiting the spatial dimension of the radio channel through multiple antennas. This thesis proposes a physical layer design for an uplink system based on SC-FDMA. The aim is to develop multiple antenna technologies compatible with SC-FDMA, leading to increased performance while keeping low-complexity detection.

Taking into account the tight implementation constraints at the mobile terminal and the presence of a nonlinear power amplifier, we show the importance of the in-band and out-of-band regulation constraints on the performance evaluation of the air interface. In realistic propagation scenarios, SC-FDMA brings significant improvements with respect to its competitors especially for users that are sensitive to high dynamic variations of the signal envelope. This is typically the case of cell-edge users having limited a priori knowledge of the propagation channel and needing to employ open-loop transmit-diversity techniques to improve their propagation conditions.

We propose a new method allowing space-frequency transmit diversity in an SC-FDMA system that keeps both the uplink framing flexibility and the low envelope variations of the signal. This new method designed for two transmit antennas is extended to four or more transmit antennas in the space-frequency or space-time-frequency domains. We also expand these strategies to spatial multiplexing so as to benefit from transmit diversity to increase of the cell and/or user throughput multi-user scenarios and/or in combination with spatial multiplexing techniques. Our analytical analysis proves that the proposed solutions keep the good envelope characteristics of SC-FDMA. Simulation results show the improvements brought by the proposed techniques compared to conventional ones in a vast number of practical scenarios.

Abrégé en français

Single-Carrier FDMA (SC-FDMA) est une technique d'accès multiple combinant les avantages des techniques multiporteuses avec les faibles variations d'enveloppe des signaux monoporteuses. SC-FDMA est robuste dans des canaux multi-trajet, autorise une gestion flexible des ressources en fréquence et a de faibles excursions d'enveloppe. Dans cette thèse, nous proposons une couche physique pour la liaison montante des systèmes de communications mobiles de future génération, basée sur le SC-FDMA. Nous proposons des techniques exploitant la présence d'antennes multiples pour améliorer les performances du système, sans augmenter la gamme dynamique du signal et tout en gardant des mécanismes de détection peu complexes.

En prenant en compte les lourdes contraintes d'implémentation sur les terminaux mobiles, mais aussi les contraintes de régulation imposées aux systèmes réels, nous avons montré l'importance de l'évaluation des performances du système en présence d'amplificateurs non-linéaires de puissance. SC-FDMA permet d'obtenir des améliorations significatives par rapport à d'autres techniques concurrentes, particulièrement pour les utilisateurs sensibles aux variations importantes de l'enveloppe du signal. Ce type d'utilisateur se trouve généralement en bord de cellule. Comme il a notamment une faible connaissance du canal, il est contraint d'utiliser des techniques de diversité d'émission en boucle ouverte pour améliorer ses condition de propagation.

Nous proposons une nouvelle méthode pour appliquer des codes espace-fréquence dans un système SC-FDMA, tout en gardant la flexibilité du système et la faible gamme dynamique du signal. Cette méthode, appelée SC-SFBC, est conçue pour deux antennes d'émission. Nous proposons aussi des extensions à quatre ou plus antennes d'émission, par codage espace-fréquence ou espace-temps-fréquence. Nous proposons enfin des stratégies adaptées à la transmission multiutilisateurs et/ou des combinaisons avec des techniques de multiplexage spatial. Les résultats de simulations mettent en valeur les améliorations que les schémas proposés apportent par rapport à des techniques existantes, dans un vaste nombre de scénarios réalistes.

Remerciements

Je tiens à remercier M. Jean François Hélard, professeur à l'Institut National des Sciences Appliquées de Rennes, et M. Michel Terré, professeur au Conservatoire National des Arts et Métiers de Paris, qui ont accepté de juger ce travail en qualité de rapporteurs. Leur travail de lecture et la qualité de leurs remarques m'ont aidée à améliorer ce manuscrit. Je remercie aussi M. Pierre Duhamel, directeur de recherche au Centre National de la Recherche Scientifique, d'avoir accepté de présider le jury, et M. Stefan Kaiser pour m'avoir fait l'honneur de faire partie de mon jury de thèse.

Toute ma reconnaissance s'adresse à mon directeur de thèse, M. Hikmet Sari, chef du Département de Télécommunications à Supélec. La confiance et le soutien qu'il m'a accordés, l'autonomie qu'il m'a permis d'acquérir, son aide et ses conseils m'ont été précieux. Il a su m'accompagner et me guider depuis mon arrivée à Supélec en tant que stagiaire, pendant mon master et jusqu'à la fin de ma thèse. Sans lui mon parcours n'aurait sans doute pas pu être le même.

Je ne remercierai jamais assez M. David Mottier, chef de la division Communications de Mitsubishi Electric R&D Centre Europe, qui a assuré l'encadrement industriel de ma thèse. Ce travail n'aurait pas été possible sans son investissement, sa patience et son sens de l'écoute, qui sont hors normes. La façon dont il a su se rendre disponible même à distance, ses conseils lors de nos longues discussions techniques, son enthousiasme, son support inconditionnel aussi bien sur le plan technique, administratif et humain m'ont été indispensables.

Je tiens aussi à remercier l'entreprise Mitsubishi Electric R&D Centre Europe, qui a financé mes travaux de thèse. J'ai trouvé au sein de l'entreprise une équipe dynamique et accueillante, forte aussi bien en compétences techniques qu'en qualités humaines, équipe dont je suis fière de faire partie aujourd'hui. Je souhaite remercier tout particulièrement M. Damien Castelain et M. Loïc Brunel dont l'expérience et le savoir-faire ont été une source d'inspiration et une aide inestimable pour l'avancement de ma thèse.

Un grand merci aussi à toute l'équipe de Supélec pour l'accueil, pour l'aide dans les questions administratives, et pour leur sens de la camaraderie. Une pensée pour tous ceux qui ont partagé mon quotidien sur le campus de Supélec pour avoir égayé les repas de midi, pour leur bonne humeur, pour les covoiturages et pour toutes ces petites choses qui ont rendu agréables les années passées à Supélec.

Mes remerciements s'adressent aussi à tous ceux qui ont posé leur empreinte sur mon parcours, qui m'ont encouragée dans mes études, qui m'ont donné l'envie de devenir ingénieur, et le désir de devenir docteur. Je pense tout particulièrement à mes professeurs de l'Ecole Polytechnique de Bucarest qui ont partagé leurs connaissances et qui m'ont donné le goût des communications numériques.

Je tiens à remercier Alexandre pour sa patience et son amour, pour avoir su composer avec les horaires prolongés, les indisponibilités et les moments de doute que tout thésard a dû connaître. Toute ma reconnaissance s'adresse à ma famille, à qui je dois énormément. Finalement, je souhaite dédier cette thèse à ma grand-mère Sonia.

Table of contents

List of figures

List of tables

Résumé en français

1 – Introduction

L'histoire des systèmes de communication sans fil, pourtant courte, est caractérisée par une évolution rapide, marquée par de nombreuses vagues d'innovation. Même si le principe fondateur des communications sans fil puise ses racines dans les travaux de Maxwell, Tesla et Marconi fin du XIXème siècle, ce domaine a connu un essor fulgurant au fil des 25 dernières années. Ainsi, si les débuts des systèmes de téléphonie mobile ont été marqués par la transmission de voix à faible débit, les futures générations ciblent des applications de haut débit mobile, comme la transmission d'images, de données ou de vidéos en temps réel, intégrant la notion de qualité de service.

La première génération de téléphonie mobile (1G), analogique, a vu le jour dans les années 70 aux États-Unis, sous le nom d'AMPS (Advanced Mobile Phone Service). La vraie révolution est venue avec la deuxième génération (2G) qui marque le passage au numérique, et le formidable succès du GSM (Global System for Mobile Communications), en exploitation commerciale depuis 1991. 80% du marché mobile d'aujourd'hui est encore représenté par le GSM. Pourtant, les 9,6 Kbits/s offerts par le GSM sont vite devenus insuffisants. Les extensions de la norme GSM, concrétisées par les systèmes GPRS (General Packet Radio Service, 2,5G) et EDGE (Enhanced Data rates for GSM Evolution, 2,75G), offrent des débits moyens par utilisateurs allant jusqu'à 40 Kbits/s en voie montante, tout en se basant sur l'architecture du réseau GSM.

La troisième génération (3G), répondant aux demandes formulées par le 3GPP (Third Generation Partnership Project) dans le standard IMT2000, a vu le jour au début du XXIème siècle avec la parution de l'UMTS (Universal Mobile Telecommunications System), basé sur la technique W-CDMA (Wideband Code Division Multiple Access) et de son correspondant américain, CDMA2000. La 3G n'aura fait qu'une courte apparition dans l'univers de la téléphonie mobile, car la plupart des opérateurs mondiaux ayant lancé des services commerciaux 3G ont rapidement fait évoluer leurs réseaux vers la 3,5G. HSDPA (High Speed Downlink Packet Access, 2005), HSUPA (High Speed Uplink Packet Access, 2008) et maintenant HSPA Evolved (2009) se sont lancés dans la course aux débits, allant jusqu'à 11.5 Mbits/s en voie montante.

Longtemps détenteurs du monopole des communications sans fil, ces systèmes se retrouvent aujourd'hui en concurrence avec les réseaux d'accès à Internet, qui évoluent vers la mobilité. Tel est le cas du WiFi et du WiMAX (Worldwide Interoperability for Microwave Access), qui intègrent désormais la mobilité.

Dans ce contexte, le travail de recherche se concentre désormais vers le développement de l'après 3G. Les systèmes B3G/4G se proposent d'offrir des débits utilisateur entre 100 Mbit/s et 1 Gbit/s. En s'appuyant sur des technologies avancées ces systèmes doivent répondre à des exigences de mobilité, de diversité des services, et de haute qualité de la transmission. Le 3GPP s'apprête à valider les spécifications large-bande LTE (Long Term Evolution), et un lancement commercial d'un réseau LTE est prévu pour la fin 2009. Les travaux de standardisation de la norme LTE-Advanced, censée représenter la 4G, sont déjà lancés depuis la fin 2008.

Les travaux de cette thèse s'inscrivent dans ce contexte, puisqu'ils portent sur l'étude de la couche physique pour la liaison montante des systèmes de radiocommunications mobiles de future génération. Le plan de la thèse est résumé ci-dessous :

- Le premier chapitre résume l'état de l'art du domaine des communications sans fil, et présente les objectifs et les principales contributions de la thèse.
- Le deuxième chapitre se concentre sur la modélisation du canal de propagation et sur ses principales propriétés dans le domaine temporel, fréquentiel et spatial. Le profile des canaux utilisés tout le long de la thèse, ainsi que les scénarios de simulation sont fixés dans ce chapitre.
- Dans le troisième chapitre, l'étude se focalise sur trois schémas d'accès multiple : OFDMA (Orthogonal Frequency Division Multiple Access), SC-FDMA (Single Carrier Frequency Domain Multiple Access) et SS-MC-MA (Spread Spectrum Multicarrier Multiple Access). Les performances de ces schémas sont évaluées et comparées dans un scénario pratique, prenant en compte les contraintes spécifiques à la liaison montante et la présence de non-linéarités. Une attention plus particulière est portée sur le SC-FDMA, qui a été depuis sélectionné comme interface pour la voie montante des systèmes LTE et LTE-Advanced, grâce à de faibles variations de l'enveloppe. Les résultats des travaux dans ce chapitre ont fait l'objet de deux communications internationales [CiMo06], [CiMo07a] et d'une publication dans une revue internationale [CiMo08a].
- L'analyse du système SC-FDMA est étendue à la dimension MIMO (Multiple-Input Multiple-Output) dans le quatrième chapitre. Les possibilités de combiner SC-FDMA avec des codes espace-temps et/ou espace-fréquence orthogonaux sont étudiées. Une allocation innovante des données sur les sous-porteuses allouées à un utilisateur est introduite, permettant d'appliquer des codes orthogonaux espace-fréquence à un signal SC-FDMA, sans augmenter les fluctuations de l'enveloppe de celui-ci et tout en gardant de bonnes performances pour la transmission. Le nouveau code espace-fréquence basé sur cette allocation innovante, nommé SC-SFBC (Single-Carrier Space-Frequency Block Coding), a été conçu pour des utilisateurs étant équipés de deux antennes de transmission. Les travaux dans ce chapitre ont abouti au dépôt de deux brevets, à deux communications internationales [CiMo07b], [CiMo07c] et à une publication dans une revue internationale [CiMo08b].
- Les principes du SC-SFBC sont généralisés dans le cinquième chapitre à des systèmes comportant plus de deux antennes d'émission. Des schémas quasi-orthogonaux, des codes espace-temps-fréquence, ainsi que des schémas combinant SC-SFBC avec des techniques de permutation de fréquence sont introduits et évalués. La valorisation de

ces travaux s'est traduite par un dépôt de brevet et une communication internationale [CiMo08c]. Les résultats les plus importants des chapitres 4 et 5 font l'objet d'un article soumis pour publication dans une revue internationale, en deuxième instance de révision.

- Le sixième chapitre s'intéresse à des schémas plus haut débit combinant des techniques de diversité d'émission avec du multiplexage spatial. Les performances de ces techniques sont évaluées dans des contextes mono- et multi-utilisateurs. Un algorithme ciblant à optimiser l'efficacité spectrale dans un contexte SC-FDMA/SC-SFBC multiutilisateurs est proposé. Les contributions apportées dans ce chapitre donnent suite à deux dépôts de brevet et à une contribution à un projet collaboratif européen.
- Finalement, le septième chapitre tire les conclusions générales de cette thèse et indique des axes d'étude pour de futurs travaux de recherche.

2 – Le canal radio mobile

Dans sa définition la plus simple, un canal de communication est défini comme étant l'entité qui effectue la transformation du message émis en message reçu. Au fil des années, le canal de communication a été représenté de différentes manières, en fonction de l'application ciblée, allant de la propagation radioélectrique à la théorie de l'information. Une bonne compréhension des paramètres physiques et des propriétés du canal, ainsi qu'une modélisation adéquate sont essentielles pour la conception de tout système de communications sans fil.

Le phénomène à la base de toute communication sans fil est la propagation électromagnétique, soumise aux lois de Maxwell. Trois mécanismes principaux représentent le fondement de la propagation des ondes dans l'espace libre : la réflexion sur de grandes surfaces lisses, la diffraction par l'extrémité du support de propagation (obstacle, arête, etc.) et la diffusion sur des surfaces rugueuses. Comme conséquence de ces phénomènes, le signal reçu est donc la superposition d'ondes venant de directions différentes, avec des atténuations et des distorsions de phase différentes : il s'agit d'une propagation par trajets multiples.

Au récepteur, la superposition des différents trajets de propagation mène, par le biais d'interférences constructives ou destructives et en fonction de la présence et l'importance des obstacles, à des fluctuations de la puissance du signal reçu, ou encore, à des fluctuations d'amplitude et de phase. Selon la durée d'observation de ces phénomènes, on distingue les fluctuations à grande échelle et celles à petite échelle. Les évanouissements à petite échelle, constatés essentiellement sur des petits déplacements (de l'ordre de la longueur d'onde) ou courts intervalles de temps, sont principalement dus à l'interférence d'ondes en provenance des trajets multiples. Il existe des modèles statistiques caractérisant les évanouissements à petite échelle, en fonction de la présence ou l'absence d'un trajet direct entre l'émetteur et le récepteur. Les plus connus sont les modèles de Rayleigh, Rice et Nakagami. À grande échelle on peut observer des évanouissements lents, mesurés sur des distances de l'ordre de plusieurs dizaines de longueurs d'onde. Il s'agit principalement d'affaiblissements de propagation dus à la distance, et de l'effet de masque (modélisé par une distribution log-normale), conséquence de la présence d'obstacles incontournables entre l'émetteur et le récepteur.

Quand un récepteur est en mouvement par rapport à l'émetteur, on observe un changement dans la fréquence reçue : c'est l'effet Doppler, qui caractérise dans le domaine fréquentiel l'évolution temporelle du canal. Cette évolution peut être caractérisée en utilisant d'autres facteurs de mérite adéquats, comme le taux de dépassements d'un seuil ou la durée moyenne des évanouissements en fonction de la fréquence Doppler.

En pratique, tous les modèles analytiques décrivant des canaux de communication se basent sur les propriétés physiques décrites ci-dessus. Il est généralement d'usage de modéliser le canal radio mobile dans la bande de base sous la forme d'un filtre linéaire variant dans le temps. Les coefficients de la réponse impulsionnelle de ce filtre sont déterminés à partir des propriétés physiques du canal de communication. Les canaux MIMO, à entrées et sorties multiples, sont modélisées sous la forme d'une matrice dont les entrées représentent chacune un canal SISO

(Single-Input Single-Output), reliant une antenne d'émission à une antenne de réception. Ces canaux ne sont pas indépendants, car il existe des corrélations entre les antennes d'émission, entre les antennes de réception et aussi des corrélations croisées entre l'émission et la réception. Il existe un grand nombre de méthodes permettant de modéliser la corrélation spatiale des canaux MIMO, dont les plus connues sont les méthodes de Kronecker et de Weichselberger.

La corrélation des variations du canal dans les dimensions temporelle, fréquentielle et respectivement spatiale a un impact immédiat sur la fiabilité et la qualité de la transmission d'informations à travers ce canal. C'est pour ces causes que l'on définit la notion de sélectivité, qui n'est pas une propriété intrinsèque du canal mais se rapporte aussi aux caractéristiques du signal à transmettre, notamment la largeur de bande et la fréquence porteuse de ce dernier. Ainsi on distingue :

- La sélectivité en fréquence, qui indique si les variations en fréquence du canal sont rapides par rapport à la largeur de bande du signal à transmettre ;
- La sélectivité en temps, qui indique si les coefficients du canal évoluent rapidement par rapport à la période d'échantillonnage du signal à transmettre ;
- La sélectivité en espace, qui indique l'espacement entre antennes à partir duquel l'on peur considérer que les signaux reçus sont indépendants.

Lorsque deux réalisations du canal sont séparées dans le domaine fréquentiel, temporel ou spatial par plus que la bande de cohérence, la durée de cohérence ou respectivement la distance de cohérence, ces deux réalisations du canal peuvent être considérées comme étant indépendantes. Les propriétés de sélectivité du canal permettent alors d'expliquer la notion de diversité, devenue un concept fondamental dans la théorie des systèmes de transmission sans fil. Si plusieurs répliques d'un signal d'information se propagent à travers des réalisations indépendantes du canal, appelées branches de diversité, alors il existe une forte probabilité pour qu'au moins une de ces répliques ne subisse pas d'important évanouissement à un instant donné. Plus on dispose de branches de diversité, plus on a de chances de récupérer correctement le signal transmis car la probabilité d'effacement est réduite.

Afin de tirer profit de la diversité, il faut utiliser des techniques appropriées de codage. L'utilisation conjointe d'un code correcteur d'erreurs et d'un entrelacement temporel permet de récupérer la diversité temporelle. Dans des systèmes utilisant des modulations multiporteuses, cette même technique aussi bien que des techniques d'étalement de spectre permettent d'exploiter la diversité fréquentielle. La diversité spatiale peut être exploitée par des techniques de codage espace-temps ou espace-fréquence. Tout au long de cette thèse, on s'appuie sur ces principes afin d'optimiser les performances du système.

3 – Techniques d'accès multiple pour la liaison montante des futurs systèmes de communications mobiles

La conception de la couche physique pour les futurs systèmes de communications mobiles doit prendre en compte à la fois les fortes demandes de débit et de qualité de services, aussi bien que les contraintes liées aux coûts ou à l'occupation spectrale. Se plier à de telles demandes souvent contradictoires s'avère être un vrai défi, d'autant plus quant il s'agit de la liaison montante où des contraintes spécifiques supplémentaires doivent être respectées. Dans les nouvelles générations de systèmes de télécommunication faisant appel à des techniques d'accès à large bande, la linéarité de l'amplificateur de puissance est un point critique. L'amplificateur de puissance est l'un des composants dissipant le plus d'énergie dans une chaîne de communication. D'un côté, pour garder une bonne autonomie du terminal il faut assurer un point de fonctionnement ayant un bon rendement en puissance. D'un autre côté, pour assurer les bonnes performances de la transmission, une bonne linéarité est indispensable. Mais de tels amplificateurs assurant la linéarité dans des zones proches de la puissance de saturation s'avèrent onéreux et incompatibles avec des demandes de bas coût du terminal mobile. Pour trouver un bon compromis, il est nécessaire d'effectuer une analyse attentive du comportement des différentes techniques d'accès multiple dans la présence des non-linéarités.

Le comportement non-linéaire des amplificateurs de puissance génère des distorsions de phase et d'amplitude sur les signaux émis. Ce comportement engendre deux types d'effets : les distorsions hors bande et les distorsions dans la bande de transmission. Les distorsions hors bande se manifestent par des remontées spectrales qui peuvent gêner la transmission des utilisateurs adjacents. Les distorsions hors bande sont encadrées par deux types de mesures : le masque d'émission spectrale (SEM, Spectrum Emission Mask), fixant un gabarit du spectre à ne pas dépasser, et l'ACLR (Adjacent Channel Leakage Ratio), fixant des bornes supérieures au rapport entre la puissance émise dans un canal adjacent et la puissance utile émise dans la bande assignée à la transmission. Le SEM et l'ACLR sont réglementés par les organismes de standardisation.

Les distorsions dans la bande se manifestent par des modifications d'amplitude et/ou de phase des symboles de modulation à émettre lors du passage par l'amplificateur, fait qui baisse la qualité de la modulation et se traduit par des erreurs supplémentaires au décodage : un rapport signal à bruit (SNR, Signal to Noise Ratio) plus important sera nécessaire pour atteindre le même taux d'erreurs qu'un système linéaire. Une mesure des distorsions dans la bande est l'EVM (Error Vector Magnitude), qui évalue la différence en pourcents entre la forme d'onde idéale et celle modifiée lors du passage par l'amplificateur.

Les effets non-linéaires sont de plus en plus prononcés lorsque la puissance des échantillons passant par l'amplificateur se rapproche de la puissance de saturation de celui-ci. Pour éviter les distorsions et respecter les gabarits fixés par le SEM et par les valeurs maximales tolérables d'ACLR et EVM, les amplificateurs de puissance sont très souvent utilisés avec un recul en puissance (back-off) dans le but d'obtenir un fonctionnement linéaire, la conséquence étant la perte de rendement. Ce recul de puissance, le plus souvent mesuré par rapport à la puissance de saturation en sortie de l'amplificateur (OBO, Output back-off), est plus important pour les signaux ayant une large gamme dynamique. Il existe plusieurs outils permettant d'apprécier la gamme dynamique d'un signal. Le plus connu est le PAPR (Peak to Average Power Ratio), qui représente le rapport entre la puissance crête et la puissance moyenne d'un signal. L'inconvénient du PAPR réside en ce que l'on ne prend en compte qu'un seul échantillon, celui avec la puissance la plus importante, parmi tous les échantillons d'un bloc (par exemple, un symbole OFDM) qui sert de base de calcul pour le PAPR. Or, la distorsion n'est pas juste provoquée par ce seul échantillon, mais est due à tous les échantillons dont la puissance dépasse un certain seuil et qui se retrouvent dans la zone non-linéaire de l'amplificateur. De ce point de vue, l'INP (Instantaneous Normalized Power) est un outil plus équitable pour évaluer la gamme dynamique d'un signal. Un troisième outil, le CM (Cubic Metric), donne une estimation empirique de l'OBO nécessaire à un système en se basant sur l'évaluation des distorsions de troisième ordre.

En dressant le bilan des pertes subies par un système où l'on prend en compte la présence d'un amplificateur de puissance par rapport au cas idéal où il n'y a pas de non-linéarité, la dégradation totale a deux composantes principales : d'un côté l'OBO nécessaire au système pour remplir les contraintes de SEM, ACLR et EVM, et d'un autre côté l'augmentation du SNR (souvent exprimé en termes d'énergie par bit utile en émission par rapport au niveau de bruit, E_b/N_0) pour atteindre le même taux d'erreurs par trame (FER, Frame Error Rate).

En se servant de ces outils, on se propose de faire une analyse comparative des techniques multiporteuses qui avaient été retenues comme candidates pour la couche physique des systèmes de communications sans fil de future génération : OFDMA, SC-FDMA et SS-MC-MA. Pour séparer les effets dus aux différences structurelles entre ces techniques de ceux engendrés par le contexte non-linéaire, l'analyse se poursuit dans un premier temps en absence de non-linéarités.

Le principe de base de l'OFDMA consiste à utiliser une transformée de Fourier inverse de taille N (IDFT, Inverse Discrete Fourier Transform) pour répartir un flux de données en $M \leq N$ flux parallèles, chaque flux étant transmis en modulant l'une des N sous-porteuses réparties de manière équidistante dans la bande du système. Chaque sous-porteuse est donc le support de transmission d'un symbole de modulation, créant ainsi des sous-canaux de transmission étroits par rapport à la bande de cohérence du canal multi-trajet, et pour lesquels la réponse fréquentielle du canal peut-être considérée comme constante. L'évanouissement du sous-canal correspondant à une certaine sous-porteuse ne mène qu'à l'effacement du symbole porté par celle-ci, sans affecter les autres symboles transmis. L'OFDMA n'arrive donc pas à récupérer la diversité fréquentielle disponible dans le canal multi-trajet en absence du codage. Les bonnes performances de l'OFDMA dépendent essentiellement de l'entrelacement et du codage correcteur d'erreurs. L'OFDMA a de nombreux avantages, comme sa bonne efficacité spectrale, sa flexibilité et la possibilité d'effectuer en réception l'égalisation et la détection de manière peu complexe dans le domaine des fréquences. Parmi ses inconvénients on dénombre la sensibilité aux glissements fréquentiels (dus, par exemple, à l'effet Doppler), mais surtout sa gamme dynamique très large.

SC-FDMA et SS-MC-MA peuvent être classés comme de l'OFDMA précodé, car elles combinent l'accès multiple de type OFDMA avec des techniques d'étalement de spectre. Cet étalement est effectué par le biais d'un précodeur placé avant l'IDFT. SC-FDMA effectue un précodage basé sur une transformée de Fourier directe (DFT, Discrete Fourier Transform), alors que SS-MC-MA s'appuie sur une transformée de Walsh-Hadamard. Chaque symbole de modulation est étalé sur l'ensemble des M sous-porteuses utiles (sur N disponibles) avant le passage par l'IDFT. Par rapport à l'OFDMA, chaque sous-porteuse ne transporte plus un seul symbole de modulation, mais une combinaison linéaire de M symboles de modulation. Il existe donc une diversité inhérente à la structure même de la transmission car chaque symbole, étant réparti sur M sous-porteuses, traverse M canaux différents. Dans des scénarios à faible codage (fort taux de codage), ou encore en l'absence de codage, les schémas précodés, qui ont des comportements similaires, ont de meilleures performances que l'OFDMA pur. Par contre, le précodage génère de l'interférence entre les codes dans le sens où l'effacement de l'information transportée par une sous-porteuse subissant un faible SNR se répercute sur tous les symboles liés par le précodage. Si cet effet a un moindre impact pour les modulations à faible nombre d'états (comme par exemple QPSK, Quadrature Phase Shift Modulation), ceci est d'autant plus gênant pour les modulations de taille plus importante où la distance minimale entre les points de la constellation est moindre (comme dans le cas de la 16 ou 64 QAM, Quadrature Amplitude Modulation, par exemple).

La conclusion qui se détache de la comparaison entre OFDMA et OFDMA précodé est qu'il existe un compromis entre la diversité, le taux de codage et l'interférence entre codes. Les schémas de type OFDMA-précodé ont des performances similaires, meilleures que celles de l'OFDMA pour les modulations à faible nombre d'états et peu codées, ou pour tout type de modulation dans l'absence du codage. Cet effet est plus prononcé dans les cas où il y a plus de diversité fréquentielle disponible (nombre plus important de sous-porteuses allouées à un utilisateur ou sous-porteuses distribuées dans la bande). Néanmoins, pour les modulations de taille plus importante, ou dans la présence d'un fort codage, l'OFDMA prend le dessus.

L'influence de la répartition des sous-porteuses dans la bande et de l'impact de l'estimation du canal sur le SC-FDMA a aussi été étudiée. On considère une structure de transmission ou chaque sous-trame correspondant à des données codées ensemble est composée de deux slots, chaque slot contenant un symbole pilote et le reste des données organisées en symboles SC-FDMA. Une allocation distribuée des sous-porteuses dans la bande offre plus de diversité fréquentielle, mais complique la tâche du module d'estimation du canal. Il semble plus intéressant d'utiliser des allocations localisées, en les combinant à faible mobilité avec des techniques de saut de fréquence entre les deux slots d'une sous-trame (FH, Frequency Hopping). À forte mobilité, l'estimation du canal dans le cas FH s'avère peu performante : les variations du canal sont très rapides et il est impossible pour le module d'estimation du canal d'effectuer une interpolation temporelle pour les suivre car les deux observations par sous-trame dont il dispose sont décorrélées à cause du saut de fréquence entre les deux slots.

Mais la prise en compte du contexte non-linéaire modifie le rapport de forces entre les trois techniques d'accès étudiées. Effectivement, l'OFDMA souffre d'une forte dynamique de l'enveloppe, concrétisée par un PAPR important. SS-MC-MA hérite aussi de ce problème : bien que légèrement inférieur, son PAPR reste très proche de celui de l'OFDMA. En revanche, SC-FDMA dispose d'un fort atout : le précodage par DFT, qui a la qualité de réduire les variations d'enveloppe du SC-FDMA au niveau de celles d'un système mono-porteuse. SC-FDMA bénéficie donc à la fois des avantages de l'OFDMA en terme d'accès multiple et flexibilité, et des faibles fluctuations d'enveloppe spécifiques aux modulations mono-porteuses.

Pour l'analyse de l'impact des non-linéarités, nous nous plaçons donc dans un contexte réaliste. Les contraintes de SEM, ACLR et EVM sont tirées des spécifications LTE. Pour représenter la non linéarité nous choisissons le modèle de Rapp avec un facteur de forme $p_{\text{Rapp}}=2$, qui est une bonne approximation pour les applications ciblées dans cette thèse. D'un point de vue spectral, c'est SC-FDMA qui tire le mieux son épingle du jeu, ayant besoin de reculs de puissance moins importants que SS-MC-MA et OFDMA pour se conformer aux gabarits imposés. Encore une fois, les allocations localisées des sous-porteuses semblent plus favorables, ayant une répartition spectrale des harmoniques de troisième ordre plus favorable que dans le cas distribué.

Le bilan est dressé par l'évaluation de la dégradation totale par rapport au cas linéaire, en prenant en compte aussi bien les contraintes spectrales que les performances des trois schémas sur un canal blanc additif gaussien et sur un canal sélectif en fréquence, dans la présence de l'amplificateur non-linéaire. En fonction de l'occupation spectrale, du type de canal et du taux de codage, SC-SFBC surpasse OFDMA de 1.5 dB à 2.9 dB quand QPSK est utilisé. SS-MC-MA n'apporte pas de bénéfice clair, n'ayant ni les bonnes propriétés de PAPR du SC-FDMA, ni les bonnes performances en termes de FER de l'OFDMA.

4 – Techniques de diversité d'émission pour des systèmes SC-FDMA avec deux antennes d'émission

Les techniques MIMO se sont imposées ces dernières années comme une solution incontournable pour augmenter les performances d'un réseau, que cela soit en termes de débit, fiabilité, efficacité spectrale, capacité ou qualité de transmission. L'utilisation d'antennes multiples à la station mobile et/ou à la station de base peut mener à une amélioration des performances au niveau lien grâce à des techniques de diversité d'émission, augmenter le débit par des méthodes de multiplexage spatial, réduire l'interférence entre les utilisateurs ou encore réaliser des compromis convenables parmi les solutions citées ci-dessus. Il existe un compromis fondamental entre le gain en diversité et le gain en multiplexage spatial, compromis similaire à celui entre le taux d'erreurs et le débit dans tout système de communications : on ne peut pas véhiculer une quantité illimitée d'information à travers une ressource limitée sans subir de pertes. Les systèmes capables de maximiser leur gain de diversité spatiale ne bénéficieront pas d'un gain de multiplexage, et vice-versa.

L'analyse du chapitre antérieur a mené à la conclusion que SC-FDMA est une technique qui apporte des bénéfices spécialement aux utilisateurs employant des modulations à faible nombre d'états et/ou sensibles aux problèmes de PAPR. Or cela est particulièrement le cas d'un utilisateur en bord de cellule, émettant à puissance maximale et à débit relativement faible, et soumis typiquement à de mauvaises conditions de propagation. L'intérêt de cet utilisateur est d'utiliser des techniques de diversité d'émission afin d'améliorer sa performance au niveau lien et donc implicitement sa couverture. Comme à cause des mauvaises conditions de propagation il est probable que cet utilisateur ne dispose pas d'information fiable sur l'état du canal, il sera contraint d'utiliser des techniques dites « open-loop », sans retour d'information. Les techniques les plus connues de cette catégorie sont CDD (Cyclic Delay Diversity), OL-TAS (Open-Loop Transmit Antenna Selection), FSTD (Frequency Switched Transmit Diversity) ou encore des techniques de codage espace-temps ou espace-fréquence basées sur le code d'Alamouti.

CDD, OL-TAS et FSTD tirent profit de la diversité spatiale en émission en la convertissant en diversité fréquentielle. CDD envoie sur les différentes antennes d'émission des répliques du même symbole, retardées de manière cyclique. Ceci est équivalent à transformer le canal MIMO en canal SIMO, ce canal transformé ayant une sélectivité fréquentielle accrue par la présence des échos virtuels produits par la technique CDD. En OL-TAS, on commute l'antenne d'émission pendant la durée de transmission d'un bloc codé. Une seule antenne d'émission est active à la fois, ce qui résulte en un canal équivalent SISO avec une diversité fréquentielle augmentée grâce au basculement de la transmission entre plusieurs antennes. FSTD est basé sur la même idée qu'OL-TAS, avec la particularité que la commutation ne se fait plus dans le domaine temporel, mais en fréquence. Toutes les antennes émettent en même temps, mais en utilisant des sous-porteuses différentes et créant ainsi un canal équivalent à forte sélectivité fréquentielle ; de différentes portions du spectre d'un même bloc codé sont transmises par différentes antennes d'émission. Toutes ces techniques se combinent naturellement avec SC-FDMA sans détériorer les bonnes propriétés de PAPR.

Les techniques de codage espace-temps ou espace fréquence font un traitement direct de la diversité spatiale. On va se cantonner ici aux codes par bloc, dont le représentant le plus remarquable est le code d'Alamouti. Ces codes sont très attractifs pour leur faible complexité et bonne flexibilité d'utilisation. Ils se focalisent sur le traitement optimal de la diversité spatiale de transmission et n'augmentent pas le débit par rapport au cas SIMO, gardant un rendement d'un symbole émis par utilisation du canal. Alamouti a découvert un code orthogonal faisant un traitement espace-temps par bloc (STBC, Space-Time Block Code), approprié pour des systèmes de transmission à bande étroite avec deux antennes d'émission.

Pour appliquer ce type de code dans un système de large bande basé sur SC-FDMA, on s'appuie sur la propriété de l'OFDMA de transformer un canal de large bande en N canaux parallèles de bande étroite, correspondant chacun à une sous-porteuse. On va appliquer le STBC au niveau des sous-porteuses ; dans un système SC-FDMA, cela correspond à appliquer le STBC après le précodage par DFT, sur les échantillons fréquentiels du signal, avant la répartition (qui précède l'IDFT) de ces échantillons sur les sous-porteuses du système. Le précodage de type Alamouti s'effectue donc au niveau de chaque sous-porteuse utile entre les échantillons de fréquence appartenant à deux symboles SC-FDMA successifs. La structure fréquentielle du signal n'est pas impactée par cette manipulation, et les signaux SC-FDMA envoyés par les deux antennes de transmission gardent de bonnes propriétés de PAPR. L'inconvénient de ce type de schéma est le manque de flexibilité qu'il impose : comme les symboles SC-FDMA sont codés par paire, chaque trame de communication doit être composée d'un nombre pair de symboles de données. Ceci peut être contraignant : les trames peuvent contenir des pilotes dynamiques, ou des symboles de contrôle de taille variable et il est difficile, voire impossible d'assurer un nombre pair de symboles dans la trame. En outre, le STBC est sensible dans des conditions de forte mobilité, quand le canal de communication risque de varier de manière importante entre la transmission des symboles formant la paire Alamouti.

Les codes originalement conçus en tant que codes espace-temps peuvent aussi être employés en tant que codes espace-fréquence (SFBC, Space-Frequency Block Code). Comme les STBC, leur rôle est de récupérer la diversité spatiale disponible. La diversité fréquentielle et temporelle sont récupérées via le codage correcteur d'erreurs. Dans un contexte SC-FDMA, employer un SFBC revient à appliquer un code d'Alamouti à l'intérieur de chaque symbole SC-FDMA entre deux échantillons de fréquence. Classiquement, ces deux échantillons sont choisis adjacents : étant répartis dans le spectre sur des sous-porteuses adjacentes (ou les plus proches possible), ils ont plus de chances de subir des évanouissements similaires à cause de la corrélation fréquentielle entre les sous-porteuses les transportant. Cela évite une perte de performances du code d'Alamouti, dimensionné pour un canal stationnaire. SFBC est donc plus flexible que STBC car il n'impose aucune contrainte sur le nombre de symboles de données composant une trame. Si l'on souhaite transmettre sur la première antenne d'émission le signal SC-FDMA d'origine, cela revient à transmettre sur la deuxième antenne un signal issu d'un signal mono-porteuse mais dont les composantes spectrales ont été permutées, complexe-conjuguées, et ont subi des changements de signe. Ce spectre ne correspond plus à un signal mono-porteuse à faibles variations d'enveloppe. On a démontré par calcul que SFBC ne changeait pas la puissance moyenne du signal correspondant, mais qu'il pouvait doubler la puissance de crête de certains échantillons dans le domaine temporel. Cette propriété est facilement explicable d'une manière intuitive en raisonnant sur la constellation équivalente dans le domaine temporel, obtenue en appliquant une IDFT de taille M au signal obtenu dans le domaine fréquentiel par la transformation spécifique au SFBC : c'est comme si cette constellation équivalente était transmise, après modulation SC-FDMA classique, sur la deuxième antenne d'émission. Or, on observe que la constellation équivalente est distordue par rapport à la constellation d'origine (QPSK, QAM, *etc.*), en ayant un PAPR plus important. Les résultats de simulation confirment une augmentation de la gamme dynamique du signal, dans l'ordre de 1 dB en termes d'INP. L'avantage du SC-FDMA par rapport à l'OFDMA se retrouve sérieusement diminué.

On propose un SFBC modifié, compatible avec les bonnes propriétés de PAPR du SC-FDMA. On s'impose les critères de construction suivants :

- Avoir une structure ou des paires d'Alamouti se retrouvant sur des couples de sous-porteuses utilisées par la première et la deuxième antenne d'émission ;
- Ne pas modifier la distribution d'amplitude de la constellation équivalente correspondant à la deuxième antenne d'émission.

L'idée consiste à trouver une méthode de choisir les couples de sous-porteuses sur lesquelles placer des paires d'Alamouti de telle manière que l'ordonnancement des composantes spectrales sur la deuxième antenne se fasse d'une manière compatible avec un signal de type mono-porteuse. L'opération qui transforme le spectre discret (de taille M) du signal d'origine dans le spectre discret du signal à transmettre sur la deuxième antenne est appelée SC_M^p. Appliquée à un vecteur de taille M, l'opération SC_M^p consiste à prendre les complexe-conjugués des éléments de ce vecteur en ordre inverse, et leur appliquer un changement alternatif de signe suivi d'un retard cyclique de p positions, où p est un paramètre pair. Ceci équivaut à lier via un code d'Alamouti la k_0-ème et la k_1-ème composante spectrale du signal d'origine, ou k_0 est pair et $k_1 = (p - 1 - k_0) \bmod M$. On nomme le code espace-fréquence résultant SC-SFBC (Single-Carrier Space-Frequency Block Code). En se basant sur les propriétés des transformées de Fourier, on peut facilement constater que la constellation équivalente, à transmettre sur la deuxième antenne d'émission après modulation SC-FDMA, est obtenue à partir de la constellation d'origine par de simples rotations de phase. Le PAPR de la constellation équivalente est égal au PAPR de la constellation d'origine, et il est possible de démontrer théoriquement et de confirmer par simulation que les distributions d'amplitude des signaux transmis sur les deux antennes d'émission sont strictement identiques.

Pour assurer les bonnes propriétés de PAPR sur les deux antennes d'émission, on a donc du relaxer la contrainte du codage sur des sous-porteuses adjacentes. Dans le cas du SC-SFBC, les sous-porteuses transportant des paires d'Alamouti sont séparées par au plus $\max(p, M-p)$ sous-porteuses utiles. En fonction de l'étalement maximal du retard du canal de communications, du type de répartition des données sur les sous-porteuses (localisé, distribué), du nombre de sous-porteuses utiles allouées à un utilisateur, *etc.*, il est possible qu'une ou plusieurs paires d'échantillons de fréquence liés par le code d'Alamouti soient placées sur des sous-porteuses subissant des évanouissements décorrélés, ce qui engendre une interférence au sein de la paire d'Alamouti, résultant dans une dégradation des performances. Si l'on veut éviter un décodage complexe à maximum de vraisemblance (ML, Maximum Likelihood), tout en gardant de bonnes performances du système, un décodage visant à minimiser l'erreur quadratique moyenne (MMSE, Minimum Mean Square Error) semble un bon compromis. Pour les solutions ciblées dans cette thèse, se rapportant à un contexte voie montante, la complexité d'un détecteur MMSE est tout à fait acceptable pour la station de base. En outre, un décodage MMSE s'impose non seulement pour SC-SFBC, mais aussi bien pour SFBC et STBC à forte mobilité, où le canal varie pendant la transmission des paires d'Alamouti.

Pour les petites allocations spectrales localisées dans la bande, il n'y a quasiment pas de dégradation de performances en termes de FER entre SC-SFBC et STBC. Dans le cas le plus défavorable des petites allocations spectrales distribuées dans la bande, une perte chiffrée à maximum 0,7 dB sur un canal Vehicular A est constatée quand on n'utilise que deux antennes de réception. Mais en pratique les stations de base sont équipées de plus de deux antennes de réception, ce qui réduit la perte en performances (seulement 0,3 dB pour quatre antennes de réception). SFBC a des performances similaires à STBC pour les allocations spectrales localisées, étant même très légèrement meilleures à très forte vitesse. Dans des scénarios distribués, il subit lui aussi une perte par rapport au STBC, à la suite de l'écart plus important entre sous-porteuses occupées.

Les autres techniques exploitant indirectement la diversité spatiale ont de moins bonnes performances que les techniques de codage espace-temps/espace-fréquence. FSTD et CDD ont des performances similaires, perdant au moins 0,6 dB par rapport aux techniques d'Alamouti. OL-TAS a une sensibilité plus prononcée aux scénarios de forte mobilité, car l'estimation du canal est moins robuste dans ce cas, où il est impossible d'interpoler dans le domaine temporel les observations du canal correspondant aux deux slots de chaque sous-trame.

SC-SFBC montre de bonnes performances dans un vaste nombre de scénarios. Il est plus flexible que STBC, a de meilleures performances que CDD, FSTD et OL-TAS, et n'engendre pas de dégradation de PAPR comme SFBC.

5 – Extensions à plus de deux antennes d'émission

Depuis l'apparition du code d'Alamouti, beaucoup d'efforts se sont concentrés sur la généralisation de ce code pour plus de deux antennes d'émission. Il a été démontré qu'il n'existait pas de code orthogonal de diversité maximale et rendement un symbole par utilisation du canal pour des systèmes utilisant des symboles complexes et plus de deux antennes d'émission. Pour créer des codes pour plus de deux antennes d'émission, plusieurs approches existent. Pour obtenir un code robuste, il faut sacrifier soit le rendement du code, soit la diversité. Il existe par exemple des codes orthogonaux de diversité maximale pour tout nombre d'antennes d'émission, mais avec un rendement 1/2. Dans le cas particulier de quatre antennes d'émission, le rendement du code peut monter jusqu'à 3/4, tout en gardant l'ordre maximal de diversité. Une autre approche est de cibler des rendements unitaires, et construire des codes qui ne sont plus orthogonaux et qui offrent juste une partie de l'ordre maximal de diversité, comme les codes quasi-orthogonaux par exemple.

Les codes quasi-orthogonaux (QO) proposés par Jafarkhani sont une extension à quatre antennes du code d'Alamouti. Chaque colonne (ou ligne) de la matrice génératrice du code est orthogonale à deux sur trois des colonnes (lignes) restantes. Le rendement du code est unitaire mais ce code ne garantit que la moitié de la diversité maximale.

La difficulté consiste à trouver des codes qui se combinent naturellement bien avec SC-FDMA, sans sacrifier les bonnes propriétés de PAPR et sans introduire des limitations de flexibilité. Appliquer un code QO en tant que code espace-temps (QOSTBC) multiplie par quatre la granularité du système, ce qui est inacceptable. Même si QOSTBC n'impacte pas l'enveloppe du SC-FDMA, le fait d'imposer que les symboles de données soient présents par multiple de quatre dans chaque trame représente une contrainte trop forte pour un système réel. QOSFBC hérite aussi bien des avantages que des inconvénients du SFBC. Si généralement, pour des raisons d'implantation des modules DFT, on dispose bien d'un nombre de sous-porteuses utiles qui est multiple de quatre (en LTE par exemple les sous-porteuses sont allouées par groupes de 12), QOSFBC est compromis par les pertes en PAPR qu'il engendre. Les signaux des trois antennes d'émission sur quatre subissent des augmentations de PAPR allant jusqu'à 1,3 dB par rapport à un signal mono-porteuse.

Pour généraliser SC-SFBC à un système avec quatre antennes d'émission, nous essayons d'appliquer le principe de quasi-orthogonalité. Il a été démontré que l'opération SC_M^p appliquée à un vecteur (conçu dans le domaine fréquentiel) le transforme dans un vecteur respectant le principe d'orthogonalité (au sens d'un code d'Alamouti) et sans engendrer de détérioration du PAPR du signal correspondant dans le domaine temporel. Nous imposons donc comme critère de construction la contrainte que, pour chaque antenne d'émission, le signal dans le domaine fréquentiel de deux antennes parmi les trois autres soit obtenu à partir du signal dans le domaine fréquentiel de cette antenne par des opérations de type SC_M^p.

Comme dans le cas du SC-SFBC, cela résulte dans un code espace-fréquence, que l'on va nommer SC-QOSFBC, qui doit être appliqué sur les échantillons de fréquence transportés par des sous-porteuses non-adjacentes, ici (k_0, k_1, k_2, k_3), avec k_0 pair et inférieur à $M/2$. En isolant des groupes de quatre sous-porteuses ainsi codées ensemble via SC-QOSFBC, on retrouve un code QO dérivé du code de Jafarhkani. Les bonnes propriétés de PAPR du SC-QOSFBC résultant sont vérifiées aussi bien par calcul théorique que par simulation numérique. Ce code peut être généralisé à plus de quatre antennes d'émission.

Pour les cas ou l'on ne dispose pas d'un nombre de sous-porteuses utiles multiple de 4, et si une granularité de deux symboles SC-FDMA dans le domaine temporel n'est pas trop encombrante, nous proposons une solution de code espace-temps-fréquence répartissant les composantes d'un code quasi-orthogonal sur deux sous-porteuses de deux signaux SC-FDMA consécutifs dans le domaine temporel.

Une autre possibilité découle de la combinaison hybride entre un schéma FSTD et un schéma SC-SFBC. Chaque bloc de données avant précodage DFT peut être séparé en deux blocs de taille deux fois inférieure. Chacun des flux ainsi généré est codé par une opération de type $\mathrm{SC}^{p}_{M/2}$, et les deux flux sont multiplexés comme en FSTD, occupant chacun la moitié des sous-porteuses utiles du spectre.

Les performances des codes décrits dans ce chapitre sont évaluées dans de différents scénarios (allocation spectrale, mobilité, nombre d'antennes de réception différentes). Les schémas QO ont de meilleures performances théoriques que les schémas combinés si la connaissance parfaite de l'état du canal est supposée en réception. Les schémas combinés bénéficient d'une estimation du canal plus robuste dans la version utilisée dans cette thèse, car la séparation en fréquence des deux flux permet l'estimation séparée de deux canaux MIMO à deux entrées chacun, ce qui s'avère plus facile que l'estimation d'un canal MIMO à quatre entrées, comme c'est le cas pour les schémas QO. SC-QOSFBC souffre de pertes de performances négligeables par rapport au QOSTBC, dans le scénario réaliste où la station de base est équipée d'au moins quatre antennes de réception.

6 – Techniques combinant le multiplexage spatial et le codage espace-temps

Jusqu'à maintenant, nous nous sommes concentrés sur des codes de rendement unitaire, où l'on tire profit de la présence des antennes d'émission pour augmenter la diversité. Un autre moyen de tirer profit de la présence d'antennes multiples serait d'augmenter le débit en utilisant des techniques de multiplexage spatial. Si l'on dispose de N_{Tx} antennes d'émission, le rendement maximal de la transmission est de N_{Tx} symboles par utilisation du canal, soit N_{Tx} fois plus important que dans les systèmes SISO, ou encore dans les systèmes utilisant des techniques de diversité d'émission à rendement unitaire.

Beaucoup d'architectures mettant en place le multiplexage spatial on été développées, parmi lesquels les plus connues sont les architectures de type BLAST (Bell Labs Layered Space-Time architecture). Pour décoder des flux multiplexés spatialement, les détecteurs performants sont très complexes. Dans de futurs systèmes de communications mobiles, où des solutions basées sur des mini-stations de base à usage résidentiel (femto cell) sont envisagées, le coût et la complexité des stations de base seront limités. Nous nous concentrons dans ce chapitre sur des solutions hybrides, réalisant un compromis entre le débit de la transmission et la diversité, ciblant des détecteurs à faible complexité.

Des schémas de type « double Alamouti » sont connus dans la littérature pour réaliser de bons compromis diversité – multiplexage spatial tout en gardant de bonnes performances. Ces schémas sont conçus pour des systèmes MIMO $4 \times N_{\mathrm{Rx}}$, transmettant en parallèle deux flux de données, chaque flux étant encodé d'après un schéma d'Alamouti. Deux cas se distinguent. Si les 4 antennes d'émission appartiennent au même terminal, et que les deux flux de données sont liés ensemble par le même code correcteur d'erreurs, il s'agit d'un scénario SU-MIMO (Single-User MIMO). Si les deux flux de données sont codés séparément (s'agissant soit de deux utilisateurs différents, chacun équipé avec deux antennes d'émission, soit d'un seul utilisateur codant ses deux flux de données séparément), nous nous trouvons dans un contexte MU-MIMO (Multi-User MIMO).

Les performances de tels systèmes, avec un détecteur sous-optimal de type MMSE, sont fortement dépendantes du taux de codage correcteur d'erreurs et du type d'interférence intercode. La sous-optimalité du détecteur mène à une perte de diversité dans le cas MU-MIMO. Le MMSE n'arrive pas à éliminer de manière optimale l'interférence entre les deux flux Alamouti ; si dans le cas SU le code correcteur d'erreurs gère l'interférence résiduelle, ceci n'est pas possible dans le cas MU, qui souffre d'une perte de diversité. Des détecteurs plus performants, capables d'annuler l'interférence d'une manière éventuellement itérative, sont nécessaires pour améliorer les performances des schémas MU. Les schémas Double Alamouti basés sur SC-SFBC ont des performances similaires à ceux basés sur du STBC.

En comparant les schémas SU Double Alamouti avec les schémas QO présentés dans le chapitre antérieur, on constate que le profil de l'interférence intercode est différent et que les résultats peuvent basculer en faveur de l'un ou l'autre des schémas, en fonction du taux de codage et du type de modulation utilisée. Pour des modulations moins sensibles à l'interférence et en présence d'un codage puissant, les schémas QO semblent avoir de meilleures performances.

Dans un contexte MU-MIMO avec des utilisateurs utilisant chacun un schéma SC-SFBC, un nouveau problème se pose. En fonction des capacités et besoins de chaque terminal mobile, des utilisateurs émettant sur des groupes de sous-porteuses qui se superposent complètement ou partiellement pourraient se voir attribuer des allocations spectrales différentes. Deux utilisateurs employant chacun des opérations de type $\mathrm{SC}_{M_0}^{p_0}$ et respectivement $\mathrm{SC}_{M_1}^{p_1}$ avec des paramètres p indépendants vont placer leurs paires d'Alamouti sur des sous-porteuses dépareillées dans le sens où, en isolant des couples de sous-porteuses, les symboles placés sur ces couples de sous-porteuses ne se trouvent pas dans une relation correspondant à un code de type Double Alamouti. En se basant sur la structure du SC-SFBC, nous proposons une méthode pour calculer les paramètres p de chaque utilisateur pour que la transmission s'effectue d'une manière coordonnée et qu'en isolant de manière convenable des couples de sous-porteuses, celles-ci transportent des paires de type Double Alamouti, facilement décodables au récepteur. Un algorithme à exécuter à la station de base qui effectue une allocation compacte dans la bande d'un nombre prédéfini d'utilisateurs avec des besoins de communications déjà identifiés est aussi proposé.

7 – Conclusions et perspectives

Cette thèse s'intéresse à l'étude des performances au niveau de la couche physique pour la voie montante des systèmes de communications mobiles de future génération. Elle se focalise sur les performances au niveau lien dans un contexte non-linéaire, ainsi que sur des techniques MIMO compatibles avec SC-FDMA.

Dans un premier temps, nous avons fait une analyse détaillée de la technique SC-FDMA, étudiant ses performances sous de nombreux aspects, en la comparant avec d'autres techniques d'accès multiple comme OFDMA et SS-MC-MA. L'analyse comparative a été conduite dans un contexte non-linéaire, prenant en compte des contraintes pratiques spécifiques aux standards des futurs systèmes de communications mobiles.

Une fois les bonnes performances du SC-FDMA établies, nous avons étendu notre étude à la dimension MIMO. Nous avons étudié différentes solutions de l'état de l'art, en mettant en évidence leurs avantages et inconvénients et nous avons proposé de nouvelles techniques de diversité d'émission compatibles avec SC-FDMA. Des schémas pour deux et quatre antennes d'émission ont été proposés et évalués, et des possibilités d'extension à d'autres nombres d'antennes d'émission ont été données.

Finalement, nous avons étudié des schémas combinant diversité d'émission et multiplexage spatial. Nous avons proposé un algorithme permettant une allocation spectrale compacte dans le cas d'un nombre donné d'utilisateurs avec des besoins différents de communication, dans un système MIMO multiutilisateurs.

La thèse ouvre la voie à plusieurs perspectives, parmi lesquelles nous citons l'étude de la diversité dans des systèmes SC-FDMA avec détection sous-optimale, ou l'extension des techniques présentées ici à des systèmes Clustered SC-FDMA.

Chapter 1

Introduction

The history of wireless communication systems, although recent, is characterized by a tremendous and rapid evolution. The bases of wireless communications as we know them today started with the work of Hertz, who discovered the existence of radio waves, and Maxwell, who developed the theory of electromagnetic waves in 1886. Shortly after, Tesla proved that it is possible to transmit information via these waves and Marconi made a first public demonstration of a wireless transmission in 1898, discovery winning him the Nobel Prize in physics in 1909. In the subsequent years, radio and television became widespread throughout the world, but it is only in the past 25 years that wireless communications systems emerged and evolved.

This evolution is phenomenal, not only from the point of view of technical progress but also from the point of view of social impact, working and communication habits. Wireless communications are today not only a profitable business, but also a daily tool more and more widespread and indispensible. With this growing importance of wireless communication in today's society comes the never-ending strive for more throughput, better quality of service, better mobility, more diversified applications, service convergence. Three generations of mobile communications systems were implemented in the past three decades and we are heading for the fourth. The demands in peak data rate passed from several kbps to 50 Mbps in uplink (1 Gbps in downlink) or more in future systems.

The first generation of mobile communications (1G) emerged in the early 70s in the US under the name of AMPS (Advanced Mobile Phone Service). This analog mobile phone system developed by Bell Labs fathered the term "cellular" because of its use of small hexagonal cells. The first big revolution was the migration from analog to digital communications, opening way to the second generation (2G) of mobile systems and its most remarkable exponent, GSM (Global System for Mobile communications). Standardization work spanned from 1982 to 1988, and the first GSM call was made in 1991. With more than 3.8 billion connections, GSM is used nowadays by 80% of the global mobile market (data provided by GSM Association, September 2008).

But the 9.6 kbps offered by GSM, which sufficed for the needs of voice services, proved to be insufficient to cover the demands in data transfer services. This is how 2.5G standards appeared. GPRS (General Packet Radio Service) for example is an extension of the GSM standard, providing uplink data rates of up to 40 kbps (115 kbps in downlink). It uses the GSM architecture for voice transmission but also allows access to data networks and Internet. The packet based transmission allows a dynamic optimization of data and voice transmission, and also allows billing per transferred traffic rather than per connection time. It was originally standardized by European Telecommunications Standards Institute (ETSI), and was taken over by the 3rd Generation Partnership Project (3GPP). Further enhancements to GSM networks are provided by Enhanced Data rates for GSM Evolution (EDGE) technology, which provides up to three times the data capacity of GPRS (100-130 kbps in uplink, 384 kbps in downlink). EDGE is considered as a 2.5G – 2.75G technology. It was standardized by 3GPP as part of the GSM family and it brings important technological advancements with respect to GPRS, such as the use of more sophisticated methods of modulation and coding, as well as link adaptation techniques.

The birth certificate of 3G was signed when International Telecommunication Union (ITU) defined a global set of demands reunited under the name of International Mobile Telecommunications-2000 (IMT-2000) standard. Several systems fulfilling the demands of IMT-2000 were developed. These systems partly emerged from the mobile telephony world, while others are developments of standards from the wireless data transfer world. In the US, CDMA2000 emerged, as an evolution of the IS95 standard, also employing Code Division Multiple Access (CDMA). The European solution to IMT2000 was given by 3GPP under the form of Universal Mobile Telecommunications System (UMTS). Currently, the most common form of UMTS uses W-CDMA (Wideband Code Division Multiple Access) as the underlying air interface. The first commercial launches of 3G systems were made in October 2001 (Japan, NTT DoCoMo) and January 2002 (South Korea, SK Telecom). In Europe, mass market 3G services started to be commercialized in 2003 (in 2004 in France), but 3G networks are confronted with the enormous costs of additional spectrum licensing fees, which considerably slowed down their development. UMTS promised data rates of 2 Mbps for fixed users and 384 kbps from a mobile location. Field tests showed data rates around 220-320 kbps, which rapidly turned out to be insufficient.

The needs for higher throughputs marked the step for the 3.5G. Standardized by 3GPP, HSPA (High Speed Packet Access) is a family of technologies embodying the evolution of 3G/UMTS (WCDMA) and providing efficient voice services in combination with mobile broadband data. HSPA includes HSDPA (High Speed Downlink Packet Access), HSUPA (High Speed Uplink Packet Access) and HSPA Evolved. These are also known as 3GPP Releases 5 through 8. The GSM Association reported, end 2008, over 297 million 3G subscribers, among which over 55 million using HSPA. HSDPA (2005) brings an important technological upgrade, utilizing hybrid automatic repeat-request (HARQ), adaptive modulation and coding or fast packet scheduling. Current HSDPA deployments support down-link speeds up to 14.4 Mbps. HSUPA (2008) utilizes the same evolved techniques as HSDPA to improve the uplink and create synchronous data transmissions of up to 5.7 Mbps. HSPA Evolved, also referred to as HSPA+, promises to enhance the downlink to provide 42 Mbps by utilizing 64QAM modulation and the uplink to 11.5 Mbps through 16QAM. A further enhancement to help achieving increased data rates is the use of MIMO (multiple input multiple output antennas). The first HSPA+ commercial launch in Europe has just been announced on March 23, 2009, in Austria.

On the same market segment, the techniques reviewed here also have some indirect competitors mainly emerged from the wireless data transfer world. We will cite here especially WiFi (Wireless Fidelity, IEEE 802.11 family) and WiMAX (Worldwide Interoperability for Microwave Access, IEEE 802.16 family). Several milestones are to be noted in the history of WiMAX. The IEEE 802.16-2004 standard forming the basis of "fixed WiMAX" was amended in 2005 to integrate support for mobility, resulting in the "mobile WiMAX" standard IEEE 802.16e-2005. More developed in the US and Asia, WiMAX commercial offers entered the European market in 2008, and WiMAX networks are under deployment and test in many European countries. The last forthcoming version, IEEE 802.16m, still under development, aims at fulfilling the requirements of IMT Advanced of the ITU.

The research effort for defining the after-UMTS era started several years ago. Beyond 3G (B3G)/4G systems are currently active in standardization bodies and are aiming high: between 100 Mbps and 1 Gbps data rates both indoors and outdoors, with premium quality and high security. 3GPP started the work on the B3G Long Term Evolution (LTE) of UMTS back in December 2004. This new radio access technology is optimized to deliver very fast data speeds of up to 100 Mbps downlink and 50 Mbps uplink for channel bandwidths from 1.25 MHz to 20 MHz, coupled with major improvements in capacity and reductions in latency. LTE incorporates MIMO in combination with Orthogonal Frequency Division Multiple Access (OFDMA) in the downlink and Single Carrier FDMA (SC-FDMA) in the uplink. The 3GPP Release 8 is to be ratified as a standard, commercial deployment being foreseen for the end of 2009. Several major mobile operators have indicated they will adopt LTE in the next few years, aiming to launch a commercial LTE network by the end of 2009 in Japan, and in 2010 in the US. Business perspectives involve a macro-cell deployment for outdoor coverage and an indoor deployment with femto-cells in order to deal with data traffic generated from homes or enterprises.

The work on the 3GPP's candidate for the 4G technologies (LTE- Advanced) has started in 2008. LTE-Advanced extends the technological principles behind LTE, incorporating higher order MIMO (4x4 and beyond). It has the ability to use non-contiguous frequency ranges to alleviate frequency range issues in an increasingly crowded spectrum. LTE-Advanced targets peak data rates of 1 Gbps. However, whereas LTE focus is on clearly the peak data rate, *i.e.*, for terminals that have already good transmission environment, LTE-Advanced also aims at improving the user experience in any situation, *e.g.*, terminals at the cell-edge with bad coverage.

This thesis addresses the design of a physical layer for the uplink of B3G/4G wireless communication systems. In the context of LTE/LTE-advanced studies, this thesis develops and evaluates transmission strategies exploiting an SC-FDMA uplink system. The outline of the thesis can be summarized as follows:

- In the present Chapter 1, we review the state-of-the-art in wireless communication systems and we point out the outline and the major achievements of this thesis.

- Chapter 2 introduces as a key constituent of wireless communications, the transmission channel, and reviews its properties in the time, frequency and space domains. Several channel models and simulation framework used throughout the thesis are given.
- Chapter 3 presents and compares three multiple access schemes suitable for the uplink air interface of future mobile systems, with a particular focus on SC-FDMA, which has the advantage of low Peak to Average Power Ratio (PAPR) over its competitors. This analysis is conducted taking into account the specific constraints of a mobile terminal, namely the presence of a high power nonlinear amplifier and the regulation constraints. In particular, we introduce a set of tools and methods for evaluating a system's performance in nonlinear context and we show the importance of a nonlinear analysis when evaluating the performance of a system. We also perform a thorough analysis of SC-FDMA, proving that it is an appropriate air interface for future communications systems. This work resulted in two conference papers [CiMo06], [CiMo07a] and one journal paper [CiMo08a].
- An innovative transmit diversity scheme compatible with SC-FDMA, coined Single-Carrier Space-Frequency Block Coding (SC-SFBC), is developed in Chapter 4. This new orthogonal scheme is designed for transmitters equipped with two transmit antennas and relies on an innovative mapping that allows Alamouti-based SFBC-type precoding, without degrading the PAPR properties of SC-FDMA. The performance of this new scheme is also investigated and compared to alternative transmit diversity schemes in realistic simulation scenarios. In particular, the benefit of such a technique is shown for power limited terminals, *e.g.*, for terminals at the cell-edge. Based on this work, we filed two patents, participated in two international conferences [CiMo07b], [CiMo07c] and published one international paper [CiMo08b].
- Chapter 5 extends the SC-SFBC concept to systems with more than 2 transmit antennas. A novel quasi-orthogonal code, as well as a combination of SC-SFBC with frequency-switching, and space-time-frequency coding are presented and evaluated. All of these schemes preserve the PAPR of SC-FDMA for a transmission rate of 1 symbol per channel use. The novel technology exposed in this chapter is protected by a patent, and resulted in one conference paper [CiMo08c]. Also, a journal paper reviewing the most important results in chapters 4 and 5 has been submitted and is under second revision.
- Schemes combining SC-SFBC transmit diversity with spatial multiplexing are investigated in Chapter 6 to allow an increase of data rates as well as an improvement of performance, while keeping nominal PAPR properties. Single-user and multi-user MIMO scenarios are distinguished and specific SC-SFBC optimization techniques are proposed. An algorithm for optimal spectrum allocation is also presented in the context of multi-user MIMO SC-FDMA. The innovative ideas in this chapter are protected by two filed patents and were included in a contribution to an European project [Codiv].
- Finally, Chapter 7 summarizes the conclusions of this work and gives some perspectives on future work.

Chapter 2

The mobile radio channel

In its simplest definition, a communication channel is the entity transforming a transmitted message into a received message. Throughout the years, many different concepts of communication channel have been developed, serving different areas of research, from electromagnetic propagation to information theory. Several approaches exist in the literature, and we will discuss in the following two main viewpoints.

A good understanding of the wireless channel, of its physical parameters, of its properties, as well as accurate channel modeling are of the utmost importance in the design of mobile communication systems. The goal of this chapter is to review the principal characteristics of the wireless channel and to evaluate the influence of the channel parameters on the transmitted signal. We will present a physical approach, where the radio channel can be seen as the physical medium which the electromagnetic wave propagates through, and an analytical approach, where the radio channel can be seen as a linear time-varying filter, mapping signals from transmit to receive data space. Different channel models to be further employed in this thesis will also be discussed.

2.1. Physical and statistical modeling for radio channels

The basis of any wireless communication is the electromagnetic wave propagation, governed by the laws of Maxwell. Theoretically, provided knowledge of the radiated waveform and of all the obstructions present in the propagation environment (and infinite computational power), one could compute the electromagnetic field impinging on the receive antenna by solving the Maxwell equations. Three main mechanisms govern the radio wave propagation from the base-station (BS) to the mobile station (MS): *reflection* on large smooth surfaces, *diffraction* on sharp edges and *scattering* on rough surfaces [Rap02]. In the literature, all the interacting objects are generally referred to as "scatterers", even when the interaction process is not scattering.

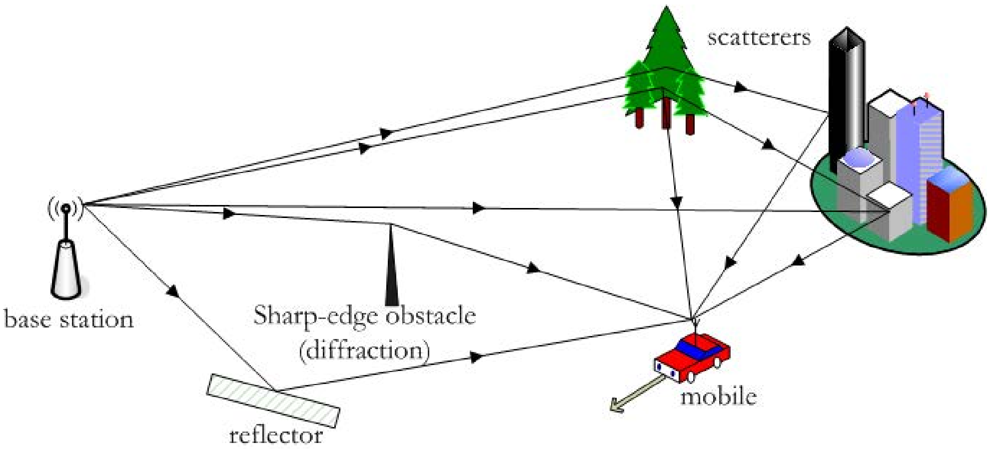

Fig. 2.1 Example of outdoor multipath propagation.

As shown in Fig. 2.1, the received signal is consequently a superposition of waves coming from different directions with different attenuations and phase rotations. This phenomenon, engendered by the mechanisms here-above cited, is called *multipath propagation*. On one hand, shadowing by large objects causes variations in signal strength that can be observed on a large scale. This is called *large-scale fading*, and the mean of the variations, decaying with the distance, is given by the path loss. On the other hand, on short distances, the multipath components arriving from different directions with different phase variations combine in a constructive or destructive manner, leading to important rapid fluctuations in the signal strength. This is known as *small-scale fading*. Large and small-scale fading are sometimes referred to as slow and respectively fast fading. Since it is too complicated to describe all the reflection, diffraction and scattering events that compose each of the multiple paths, statistical approaches are preferred to describe the fading process.

2.1.1. Propagation mechanisms

Reflection and transmission

Specular reflection (Fig. 2.2-(a)) occurs when a radio wave is incident to a smooth object considered large with respect to the radiation wavelength. If the incident object is a perfect conductor all the wave energy is reflected back into the original medium. When the incident object is a dielectric layer (*e.g.*, a wall), the incident wave is partly reflected and partly transmitted. The incidence angles of the reflected and transmitted wave are given by Snell's law:

$$\begin{cases} \theta_{\mathrm{r}} = \theta_{\mathrm{i}} \\ \sqrt{\delta_2}\sin\theta_{\mathrm{t}} = \sqrt{\delta_1}\sin\theta_{\mathrm{i}} \end{cases}, \tag{2.1}$$

where $\theta_{\mathrm{i/r/t}}$ stands for the angle of the incident, reflected and respectively transmitted (refracted) wave, and $\delta_{1,2}$ is the complex dielectric constant of the two mediums. In highly lossy materials,

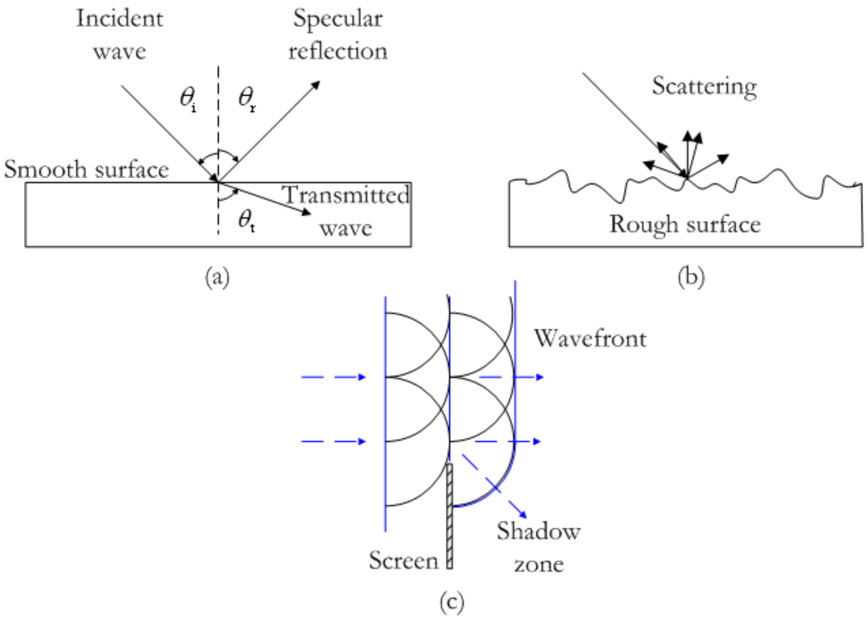

Fig. 2.2 Reflection, scattering and diffraction.

Snell's law is not applicable. The transmission phenomenon is very important for wave propagation inside buildings for example, when the waves need to penetrate a wall to get to the receiver.

Diffraction

Diffraction appears when the wave direction is obstructed by a sharp-edge obstacle. The secondary waves generated on the obstacle's discontinuity propagate behind the obstacle: the wave "bends" behind the obstacle, generating an electromagnetic field even in the shaded areas when no direct line of sight (LOS) exists between the transmitter (Tx) and the receiver (Rx) (this is explained by the Huygens-Fresnel principle, which states that each point of a wavefront can be considered the source of a spherical wave [Str41], as depicted in Fig. 2.2 – (c)). Computing the diffracted field at the receiver is a rather complex problem. In the ideal case of an absorbing semi-infinite screen, a closed form solution based on the Fresnel integral exists. If diffraction occurs on a single wedge structure, a formula for the far field is given in [VaAn03]. Except for several special cases, closed form solutions do not exist when multiple obstacles contribute to the diffraction mechanism (which is always the case in practice). A multitude of approximate methods exist: Bullington [Bul47], Epstein – Peterson [EpPe53] and Deygout [Dey66].

Scattering

Scattering occurs as the result of an interaction between a radio wave and rough surfaces or small irregular shapes (Fig. 2.2-(b)). The dimension of the irregularity is understood to be on the order of the wavelength, or smaller. The irregularities scatter the incident waveform into all directions, which makes impossible to determine the exact amount of energy radiated on a given direction. The elements generating scattering are raindrops, snowflakes, leaves and more generally any small object not included in the used maps and building plans.

Scattering was largely investigated, mainly due to its great importance for radar techniques [BaFu79] [VaAn03]. Two main theories emerged in the study of rough surfaces, namely the Kirchhoff theory and the perturbation theory [Mol05]. The Kirchhoff theory assumes that the different scattering points onto the surface are sufficiently small so as not to influence each other: The probability density function of the surface height suffices to model the scattering. The perturbation theory generalizes the Kirchhoff theory by using not only the probability density function of the surface height but also its spatial correlation function.

2.1.2. Small-scale fading

Small-scale fading characterizes the fast variation of the signal strength over small distances (in the order of the carrier wavelength) due to the interference of the multipath components. Small scale fading can be further classified as flat/frequency selective fading, notions to be clarified in section 2.2.3, since they are not intrinsic to the channel, but depend on the system properties (bandwidth, carrier frequency etc.).

Rayleigh fading

Let us consider the propagation from a BS to a MS in a multipath environment with no dominant component (NLOS). Evaluating the electric field $E(t)$ impinging the MS at a certain moment t shows that both its in-phase and quadrature-phase components are the sum of many random variables. Consequently, the central limit theorem ensures us that they can be modeled by a zero-mean Gaussian random variable. Separating the real and the imaginary part derives the independent statistics of amplitude $\left(r = |E|\right)$ and phase $\left(\psi = \arg(E)\right)$ of the received signal. The amplitude follows a Rayleigh distribution with probability density function:

$$pdf\,(r) = \frac{r}{\sigma^2}\exp\left(-\frac{r^2}{2\sigma^2}\right),\ \ 0 \le r < \infty\,, \tag{2.2}$$

while the phase is uniformly distributed in [0, 2π). σ stands for the standard deviation of r. The Rayleigh distribution (2.2) is an excellent approximation in a large number of NLOS scenarios. Also, it can be perceived as a worst case scenario from the point of view of the received power, as in the absence of LOS component there is a large number of fading dips.

Rice fading

Should we assume a LOS component added to the previous scenario, we can prove in a similar way that the received signal amplitude follows a Rice distribution with probability density function:

$$pdf(r) = \frac{r}{\sigma^2} \exp\left(-\frac{r^2 + A^2}{2\sigma^2}\right) \cdot \mathrm{I}_0\left(\frac{rA}{\sigma^2}\right),\ 0 \le r < \infty\,, \tag{2.3}$$

where $\mathrm{I}_0(.)$ is the modified Bessel function of the first kind, zero order [Bow58], and A represents the amplitude of the LOS component. The higher the amplitude of the LOS component, the less probable the occurrence of deep fades. Rice distribution is a good approximation when besides the dominant component a large number of non-dominant components exist.

Nakagami fading

The Nakagami distribution is employed when the central limit theorem is not necessarily valid for the non-dominant components and the Rice distribution is not appropriate (*e.g.*, ultra-wideband channels) [Nak60]. The amplitude distribution is given as:

$$pdf_r(r) = \frac{2}{\Gamma(m)} \left(\frac{m}{\Xi}\right)^m r^{2m-1} \exp\left(-\frac{m}{\Xi} r^2\right),\ 0 \le r < \infty,\ m \ge 1/2\,, \tag{2.4}$$

where $\Gamma(m)$ is Euler's Gamma function [AbSt72], $\Xi = \overline{r^2}$ is the mean square value of r and the parameter m is given by $m = \Xi^2 / \overline{(r^2 - \Xi)^2}$.

2.1.3. Large-scale fading

As pointed out before, small-scale fading changes rapidly over a small spatial scale of the order of the wavelength. If the field strength E is averaged over a small area (in the order of tens of wavelengths), we obtain a small-scale averaged field strength (and a corresponding received power) that varies slowly when the MS moves at a fixed distance from the BS, *e.g.*, on a circle around the BS. The reason of these variations is shadowing by large objects and will be statistically described in the following. At a large scale, the mean of the shadowing variation itself is inversely proportional to the BS-MS distance and is linked to the deterministic path loss.

Path loss

The path loss represents the difference between the transmitted and the received power (in dB), due to the attenuation introduced by the propagation channel.

The free-space path loss can be directly derived from the Frii's law [Mol05] as:

$$L_{(\mathrm{dB})} = 10\log_{10}\left(\frac{P_{\mathrm{Tx}}}{P_{\mathrm{Rx}}}\right) = -10\log_{10}\left(G_{\mathrm{Tx}} G_{\mathrm{Rx}} \frac{\lambda^2}{(4\pi)^2 d^2}\right), \tag{2.5}$$

where:

- $P_{\mathrm{Tx/Rx}}$ is the Tx/Rx power;

- $G_{\mathrm{Tx/Rx}}$ is the Tx/Rx antenna gain;
- d is the distance between the transmitter and the receiver;
- $\lambda = c / f_{\mathrm{c}}$ is the radiation wavelength, where $c = 3 \cdot 10^8$ m/s is the speed of light and f_{c} stands for the carrier frequency.

The factor $(4\pi d / \lambda)^2$ is also called the free space loss factor. The free-space loss in (2.5) is inversely proportional to the square of the distance. In practice, the assumption of having only a direct LOS path is unrealistic, as discussed above. Should we assume that besides a direct LOS wave a second ground-reflected wave is impinging on the Rx antenna, an approximate estimation of the path loss can be deduced to replace the standard Frii's law:

$$L_{\mathrm{(dB)}} \simeq -10 \log_{10}\left(G_{\mathrm{Tx}} G_{\mathrm{Rx}} \frac{h_{\mathrm{Tx}}^2 h_{\mathrm{Rx}}^2}{d^4} \right), \tag{2.6}$$

where $h_{\mathrm{Tx/Rx}}$ stand for the heights of the Tx/Rx antennas. The received power is no longer dependent on the carrier frequency and decays with the fourth power of the distance: since the sign of the electric field is reverted on the reflected path, the two waves interfere and start cancelling each other, which explains the faster decay of the received power. This is also known as the d^{-4} power law. Considering such a decay factor of 4 is valid for large distances and is particularly useful in rural areas, where the two-ray model is a good approximation.

In practice these laws do not give accurate results, as the decay factor strongly depends on the environment; the radio wave will be obstructed by multiple incident obstacles, which will absorb a part of the incident energy while scattering the rest. [Jak94] reports decay factors from 3 to 5 for mobile radio channels and even exponential decays at very large distances. Several empirical or semi-empirical laws exist for different types of scenarios (metropolitan, urban, suburban, LOS/NLOS, etc.). The empirical laws are based solely on measurements, while the semi-empirical laws take into account theoretical laws modified by correction factors that have been deduced via experimental measurements. Amongst the most well known such laws we shall cite: Okumura - Hata [Oku68] [Hat80], Walfish - Ikegami [WaBe88] [Ike84], CCIR [CCIR82]. Accurate path loss evaluation is very important in the design of a mobile cellular system, as it determines the number of cells and the position of the base-stations: the dimension of the cell is dictated by the maximum tolerable path loss. Since the path loss is very dependent on the physical environment, practical channel measurements are indispensable for the deployment of a cellular network.

Shadowing

Measurements performed in practice show that the average received power has stochastic variations for a fixed given distance and cannot be simply computed in a deterministic manner by solely evaluating the path loss. Imagine a mobile moving in a given environment, in the shadow of large obstacles like tall buildings or a hill. Since the relative position of the mobile with respect to the obstacles is constantly changing, the conditions of propagation (*e.g.*, diffraction coefficient, reflection angles) are also changing, but it might take a large distance (in the order of several tens of wavelengths) in order to significantly change the received field strength. This phenomenon engenders slow variations which are referred to as shadowing.

The received small scale averaged field strength E follows a lognormal distribution [Mol02]:

$$pdf_{\mathcal{E}}(\mathcal{E}) = \frac{20/\ln(10)}{\mathcal{E}\sqrt{2\pi\sigma_{\mathcal{E}}^2}} \exp\left(-\frac{\left(20\log_{10}(\mathcal{E}) - \mu_{\mathrm{dB}}\right)^2}{2\sigma_{\mathcal{E}}^2} \right), \tag{2.7}$$

where $\sigma_{\mathcal{E}}$ is she standard deviation of $\mathcal{E}$, and μ_{dB} is the mean of the values of $\mathcal{E}$, expressed in dB. Indeed, should we consider that the mobile station undergoes several random reflections and diffractions, the loss caused by each of these mechanisms corresponds to adding or substracting a random loss (expressed in dB) from the path loss average value. We can thus model this effect as a sum of random variables expressed in dB, which follows a lognormal distribution. Since the mechanism described here-above is not a valid scenario in all physical situations, other explanations for (2.7) exist, such as [And02].

The combined effect of path loss and shadowing are reflected by an overall resulting attenuation also called the Local Mean (LM) attenuation, used to predict the average received signal power from random locations. Other statistics exist to include both large scale fading and small scale interference effects, *e.g.*, the Suzuki distribution [Suz77].

2.1.4. Doppler spectrum

When a receiver is in relative motion with respect to the source of the transmitted wave or when the propagation environment itself includes moving obstacles, the receiver observes a change in the received frequency and wavelength. This is called the Doppler effect. The difference between the received carrier frequency f_{Rx} and the transmitted carrier frequency f_{c}, $\nu = f_{\mathrm{Rx}} - f_{\mathrm{c}}$ is called the Doppler shift. It depends on the speed of movement in the direction of the wave propagation ($|\mathbf{v}|\cos(\alpha)$, see Fig. 2.3-(a)) and the wavelength λ:

$$\nu = -\frac{|\mathbf{v}|}{\lambda}\cos(\alpha) = -\nu_{\mathrm{D,max}}\cos(\alpha). \tag{2.8}$$

Let us now consider that a sine wave (narrowband case) is transmitted in a multipath environment. Different multipath components have different directions of arrival and are thus received with different Doppler shifts in the range $f_{\mathrm{c}} - \nu_{\mathrm{D,max}} \cdots f_{\mathrm{c}} + \nu_{\mathrm{D,max}}$. Here, $\nu_{\mathrm{D,max}}$ stands for the maximum Doppler shift. A commonly used assumption is that of an isotropic scattering: The angles of arrival are uniformly distributed in $[0, 2\pi)$. This yields the so-called Jakes Doppler power spectrum [Jak94] given by:

$$\mathbf{S}_{\mathrm{D}}(\nu) = \frac{1}{\pi\sqrt{\nu_{\mathrm{D,max}}^2 - \nu^2}}, \ \forall\, \nu_{\mathrm{D}} \in \left(-\nu_{\mathrm{D,max}}, \nu_{\mathrm{D,max}}\right). \tag{2.9}$$

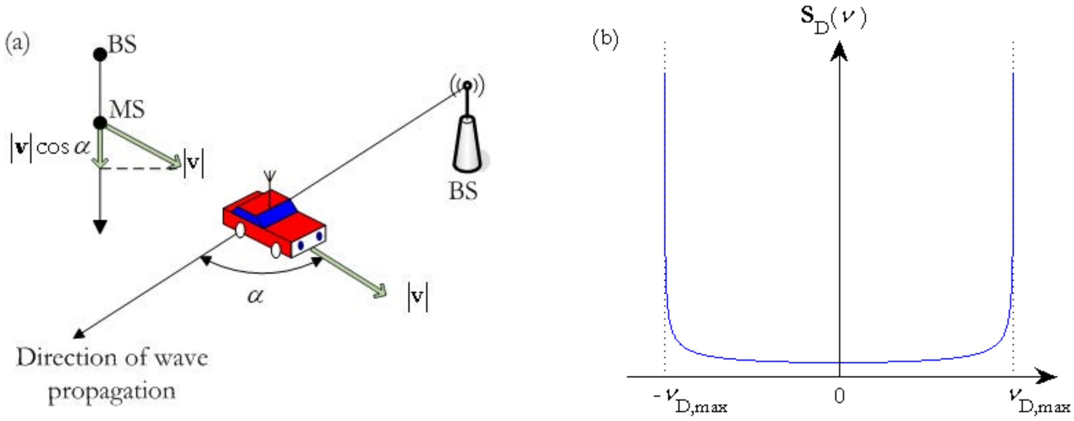

Fig. 2.3 (a)- Movement in a propagation environment; (b)- Jakes Doppler power spectrum of a single sine wave.

The "bathtub" shape of the Jakes spectrum is depicted in Fig. 2.3-(b). The Doppler spectrum describes the frequency dispersion of the channel, particularly disturbing in narrowband systems where it leads to transmission errors (*e.g.*, in Frequency Shift Keying (FSK) modulations, frequency shifts lead to demodulation errors) or in wideband systems like OFDM (Orthogonal Frequency Division Multiplexing) where Doppler shifts can lead to inter-carrier interference. Since the power distribution spectrum and the autocorrelation function are Fourier pairs, the Doppler spectrum is a measure of the temporal statistics of the channel fading. The tools described in 2.1.5 give a more intuitive insight on the temporal behavior of the channel.

2.1.5. Time-domain characterization of fading

Level Crossing Rate

The Level Crossing Rate (LCR) is defined as the average rate with which the amplitude r of the received signal crosses a certain level r_0 in the positive direction (r_0 defines the depth of the fading dips). For Rayleigh fading for example, the LCR can be computed as [Rap02]:

$$\mathrm{LCR}(r_0) = \sqrt{2\pi}\nu \frac{r_0}{\sqrt{2\sigma^2}} \exp\left(-\frac{r_0^2}{2\sigma^2}\right). \tag{2.10}$$

ν stands for the Doppler shift and σ is the standard deviation of the amplitude of the signal. LCR is proportional to the MS speed.

Average Fade Duration

The Average Fade Duration (AFD) determines, in average, how long the amplitude r of the received signal remains below a certain level r_0. It is consequently the ratio between the cumulative distribution function (CDF), *i.e.*, the probability that the amplitude r of the received signal be inferior to a threshold r_0, over the crossing rate of that threshold [Mol05]. For Rayleigh fading, with the notations in the previous subsection, this gives:

$$\mathrm{AFD}(r_0) = \frac{1 - \exp\left(-\frac{r^2}{2\sigma^2}\right)}{\mathrm{LCR}(r_0)} . \tag{2.11}$$

The AFD is a good indicator if we want to determine, *e.g.*, how many bits are likely to be lost during a fade. AFD decreases when the mobile speed increases: At higher speeds, long fade dips are less and less probable.

2.2. Analytical modeling of the wireless channel

Section 2.1 described the physical phenomena that occur during propagation and their statistical properties. But one might only be interested by the transformation between transmitted and received signals, without having to model all the physical phenomena behind the propagation mechanism. To this end, the multipath channel can be modeled as a linear time-varying filter performing the mapping of the transmitted symbols set to the received symbols set. The coefficients of this filter will have statistical properties motivated by the physical propagation phenomena, but their interpretation will be system-dependent.

2.2.1. The wireless channel as a linear filter

Let us denote by $x(t)$ an arbitrary transmitted signal with non-zero bandwidth W. In a multipath environment, due to the multiple scatterers, the received signal $y(t)$ is of a sum of delayed and attenuated copies of the original signal:

$$y(t) = \sum_i a_i(t) x(t - \tau_i(t)) , \tag{2.12}$$

where $a_i(t)$ and $\tau_i(t)$ are respectively the attenuation and the delay of the ith path at time t. Since the channel is linear, let us define by $h(\tau, t)$ the impulse response of the channel at time t to an impulse transmitted at time $t - \tau$. The input signal filtered by $h(\tau, t)$ yields:

$$y(t) = \int_{-\infty}^{\infty} h(\tau, t) x(t - \tau) d\tau . \tag{2.13}$$

In conjunction with (2.12), we can deduce the impulse response of the fading channel as:

$$h(\tau, t) = \sum_i a_i(t) \delta(\tau - \tau_i(t)) . \tag{2.14}$$

This shows that the channel can be seen as a linear time-varying filter, encompassing all the physical channel properties, and reducing the complexity of solving Maxwell's equations to the input-output relationship (2.13). Fourier and inverse Fourier transforms $\left(\mathcal{F} / \mathcal{F}^{-1}\right)$ can be defined for both time (t) and delay (τ) variables, resulting in the functions in Fig. 2.4. For example, we can define a time-varying frequency response of the channel as the Fourier transform of the time-varying impulse response function with respect to the delay variable τ:

$$H(f,t) = \int_{-\infty}^{\infty} h(\tau,t)\exp(-j2\pi f\tau)d\tau = \sum_i a_i(t)\exp(-j2\pi f\tau_i(t)) . \tag{2.15}$$

$H(f,t)$ is a slowly varying function of t and we can interpret it as the frequency response of the channel around a fixed time t. By taking the Fourier transform of the transmitted/received signal, eq. (2.13) can be re-written:

$$Y(f,t) = H(f,t)X(f,t) . \tag{2.16}$$

In (2.14), the channel is modeled as a tapped delay line. A common practice is the WSSUS assumption (Wide Sense Stationary, with Uncorrelated Sources) [Bel63]. WSS means that the second-order amplitude statistics do not vary with time; US defines contributions with different delays as uncorrelated. Overall, from a physical point of view, the WSSUS assumption implies that at all the taps $a_i(t)$ are fading independently and that their average power does not depend on time. For each tap, the time variations are described by a Doppler spectrum. Let us also define here the power delay spectrum, more popularly known as the power delay profile (PDP):

$$P_h(\tau) = \int_{-\infty}^{\infty} |h(t,\tau)|^2 \, dt . \tag{2.17}$$

The PDP describes how much power from a transmitted unitary impulse arrives at the receiver with a delay between $[\tau, \tau + d\tau]$. Equation (2.17) is valid under the assumption that $h(t,\tau)$ is ergodic and thus $P_h(\tau)$ also represents the statistical expectation of $|h(t,\tau)|^2$.

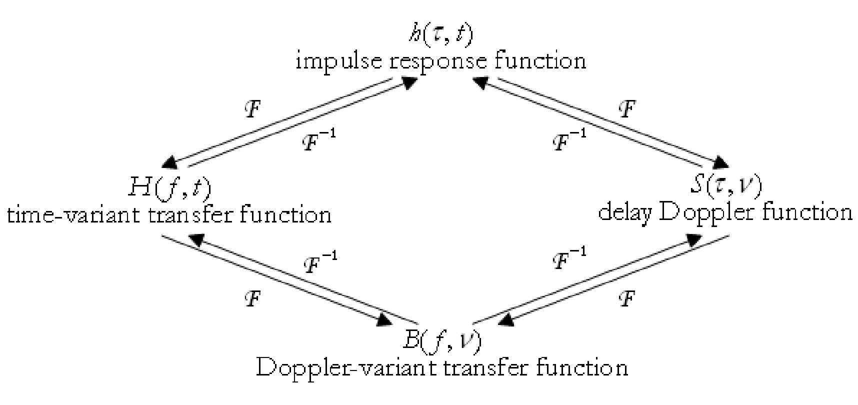

Fig. 2.4 Deterministic system functions.

A simplified block diagram modeling the impacts of the transmission is presented in Fig. 2.5. A noise component $n(t)$ is generally introduced in order to model the internal noise due to the electrical system components. It is assumed to be AWGN (additive white Gaussian noise).

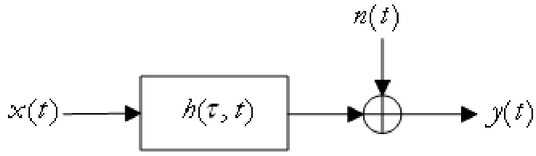

Fig. 2.5 Simplified model of the transmission.

2.2.2. Discrete time baseband model

In typical wireless applications, most of the signal processing (coding/decoding, modulation/demodulation, equalization, etc.) is performed in the baseband $\left(-W/2\ldots W/2\right)$, *i.e.*, before up-conversion and after down-conversion. It is then of interest to consider the complex baseband equivalent:

$$h_{\mathrm{b}}(\tau,t)=\sum_i \underbrace{a_i(t)\exp(-j2\pi f_c\tau_i(t))}_{a_i^{\mathrm{b}}(t)}\delta(\tau-\tau_i(t)) \tag{2.18}$$

In the sequel, all signals will be considered to be represented by their complex baseband equivalent (subscript b will be ignored). Also, it is of interest to convert the continuous time channel model into a discrete time channel model. The impulse response can be represented by a sampled version of the continuous time impulse response, where the distance between the taps is fixed by the Nyquist theorem. The channel model becomes system-specific, as its representation depends on system parameters such as bandwidth and carrier frequency. We can re-write (2.14):

$$y[m]=\sum_k h_k[m]x[m-k], \tag{2.19}$$

where $h_k[m]$ is the kth complex channel filter tap at time m. If we define $\mathrm{sinc}(t)\triangleq\sin(\pi t)/(\pi t)$, we can write [TsVi05]:

$$h_k[m]=\sum_i a_i^{\mathrm{b}}(m/W)\,\mathrm{sinc}[k-\tau_i(m/W)W]. \tag{2.20}$$

Each time-variant tap $h_k[m]$ mainly collects the contributions $a_i^{\mathrm{b}}(t)$ of those paths i whose delays $\tau_i(t)$ are close to k/W, and more specifically in the window $k/W\pm 1/(2W)$. The rest of the contributions can be neglected due to the decaying properties of the sinc function. If we assume that a large number of statistically independent multipath components contribute to each filter tap, it is reasonable to model $h_k[m]$ as a zero-mean circularly symmetric Gaussian random variable of power P_k [TsVi05]. This Rayleigh fading model with $P_h(k)=P_k$ is widely used.

2.2.3. Time and frequency selectivity

Doppler spread and time selectivity

Let us concentrate on the variations of the taps $h_k[m]$ as a function of time *m*. By analyzing (2.20), we notice that when the different paths contributing to the *k*th tap have significantly different Doppler shifts, the magnitude of the tap can vary significantly at a time scale inversely proportional to the Doppler spread $\Delta D_{\mathrm{s}} = \max_{i,j} \left| \nu_i - \nu_j \right|$. The larger the Doppler spread, the smaller the coherence time. The coherence time T_{coh} is perceived as the interval over which the tap $h_k[m]$ significantly changes as a function of the discrete time *m*. It is defined as

$$T_{\mathrm{coh}} \sim \frac{1}{\Delta D_{\mathrm{s}}}. \tag{2.20}$$

Delay spread and frequency selectivity

Let us now analyze the variations of the channel transfer function $H(f,t)$ with respect to the frequency *f*. By analyzing (2.15), we note that the combination of different paths with different delays lead to a frequency-varying channel: The spectrum of the received signal undergoes different attenuations for different frequency components. The severity of this variation is reflected by the coherence bandwidth $\mathrm{B}_{\mathrm{coh}}$ and is dictated by the phase difference between multiple path components. It is thus inversely proportional to the delay spread $\Delta T_{\mathrm{d}} = \max_{i,j} \left| \tau_i(t) - \tau_j(t) \right|$:

$$B_{\mathrm{coh}} \sim \frac{1}{\Delta T_{\mathrm{d}}}. \tag{2.21}$$

The larger the delay spread, the smaller the coherence bandwidth. The coherence bandwidth shows us how quickly the channel changes in frequency. It is a dual notion to the coherence time $\mathrm{T}_{\mathrm{coh}}$ presented in the previous subsection. Channels can be categorized as "flat" or "frequency-selective" fading. These categories are also system dependent, as the coherence bandwidth B_{coh} can be large or small with respect to the system bandwidth *W*. When $W << B_{\mathrm{coh}}$, the channel is referred to as flat fading: The transfer function $H(f,t)$ is nearly constant within the bandwidth *W* and a single channel tap is sufficient to represent the channel. When $W >> B_{\mathrm{coh}}$, the transfer function $H(f,t)$ significantly varies within the signal bandwidth *W* and the channel needs to be represented by multiple taps. This is called frequency-selective fading.

2.3. MIMO channel modeling

So far we have implicitly considered that the transmitter and the receiver are each one equipped with one single antenna: This corresponds to what is called a SISO (Single Input Single Output channel). MIMO (Multiple Input Multiple Output) systems use multiple transmit and receive antennas, which can bring much benefit to the system performance. Also, multiple antennas can for example be used only at the Tx/Rx side, which would lead to the self-explanatory terms MISO/SIMO.

2.3.1. Matrix representation of the MIMO channel

The simplest way of representing a MIMO channel for a system with N_{Tx} transmit antennas and N_{Rx} receive antennas is to see it as a set of $N_{\mathrm{Tx}}N_{\mathrm{Rx}}$ SISO channels (see Fig. 2.6, where $h_{m,n}(t)$ stands for the SISO channel relying the *n*th Tx antenna to the *m*th Rx antenna). Let us consider for simplicity the case of a narrowband deterministic MIMO channel. The extension to a statistical channel model is immediate. Let us define the N_{Tx} -sized transmit vector:

$$\mathbf{x}(t) = [x_0(t), x_1(t), \ldots, x_{N_{\mathrm{Tx}}-1}(t)]^T, \tag{2.22}$$

where $x_n(t)$ is the signal transmitted at the *n*th Tx antenna and $[.]^T$ denotes the transpose operation. Similarly,

$$\mathbf{y}(t) = [y_0(t), y_1(t), \ldots, y_{N_{\mathrm{Rx}}-1}(t)]^T \tag{2.23}$$

is the received N_{Rx} -sized vector. The vectors $\mathbf{x}(t)$ and $\mathbf{y}(t)$ are then related by:

$$\mathbf{y}(t) = \mathbf{H}(t)\mathbf{x}(t) + \mathbf{n}(t), \tag{2.24}$$

where $\mathbf{n}(t)$ is the N_{Rx} -sized AWGN vector and $\mathbf{H}(t) \in \mathbb{C}^{N_{\mathrm{Rx}} \times N_{\mathrm{Tx}}}$ is the complex MIMO narrowband channel matrix:

$$\mathbf{H}(t) = \begin{bmatrix} h_{0,0}(t) & h_{0,1}(t) & \cdots & h_{0,N_{\mathrm{Tx}}-1}(t) \\ h_{1,0}(t) & h_{1,1}(t) & \cdots & h_{1,N_{\mathrm{Tx}}-1}(t) \\ \vdots & \vdots & \ddots & \vdots \\ h_{N_{\mathrm{Rx}}-1,0}(t) & h_{N_{\mathrm{Tx}}-1,1}(t) & \cdots & h_{N_{\mathrm{Rx}}-1,N_{\mathrm{Tx}}-1}(t) \end{bmatrix}. \tag{2.25}$$

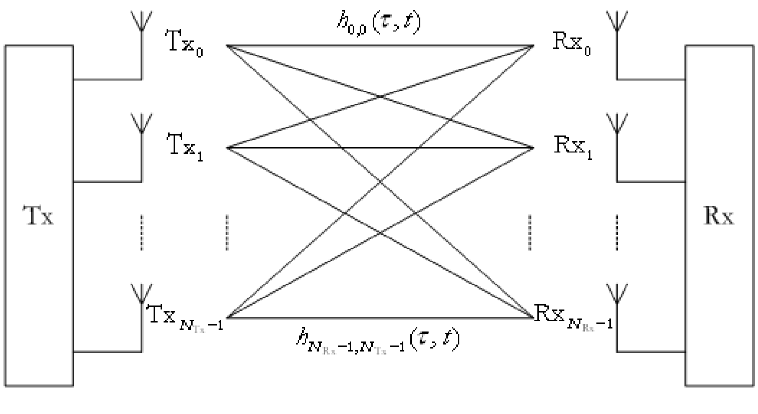

Fig. 2.6 MIMO channel.

$\mathbf{H}(t)$ is the matrix channel gain representation of a MIMO channel. All the relationships above can be mapped into the discrete time domain, similarly to subsection 2.2.2. For a wideband channel model, (2.25) becomes:

$$\mathbf{H}(\tau,t) = \left[h_{n_{\mathrm{Rx}},n_{\mathrm{Tx}}}(\tau,t) \right], \quad n_{\mathrm{Rx}} = 0 \ldots N_{\mathrm{Rx}} - 1,\ n_{\mathrm{Tx}} = 0 \ldots N_{\mathrm{Tx}} - 1 . \tag{2.26}$$

2.3.2. Angular spread and space selectivity

The most natural way of physically modeling a MIMO channel is in the angular domain. Different signal paths for example arrive with different DoA (direction of arrival) angles. Subpaths arriving with very close angles (dispersion smaller than the angular antenna resolution) aggregate to form one single path. In the same way we defined the power delay profile/delay spread and the Doppler spectrum/Doppler spread, one can define the power azimuth spectrum (PAS)/angle spread. Let us denote by $\Delta\theta$ the maximum angle separation given by the range within which the power azimuth spectrum is non-null. The smaller $\Delta\theta$, the stronger the spatial correlation between transmit antennas. We can define a coherence distance, inversely proportional to $\Delta\theta$, given by [Fle00]:

$$D_{\mathrm{coh}} \le \frac{\lambda_{\mathrm{c}}}{2\sin(\Delta\theta/2)} . \tag{2.27}$$

The coherence distance D_{coh} indicates the minimum antenna spacing required to have independent uncorrelated fading channels. We have thus a notion of spatial selectivity. Just as time or frequency selectivity, space selectivity is not a standalone property of the channel, but depends on the system parameters (antenna configuration, carrier wavelength λ_{c}).

2.3.3. Analytical modeling of the MIMO channel

To derive a statistical analytical model of the MIMO channel we can follow the same reasoning as in the statistical modeling of frequency-selective fading channels in subsection 2.2. The physical MIMO model is extremely complex and difficult to manipulate. From a signal-processing point of view, it is of more interest to model the gains of the taps of the discrete-time sampled channel rather than the physical paths in the angular domain. Directly modeling the taps also has the advantage that paths aggregation renders the statistical modeling more reliable.

A very common MIMO fading model assumes that all the taps of the discrete channel gain matrix $\mathbf{H}[m]$ are i.i.d. (independent identically distributed) circular symmetric Gaussian variables. This is called the i.i.d. Rayleigh model and it is the simplest MIMO analytical channel model. It has been shown in [TsVi05] that, in a richly scattering environment with sufficiently spaced antennas (more than a half of carrier wavelength), the i.i.d. Rayleigh assumption gives a reasonable model. This model needs to be refined in order to take into account the fact that, in practice, correlation between signals transmitted or received from multiple collocated antennas exists, and thus the tap gains are not completely independent. This correlation is not to be neglected in the design of a system, since it is the limiting factor for the capacity of MIMO channels. The channel capacity is defined as the quantity of information that can be transmitted without errors through that channel.

Let us denote by **G** an $N_{\mathrm{Rx}} \times N_{\mathrm{Tx}}$ matrix with i.i.d. complex Gaussian entries. For the i.i.d Rayleigh model, **H**=**G**. Also, we denote by $\mathrm{vec}(.)$ a function that stacks up the columns of a $M \times N$ matrix, transforming it into a $MN \times 1$ vector, and by $\mathrm{unvec}(.)$ the inverse of $\mathrm{vec}(.)$ function. The channel correlation matrix is usually defined in the literature as an $N_{\mathrm{Rx}}N_{\mathrm{Tx}} \times N_{\mathrm{Rx}}N_{\mathrm{Tx}}$ matrix given by:

$$\mathbf{R_H} \triangleq E\left\{\mathrm{vec}(\mathbf{H})\,\mathrm{vec}(\mathbf{H})^H\right\}. \tag{2.28}$$

$\mathbf{R_H}$ is symmetric because it is Hermitian matrix and it is also called "channel-oriented" because one dimension of the correlation matrix has the same number of elements as the channel matrix. The most general MIMO correlated channel model is given by:

$$\mathbf{H} = \mathrm{unvec}\left(\mathbf{R_H}^{1/2}\,\mathrm{vec}\left(\mathbf{G}\right)\right), \tag{2.29}$$

where all the $N_{\mathrm{Rx}}N_{\mathrm{Tx}}$ correlation terms between all the channel taps were considered.

This model can be simplified by making convenient assumptions on the properties of the correlation matrix $\mathbf{R_H}$. The most largely employed simplified models are the Kronecker and the Weichselberger models. Other models were also proposed in [GeBo02] and [Say02].

Kronecker MIMO channel model

The Kronecker model [ChKa98] is the most popular and commonly used analytical MIMO model. The spatial properties of the MIMO channel are simplified and separated to the link ends: This model assumes separable Tx and Rx correlation. The correlation matrix $\mathbf{R_H}$ defined in (2.30) appears as a Kronecker product between a N_{Tx}xN_{Tx}-sized transmit correlation matrix $\mathbf{R}_{\mathrm{Tx}}$ and a N_{Rx}xN_{Rx}-sized receive correlation matrix $\mathbf{R}_{\mathrm{Rx}}$, which are assumed independent:

$$\mathbf{R_H} = \frac{1}{P_{\mathbf{H}}}\mathbf{R}_{\mathrm{Tx}} \otimes \mathbf{R}_{\mathrm{Rx}}, \tag{2.31}$$

where $P_{\mathbf{H}}$ is the total channel power and $\otimes$ is the Kronecker product. Inserting the assumption (2.31) into the general model (2.29), we obtain the formulation of the Kronecker model:

$$\mathbf{H} = \frac{1}{\sqrt{P_{\mathbf{H}}}}\mathbf{R}_{\mathrm{Rx}}^{1/2}\mathbf{G}\left(\mathbf{R}_{\mathrm{Tx}}^{1/2}\right)^T. \tag{2.32}$$

In practice, a common way of estimating the correlation matrices at the transmitter and receiver sides is to consider:

$$\begin{cases} \mathbf{R}_{\mathrm{Tx}} = E\left\{\mathrm{H}^T\mathrm{H}^*\right\} \\ \mathbf{R}_{\mathrm{Rx}} = E\left\{\mathrm{H}\mathrm{H}^H\right\} \end{cases}. \tag{2.33}$$

The fact that the full MIMO correlation matrix is decomposed into one-sided Tx and Rx correlation matrices with no cross-dependence has severe consequences. All relationship between the directions of arrival (DoA) and directions of departure (DoD) is suppressed, and fundamentally different MIMO channels might be reduced to the same model. Since the multipath structure of the channel is not rendered correctly, the mutual information of the channel is typically underestimated [BoÖz03]. [ÖzHe03] points out the main deficiencies of this model.

The Kronecker model is very popular due to its simplicity. It facilitates the analytical treatment as well as the separate optimization of the Tx and Rx signal processing algorithms or antenna hardware. Measurements show good agreement to the model for scenarios with low number of antenna elements [KeSc02]. When the number of antenna elements increases, model errors become important.

Weichselberger MIMO channel model

In the Weichselberger model [Wei03], [WeÖz03], [WeÖz03] the spatial correlation properties of the channel are not divided into separate contributions from transmitter and receiver. Instead, the joint correlation properties are modeled by describing the average coupling between the eigenmodes of the two link ends. The Weichselberger model is able to reproduce the multipath structure and the mutual information significantly better than the Kronecker model, which can be viewed as a particular simplified case of the Weichselberger model.

Let us denote by $\mathbf{U}_{\mathrm{Tx}}$ and $\mathbf{U}_{\mathrm{Rx}}$ the eigenvector matrices corresponding to the eigenvalue decomposition of $\mathbf{R}_{\mathrm{Tx}}$ and $\mathbf{R}_{\mathrm{Rx}}$ respectively. The fact that the transmitter and the receiver have joint correlation properties is represented by a $N_{\mathrm{Rx}}\mathrm{x}N_{\mathrm{Tx}}$-sized coupling matrix $\mathbf{\Omega}$ whose coefficients $\mathbf{\Omega}_{m,n}$ specify how much power is averagely coupled from the nth Tx eigenmode to the mth Rx eigenmode. The channel model is given by:

$$\mathbf{H} = \mathbf{U}_{\mathrm{Rx}}\left(\tilde{\mathbf{\Omega}} \odot \mathbf{G}\right)\mathbf{U}_{\mathrm{Tx}}, \tag{2.34}$$

where $\odot$ denotes the Schur-Hadamard (element-wise) product and $\tilde{\mathbf{\Omega}}$ is the element-wise square root of $\mathbf{\Omega}$. In practice, we can easily compute measurement-based estimates for $\mathbf{R}_{\mathrm{Tx}}$ and $\mathbf{R}_{\mathrm{Rx}}$ as in (2.33). A good estimate for $\mathbf{\Omega}$ is given by:

$$\mathbf{\Omega} = E\left\{\left(\mathbf{U}_{\mathrm{Rx}}^H\mathbf{H}\mathbf{U}_{\mathrm{Tx}}^*\right)\odot\left(\mathrm{U}_{\mathrm{Rx}}^T\mathbf{H}^*\mathbf{U}_{\mathrm{Tx}}\right)\right\}. \tag{2.35}$$

For systems with large number of Tx/Rx antennas (typically more than 4), the Weichselberger model gives more accurate results than the Kronecker model [HeGr04].

2.4. Normalized channel models; Practical simulation scenarios

Simulating, designing and analyzing of wireless systems need to rely on channel models. The mathematical descriptions of such models can rely on different approaches. Basically, tree main types of channel models can be found in the literature.

Deterministic channel models rely on Maxwell's propagation equations and take into account all the geographical and morphological properties of the propagation environment. As modeling methods, we note the ray tracing and the ray launching approaches. Deterministic models are highly accurate, but pay the price of a very high complexity and need exhaustive knowledge of the scattering environment.

Empirical models are based on real channel measurements. They usually need extensive measurement campaigns and their accuracy level depends on the level of detail of the measurements. Examples are the models Okumura-Hata or Walfish-Ikegami (COST 231).

Statistical channel models make use of random variables, whose statistical properties are determined by making a set of assumptions on the radio propagation.

In practice, hybrid combinations of the here-above models can be found, yielding for a trade-off between accuracy and computational complexity. Let us briefly describe the channel models which will be used in simulations throughout this thesis.

2.4.1. 3GPP / 3GPP2 channel models

The Spatial Channel Model (SCM) proposed by the 3rd Generation Partnership Project (3GPP) is one of the most elaborated channel models. It specifies parameters and methods associated with the spatial channel modeling that are common to the needs of the 3GPP and 3GPP2 organizations. The scope includes development of specifications for both system- and link-level evaluations, with an emphasis on system-level. A full description of this channel is given in [TR25996]. It is a MIMO ray-based correlated model, taking into account 6 paths, each path consisting in a superposition of 20 subpaths scattered by a cluster of scatterers. Any antenna configuration is possible.

The system-level approach explicitly models the sub-paths, whose amplitudes, phases and angles are random variables drawn from probability density functions which are statistically correlated, specified for different propagation conditions. Due to random realizations in spatial and temporal domains, large amount of simulations are needed to get accurate statistics, which renders the generation procedure rather tedious. A link-level approach is also given for calibration purposes, with parameters described in Appendix A, Table A.1. An example of PDP for the Vehicular A channel is depicted in Fig. 2.7 – (a). The link-level model assumes a set of spatial parameters that correspond to static channel conditions. Antenna patterns are targeted for diversity-oriented implementations (large antenna spacing). Also, [TS45005] indicates some normative channel propagation models as the typical urban (TU) profile described in Table A.2.

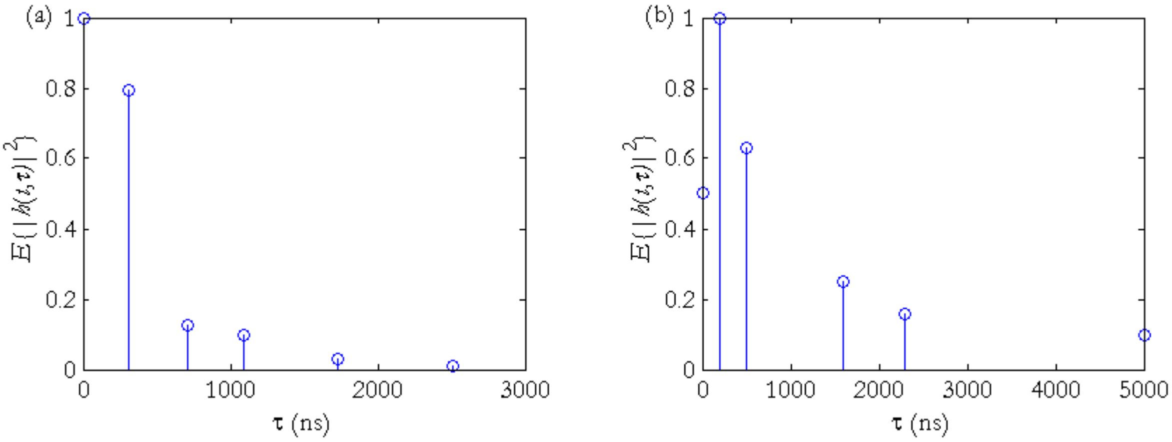

Fig. 2.7 Power delay profile: (a)- SCM Vehicular A channel; (b)- 3GPP TU channel.

2.4.2. Practical simulation scenario

Let us present an approach used for building a practical channel model for simulation purposes. As previously discussed, some ready-to-use channel models conceived for system level simulations (*e.g.*, 3GPP SCM) are rather tedious to use for link-level simulations because of their high complexity; Others (*e.g.*, BRAN E) were originally conceived for simple SISO systems and there is no standardized extension to a MIMO scenario.

We present a simulation approach used for generating the time-variant channel impulse response $h(\tau,t)$ with a given PDP and Jakes Doppler spectrum. We then extend the model to a MIMO channel $\mathbf{H}(t)$ with spatial correlation. In order to generate a simple link-level simulation model corresponding to a desired channel profile, we will proceed as in the following:

- Step 1: Choose the desired channel profile (TU, Vehicular A, etc.). The channel profile is specified by a set of L delays $\left\{\tau_k, k=0 \ldots N_{\text{paths}}-1\right\}$ of the N_{paths} channel paths and the corresponding PDP $P_k = 2\sigma_k^2$.
- Step 2: Generate a Rayleigh uncorrelated channel model in the (Doppler) frequency domain. For each path k of a SISO channel we generate a random zero-mean Gaussian complex vector of complex variance $2\sigma_k^2$ (real variance σ_k^2 onto each real branch), corresponding to the delay Doppler function $S\left(\tau_k,\nu\right)$ depicted in Fig. 2.4. This is coherent with the assumptions in 2.2.1: If $h(\tau_k,t)$ is a Gaussian random variable, then its Fourier transform with respect to time t, $S\left(\tau_k,\nu\right)$, is also Gaussian.
- Step 3: Model the MS velocity by shaping the Doppler spectrum. So far, $S\left(\tau_{k_i},\nu\right)$ has a white power spectrum. We perform filtering in the frequency domain ν by the square root of the Jakes Doppler spectrum $\sqrt{\mathbf{S}_{\text{D}}(\nu)}$, where $\mathbf{S}_{\text{D}}(\nu)$ is given in (2.9). The filtered $S\left(\tau_k,\nu\right)$ now contains the time-domain correlation due to the Doppler effect; Performing an inverse Fourier transform with respect to the variable ν results in the model of the kth channel path $h(\tau_k,t)$. The impulse response function of the SISO

channel with temporal correlation is given by the accumulation of the N_{paths} channel paths, $h(\tau,t)=\sum_{k=0}^{L-1} h(\tau_k,t)\delta(\tau-\tau_k)$. Here, we assumed that all the independent channel paths have the same Doppler-delay profile. The time-variant transfer function $H(f,t)$ of this SISO channel can be computed by taking the Fourier transform of the impulse function $h(\tau,t)$ with respect to the delay variable τ.

- Step 4: Model the correlation profile. A MIMO channel will be modeled as a $N_{\text{Rx}} \times N_{\text{Tx}}$ accumulation of SISO channels, supposed to have all the same PDP. Let us denote this accumulation by $\mathbf{G}(t)$. At each time t, the different elements of $\mathbf{G}(t)$ are independent. We can now apply a spatial correlation model, for example the Kronecker model (2.32) and obtain the time-variant channel matrix $\mathbf{H}(t)$ with spatial and temporal correlation.

The filtered white noise method proposed in steps 1-2 presents some implementation questions: Which high-order filters to approximate the irrational square-root function (2.9)? Which rate to use to sample the Gaussian waveform? Sometimes it is replaced by the "sum of sines" method [Jak94]. This method assumes that scatterers are uniformly distributed on a circle with a large number of rays emerging from each scatterer. Each Rayleigh fading variable $h(\tau_k,t)$ appears as a large sum of sinusoids with random phases. A simplified "sum of sines" method is given in [Den93].

2.5. Time, frequency and space diversity; Degrees of freedom

A diversity scheme refers to a method for improving the reliability of a message signal by utilizing two or more communication channels with different characteristics. If transmission is performed over one single signal path, there is a significant probability that this path be in a deep fade. To improve performance, one natural solution is to send the information symbols through different independent signal paths, so that the communication is possible as long as there is at least one strong available signal path. Multiple versions of the same signal may be transmitted and/or received and combined in the transmitter and/or receiver, resulting in an important performance improvement. Diversity plays an important role in combating fading and avoiding error bursts. To improve system performance, forward error correcting codes (FEC) are generally employed in all practical transmission systems. Redundancy is added to the transmitted information using a predetermined algorithm, designed to detect and correct the errors occurred during transmission. Coded systems provide a coding gain: less signal to noise ratio (SNR) is needed in order to achieve the same bit error rate (BER) performance as an uncoded system. Coding also plays an important role in recuperating the available diversity. Data coded together (and forming a codeword) is sent through multiple signal paths, which allows recovering in the decoding process the data loss caused by deep fades.

Diversity can be obtained by exploiting in a convenient way the channel selectivity. It is not an intrinsic property of the channel, but it is a measure of how well a coding scheme can take advantage of the channel properties. Diversity is effective when the different channel diversity branches are uncorrelated and carry independently faded copies of the signal. Any correlation between these transmission channels leads to a decrease in diversity. Let us admit that the SNR is measured at the receiver, and assume coherent detection with perfect channel knowledge at the receiver. If the channel has L branches of diversity, at high SNR the BER decays like:

$$\mathrm{BER} \approx c \cdot \mathrm{SNR}^{-L} . \tag{2.36}$$

Here, L is the diversity of the system, and c represents the coding gain. Let us separately analyze these effects.

Time diversity is achieved by averaging the fading of the channel over time. In order to have L independent channel realizations in the time domain, the signal must span at least L coherence periods T_{coh}. This can be achieved in several ways, for example by repetition coding: Repeating the same codeword over different coherence periods recovers all the available time diversity in the channel, but is highly bandwidth inefficient. More efficient solutions are, *e.g.*, automatic repeat request (ARQ) or a combination of coding and interleaving. When there are strict delay constraints or when T_{coh} is very large, exploiting the time diversity may be not possible.

Frequency diversity is achieved in frequency-selective channels by sending signals onto frequencies spaced apart by more than the coherence bandwidth B_{coh}. Let us for example assume that one single symbol is sent through a channel modeled as in (2.19) and having L taps. The receiver observes L delayed independent copies of the signal, because the L channel taps are assumed to be independent. The channel provides thus L diversity branches. There are many ways for a system to achieve frequency diversity. Spread spectrum systems like IS-95 CDMA (Code Division Multiple Access) spread information symbols over a large bandwidth by multiplication with a pseudo-noise sequence. Multi-carrier systems using coded OFDM send a same codeword jointly encoded information symbols over a group of subcarriers. Frequency hopping techniques send different parts of the same codeword onto groups of carrier frequencies that change from one OFDM symbol to another.

Space diversity is obtained in multi-antenna systems by exploiting the space selectivity of the channel. If the antennas are placed sufficiently apart (spaced by at least D_{coh}), independent signal paths are created. For a mobile (close to the ground, with many scatterers around), the coherence distance is in the order of half to one carrier wavelength. For base stations, typically mounted on high towers with no closed scatterers, antennas decorrelate over several tenths of wavelengths. Space diversity can be retrieved for example at the receiver by combining the multiple copies of the transmitted signal (receive diversity, SIMO transmission, each added antenna also provides a power gain). Transmit diversity techniques spread the transmitted codewords onto multiple transmit antennas (MISO or MIMO channels). The amount of available space diversity of a MIMO channel equals the number of independent faded paths between the transmitter and the receiver.

More complex coding schemes cannot achieve more diversity gain than the one available in the channel; on the other hand, they can make more judicious use of the channel properties and increase the coding gain. Let us define the number of degrees of freedom available in the channel as the dimension of the received signal vector space [TsVi05]. It dictates the number of different transmitted independent signals that can be reliably distinguished at the receiver. Different schemes use more or less of the available degrees of freedom, resulting in different coding gains. Code design criteria can be derived to make maximum use of the available degrees of freedom. For time diversity, it has been proven that the optimal strategy is to maximize the minimum product distance between the codewords. For space-time codes, the determinant criterion stands. For example, in a 2x1 uncorrelated MISO channel, one single degree of freedom is available for a 2-fold diversity order: the received signal space has only one single-dimensional element A repetition coding scheme sending the same symbol successively from the two antennas recovers all the spatial diversity, but uses only one half degree of freedom (one symbol sent over two periods of time).

In MIMO channels, the available degrees of freedom allow us to multiplex several independent streams and thus increase the system throughput. An i.i.d. Rayleigh channel with N_{Tx} transmit antennas and N_{Rx} receive antennas provides $\min(N_{\mathrm{Tx}}, N_{\mathrm{Rx}})$ degrees of freedom and $N_{\mathrm{Tx}}N_{\mathrm{Rx}}$ space diversity branches. In a fast fading scenario, averaging over the channel variations over time allows us to reliably use the degrees of freedom of the channel and communicate to a rate close to the channel capacity. In slow fading scenarios, no such averaging is possible and the key performance measure is the diversity gain. To achieve the maximum diversity gain, one needs to sacrifice its spatial multiplexing capabilities and communicate at a fixed rate vanishingly small with respect to the fast fading channel capacity. This gives a fundamental trade-off between the multiplexing capabilities of the channel and the achievable diversity gain [TsVi05].

The diversity and multiplexing aspects in wireless communications will be re-discussed in all the chapters of this thesis.

2.6. Summary and conclusions

This chapter presents the conventional model of the radio channel. All models are based on the physical properties of the channel, explained by propagation mechanisms. In wireless channels, transmitted waves suffer reflection, diffraction and scattering, which lead to the multipath phenomenon: Information propagates from the transmitter to the receiver through multiple paths. The channel variations have two main components: at large scale, shadowing produces slow variations of stochastic nature around a deterministic mean given by the path loss. At small scale, fast variations due to the constructive and/or destructive recombination of multipath components leads to small-scale fading. Conveniently exploiting the time and frequency selectivity in wireless channels leads to a diversity gain, which may be employed to improve the performance of wireless communications systems. In MIMO channels, a supplementary dimension is available, which can be exploited to increase system capacity. In the sequel, the presented channel model(S) will be employed to design and evaluate new MIMO uplink transmission strategies that make use of transmit diversity and spatial multiplexing capabilities.

Chapter 3

Multiple access schemes for the uplink of future wireless systems

One of the main challenges of designing an air interface for the next generation mobile systems relies in identifying and understanding the requirements of such a system. Future generations of wireless communications will need to cope with the ever increasing demands in quality and performance. Multimedia services with peak data rates of the order of tens-to-hundreds of Mbps in a high mobility environment need to be foreseen, and spectrum efficiency will become a stringent requirement since the spectrum is a limited resource. In the uplink, specific requirements need to be taken into account. For example, users will need good coverage while benefiting of low-cost terminals with long battery life. These constraints are sometimes contradictory, and a trade-off must be found. An exhaustive survey of candidate air interface technologies imposes itself.

3.1. Uplink-specific terminal constraints

The tasks enumerated here are even more challenging on the uplink due to the limited power of high power amplifier (HPA) of the user terminal. The power amplifier should be as power efficient as possible to limit cost and increase battery life. To ensure good performance, the signal must lie into the linear zone of the power amplifier and thus avoid distortion. If the signal's dynamic range is high, it requires an HPA with a good linearity, or equivalently a costly HPA.

3.1.1. HPA parameters and models

HPA baseband models

Let us first describe the baseband HPA models present in the literature. In the following, $v_{\mathrm{IN(OUT)}}(t)$ will represent the time-variant baseband complex signals present at the input (output) of the HPA, with saturation level $v_{\mathrm{IN(OUT),Sat}}$. The variable t will be omitted whenever possible. An

HPA model is usually given by a double dependence: On one hand the AM/AM characteristic, giving the output amplitude $|v_{\mathrm{OUT}}|$ as a function of the input amplitude $|v_{\mathrm{IN}}|$, and on the other hand the AM/PM characteristic giving the output phase distortion $\Delta\phi = \arg(v_{\mathrm{OUT}}) - \arg(v_{\mathrm{IN}})$ in function of the input phase $\arg(v_{\mathrm{IN}})$ and amplitude $|v_{\mathrm{IN}}|$.

The simplest HPA model is the ideal clipper: all peaks above a certain saturation level are clipped, and all the others remain unchanged (Fig. 3.1, black solid line curve). Since no phase change is performed, the AM/PM characteristic is null and the input-output relationship can be globally expressed as:

$$\frac{v_{\mathrm{OUT}}}{v_{\mathrm{OUT,Sat}}} = \begin{cases} \dfrac{v_{\mathrm{IN}}}{v_{\mathrm{IN,Sat}}}, & |v_{\mathrm{IN}}| \le v_{\mathrm{IN,Sat}} \\ 1, & \text{otherwise} \end{cases}. \tag{3.1}$$

HPA's linear gain is given by $G_1 = v_{\mathrm{OUT,Sat}} / v_{\mathrm{IN,Sat}}$. Still, the assumption of a perfectly linear amplifier characteristic is highly unrealistic. Another simple model is the solid state Rapp model [Rapp91]. It assumes null AM/PM. The AM/AM characteristic depends on a knee factor p_{Rapp}:

$$v_{\mathrm{OUT}} = \frac{v_{\mathrm{IN}}}{\left(1 + \left(|v_{\mathrm{IN}}| / v_{\mathrm{OUT,Sat}}\right)^{2 p_{\mathrm{Rapp}}}\right)^{\frac{1}{2 p_{\mathrm{Rapp}}}}}. \tag{3.2}$$

The factor p_{Rapp} controls the transition for the amplitude gain as the input amplitude approaches saturation, dictating the smoothness of the curve. Small p_{Rapp} factors correspond to smooth AM/AM characteristics with a pronounced nonlinear zone. High p_{Rapp} factors correspond to rather linear HPAs. When p_{Rapp} tends to infinity, the Rapp model approaches the clipper ideal model (Fig. 3.1). The Rapp solid state amplifier baseband model with $p_{\mathrm{Rapp}} = 2$ is considered to be a good approximation [Kai01] for typical HPAs in the sub-10 GHz range. In the following we will consider implicitly a knee factor of 2 for the Rapp model, unless stated otherwise.

Other more complex models exist. In some applications (*e.g.*, when studying the effect of nonlinearities on phase modulations), it is important to take into account the phase distortions caused by the HPA. We shall cite here the popular Saleh model [Sal81], whose AM/AM - AM/PM characteristics and input-output relationships are given below and plotted in Fig. 3.2:

$$|v_{\mathrm{OUT}}| = \frac{\alpha |v_{\mathrm{IN}}|}{1 + \beta |v_{\mathrm{IN}}|^2}, \ \Delta\phi = \frac{\pi}{3} \frac{\alpha_p |v_{\mathrm{IN}}|^2}{1 + \beta_p |v_{\mathrm{IN}}|^2}. \tag{3.3}$$

$$v_{\mathrm{OUT}} = |v_{\mathrm{OUT}}| \exp\left(j\left(\phi_{\mathrm{IN}} + \Delta\phi\right)\right) = \frac{\alpha v_{\mathrm{IN}}}{1 + \beta |v_{\mathrm{IN}}|^2} \exp\left(j \frac{\pi}{3} \frac{\alpha_p |v_{\mathrm{IN}}|^2}{1 + \beta_p |v_{\mathrm{IN}}|^2}\right). \tag{3.4}$$

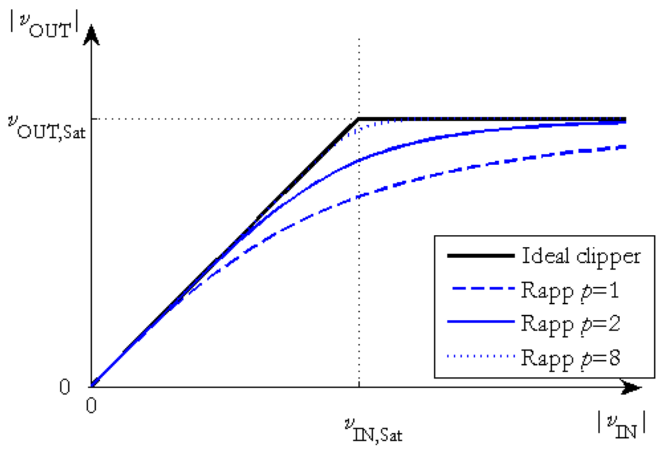

Fig. 3.1 AM/AM characteristics for ideal clipper and Rapp model with different knee factors.

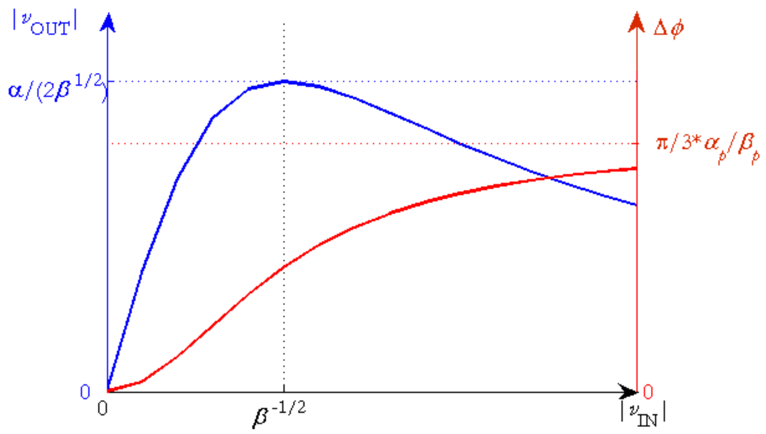

Fig. 3.2 AM/AM and AM/PM characteristics for Saleh model.

Input and output back-off

To make good use of the available power, it is necessary to operate the HPA near saturation. For the same operating point, the effect of the HPA on the input signal and the amount of caused distortion depends on the dynamic range of the signal. Let us consider two signals with different dynamic ranges present at the input of a HPA like in Fig. 3.3, where for simplicity reasons we considered an ideal HPA. The blue signal in Fig. 3.3 has a low dynamic range and can use the HPA in an efficient manner, in a working point I_1 close to the saturation level. The red signal has higher dynamic range. If it uses the same working point as the blue signal (red dotted line scenario), some of the signal peaks go into saturation and get clipped. To avoid this signal distortion, the signal needs to be "backed-off" to the working point I_2 (red solid line).

Let us denote by:

$$P_{\mathrm{IN(OUT),Avg}} = \lim_{T\to\infty} \frac{1}{T} \int_0^T \left| v_{\mathrm{IN(OUT)}}(t) \right|^2 dt \tag{3.5}$$

the mean power of a signal $v(t)$ at the HPA's input (output). $P_{\mathrm{IN(OUT),Sat}} = \left| v_{\mathrm{IN(OUT),Sat}} \right|^2$ represents the input (output) saturation power. We define the input back-off (IBO) and output back-off (OBO) with respect to the saturation values as respectively:

$$\mathrm{IBO}\big|_{dB} = -10\log_{10} \frac{P_{\mathrm{IN,Avg}}}{P_{\mathrm{IN,Sat}}}, \tag{3.6}$$

$$\mathrm{OBO}\big|_{dB} = -10\log_{10} \frac{P_{\mathrm{OUT,Avg}}}{P_{\mathrm{OUT,Sat}}}. \tag{3.7}$$

In order to obtain a satisfactory degree of linearity, the input signal power needs therefore to be backed-off to the linear region. This power reduction represents a loss of HPA power efficiency. In practice we usually focus on the output levels and we consider the amount of necessary OBO as a system loss with respect to an ideal linear system. Obviously, the amount of necessary OBO depends on the dynamic range of the signal and of the system constraints, as it will be discussed in the sequel.

While the signal lies in the linear region of the HPA, OBO and IBO have a linear dependence. In the nonlinear region, the relationship between OBO and IBO is nonlinear and depends on the HPA characteristics and on signal's dynamic range. An example for the Rapp HPA with p=2 is given in Fig. 3.4. Signals with higher dynamic ranges are more distorted when

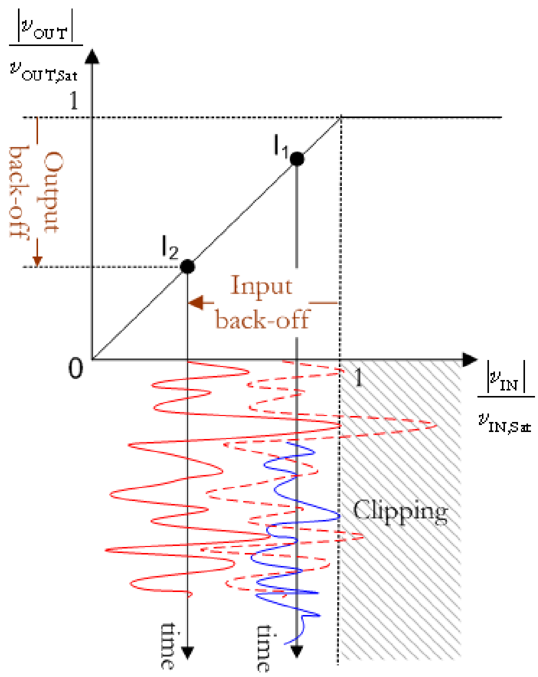

Fig. 3.3 Backing-off signals with different dynamic ranges.

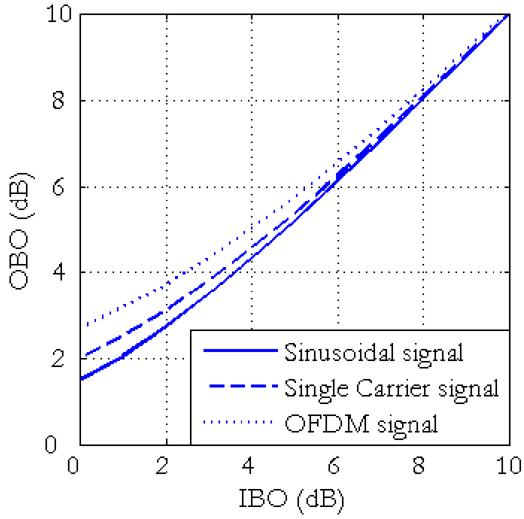

Fig. 3.4 OBO-IBO dependence for a Rapp HPA with $p_{Rapp}=2$ and different types of input signals.

passing through the HPA and thus the impairment between OBO and IBO is higher. The results in Fig. 3.4 are explained by the fact that multicarrier signals (here, OFDM with 512 subcarriers) have high envelope fluctuations while single-carrier signals have low envelope variations and sinusoidal signals have no envelope fluctuations (the peak power equals the mean power). Further discussion of the envelope fluctuations of several types of signals will be presented in subsection 3.6.1.

3.1.2. Effects of HPA nonlinearities

As discussed in the previous section, if no sufficient back-off is performed the signals suffer distortion. Working with high back-offs is highly power-inefficient. In practical systems some amount of distortion and/or clipping needs to be tolerated. At system level, HPA nonlinearity has two main consequences: It causes performance degradation and spectral regrowth. While performance degradation translates into an SNR loss at a given BER or frame error rate (FER), spectrum regrowth causes out-of-band radiation. Let us separately analyze these effects.

In-band distortion

When passing through the HPA, the signal samples lying in the nonlinear region will suffer amplitude and/or phase distortion that will affect the in-band structure of the transmitted signal. Let us consider for example an OFDM signal with 16 QAM (Quadrature Amplitude Modulation) signal mapping and using 512 subcarriers. Fig. 3.5 presents the corresponding constellation before (red dots) and after (blue dots) passing through the HPA. The constellation was assumed normalized to unitary mean power. We notice that the presence of the HPA distorts the transmitted signal. This means that the system will suffer some performance degradation even in the absence of noise and channel distortions. When using the Rapp model with knee factor 2, only amplitude distortion is present (Fig. 3.5 – (a)) and this can be interpreted as a noise enhancement. With the Saleh model (α=1, β=1/4 and α_p=β_p=1), phase distortion is also present. We backed-off the signal at an IBO=6 dB, corresponding to OBO=6.5 dB and 2.9 dB for the Rapp and Saleh models, respectively.

The impact of the nonlinear distortion translates into supplementary decoding errors: a higher SNR is needed to attain the same BER/FER target compared to the case where no HPA would be present. Together with the OBO loss, this SNR loss is a second factor in evaluating the total system degradation. This will be more thoroughly analyzed in 3.1.4. The quality of the transmitted modulation is obviously affected. The modulation quality is quantified in practice under the form of the Error Vector Magnitude (EVM). The EVM is a measure of the difference between the reference waveform and the measured waveform, defined as the square root of the ratio of the mean error vector power to the mean reference power expressed as a percentage. In the example of Fig. 3.5, the Rapp amplifier introduces an EVM on the absolute amplitude of 8.9% while the Saleh HPA lowers the quality of the transmitted modulation by 47.6%. At spectral level, passing through an HPA has as effect a spectral regrowth phenomenon depicted in Fig. 3.6. We took as example an OFDM signal with 512 subcarriers in the band of 5 MHz present at the input of a Rapp HPA and plotted the power spectrum when an IBO of 3 dB, 6 dB and 10 dB (corresponding OBO of 4.3 dB, 6.5 dB and respectively 10.1 dB, which is coherent with the results in Fig. 3.4). Strong back-offs avoid important distortion.

Out-of-band radiation

In all communications systems strict limits are imposed on the allowed emission bands and out-of-band radiation. The out-of-band emissions are unwanted emissions immediately outside the assigned channel bandwidth resulting from the modulation process and nonlinearity in the transmitter. This out-of-band emission limit is specified in terms of a spectrum emission mask and an Adjacent Channel Leakage power Ratio (ACLR).

Power of any MS emission shall not exceed the levels specified by the spectrum emission masks. For example, the 3GPP defined the minimum requirements for the Evolved Universal Terrestrial Radio Access (E-UTRA) [TS36101] as in Appendix B, Table B.1. For the 5 MHz bandwidth, this spectrum mask is plotted in Fig. 3.6. If no sufficient OBO is performed (e.g., OBO=4.3 dB in Fig. 3.6), the spectral mask constraints are not respected.

The ACLR describes the maximum acceptable levels of radiation that a user is allowed to transmit in the neighboring bands. It is defined as the ratio of the filtered mean power centered on the assigned channel frequency (yellow band in Fig. 3.6) to the filtered mean power centered on an adjacent channel frequency (blue band in Fig. 3.6). The measurement scenarios are usually given by standard regulations. For example, 3GPP LTE (Long Term Evolution) assumes that the E-UTRA channels are measured with rectangular filters (with bandwidths conform to Table B.2) and imposes a minimum ACLR value of 30 dB [TS36101]. The three distorted signals in Fig. 3.6 present ACLRs of 26 dB, 31.3 dB and respectively 36.8 dB. The accepted ACLR level also imposes a constraint on the necessary level of OBO. In a practical scenario, a system analysis is necessary in order to determine whether it is the ACLR, the spectrum mask, the EVM or the SNR degradation that is the first limiting factor in determining the HPA working point.

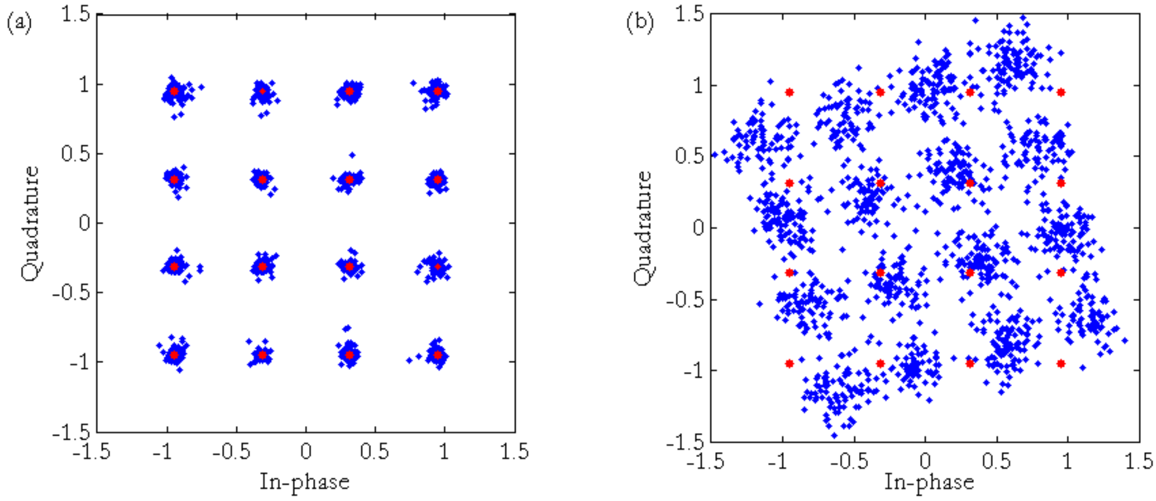

Fig. 3.5 Effect of HPA nonlinearities onto an OFDM signal with 16 QAM mapping: (a) – Rapp HPA with $p_{\mathrm{Rapp}}=2$; (b) – Saleh HPA with $\alpha=1$, $\beta=1/4$ and $\alpha_p=\beta_p=1$

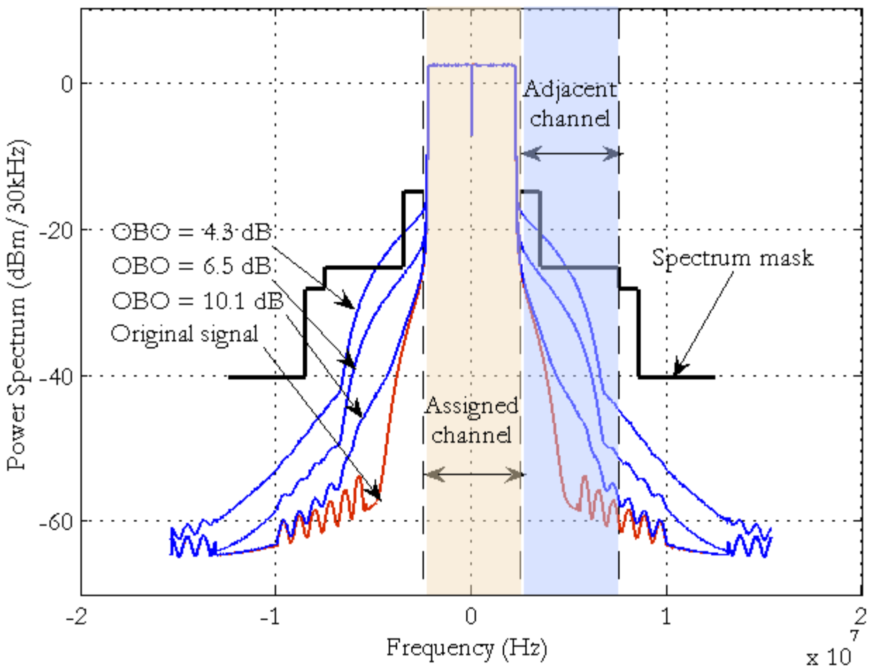

Fig. 3.6 Out-of-band radiation of an OFDM signal at different OBO levels.

3.1.3. Measures of the signal dynamic range

We have seen in the previous subsections that signals with different dynamic ranges are affected differently when passing through an HPA. Let us now analyze more precisely how we can measure the dynamic range of a signal.

Peak to Average Power Ratio

One of the most popular ways of giving a measure of a signal's dynamic range is the Peak to Average Power Ratio (PAPR). It is used to quantify the envelope excursions of a signal $v(t)$ over a time interval $\mathcal{T}$:

$$\mathrm{PAPR}\left(v(t)\big|_{t\in\mathcal{T}}\right) = \left.\frac{\max\limits_{t\in\mathcal{T}} |v(t)|^2}{E\left\{|v(t)|^2\Big|_{t\in\mathcal{T}}\right\}}\right|_{\mathrm{dB}} . \tag{3.8}$$

The PAPR thus represents the ratio of the maximum instantaneous peak power to the average power of the signal over the observation period $\mathcal{T}$ and is usually expressed in dB. Throughout this thesis, the PAPR will be understood as referring to the baseband signal.

In practice, since the cost and power dissipation of the analog components are of great importance in the design of a system, we are interested in the dynamic range of signals after digital to analog (D/A) conversion, at the input of the HPA. It is thus the continuous-time PAPR that we need to evaluate. Nevertheless, it is more practical to analyze the digital samples before D/A conversion, since it is at this level that we can intervene on the signal's properties. Equation (3.8) can be re-written in discrete-time by replacing the continuous-time signal $v(t)$ by its samples $v[n]$. Special precautions need to be taken when evaluating a signal's dynamic range in discrete time. Let us take the example of a single-carrier signal composed of QPSK (Quadrature Phase Shift Keying) symbols. If we evaluate the PAPR by taking into account the signal at its nominal sampling rate ($v[n]$ represents one QPSK symbol), we conclude that the PAPR would be 1: All signal samples have the same amplitude. But this would be a false conclusion, since the QPSK continuous-time waveform is not a constant-amplitude signal. A more careful analysis shows that oversampled signals may have a more important PAPR than critically sampled signals, since all the "missing" samples are estimated as a large linear combination of the available samples. When the oversampling factor increases, there are more and more samples that are susceptible of increasing the PAPR, but these extra samples become more and more correlated to their neighbors. At a certain point, further increase of the oversampling factor does not significantly modify the PAPR. It has been shown [Tel99] that an oversampling factor $L_{\mathrm{ovs}} = 4$ is sufficient to get a good estimate of the continuous-time PAPR. In the following we will consider that the PAPR corresponds to a sufficiently oversampled digital signal and that it is performed over blocks of N_{s} signal samples $\mathbf{v} = \left[v[0], v[1], ... v[N_{\mathrm{s}}-1]\right]$:

$$\mathrm{PAPR}(\mathbf{v}) = \left. \frac{\max\limits_{0 \le n < N_s} |v[n]|^2}{\frac{1}{N_s} \sum\limits_{n=0}^{N_s-1} |v[n]|^2} \right|_{\mathrm{dB}}. \tag{3.9}$$

Estimating the PAPR of a signal over a very large time interval T (theoretically $T \to \infty$) correctly indicates the envelope excursion of the signal, but is of little practical interest: This PAPR bound indicates the value of the highest peak of the signal, but give no further indication on the signal statistics. Usually the signal is analyzed on a block-by block basis, where the considered blocks are long enough in order to provide a good statistics for computing the average signal power. With this assumption, the PAPR per block can be seen as a random variable and we can focus on its distribution function in order to get some information on the signal dynamic range. It is usual to express the signal's variations under the form of Complementary Cumulative Distribution Function (CCDF) of PAPR, defined as:

$$\mathrm{CCDF(PAPR)} = \Pr\left\{\mathrm{PAPR} > \gamma^2\right\}. \tag{3.10}$$

Parameter γ^2 is a threshold, expressed in dB, and the CCDF value indicates the probability that the PAPR surpasses this threshold. Should we consider a signal (normalized to unitary mean power, for simplicity) passing through an ideal clipper HPA, γ^2 has a direct physical interpretation: It can be assimilated to the input back-off. Indeed, for a signal working at γ^2 dB of IBO to go into saturation and suffer clipping, it would be necessary that its PAPR be higher than γ^2. The probability in (3.10) is also called clipping probability.

Instantaneous Normalized Power

While the CCDF of PAPR is a very popular notion, it has one important drawback. A certain clipping probability ensures that at least one peak per block has an important amplitude and is susceptible to suffer clipping or severe distortion, but gives no information on how many samples in that block are distorted. Yet, in practical scenarios it is of great interest to know how many samples have a certain level and are thus susceptible to be distorted, as all of these samples cause degradation [CiBu05]. Indeed, severely clipping one single peak in a large block has a negligible effect on the EVM or spectrum shape, while distortion (even mild) of a large number of samples might have unacceptable consequences. From this point of view, it is important to consider a more refined analysis taking into account all the signal samples. This can be done by means of considering the distribution of the Instantaneous Normalized Power (INP):

$$\mathrm{CCDF(INP)} = \Pr\left\{ \overbrace{\frac{|v[n]|^2}{\frac{1}{N_s} \sum\limits_{k=0}^{N_s-1} |v[k]|^2}}^{\mathrm{INP}(\mathbf{v})} > \gamma^2 \right\}. \tag{3.11}$$

The CCDF of INP indicates the probability that the INP at a sample level exceeds a certain threshold γ^2. If we look at the range of important values of γ^2 for the CCDF of PAPR, the probability that one sample in a block exceeds such a level is very weak, and should a sample exceed this level it is highly likely to be the only one in that block: The CCDF of INP and the CCDF of PAPR tend asymptotically to the same value, which is the PAPR defined as in (3.8) for $\mathcal{T} \to \infty$. But in the range of lower values of γ^2 the CCDF of INP has a better resolution and shows effects that CCDF of PAPR tends to mask.

The INP is a good measure when comparing the performance of two systems. For CCDF of INP representations where the signals are normalized to unitary mean power, the parameter γ^2 can be assimilated to the IBO, which is closely related to the OBO. Moreover, the analysis in [CiBu05] and [CiMo08a] shows that, when using an ideal clipper-type HPA, the OBO difference in order for two systems to have similar spectral behavior (respect the same SEM) can be roughly estimated by the difference between the CCDF of INP curves corresponding to these two systems, evaluated at values of γ^2/IBO corresponding to the desired working point. When the amplifier is not ideal, this approximation is less accurate, but the CCDF of INP difference still gives a good idea of the maximum OBO gain between two systems.

Cubic Metric

The CCDF of PAPR and INP are signal-specific statistics computed on the signal samples and do not assume nor take into account the presence of an HPA. The indications given by these statistics help us roughly anticipate the behavior of the signal when passing through an HPA but the actual distortion level is subject to HPA properties. Moreover, if CCDF of PAPR/INP can sometimes be related to the IBO, such statistics give no indication on the necessary OBO, since the OBO-IBO relationship is not one-to-one and it depends on both HPA's and input signal's characteristics. In practice the important parameter is the necessary OBO (sometimes also called power de-rating) in order to achieve target performance. This yields another means of expressing the behavior of a signal in the presence of nonlinearities, which is the Cubic Metric (CM).

The CM tries to empirically estimate the actual necessary OBO for a signal passing through a typical HPA in a mobile handset. In 3GPP-LTE, CM has been analyzed in [Mot04] in an OFDMA-type context. In amplifier circuits, the primary cause of ACLR is the third order nonlinearity of the amplifier's gain characteristic. Ignoring any other causes of nonlinearity, the amplifier input-output characteristics in the non-saturated zone may be approximately written as:

$$v_{\mathrm{OUT}} \simeq G_1 v_{\mathrm{IN}} + G_3 v_{\mathrm{IN}}^3 . \tag{3.12}$$

Linear and respectively nonlinear gain G_1, G_3 depend only on the amplifier design, and will not change regardless of the input signal. The cubic term in (3.12) is at the origin of nonlinear distortion. For a given amplifier, the total energy in the cubic term will be determined only by the input signal, and this total energy will be distributed among the various distortion components in some predefined, signal-dependent way.

In order to generate a metric that reflects the power in the cubic term above, the given voltage signal v is first normalized to unitary root mean square (rms) value $v_{\text{norm}} = v / P_{\text{Avg}}^{1/2}$, then cubed. The rms value of this cubed waveform is then computed and converted to dB. Cubic metric has been defined as [Mot06]:

$$\text{CM}\big|_{\text{dB}} = \frac{20\log_{10}\left\{\text{rms}(v_{\text{norm}}^{3})\right\} - 20\log_{10}\left\{\text{rms}(v_{\text{Ref}}^{3})\right\}}{K}(+0.77)\,. \tag{3.13}$$

Terms in (3.13) have the following significance:

- $20\log_{10}\left\{\text{rms}(v_{\text{norm}}^{3})\right\}$ is called the raw CM and is a measure of the third order distortion that v is susceptible to cause;
- $20\log_{10}\left\{\text{rms}(v_{\text{Ref}}^{3})\right\} = 1.52\text{ dB}$ is the raw CM of a reference voice signal;
- K is an empirically determined factor, with value 1.56 for 3GPP-LTE signals [Mot06].

A correction factor of 0.77 dB is applied for E-UTRA signals (omitted for UTRA); This correction factor takes into account the fact that even if the raw CM is not affected by the amount of occupied bandwidth, the ACLR is, which leads to the necessity of increased OBO. Equation (3.13) is determined on empirical basis, so as to fit the OBO measurements performed onto a set of practical HPAs. Results in [Mot06] state that the prediction accuracy of CM is superior to that of PAPR. Nevertheless, we must take into account the fact that these statistics are based on rather restrictive assumptions onto the type of signals and HPA, and it is calibrated for a 3GPP-LTE typical context.

3.1.4. Total system degradation

We have seen so far that nonlinearities introduce different types of effects, resulting in relative distortion-related SNR loss (ΔSNR) and OBO loss with respect to an ideal linear transmission. To perform an overall analysis, the losses with respect to an ideal linear system can be summed under the form of a total degradation:

$$\text{Total degradation} = \Delta\text{SNR} + \text{OBO}\,. \tag{3.14}$$

We proceed as follows: Fix a target performance level (*e.g.*, BER=10^{-4}, FER=1%, etc.); at this target, analyze how much total degradation the system suffers when a certain amount of OBO is performed. This results into a total degradation curve like the one in Fig. 3.7, where an uncoded OFDM signal passing through Rapp HPA before AWGN channel and for a target BER of 10^{-4} is presented as generic example. When the back-off is high, there is virtually no in-band distortion and thus no distortion-related BER loss (ΔSNR<<OBO). When working at low OBO, in-band distortions increase, ΔSNR loss is important and becomes the predominant term in the total degradation. There is an optimal working point I_{opt}, which ensures a compromise between OBO and ΔSNR and yields a minimum total degradation. In coded systems, the importance of the ΔSNR term is reduced and the optimum working point I_{opt} is pushed into the low-OBO region.

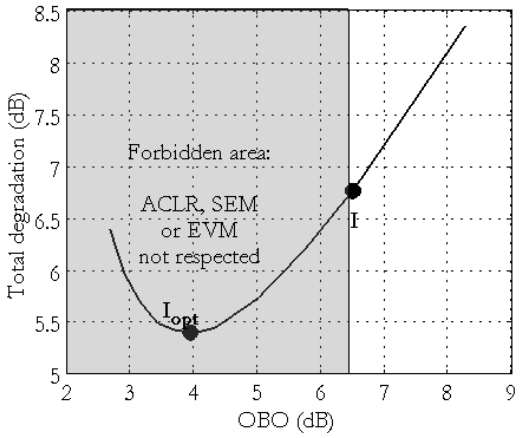

Fig. 3.7 Total system degradation at different operating points.

While operating in the point I_{opt} is optimum from a total in-band degradation point of view, this might not be always possible in practical systems. Indeed, I_{opt} lies in the low OBO region (especially in coded systems) which implies out-of-band degradations, *i.e.*, high levels of spectral regrowth, and might also cause high EVM. Usually, the operating point I is the closest point to I_{opt} where all system constraints (ACLR, SEM, EVM) are simultaneously respected. This will be thoroughly detailed in 3.6.3.

3.2. Multiple access techniques

Cellular communications systems must accommodate multiple users. These users need to share the available system resource in such a manner that all active users have a satisfactory quality of access. Multiple access techniques describe the way the available resources are shared between multiple users.

First, there are two basic techniques to separate the uplink (UL) and the downlink (DL). These are frequency-division duplexing (FDD) and time-division duplexing (TDD). For example, conventional telephony uses FDD and DECT (Digital Enhanced Cordless Telecommunications) uses TDD. Classical multiple access schemes are TDMA (Time Division Multiple Access) and FDMA (Frequency Division Multiple Access), which are illustrated in Fig. 3.8 – (a) and (b) respectively. In TDMA, users transmit in rapid succession, one after the other, each one using its own time slot. This allows multiple MSs to share the same frequency band while using only a part of the channel capacity. TDMA is used in the digital 2G cellular systems such as GSM, IS-136, Personal Digital Cellular and also in some satellite communications systems. In FDMA systems, the users are individually allocated one or several frequency bands, allowing them to access the radio system without interfering with each other. It can obviously be combined either with TDD (*e.g.*, DECT) or FDD (*e.g.*, Advanced Mobile Phone System AMPS). In recent broadband mobile systems, FDMA evolved into Orthogonal FDMA (OFDMA) [SaLe96a], [SaLe96b], [SaLe97], [Sar97], [StMo98], [SaKa98], which will be largely discussed in 3.3.2.

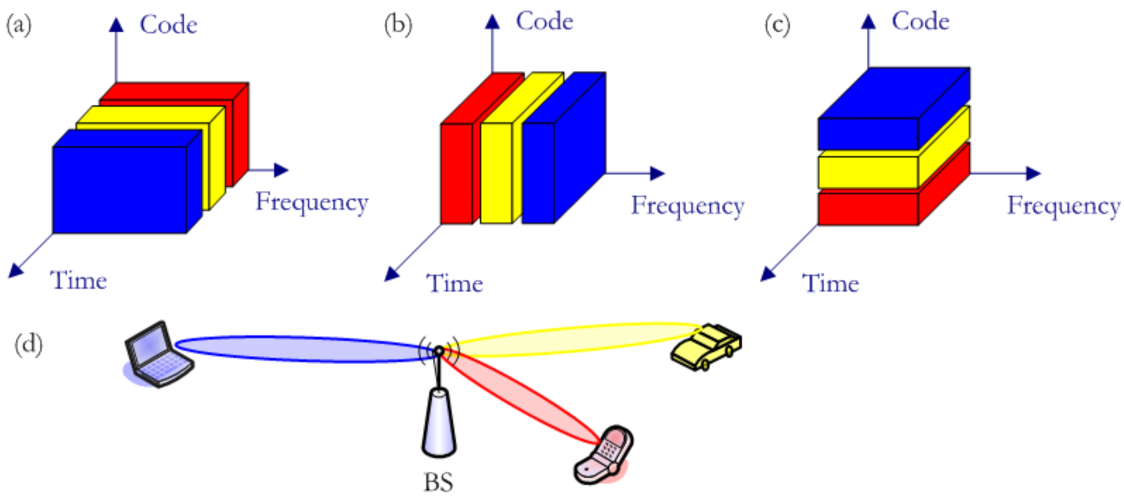

Fig. 3.8 Multiple access schemes: (a) – TDMA; (b) – FDMA; (c) – CDMA; (d) - SDMA.

Another multiple access scheme allowing all the users to simultaneously share all the system bandwidth is CDMA. Each user is allocated a code drawn from a set of sequences, which are usually orthogonal to each other. This code, with a chip rate several times superior to user's data rate, spreads the user's signal into the whole available bandwidth. All users use the same bandwidth at the same time, each user being identified by its code (Fig. 3.8 - (c)). At the receiver, each user is detected due to its unique spreading code. Although very flexible, CDMA has its own limitations: Every user is a source of noise for all other users, and thus increasing the number of users also increases the interference level, degrading the performance for all users. CDMA was first used in the 2G standard IS-95 (Interim Standard 95), also known as cdmaOne. It was also adopted in 2.5G/3G systems under the form of CDMA2000 and evolved into W-CDMA in 3G networks.

Recently, the use of multiple antenna systems opened the way to a new exploitable resource: the space dimension. SDMA (Space Division Multiple Access) is a technique allowing multiple users to be multiplexed due to their different spatial signatures. In contrast to the previous schemes, SDMA does not really separate the signals coming from different users, but rather takes benefit from their geographical separation. Of course, the problem of collocated users must be resolved using other multiple access schemes.

3.3. Multicarrier frequency-domain based air interfaces

MC air interfaces have become popular due to their robustness to deep fading. on the other hand, air interfaces based on frequency-domain transmission and reception are known to fulfill requirements of high spectral efficiency and scalability of the cost of the terminal with respect to the data rate. Both MC interfaces and those based on frequency-domain techniques can be unified under the generic term of Generalized Multicarrier Transmission.

3.3.1. Generalized multicarrier transmitter

Let us first make the following notation conventions:

- $(.)^{-1}$, $(.)^{\dagger}$, $(.)^{\mathrm{T}}$, $(.)^{\mathrm{H}}$ and $(.)^{*}$ will stand for the inverse, pseudo-inverse, transpose, Hermitian and complex conjugate of a vector or matrix, respectively;
- $\otimes$ denotes the Kronecker product;
- $\omega_N = \exp(j2\pi / N)$ is a primitive root of unity;
- $\mathbf{F}_N$ is the N-point normalized Discrete Fourier Transform (DFT) under the form of an $N \times N$ matrix with elements $F_{k,n} = \omega_N^{kn} / \sqrt{N}$ on the k-th row and n-th column, where $k,n = 0 \ldots N-1$;
- $\mathbf{F}_N^{-1} = \mathbf{F}_N^{\mathrm{H}} = \mathbf{F}_N^{*}$ is the Inverse DFT (IDFT) matrix;
- $\mathbf{0}_{M\times N}$ is the all-zero matrix of size $M \times N$;
- $\mathbf{I}_M$ is the $M \times M$ identity matrix.

Fig. 3.9 presents the baseband structure of a generalized MC transmitter, which applies to all types of SC (single carrier) or MC modulation signals transmitted in blocks [Taf06]. Let us denote by x_k the information symbols (*e.g.*, QAM symbols) which are parsed into data blocks $\mathbf{x}$ of size M. The i-th data block $\mathbf{x}^{(i)}$ can thus be written as:

$$\mathbf{x}^{(i)} = \left[x_0^{(i)},\ldots,x_{M-1}^{(i)}\right]^{\mathrm{T}}. \tag{3.15}$$

Data blocks $\mathbf{x}^{(i)}$ belonging to a certain user, are precoded with an $M \times M$ matrix $\mathbf{M}$. The user-specific M-sized output:

$$\mathbf{s}^{(i)} = \mathbf{M}\mathbf{x}^{(i)} \tag{3.16}$$

is then mapped onto a set of M out of N inputs of the inverse DFT conveniently chosen by the user-specific subcarrier mapping $N \times M$ matrix $\mathbf{Q}$, resulting in the N-sized vector:

$$\mathbf{y}^{(i)} = \mathbf{F}_N^{\mathrm{H}}\mathbf{Q}\mathbf{M}\mathbf{x}^{(i)}. \tag{3.17}$$

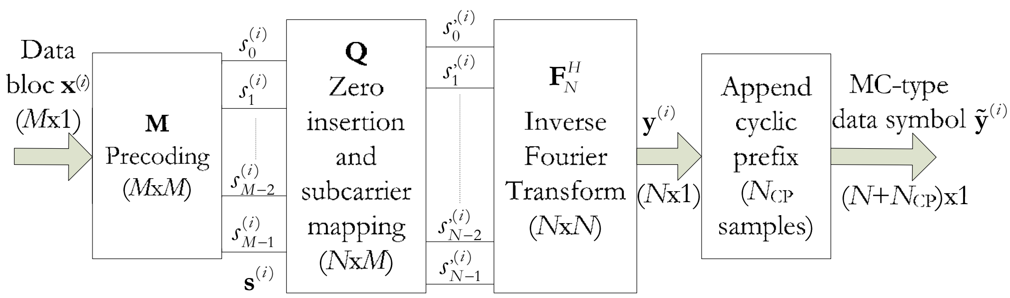

Fig. 3.9 Generalized MC transmitter for SISO transmission.

The form of the matrix $\mathbf{Q}$ might lead to contiguous, distributed, mixed or even channel dependent subcarrier allocation. Let us consider, for simplicity, that N is a multiple of M, *i.e.*, $N = KM$. The form of Q for localized and distributed carrier assignments are given by (3.18) and respectively (3.19):

$$\mathbf{Q}_{N\times M} = \begin{pmatrix} \mathbf{0}_{q\times M} \\ \mathbf{I}_M \\ \mathbf{0}_{(N-q-M)\times M} \end{pmatrix}, \tag{3.18}$$

$$\mathbf{Q}_{N\times M} = \mathbf{I}_M \otimes \begin{pmatrix} \mathbf{0}_{n\times 1} \\ 1 \\ \mathbf{0}_{(K-n-1)\times 1} \end{pmatrix}. \tag{3.19}$$

A cyclic prefix (CP), of length N_{CP} longer than the largest multipath delay, is usually inserted before transmission (and removed at the receiver before demodulation) to eliminate the intersymbol interference arising from multipath propagation. The role of CP will be further discussed in 3.4. Resulting signal $\tilde{\mathbf{y}}^{(i)}$ undergoes D/A conversion and is sent into the time-varying channel $h(\tau,t)$ via an HPA. Since adding CP is equivalent to circularly repeating signal samples, CP insertion does not modify the signal's dynamic range. $\mathbf{y}^{(i)}$ and $\tilde{\mathbf{y}}^{(i)}$ have the same distribution and thus it will suffice to analyze the properties of $\mathbf{y}^{(i)}$ (in the conditions described in 3.1.3) in order to estimate the impact of nonlinearities.

Transmitter structure in Fig. 3.9 is very generic and can be employed to model a large class of signals such as OFDMA, precoded OFDMA, MC-CDMA, DS-CDMA (Direct Sequence CDMA), SS-MC-MA (Spread Spectrum MC Multiple Access) and FDOSS (Frequency-Domain Orthogonal Signature Sequences) [WWRF08].

3.3.2. OFDMA

Let us consider the trivial case where precoding is performed with the identity matrix, $\mathbf{M} = \mathbf{I}_M$. This results in OFDMA. Let us focus first on the case $M = N$ which corresponds to OFDM transmission with $\mathbf{Q} = \mathbf{I}_M$. The IDFT operation is equivalent to splitting the information into N parallel data streams, each one being transmitted by modulating N distinct subcarriers equally spaced in the system bandwidth W. Each k-th subcarrier at frequency $f_k = kW / N$ carries one modulation symbol $x_k^{(i)}$. It can easily be seen that these critically-spaced subcarriers are orthogonal: Let T be the duration of an OFDM symbol $\mathbf{y}^{(i)}$ and $T_{\mathrm{c}} = T / N$ the duration of a symbol at the input of the IFFT (here, a modulation symbol $x_k^{(i)}$), we have:

$$\int_{kT_{\mathrm{c}}}^{(k+1)T_{\mathrm{c}}} \exp(j2\pi f_m t)\exp(-j2\pi f_n t)dt = \delta[m-n], \tag{3.20}$$

where $\delta[.]$ is the discrete Dirac function. Fig. 3.10 shows the principle of OFDM in the "analog" frequency domain. Supposing rectangular pulse shaping in the time domain, the spectrum of each modulated subcarrier is represented by a cardinal sinus (sinc) function. Due to the orthogonality property, the spectra of different subcarriers overlap but do not interfere, each subcarrier being in the spectral nulls of all the other subcarriers.

For multiple access, OFDM can be combined with TDMA, FDMA or CDMA. Combination with FDMA leads to OFDMA, where the user-specific data block $\mathbf{x}^{(i)}$ of size $M < N$ is directly mapped onto a subset of M subcarriers, conveniently chosen by the user-specific subcarrier mapping matrix $\mathbf{Q}$. Vector $\mathbf{Qx}^{(i)}$ is fed to the entries of the IDFT, resulting in:

$$\mathbf{y}^{(i)} = \mathbf{F}_N^{\mathrm{H}}\mathbf{Qx}^{(i)}. \tag{3.21}$$

Unoccupied carriers can be allocated to other users, enabling the multiple access. OFDMA has multiple advantages, which render this scheme a serious candidate for the air interface of future generation systems. It attains high spectral efficiency by exploiting the orthogonality between subcarriers with overlapping spectra. Indeed, traditional FDMA would need large frequency spacing between subcarriers to multiplex different users. Frequency-domain implementation based on the block diagram in Fig. 3.9 is extremely simple and flexible. Low-complexity receivers can be also implemented in the frequency domain. Nevertheless, OFDMA has several disadvantages, such as its sensitivity to the loss of orthogonality (due to, *e.g.*, Doppler shifts or frequency errors). But the major drawback of OFDMA is its high dynamic range.

Let us consider again an OFDM scenario. Each sample $y_k^{(i)}$ at the output of the IDFT can be represented as:

$$y_k^{(i)} = \frac{1}{\sqrt{N}} \sum_{n=0}^{N-1} x_n^{(i)} \omega_{\mathrm{N}}^{kn} . \tag{3.22}$$

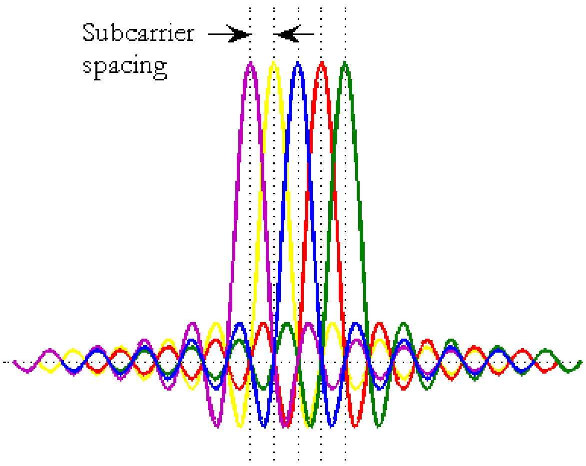

Fig. 3.10 Principles of OFDM.

Each sample appears as the sum of N independent random variables. For large N, we can state that, in conformity with the central limit theorem, both in-phase and quadrature components of $y_k^{(i)}$ are asymptotically Gaussian. This approximation stands in the case treated here, as we generally consider N=512 or higher. Further increasing N does not significantly increase the envelope fluctuations [Tel99]. This yields a Rayleigh distribution for the amplitude $\left|y_k^{(i)}\right|$ and a chi-square distribution with two degrees of freedom for the INP. As a result, even if most of the samples have powers concentrated around the mean value, samples with very important amplitudes exist. This explains the high PAPR in OFDM signals. OFDMA obviously inherits this PAPR problem, which is common to MC systems.

The reasoning above leads to closed-form expressions of the CCDF of PAPR corresponding to the critically-sampled signal $\mathbf{y}^{(i)}$. As explained in 3.1.3, this underestimates the continuous-time PAPR. Other analytical approximations are given in [OcIm01]. Upper bounds for the oversampled case are discussed in [Tel99].

From a performance point of view, OFDMA does not benefit from any built-in diversity. In a system where no FEC coding is employed, each carrier contains a modulation symbol uncorrelated with other transmitted data. When passing through a frequency-selective channel, if an occupied carrier is in a deep fade, all the information carried by this carrier is lost. We can say that uncoded OFDMA retrieves a frequency diversity order of 1 (out of L diversity branches available in a frequency selective channel with L non-null taps). Therefore, employing FEC coding is essential in order to have good performance in an OFDMA system.

3.3.3. SC-FDMA

As opposed to MC-FDMA schemes, SC-FDMA combines a SC signal with an OFDMA-like multiple access, trying to take advantage of the strengths of both techniques: Low PAPR and flexible dynamic frequency allocation. Depending on the way the subcarriers are allocated to each user or on the techniques used to generate the signal, SC-FDMA can be found in the literature under different names. Let us review the origin of SC-FDMA signals before explaining how it can be seen as a particular case of Fig. 3.9.

SC-FDMA was first conceived in a time-domain implementation [SoBr98] called IFDMA (Interleaved Frequency Division Multiple Access). At instant (i), blocks of M data symbols are parsed into data blocks $\mathbf{x}^{(i)}$ like in (3.15). $\mathbf{x}^{(i)}$ is of duration $T = MT_s$, where T_s is the QAM symbol duration. These blocks are K-time compressed and K-time replicated to form the IFDMA signal $\mathbf{y}^{(i)}$ with the same duration $T = NT_c$ as depicted in Fig. 3.11. Here, $N = KM$ and $T_s = KT_c$, T_c being the chip duration. As theoretically proven in [FrKl05], this manipulation has a direct interpretation in the frequency domain: The spectrum of the compressed and K-times replicated signal $(\mathbf{F}_N\mathbf{y}^{(i)})$ has the same shape as the spectrum of the original signal $(\mathbf{F}_N\mathbf{x}^{(i)})$, with the difference that it includes exactly K-1 zeros between two data subcarriers, as it can be seen in the example in Fig. 3.12. This feature enables us to easily interleave a maximum of K different users in the frequency domain by simply applying to each user a specific frequency shift, or equivalently, by multiplying the time-domain sequence by a specific phase ramp.

Obviously, this structurally imposes a distributed subcarrier allocation.

The spectral considerations above open the way to a frequency-domain implementation of SC-FDMA [TS25814], sometimes called DFT-spread OFDM, and which is in fact a classical precoded OFDMA scheme, where precoding is done by means of a DFT. This results in taking:

$$\mathbf{M} = \mathbf{F}_M \tag{3.23}$$

in Fig. 3.9. In a vector form, the generated SC-FDMA symbol can be described as:

$$\mathbf{y}^{(i)} = \mathbf{F}_N^{-1}\mathbf{Q}\mathbf{s}^{(i)} = \mathbf{F}_N^{-1}\mathbf{Q}\mathbf{F}_M\mathbf{x}^{(i)}. \tag{3.24}$$

The form of the matrix $\mathbf{Q}$ might lead to contiguous [TS25814], distributed [SoBr98], mixed [FrKl05] or even channel-dependent subcarrier allocation. In a distributed subcarrier allocation scenario, frequency-domain generated SC-FDMA is strictly identical to time-domain generated IFDMA. The advantage of frequency-domain implementations is their flexibility, since we can

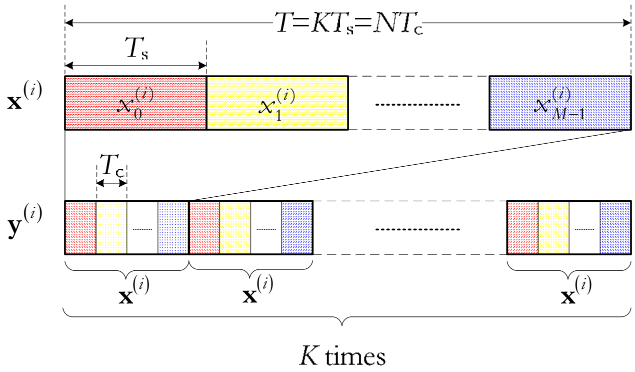

Fig. 3.11 IFDMA signal generation.

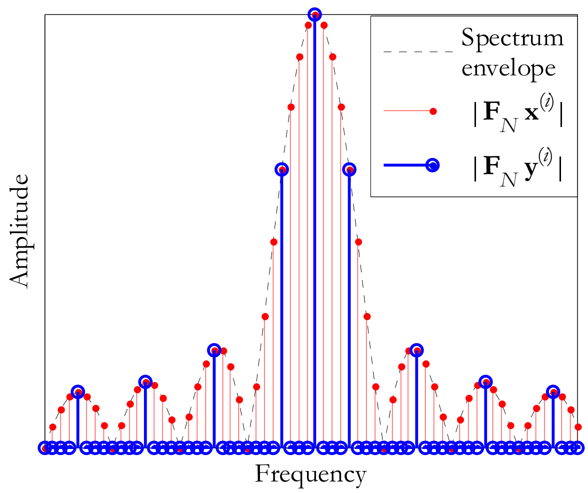

Fig. 3.12 IFDMA generation, a spectral point of view; example for N=64, K=4.

choose convenient subcarrier allocation. Also, pulse-shape filtering and/or time windowing are easily implemented in the frequency domain.

The role of the DFT precoder is a double one. On one hand, this precoding restores the SC-like properties of the signal envelope, alleviating the PAPR problem that OFDMA signals have. Indeed, we have seen that in the distributed case $\mathbf{y}^{(i)}$ is simply the condensed repeated version of $\mathbf{x}^{(i)}$, and thus an SC signal. In a localized scenario, the spectrum of the SC signal $\mathbf{x}^{(i)}$ is simply mapped into a portion of the spectrum of $\mathbf{y}^{(i)}$ just like in a conventional FDMA system. While this frequency up-conversion could slightly modify the PAPR, we do not expect significant changes. This will be verified in 3.6.1.

On the other hand, DFT performs a spreading operation, like all precoders. As a consequence, each modulation symbol $x^{(i)}$ is spread over M subcarriers. As opposed to OFDMA, losing the information on one subcarrier because of a fading dip does not automatically mean losing all the information in a modulation symbol. Uncoded SC-FDMA is thus capable of retrieving some of the frequency diversity offered by the channel, and the amount of recovered diversity obviously depends on the number of allocated carriers M and on the type of subcarrier mapping $\mathbf{Q}$.

Spreading has not only beneficial consequences, but it also causes some intercode interference. Frequency selective fading among the set of allocated carriers can be interpreted as a loss of orthogonality between the M-sized Fourier codes (orthogonality only remains on a flat channel): This impacts onto all the modulation symbols composing $\mathbf{x}^{(i)}$, and the effect is especially disturbing for high-order modulations.

3.3.4. SS-MC-MA

SS-MC-MA is a multiple access technique derived from MC-CDMA (Multicarrier CDMA), especially conceived for the uplink. Let us consider in Fig. 3.9 a precoding matrix:

$$\mathbf{M} = \mathbf{WH}_M = \left[\mathbf{WH}_M^{(0)}, \mathbf{WH}_M^{(1)}, \ldots, \mathbf{WH}_M^{(M-1)}\right], \tag{3.25}$$

where the column vectors $\mathbf{WH}_M^{(k)}$, $k = 0 \ldots M-1$, are orthogonal Walsh-Hadamard (WH) sequences of length M. The precoding matrix $\mathbf{M}$ becomes a Hadamard matrix of order M, $\mathbf{WH}_M$, performing a WH transform. This type of precoded OFDMA was coined SS-MC-MA [KaFa97], [KaKr99]. The precoding operation $\mathbf{WH}_M \mathbf{x}^{(i)}$ consists in spreading the data symbols by multiplication with orthogonal WH sequences and superimposing them on the same set of subcarriers according to matrix $\mathbf{Q}$. If $M = N$, this results in MC-CDMA. Hadamard orthogonal matrices are known and employed for a very long time in mathematics [Syl67]. The existence and generation of WH codes has been extensively studied recently since they are very commonly used in all CDMA-based systems. While generating Hadamard matrices is simple for all M of type $M = 2^m$ with $m \in \mathbb{N}$, the problem is more complicated for more general cases. It is known that $\mathbf{WH}_M$ exists for all M that are integer multiples of 4, but the problem of generating $\mathbf{WH}_M$ is solved only in some particular cases. Appendix C details some useful Hadamard matrices.

In MC-CDMA, users separated by orthogonal spreading codes in the frequency domain transmit over all the available bandwidth, taking maximum advantage of the available frequency diversity. However, in uplink, MC-CDMA degrades significantly due to time and frequency misalignments of different users who share the same frequency grid, which generates a loss of orthogonality between the codes and results in important increases of the interference level. Furthermore, channel estimation turns out to be a very complicated task in such a scenario.

Therefore, while in downlink scenarios MC-CDMA may be a good choice, for uplink the alternative SS-MC-MA is preferable. In SS-MC-MA different users are frequency multiplexed on different sets of carriers in an OFDMA-like manner with matrix $\mathbf{Q}$, and each user, within its own carriers, spreads M different symbols $x_{0\ldots M-1}^{(i)}$ with M spreading vectors of $\mathbf{WH}_M$ as if they were M "virtual users". Performance approaches that of MC-CDMA in downlink. Note that SS-MC-MA does not necessarily need to be in "full-load" conditions, but may employ blocks $\mathbf{x}^{(i)}$ of $M' < M$ symbols to be spread onto the M used subcarriers using only M' out of M vectors from $\mathbf{WH}_M$.

Both SC-FDMA and SS-MC-MA appear as precoded OFDMA schemes, with precoding via DFT and WH orthogonal transform, respectively. It is expected that precoding has the same effects on system performance in both cases, so the diversity and code interference reasoning remains unchanged with respect to the discussion in 3.3.3. On the other hand, from a PAPR point of view, precoding via WH does not "revert" the effect of the IDFT onto the signal statistics so we expect the SS-MC-MA signal to have high OFDMA-like PAPR.

3.4. Receiver structure

Let us now focus on how a MC signal generated by a transmitter like in Fig. 3.9 can be decoded. Classically, SC systems employed time-domain equalization. The complexity of these detectors grows exponentially with the bandwidth - delay spread product, which becomes unsustainable in MC wideband systems. Part of the success of OFDM-based systems is due to the fact that temporal equalization can simply be avoided and robust frequency-domain equalization techniques exist. For all types of signals with block-based transmitters described in Fig. 3.9, frequency-domain equalization is rendered possible by the insertion of a CP, at the cost of a very small penalty in channel capacity.

Also, in this subsection we will not model the presence of the HPA, because doing so would imply building a receiver dependent on the HPA characteristics. Or, in practice, this would not be a sensible choice: Different users may possess mobile devices with different characteristics, built by different constructors and this cannot impact on the structure of the BS which needs to correctly demodulate the signals of all users. We will therefore not take explicitly into account the presence of the HPA when deriving the receiver's structure.

3.4.1. General structure of an MC receiver

The general structure of a receiver capable of demodulating the class of signals described in subsection 3.3 is presented in Fig. 3.13. This receiver basically needs to invert the operations in Fig. 3.9, the purpose being to give an estimate $\hat{\mathbf{x}}^{(i)}$ of the transmitted data block $\mathbf{x}^{(i)}$. Let us comment on the structure of this general receiver.

Let us suppose that the time necessary to the transmission of an OFDMA-like symbol $\tilde{\mathbf{y}}^{(i)}$ is inferior to the coherence time T_{coh}, which allows us to consider that the channel $h(\tau,t)$ is stationary during the transmission of an OFDMA-like symbol. The baseband discrete channel model can thus be assumed to have L taps and can be expressed under the form of the N-sized vector:

$$\mathbf{h}^{(i)} = \left[h_0^{(i)}, h_1^{(i)}, ..., h_{L-1}^{(i)}, \mathbf{0}_{1\times(N-L)} \right]^{\mathrm{T}}. \tag{3.26}$$

Mathematically speaking, the insertion of the CP transforms the convolution product between the emitted signal $\tilde{\mathbf{y}}$ and the channel under its discrete form into a circular convolution product at block level:

$$\tilde{\mathbf{y}}^{(i)} * \mathbf{h}^{(i)} = \mathbf{y}^{(i)} \,\tilde{*}\, \mathbf{h}^{(i)}, \tag{3.27}$$

where $\tilde{*}$ denotes the circular convolution. Physically speaking, this operation removes the interference between $\mathbf{y}^{(i)}$ and the previous/following block $\mathbf{y}^{(i\pm1)}$, as long as CP is long enough. Mathematically speaking, this allows us to transform the time-domain circular convolution into frequency-domain element-wise multiplication:

$$\mathbf{F}_N \left(\mathbf{y}^{(i)} \,\tilde{*}\, \mathbf{h}^{(i)} \right) = \mathbf{F}_N \mathbf{y}^{(i)} \odot \mathbf{F}_N \mathbf{h}^{(i)}. \tag{3.28}$$

This property is of great importance, since it opens the way to frequency-domain equalization (FDE): The effect of the channel onto the transmitted signal can be inverted by simple multiplication in the frequency domain with a one-tap equalization coefficient for each subcarrier.

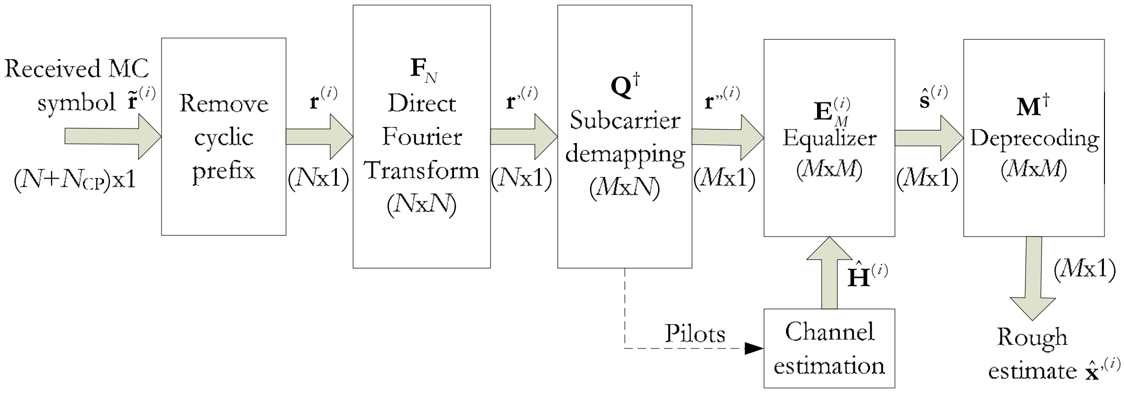

Fig. 3.13 Generalized MC receiver for SISO transmission.

Let us express (3.28) in matrix form. We denote by $\mathbf{r}^{(i)}$ the received signal and by $\mathbf{H}_{\mathrm{c}}^{(i)}$ the circulant channel matrix defined as:

$$\mathbf{H}_{\mathrm{c}}^{(i)} = \mathrm{circ}\left(\mathbf{h}^{(i)}\right) = \begin{bmatrix} h_0^{(i)} & 0 & 0 & 0 & h_{L-1}^{(i)} & \cdots & h_1^{(i)} \\ h_1^{(i)} & h_0^{(i)} & 0 & \vdots & 0 & \ddots & \vdots \\ \vdots & h_1^{(i)} & \ddots & 0 & \vdots & 0 & h_{L-1}^{(i)} \\ h_{L-1}^{(i)} & \vdots & \ddots & h_0^{(i)} & 0 & \vdots & 0 \\ 0 & h_{L-1}^{(i)} & & h_1^{(i)} & h_0^{(i)} & 0 & \vdots \\ \vdots & 0 & \ddots & \vdots & \ddots & \ddots & 0 \\ 0 & 0 & \ldots & h_{L-1}^{(i)} & \cdots & h_1^{(i)} & h_0^{(i)} \end{bmatrix}. \tag{3.29}$$

With these notations, the circular convolution product between $\mathbf{y}^{(i)}$ and $\mathbf{h}^{(i)}$ can be re-written in matrix form:

$$\mathbf{r}^{(i)} = \mathbf{H}_{\mathrm{c}}^{(i)}\mathbf{y}^{(i)} + \mathbf{n}^{(i)}, \tag{3.30}$$

where $\mathbf{r}^{(i)}$ is the N-point vector corresponding to the received signal after CP removal, $\mathbf{H}_{\mathrm{c}}^{(i)}$ is the $N \times N$ circulant matrix (3.29) describing the channel and $\mathbf{n}^{(i)}$ represents AWGN.

Passing in the frequency-domain results in computing the N-point DFT of $\mathbf{r}^{(i)}$ as:

$$\mathbf{F}_N\mathbf{r}^{(i)} = \mathbf{F}_N\mathbf{H}_{\mathrm{c}}^{(i)}\mathbf{y}^{(i)} + \mathbf{F}_N\mathbf{n}^{(i)} = \mathbf{F}_N\mathbf{H}_{\mathrm{c}}^{(i)}\mathbf{F}_N^{\mathrm{H}}\mathbf{s}'^{(i)} + \mathbf{F}_N\mathbf{n}^{(i)}. \tag{3.31}$$

It is known from the theory of circulant matrices [Lan69] [Dav79], that the eigenvectors of a circulant matrix of given size are the columns of the DFT matrix of the same size. From the spectral theorem [Hal63] applied to $\mathbf{H}_{\mathrm{c}}^{(i)}$, it results that the eigenvalues of $\mathbf{H}_{\mathrm{c}}^{(i)}$ are given by the DFT of the first row of $\mathbf{H}_{\mathrm{c}}^{(i)}$, which is equivalent to:

$$\mathbf{F}_N\mathbf{H}_{\mathrm{c}}^{(i)}\mathbf{F}_N^{\mathrm{H}} = \mathrm{diag}\left(\mathbf{F}_N\mathbf{h}^{(i)}\right) = \mathrm{diag}\left(H_N[k,i]\big|_{k=0\ldots N-1}\right), \tag{3.32}$$

where $H_N[k,i]$ is the discrete version of the time varying channel transfer function $H(f,t)$ as defined in Chapter 2 (operator $\mathbf{F}_N$ performs Fourier transform in the time-delay domain).

Moreover, since the mapping/demapping operations $\mathbf{Q}/\mathbf{Q}^{\dagger}$ consist only in adding/removing null rows and columns, it is easy to verify that $\mathbf{Q}^{\dagger}\mathbf{F}_N\mathbf{H}_{\mathrm{c}}^{(i)}\mathbf{F}_N^{\mathrm{H}}\mathbf{Q}$ is also diagonal, containing on its main diagonal only the M (out of N) elements of $\mathbf{F}_N\mathbf{h}^{(i)}$ corresponding to the allocated subcarriers:

$$\mathbf{H}^{(i)} \triangleq \mathbf{Q}^{\dagger}\mathbf{F}_N\mathbf{H}_{\mathrm{c}}^{(i)}\mathbf{F}_N^{\mathrm{H}}\mathbf{Q} = \mathrm{diag}\left(H[k,i]\big|_{k=0\ldots M-1}\right), \tag{3.33}$$

where $H[k,i]$ is the discrete version of the time varying channel transfer function $H(f,t)$ corresponding only to the used subcarriers.

It is therefore after the precoding operation $\mathbf{M}$ at the transmitter side that the system "sees" an equivalent diagonal channel. This diagonalization property allows simple FDE at the receiver side, before the deprecoding operation, by multiplication with coefficients derived from classical low-complexity linear equalization methods, *e.g.*, MMSE (Minimum Mean Square Error) or ZF (Zero Forcing).

Let us suppose that the linear FDE is represented in matrix form by an $M \times M$ equalization matrix $\mathbf{E}_M^{(i)}$. The estimated data vector $\hat{\mathbf{x}}$' at the receiver can be expressed in a first instance as:

$$\hat{\mathbf{x}}'^{(i)} = \mathbf{M}^{\dagger}\mathbf{E}_M^{(i)}\mathbf{Q}^{\dagger}\mathbf{F}_N\mathbf{r}^{(i)} . \tag{3.34}$$

This results in:

$$\begin{aligned}\hat{\mathbf{x}}'^{(i)} &= \underbrace{\mathbf{M}^{\dagger}\mathbf{E}_M^{(i)}\mathbf{Q}^{\dagger}\mathbf{F}_N\mathbf{H}_{\mathrm{c}}^{(i)}\mathbf{F}_N^{\mathrm{H}}\mathbf{Q}\mathbf{M}}_{\triangleq\mathbf{A}^{(i)}}\mathbf{x}^{(i)} + \mathbf{M}^{\dagger}\mathbf{E}_M^{(i)}\mathbf{Q}^{\dagger}\mathbf{F}_N\mathbf{n}^{(i)} = \\ &= \underbrace{\mathrm{diag}(\mathbf{A}^{(i)})\mathbf{x}^{(i)}}_{\text{useful signal}} + \underbrace{\left(\mathbf{A}^{(i)} - \mathrm{diag}(\mathbf{A}^{(i)})\right)\mathbf{x}^{(i)}}_{\text{interference}} + \underbrace{\mathbf{M}^{\dagger}\mathbf{E}_M^{(i)}\mathbf{Q}^{\dagger}\mathbf{F}_N\mathbf{n}^{(i)}}_{\text{noise}} .\end{aligned} \tag{3.35}$$

When $\mathrm{diag}(\mathbf{A}^{(i)})$ differs from the identity matrix $\mathbf{I}_M$, a normalization (that can be seen as a per-carrier post-equalization) needs to be applied. Since the inverse of a diagonal matrix is straightforward to compute, matrix multiplication with:

$$\mathrm{diag}^{-1}(\mathbf{A}^{(i)}) = \mathrm{diag}\left(\frac{1}{A_{0,0}^{(i)}} \quad \dots \quad \frac{1}{A_{M-1,M-1}^{(i)}}\right) \tag{3.36}$$

will suffice to compute an estimate of the transmitted sequence:

$$\hat{\mathbf{x}}^{(i)} = \mathbf{x}^{(i)} + \underbrace{\mathrm{diag}^{-1}(\mathbf{A}^{(i)})\left(\mathbf{A}^{(i)} - \mathrm{diag}(\mathbf{A}^{(i)})\right)\mathbf{x}^{(i)}}_{\text{interference}} + \underbrace{\mathrm{diag}^{-1}(\mathbf{A}^{(i)})\mathbf{M}^{\dagger}\mathbf{E}_M^{(i)}\mathbf{Q}^{\dagger}\mathbf{F}_N\mathbf{n}^{(i)}}_{\triangleq\mathbf{N}^{(i)}} \tag{3.37}$$

Let us comment on the implications of (3.35)-(3.37) on the decoding process. When $\mathbf{x}$ is drawn, *e.g.*, from a QPSK modulation alphabet, the normalization (3.37) is not necessary and the rough estimate $\hat{\mathbf{x}}$' is sufficient in order to compute the soft bit estimates. When a higher order modulation is employed, (3.37) is indispensible in order to correctly detect the constellation symbols. In a SISO transmission like in Fig. 3.9-Fig. 3.13 with linear FDE, $\mathbf{E}_M^{(i)}$ is a diagonal matrix. In an OFDMA system,

$$\mathbf{A}^{(i)}\Big|_{\mathrm{OFDMA}} = \mathbf{E}_M^{(i)}\mathbf{Q}^{\dagger}\mathbf{F}_N\mathbf{H}_{\mathrm{c}}^{(i)}\mathbf{F}_N^{\mathrm{H}}\mathbf{Q} \tag{3.38}$$

is diagonal. In this case, since $\mathbf{A} = \mathrm{diag}(\mathbf{A})$, the interference term in (3.42) disappears: OFDMA does not suffer from intercode interference. On the other hand, for SC-FDMA systems,

$$\mathbf{A}^{(i)}\Big|_{\text{SC-FDMA}} = \mathbf{F}_M^{\mathrm{H}} \underbrace{\mathbf{E}_M^{(i)}\mathbf{Q}^{\dagger}\mathbf{F}_N\mathbf{H}_{\mathrm{c}}^{(i)}\mathbf{F}_N^{\mathrm{H}}\mathbf{Q}}_{\triangleq\tilde{\mathbf{A}}^{(i)}}\mathbf{F}_M \tag{3.39}$$

is not diagonal, which makes explicitly appear in (3.37) the intercode interference mentioned in 3.3.3. We should note here that a special simplification occurs in this case. Due to the fact that $\tilde{\mathbf{A}}^{(i)}$ is diagonal, if we denote by $\tilde{\alpha}^{(i)}$ the mean value of $\mathrm{diag}(\tilde{\mathbf{A}}^{(i)})$, we obtain by applying the properties of the unitary DFT transform:

$$\mathrm{diag}(\mathbf{A}^{(i)})\Big|_{\text{SC-FDMA}} = \mathrm{diag}(\mathbf{F}_M^{\mathrm{H}}\tilde{\mathbf{A}}^{(i)}\mathbf{F}_M) = \tilde{\alpha}^{(i)}\mathbf{I}_M\,. \tag{3.40}$$

Similar reasoning can be applied in the SS-MC-MA case.

After the constellation normalization (3.37), constellation detection allows to compute the soft bit estimates in the form of Log Likelihood Ratio (LLR). At this stage, the variance of the equivalent noise plus interference term in (3.37) needs to be computed and taken into account in order for the LLR estimates to be correctly normalized before soft-input channel decoding (Viterbi or turbo decoding).

Suppose that N_{Sym} MC symbols are coded together (*e.g.*, with a convolutional or turbo FEC), corresponding to the transmission of $\mathbf{x} = \begin{bmatrix}\mathbf{x}^{(0),\mathrm{T}} & \mathbf{x}^{(1),\mathrm{T}} & \dots & \mathbf{x}^{(N_{\text{Sym}}-1),\mathrm{T}}\end{bmatrix}^{\mathrm{T}}$. Let us denote by A the overall system transfer function:

$$\mathbf{A} = \mathrm{blkdiag}(\mathbf{A}^{(i)}) = \begin{bmatrix} \mathbf{A}^{(0)} & \mathbf{0}_{M\times M} & \cdots & \mathbf{0}_{M\times M} \\ \mathbf{0}_{M\times M} & \mathbf{A}^{(1)} & & \vdots \\ \vdots & & \ddots & \mathbf{0}_{M\times M} \\ \mathbf{0}_{M\times M} & \cdots & \mathbf{0}_{M\times M} & \mathbf{A}^{(N_{\text{Sym}}-1)} \end{bmatrix}, \tag{3.41}$$

and by $\mathbf{N} = \mathrm{blkdiag}(\mathbf{N}^{(i)})$, $i = 0 \dots N_{\text{Sym}-1}$ the overall noise. The transmission of this coded modulation through the system is characterized by:

$$\hat{\mathbf{x}} = \mathbf{x} + \underbrace{\mathrm{diag}^{-1}(\mathbf{A})\big(\mathbf{A} - \mathrm{diag}(\mathbf{A})\big)\mathbf{x} + \mathbf{N}}_{\text{equivalent interference + noise}}\,. \tag{3.42}$$

Since $\mathbf{A}$ is block diagonal, it is obvious that overall detection can be split into N_{Sym} separate blocks, which allows simple receiver structure in this case.

From this analysis, it appears that for coded OFDMA systems ZF equalization is a good detection strategy when we want to avoid complex Maximum Likelihood (ML) detection: No intercode interference is present and the noise enhancement that characterizes ZF detection is compensated by correct LLR normalization, which would not have been possible in the uncoded case. For precoded OFDMA systems, the intercode interference needs to be minimized, which points out MMSE as a good strategy.

Some details on MIMO receivers will be discussed in Chapter 4.

3.4.2. Pilot-symbol based channel estimation

We focus in this subsection onto the channel estimation presented in Fig. 3.13, whose purpose is to compute an estimate of the channel at each time i. We take into account a scenario of coherent detection. Differential modulation and detection, where information is coded in transition between consecutive data symbols, will not be discussed here. As explained in Chapter 2, the channel experienced by a wideband system is frequency selective and time varying. To correctly retrieve the transmitted message, a dynamic estimation of the channel is necessary before the demodulation.

The construction of OFDMA-based systems allows, as explained in subsection 3.3.2, to transform the wideband frequency-selective channel into N parallel narrowband (non-frequency-selective) channels. From a channel estimation point of view, this allows us to avoid complex time-domain estimation (*i.e.*, before DFT at the receiver), which would require evaluating both time delays and amplitudes of each multipath component. In the frequency-domain (*i.e.*, after DFT at the receiver, as represented in Fig. 3.13), one single coefficient per subcarrier needs to be estimated, since the wideband channel is equivalent to N one-tap channels.

Different methods of channel estimation have been proposed in the literature, divided into two main classes: blind channel estimation and pilot-symbol aided channel estimation. Hybrid methods also exist. The advantage of blind estimation techniques, which rely on some statistical properties of the transmitted signal, is that they do not affect the spectral efficiency of the system. Nevertheless, such methods [HeGi99], [MuCo02] have the handicap of long convergence times and high complexity.

We will concentrate in the following onto pilot-symbol aided channel estimation. These methods assume the insertion of known symbols onto predetermined pilot positions within the sent frame, from which a channel fading coefficient can be evaluated. This consumes of course a part of the available resources, leading to a small loss in spectral efficiency. To minimize this loss, one needs to minimize the number of inserted pilots while keeping good quality of the estimation. Usually, the pilots are placed into the frame according to a predefined pilot-symbol grid. Channel coefficients corresponding to data positions are estimated by interpolation techniques from the known coefficients onto the pilot grid.

Some examples are provided in Fig. 3.14. The first two cases (a) and (b) exemplify the case where entire MC symbols and entire subcarriers are allocated to pilot transmission, and interpolation needs to be performed in time and respectively frequency domain. In example (c), interpolation needs to be performed in both dimensions. Other types of grids are of course possible. In all cases, the pilots provide the receiver with a noisy sampled version $H^{'}[k,i]$ of the time varying channel transfer function $H\left(f,t\right)$ as defined in Chapter 2. In order for the interpolation to be possible, two different observations cannot be separated by more than the coherence time T_{coh} in the time domain and by more than the coherence bandwidth B_{coh} in the frequency domain, respectively. Since the observations are imperfect (affected by noise, *etc.*), in practice it is considered that interpolation leads to good results when the time/frequency separation does not exceed half of the coherence time/bandwidth [HoKa97].

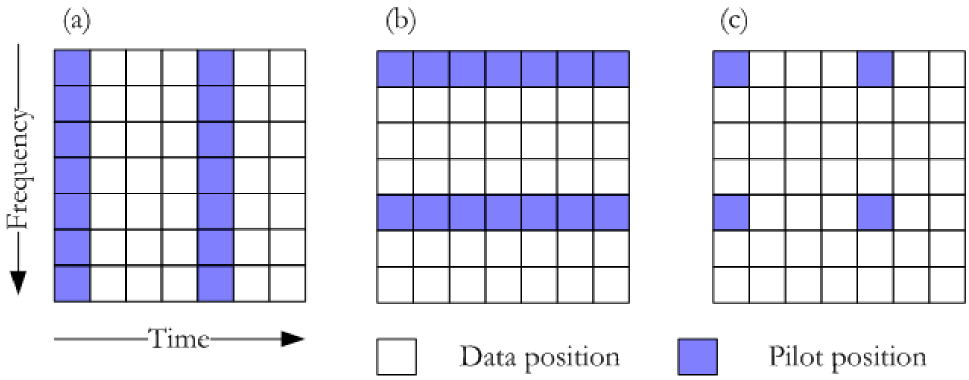

Fig. 3.14 Pilot grids: (a) – Pilot symbols; (b) – Pilot subcarriers; (c) – Rectangular grid

Ideally, a two-dimensional filter, different for each estimated position and with a number of coefficients equal to the number of pilot positions in the frame would need to be constructed for optimal interpolation. Let us consider that pilot symbols $s_{\mathrm{P},k_{\mathrm{P}}}^{(i_{\mathrm{P}})}$ are inserted in the transmission frame at position (i_{P}) in time and k_{P} in frequency. Since this training sequence is known by the receiver, we can dispose of the discrete channel observations:

$$H^{'}[k_{\mathrm{P}},i_{\mathrm{P}}] = r_{\mathrm{P},k_{\mathrm{P}}}^{''(i_{\mathrm{P}})} / s_{\mathrm{P},k_{\mathrm{P}}}^{(i_{\mathrm{P}})} = H[k_{\mathrm{P}},i_{\mathrm{P}}] + \eta_{\mathrm{P},k_{\mathrm{P}}}^{(i)}, \text{ with } k_{\mathrm{P}}, i_{\mathrm{P}} \in \text{pilot grid}. \tag{3.43}$$

In the most general case, the "missing" positions corresponding to the transmitted data are estimated by two-dimensional interpolation. The channel sample $H[k,i]$ in position (k,i) appears as a linear combination of those observations $H^{'}[k_{\mathrm{P}},i_{\mathrm{P}}]$ on the pilot grid that are spaced by less than the coherence time/bandwidth with respect to $H[k,i]$. If we define by $S_{\mathrm{P}(k,i)}$ the set of these positions, where the observation remains correlated to the sample in position (k,i) to be estimated, then:

$$\hat{H}[k,i] = \sum_{k_{\mathrm{P}},i_{\mathrm{P}} \in S_{\mathrm{P}(k,i)}} w_{k,i,k_{\mathrm{P}},i_{\mathrm{P}}} H^{'}[k_{\mathrm{P}},i_{\mathrm{P}}]. \tag{3.44}$$

The optimum linear filter for (3.44) is a two-dimensional Wiener filter [Wie49], [Hay96], employing the MMSE principle in order to minimize the mean square error between the channel coefficients and their estimates. Nevertheless, such a solution has high complexity and generates system latency, since filtering is performed over several MC-type symbols. In practice, it is preferable to perform two times one-dimensional filtering, separately in the time and frequency domain [HoKa97]. Even if performance does not depend on the order of the filtering, in practice frequency filtering is performed first, to avoid system latency. Good performance can be achieved with a relatively small number of filter taps. For a one-dimensional filter in the frequency-domain, (3.44) becomes:

$$\hat{H}[k] = \sum_{k_{\mathrm{P}} \in S_{\mathrm{P}(k)}} w_{k,k_{\mathrm{P}}} H^{'}[k_{\mathrm{P}}]. \tag{3.45}$$

Since filtering is performed in the frequency domain, index i is omitted. If we consider filtering with a predetermined number of coefficients N_{Taps}, $S_{\text{P}(k)}$ contains the N_{Taps} positions from the pilot grid closest to the estimated position k. An example for $N_{\text{Taps}} = 3$ is presented in Fig. 3.15. A set of coefficients $\mathbf{w}_k$ needs to be computed for each estimated position k. This can result in either symmetric ($\mathbf{w}_{15}$) or asymmetric ($\mathbf{w}_2$) designs depending on the position of the coefficient to be estimated with respect to the distribution of the pilots.

The coefficients $\mathbf{w}_k$ minimizing the MSE for position k:

$$\text{MSE}_k = E\left\{\left|\hat{H}[k] - H[k]\right|^2\right\} \tag{3.46}$$

are computed based on the N_{Taps}–sized cross-correlation function $\boldsymbol{\rho}_{\text{C},k}$ between the channel coefficients $H[k]$ and its observations $H^{'}[k_{\text{P}}]\Big|_{k_{\text{P}} \in S_{\text{P}(k)}}$ with elements:

$$\rho_{\text{C}}[k, k_{\text{P}}] = E\left\{H[k]H^{'*}[k_{\text{P}}]\right\}\Big|_{k_{\text{P}} \in S_{\text{P}(k)}} \tag{3.47}$$

and respectively the $N_{\text{Taps}} \times N_{\text{Taps}}$ autocorrelation function of the observations in Toeplitz matrix form $\mathbf{R}^{'}$, with elements:

$$\rho_{\text{A}}[k_{\text{P}}^{'}, k_{\text{P}}^{''}] = E\left\{H^{'}[k_{\text{P}}^{'}]H^{'*}[k_{\text{P}}^{''}]\right\}\Big|_{k_{\text{P}}^{'}, k_{\text{P}}^{''} \in S_{\text{P}(k)}}. \tag{3.48}$$

The set of coefficients $\mathbf{w}_k$ can thus be computed as:

$$\mathbf{w}_k = \mathbf{R}^{'-1}\boldsymbol{\rho}_{\text{C},k}. \tag{3.49}$$

Let us concentrate on the uplink. At BS, the channels of different users sharing the same resource need to be estimated. A solution would be to employ dedicated pilot positions specific

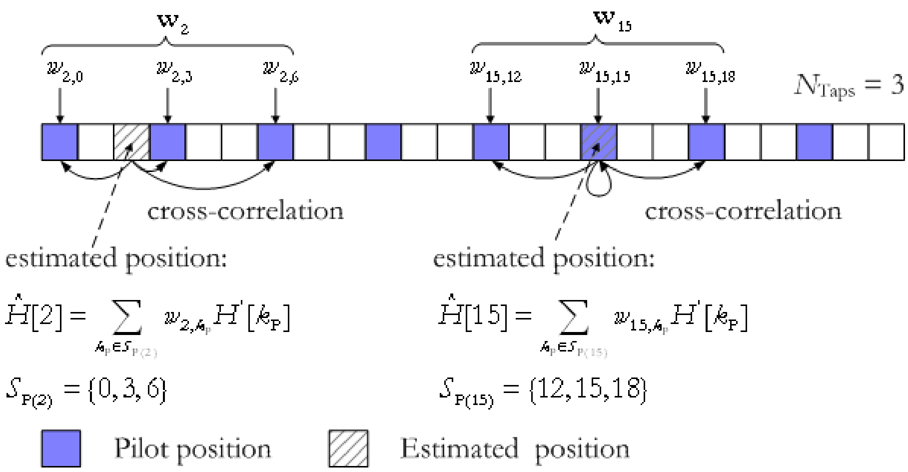

Fig. 3.15 Example of a one-dimensional 3-tap Wiener filter.

to each user, as in downlink, but this may lead to significantly increased pilot overhead, which gets prohibitive for large number of users [Säl04].

Solutions like the one in Fig. 3.14 – (a) are preferred in the uplink. Each user uses a dedicated training sequence and all users send their pilots within the same dedicated MC-type symbols. Constant Amplitude Zero Autocorrelation (CAZAC) sequences are a classical choice of training sequence. 3GPP LTE for example uses Zadoff-Chu polyphase CAZAC sequences as reference pilot signals [TS36211]. These sequences exhibit the useful property that cyclic-shifted versions of themselves remain orthogonal to one another, property important in the MIMO cases. A Zadoff–Chu sequence that has not been shifted is known as a root sequence. The n-th position of the q-th root Zadoff-Chu sequence of length N_{ZC} is defined as:

$$z_q[n] = \exp\left(-j\pi q \frac{n(n+1)}{N_{\mathrm{ZC}}}\right),\ n = 0 \ldots N_{\mathrm{ZC}} - 1. \qquad (3.50)$$

In order for the cross-correlation between two root sequences to be low, N_{ZC} needs to be prime. Let us detail the approach that will be used in the present work to study the impact of real channel estimation on the system performance. We are considering a solution like the one in Fig. 3.14 – (a), where one or several full MC-type symbols per frame are dedicated to carry the pilots. In this case, since we dispose of observations for all the used subcarriers, no interpolation is necessary in the frequency domain and the number of coefficients to be computed can be reduced. The role of the Wiener filter is to perform smoothing in the frequency-domain, reducing thus the estimation noise level $\sigma_{\eta_{\mathrm{P}}}$. Complexity is reduced by assuming fixed filter design: coefficients $\mathbf{w}_k$ are computed only once and applied to all pilot symbols as long as the statistical properties of the channel are assumed invariant. Asymmetric filters are computed for the border positions. One symmetric filter, shifted accordingly, is used for the center positions. For example, in a system with $M = 12$ used subcarriers and $N_{\mathrm{Taps}} = 5$, we need to compute 4 asymmetric filters (2 for each border side) and one symmetric filter for the rest of the band.

To compute the filter coefficients, some assumptions on the statistical properties of the channel need to be made. Wiener design relies on the cross-correlation and autocorrelation functions in (3.47), (3.48), which are generally unknown. These functions may be estimated from the channel observations, but this implies frequent updates of the filter coefficients. Another approach is to assume that the channel PDP has a rectangular shape [Säl04]. Common assumptions suppose this duration to equal either the delay spread $\tau_{\max}$ or the duration of the cyclic prefix T_{CP}:

$$P_h(\tau) = \begin{cases} \dfrac{1}{T_{\mathrm{CP}}}, & \tau \in [0, T_{\mathrm{CP}}) \\ 0, & \text{otherwise} \end{cases}. \qquad (3.51)$$

This leads to:

$$\rho_{\mathrm{C}}[k,k_{\mathrm{P}}]=\mathrm{sinc}(T_{\mathrm{CP}}\Delta f(k-k_{\mathrm{P}}))\exp(-j\pi T_{\mathrm{CP}}\Delta f(k-k_{\mathrm{P}})),\quad k,k_{\mathrm{P}}=0...M-1 \tag{3.52}$$

and respectively:

$$\begin{aligned}\rho_{\mathrm{A}}[k_{\mathrm{P}}^{'},k_{\mathrm{P}}^{''}]=\mathrm{sinc}(T_{\mathrm{CP}}\Delta f(k_{\mathrm{P}}^{'}-k_{\mathrm{P}}^{''}))\exp(-j\pi T_{\mathrm{CP}}\Delta f(k_{\mathrm{P}}^{'}-k_{\mathrm{P}}^{''}))+\sigma_{\eta_{\mathrm{P}}}^{2}\delta[k_{\mathrm{P}}^{'}-k_{\mathrm{P}}^{''}],\\ k_{\mathrm{P}}^{'},k_{\mathrm{P}}^{''}=0...M-1\end{aligned} \tag{3.53}$$

Fixed filter design based on the assumption of an uniform delay power spectrum of the channel is a good trade-off between complexity and performance and provides a robust design. To keep a fixed filter design, $\sigma_{\eta_{\mathrm{P}}}^{2}$ is generally taken as a constant, underestimated with respect to its real value according to the predefined system operating point. This model, presented here in SISO context, is applicable to SIMO transmission as well and can be easily extended to MIMO systems. To distinguish between different transmit antennas, cyclic-shifted versions of the same CAZAC sequence are sent onto different antennas. When estimating the channel from one particular Tx antenna, the role of the Wiener filter is to eliminate not only the transmission noise but also the jammer signal consisting in the pilots of the other Tx antennas. Equation (3.53) needs to be modified accordingly.

3.5. Performance of the conventional single-antenna system

In this chapter we have so far separately analyzed the main features of three systems that are good candidates for the air interface of future mobile systems. Let us now perform a numerical analysis of the presented systems, comparing their performance in realistic scenarios for B3G/4G systems. We will choose a simulation configuration drawn from practical specifications [TS36211] referring to the LTE Physical Uplink Shared Channel (PUSCH). The basic unit of transmission is a sub-frame of duration 1ms. Groups of 10 sub-frames constitute a frame, of duration 10ms. Each sub-frame is composed of 2 slots, each slot comprising 7 OFDMA-like symbols, among which 6 are data symbols and one is reserved for pilot sequences, as depicted in Fig. 3.16.

Let us consider a system with $N=512$ subcarriers, among which $M_{\max}$=300 are active data carriers, to fit a bandwidth W of 5 MHz. One DC subcarrier is allocated when pure OFDMA is employed. Remaining 211/212 subcarriers are used as guard interval. This allocation corresponds

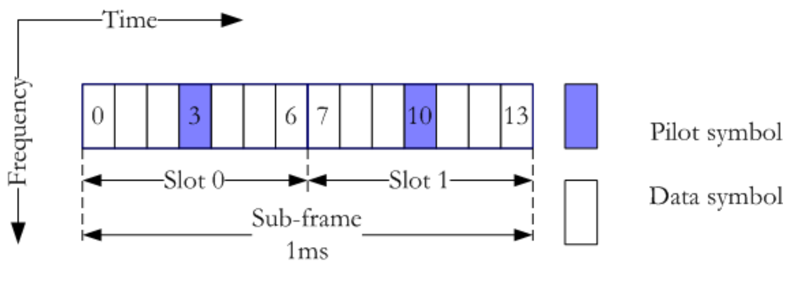

Fig. 3.16 Uplink sub-frame structure.

to a sampling frequency $F_s = 7.68$ MHz. Simulation parameters are summarized in Table 3.1. Active subcarriers are divided into 25 resource blocks (RBs) of 12 data subcarriers each. Each active user is allocated M subcarriers, where M is a multiple of 12 (integer number of RBs), and we will investigate here typical uplink cases when less than 5 RBs are allocated to each user. To retrieve frequency diversity, groups of $N_{\text{Sym}} = 12$ OFDMA-like symbols based on QAM constellations are encoded together. Data is scrambled before coding and interleaved prior to QAM mapping. FEC is a turbo code (TC) using the LTE interleaving pattern [TS36212].

A cyclic prefix with a length of $N_{\text{CP}} = 31$ samples is employed. We consider an uncorrelated SCM Vehicular A channel profile with 6 taps and a maximum delay spread of 2.51 μs. This corresponds to a coherence bandwidth of 400 kHz, or about 26 subcarriers in the present simulation scenario. Fig. 3.17 presents a frequency-domain realization of the channel against the subcarrier index. An example of localized and distributed spectral allocation is also presented, for 1 RB (12 allocated subcarriers). 12 localized subcarriers are strongly correlated, while 12 distributed subcarriers experience independent channel fadings. These properties influence the trade-off between intercode interference and diversity, as it will be seen in the sequel.

At the receiver, we assume either perfect channel state information (CSI), or real channel estimation. In this latter case, the pilot symbol splitting each slot is a Zadoff-Chu sequence (3.50) of prime N_{ZC} length. Channel estimation is performed by frequency smoothing with a Wiener filter (3.49) of length $N_{\text{Taps}} = 11$, followed by time-domain interpolation when possible. The Wiener filter is based on a fixed design relying on assumptions (3.51)-(3.53).

Table 3.1 Simulation parameters

Parameter	**Value**
Bandwidth W	5 MHz
Sampling frequency F_s	7.68 MHz
Carrier frequency F_c	2 GHz
Modulation scheme	OFDMA, SC-FDMA or SS-MC-MA
Constellation mapping	QPSK, 16QAM or 64QAM
FFT size N	512
Number of data subcarriers $M_{\max}$	300
Number of used subcarriers M	12 or 60 (1 or 5 RBs)
CP length N_{CP}	31 samples
FEC	TC 1/2, 3/4, 5/6 or uncoded
Data symbols per sub-frame N_{Sym}	12
Pilots per sub-frame	2, in position 3 and 10
Channel	SCM Vehicular A
MS velocity	0, 30, 120 or 300 kmph
Channel estimation	Either perfect CSI or Wiener filtering
Equalization	Phase compensation for OFDMA, MMSE otherwise

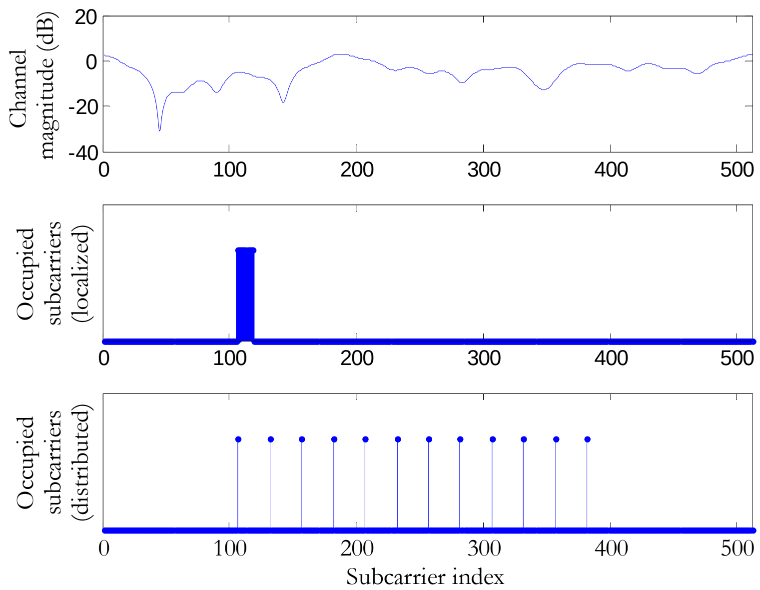

Fig. 3.17 Channel magnitude and spectral allocation.

MMSE equalization is performed for SC-FDMA and SS-MC-MA. In the case of OFDMA, the used equalization scheme has little importance, as they all would lead to the same performance: Indeed, following the reasoning in 3.4.1, it appears that the process of equalization followed by LLR correction is equivalent to only applying a phase correction factor, the effect of the amplitude equalization being cancelled (after soft demapping) by the LLR correction.

In this subsection we neglect the presence of nonlinearities.

3.5.1. OFDMA versus SC-FDMA and SS-MC-MA performance

In a first instance, we consider perfect CSI at the receiver: $\hat{\mathbf{H}} = \mathbf{H}$ and the equalizer is capable of perfectly compensating the effects of the frequency selective channel. 60 distributed subcarriers (5 RBs) are allocated to a static user. In Fig. 3.18 QPSK is employed. SC-FDMA and SS-MC-MA have similar Frame Error Rate (FER) performances because they both tend to recover the frequency diversity in the same manner thanks to their symbol energy spreading property. Since OFDMA has no built-in diversity, its performance is very dependent on the coding rate. When a high coding rate or an uncoded system is employed, OFDMA performs poorly because coding does not manage to compensate the influence of carriers with a low SNR. When stronger coding is present (*e.g.*, rate 1/2), OFDMA benefits from the coding diversity and thus it recovers the difference and even outperforms SC-FDMA/SS-MC-MA by 0.5 dB at FER=1%. With higher level modulations, there is a tradeoff [GaFu05] between the frequency diversity gain (due to the spreading performed in SC-FDMA / SS-MC-MA), coding gain and intercode interference.

Let us examine the FER results in Fig. 3.19 - Fig. 3.20, centered on a target FER of 1%. We omitted the performance of SS-MC-MA, since it is completely equivalent to that of SC-FDMA.

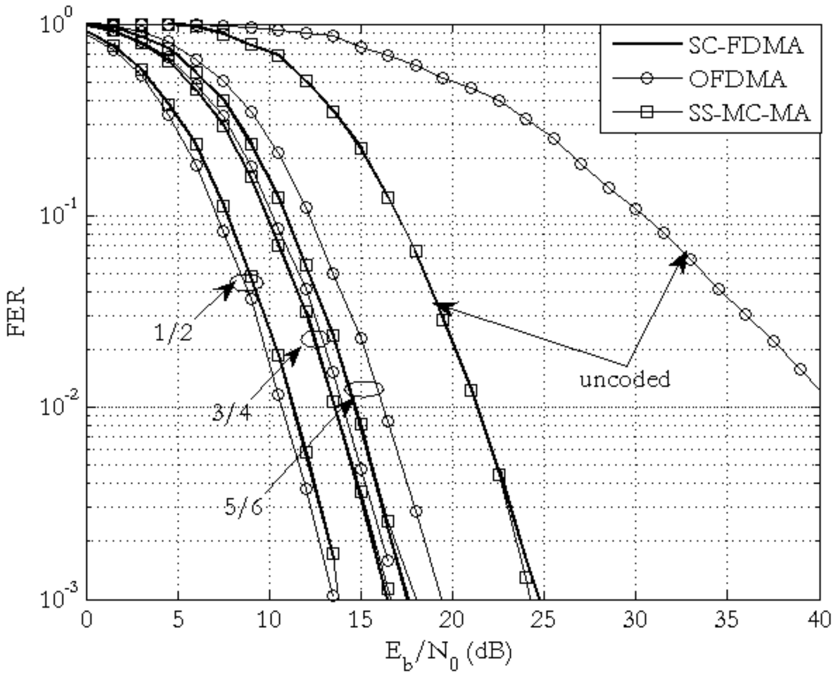

Fig. 3.18 FER performance, QPSK at different coding rates, 5 distributed RBs, no HPA, Vehicular A channel.

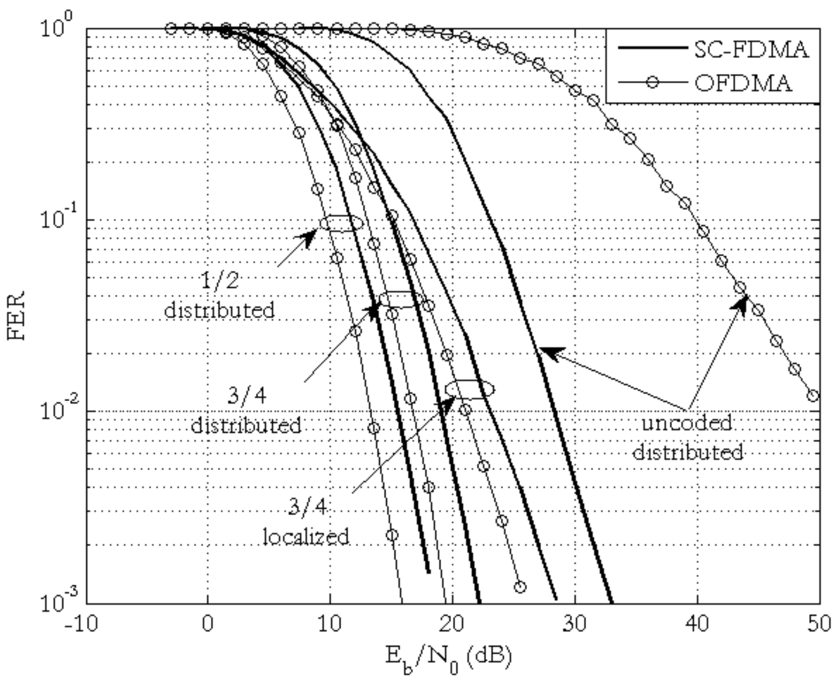

Fig. 3.19 FER performance, 16QAM at different coding rates, 5 RBs, no HPA, Vehicular A channel, perfect CSI.

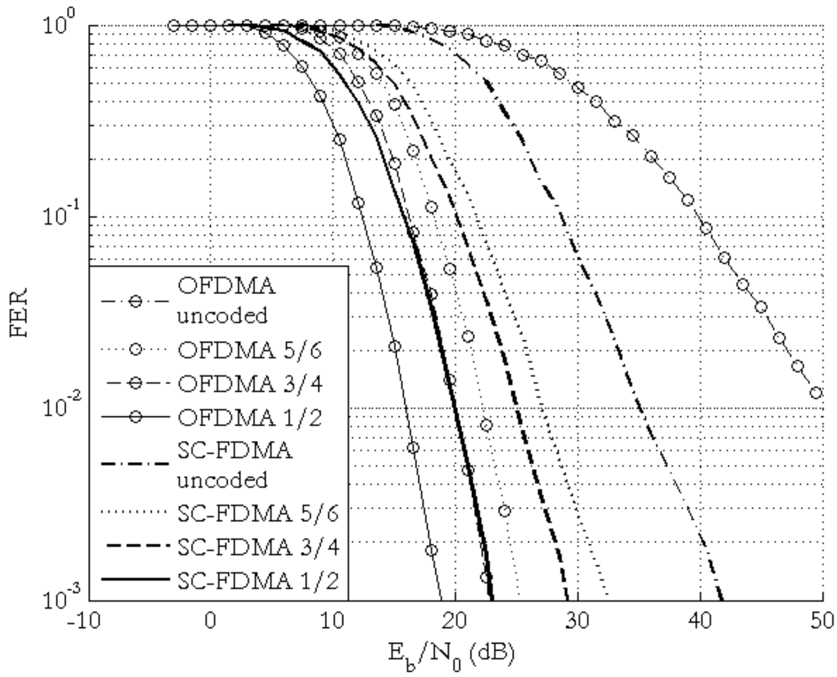

Fig. 3.20 FER performance, 64QAM at different coding rates, 5 distributed RBs, no HPA, Vehicular A channel, perfect CSI.

Distributed over localized results will be discussed later in this subsection. Let us now concentrate of the performance behavior for different modulation orders. We notice that SC-FDMA is more sensitive to intercode interference when the modulation order increases (16QAM, 64QAM). In that case, coded OFDMA has better performance. The higher the modulation order, the more accentuated this effect is: OFDMA TC1/2, for example, outperforms SC-FDMA by 0.6 dB, 2.2 dB and 3.9 dB when employing QPSK, 16QAM and 64QAM respectively. The numerical results reported in Table 3.2 show the gain of OFDMA over SC-FDMA at 10% FER in a large number of scenarios (NB: 10% FER is a reasonable operating point as Automatic Repeat reQuest –ARQ– may decrease FER down to 1%).

SC-FDMA outperforms OFDMA when low modulation order (QPSK) or uncoded modulation is employed. When the strength of the code decreases, OFDMA starts to perform poorly. There is a trade-off between frequency diversity gain and intercode interference. In distributed uncoded scenarios the gain of SC-FDMA over OFDMA is greater than in localized uncoded scenarios (*e.g.* 5.5 dB of difference for QPSK 5 RBs between the relative gain in distributed and respectively localized scenarios) because more frequency diversity is present. But when the modulation order increases, this relative gain decreases as the intercode interference affects SC-FDMA. This effect is more pronounced for distributed scenarios, where channel frequency selectivity is more important and thus the intercode interference gets larger. For 64QAM 5 RBs, only 2.1 dB of difference exist between the relative gains of localized and distributed scenarios.

Table 3.2 Gain of OFDMA over SC-FDMA in terms of E_b/N_0 (dB) at different coding rates with 1 or 5 allocated RBs, distributed and localized.

FER=1%		QPSK (dB)		16QAM (dB)		64QAM (dB)	
		1 RB	5 RBs	1 RB	5 RBs	1 RB	5 RBs
localized	1/2	0.4	0.5	1.8	2.6	2.5	4.4
	3/4	-0.8	-0.8	1.1	2.0	1.9	4.8
	5/6	-1.7	-1.8	0.3	1.0	1.2	3.9
	uncoded	-4.2	-13.6	-3.8	-13.2	-3.5	-12.8
distributed	1/2	0.6	0.6	2.9	2.2	6.7	3.9
	3/4	-1.4	-0.5	3.8	2.3	7.9	5.2
	5/6	-2.0	-1.6	3.1	1.4	6.7	4.9
	uncoded	-13.4	-19.3	-10.3	-17.5	-8.63	-14.9

Let us revisit Fig. 3.19, where distributed versus localized scenarios are also presented. Localized subcarrier mapping has poorer performance as it recovers less diversity than distributed mapping. Indeed, when data is spread in the whole bandwidth, the signal has more chances to experience different channel fades than in the case where all allocated carriers are contiguous. In this second case, due to the fact that adjacent carriers are correlated, less diversity can be recovered. Some partial results considering convolutional FEC and a channel profile with more available diversity have been discussed in [CiMo08a], leading to results consistent with the ones presented here. Some partial results considering convolutional FEC and a channel profile with more available diversity have been discussed in [CiMo08a], leading to results consistent with the ones presented here.

The results tend to be in favor of distributed allocation and OFDMA. Nevertheless, further investigation needs to be performed by taking into account the impact of channel estimation and HPA in order to draw clear conclusions. This will be dealt with in subsection 3.5.2 and 3.6.

3.5.2. Distributed versus localized and localized FH subcarrier mapping

In practice, this loss between localized and distributed carrier mapping shown in the previous subsection is compensated by employing frequency hopping (FH) techniques. Localized mapping is used for each slot, but the allocated bandwidth changes between the first and the second slot of a sub-frame. Since all OFDMA-like symbols in a sub-frame correspond to a single codeword, the transmitted signal experiences two different channel realizations and manages to recover more diversity than in a localized scenario. The advantage of this technique is that it does not need any a priori CSI at the transmitter as opposed to, *e.g.*, localized mapping with scheduling which would allocate to each user a portion of the spectrum where the channel has a convenient realization.

When comparing distributed, localized and frequency hopping techniques, channel estimation can no longer be neglected as it impacts differently on different subcarrier allocation scenarios. Fig. 3.22 presents the FER performance of a SC-FDMA system with distributed, localized and frequency hopping subcarrier mapping, using perfect CSI and real channel estimation at the receiver respectively. The user is allocated 60 RBs and has a velocity of 3 kmph.

Employing FH recovers some more diversity than employing localized frequency mapping, but less than the distributed case. Using channel estimation obviously leads to some performance loss with respect to the case of perfect CSI at the receiver: 3.4 dB, 1.1 dB and 1.3 dB at FER=1% when distributed, localized and FH is employed, respectively. These different degradations result from the fact that different processing needs to be employed to estimate the channel. For localized subcarrier mapping, the Wiener filter takes advantage of the channel's correlation profile in the frequency domain to maximize the SNR of the estimation as in (3.45). The time-domain variations introduced by the Doppler effect are tracked by time-domain interpolation.

For distributed subcarrier mapping, since pilots are placed rather far away from each other, they experience almost uncorrelated channel realizations. In this case, Wiener filtering is not possible because in the vicinity of the estimated position there is no other position from the pilot grid correlated to the estimated position. Channel estimation module simply divides the received noisy pilot by its original value to determine $\hat{H}[k_p, i_p] = H'[k_p, i_p]$ as in (3.43). Estimation noise is higher than in the localized case, which leads to a lower performance of the channel estimation module. Time-domain interpolation is still possible. Also, distributed systems are known to be more vulnerable to frequency offsets.

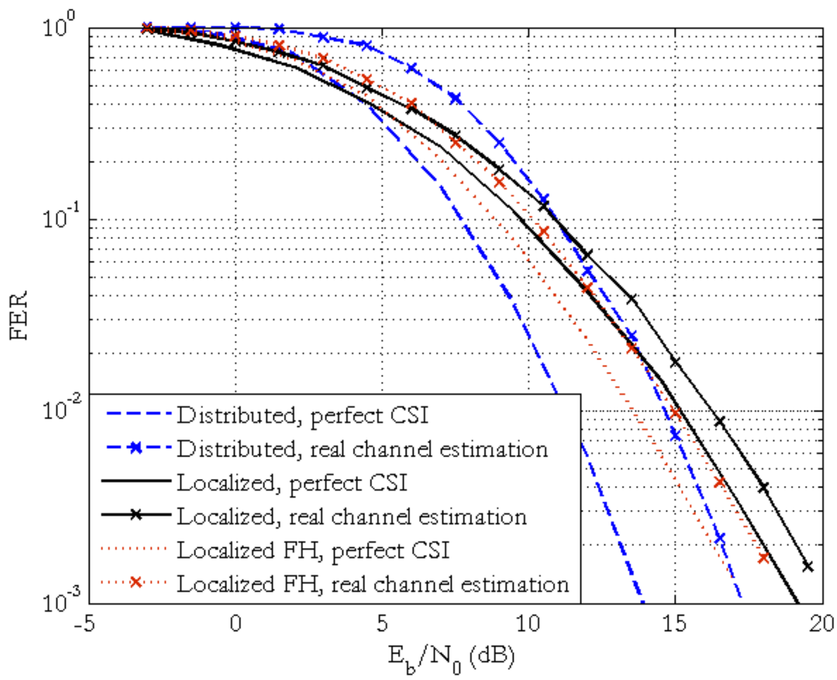

Fig. 3.21 FER performance, SC-FDMA, QPSK TC1/2, 5 RBs with different subcarrier mappings, no HPA, Vehicular A channel, 3 kmph.

In the FH case, Wiener filtering can be applied in the frequency domain, just as in a localized scenario. On the other hand, since each slot will experience a different channel realization, time-domain interpolation is no longer possible between the two channel observations. The channel corresponding to the transmission of each slot will be estimated as being time-domain invariant and equal to the estimate performed in the pilot position. When the channel does not vary much in the time domain, this estimation technique leads to good results, as seen in Fig. 3.21, where the channel has negligible time-domain variations due to low user mobility.

Let us now analyze the results in Fig. 3.22, where the performance of the FH technique is estimated in different mobility scenarios. With perfect CSI, performance improves at high velocities because the system gains in time diversity. In practice, with real channel estimation, performance quickly deteriorates in high mobility scenarios. While at 30 kmph degradation remains acceptable, at 300 kmph estimation errors are no longer manageable. The impossibility of tracking the time variations of the channel when FH techniques are employed leads to high estimation errors and thus to an error floor, higher at high velocities. Moreover, we also note a tendency of further deterioration of the FER performance at high SNR, which comes from the fact that the MMSE equalizer is based on the knowledge (perfect or estimated) of the variance σ^2 of the AWGN affecting the channel, which becomes vanishing. Yet, the important level channel estimation error disrupts the functioning of the MMSE equalizer expecting low input noise. This can be alleviated by using overestimated values $\hat{\sigma}^2 > \sigma^2$ when σ^2 falls below a certain threshold, or designing specific estimation techniques for σ^2 which take into account the effects of channel estimation noise.

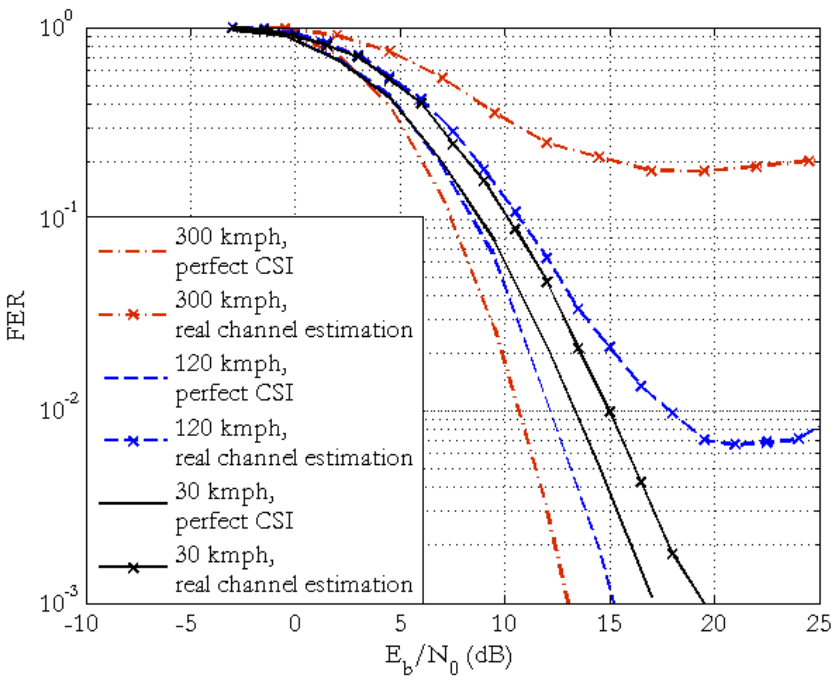

Fig. 3.22 FER performance, SC-FDMA, QPSK TC1/2, 5 localized RBs with frequency hopping, no HPA, Vehicular A channel.

Present results do not take into account any error control methods (*e.g.*, HARQ). To estimate the comparative performance of the three presented scenarios, it seems reasonable to interpret the FER curves with channel estimation for a target FER between 1% and 10%. In Fig. 3.21, this leads to the conclusion that distributed and localized systems have similar performance, while FH has a slight advantage (0.8 dB) at low velocities. Localized and localized FH techniques can be further improved by using more complex channel estimation methods. Localized frequency mapping with scheduling is susceptible of giving better performance than its competitors at the expense of a scheduling effort. FH techniques are suitable choices in pedestrian or low velocities scenarios, but are very sensitive to important Doppler shifts.

3.6. Impact of nonlinearities

Results in the previous subsection give a good idea about the relative performance of the three analyzed schemes in a linear environment. Let us see how the presence of a nonlinear HPA affects the behavior of these systems. To evaluate this impact, we impose realistic constraints on the system's behavior. We will consider a set of requirements similar to the ones demanded by 3GPP LTE [TS36101]. Table 3.3 summarizes the requirements considered in this subsection.

3.6.1. Signal envelope variations

Let us consider that 5 RBs are allocated to each user. Fig. 3.23 presents the CCDF of INP of SC-FDMA, OFDMA and SS-MC-MA with QPSK, 16QAM and 64QAM signal mappings. An oversampling factor $L_{\mathrm{ovs}} = 4$ is considered. The SC properties of SC-FDMA result in low envelope variations for all subcarrier mapping types: At a clipping probability per sample of 10^{-4}, SC-FDMA outperforms OFDMA by 2.7 dB, 1.9 dB and 1.8 dB when QPSK, 16QAM and 64QAM are employed, respectively. OFDMA exhibits high envelope variations for all subcarrier mappings. SS-MC-MA has somewhat lower PAPR than OFDMA, but still largely superior to SC-FDMA.

Distributed and localized SC-FDMA exhibit the same good performance for all subcarrier mapping types (results for 16QAM and 64QAM are not plotted here for better figure readability). This result can be confirmed for all spectral allocations (1 to 25 RBs allocated to the same user). Note that this evaluation compares localized and distributed frequency-domain implementations of SC-FDMA, generated by the structure described in Table 3.1. No pulse shape filtering or time

Table 3.3 Minimum spectral requirements.

Parameter	Requirement
Spectrum mask	LTE for 5 MHz E-UTRA [TS36101]
Minimum ACLR	30 dB
Maximum EVM for QPSK	17.5%
Maximum output power P_{out}(QPSK, <8 RBs)	24 dBm

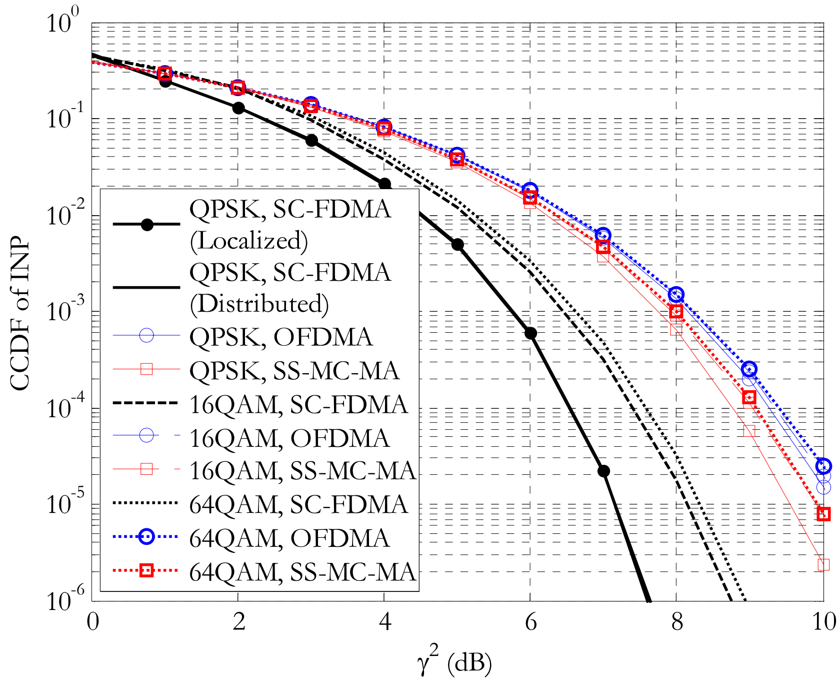

Fig. 3.23 CCDF of INP for SC-FDMA, OFDMA and SS-MC-MA, 5 localized RBs, QPSK/16QAM/64QAM.

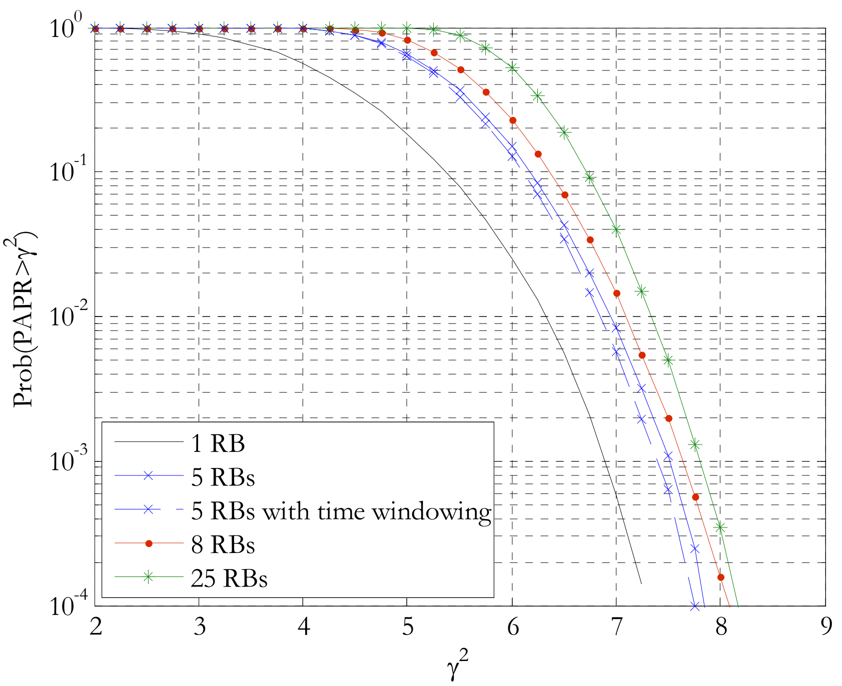

Fig. 3.24 CCDF of PAPR, localized SC-FDMA, QPSK, different number of RBs.

windowing were performed. Ideal IFDMA (with no guard intervals) is reported to have a somewhat lower PAPR than SC-FDMA [Lge05], since introducing the guard intervals increments the PAPR with respect to the ideal case. Increasing modulation order has a greater impact on SC-FDMA than on OFDMA, whose samples can be approximated with Gaussian variables for any modulation order, as discussed in subsection 3.3.2.

Just as for OFDMA, the PAPR of SC-FDMA increases when the number of allocated subcarriers increases. Indeed, each sample of the SC-FDMA signal is a weighted sum of M modulation symbols. When M is low, the probability that this weighted sum attains a high value is lower than when M has important values, but the nature of the signal does not change: Varying M has an impact on the CCDF of PAPR curves, but almost no impact on the CCDF of INP curves. Fig. 3.24 presents comparative results of the CCDF of PAPR for localized SC-FDMA, QPSK, with 1, 5, 8 and 25 RBs, respectively. At a clipping probability (per SC-FDMA symbol) of 10^{-3}, the PAPR increases by 0.6 dB, 0.7 dB and 0.9 dB when 5, 8 and 25 RBs respectively are used with respect to the case when one single RB is used. CCDF of INP results are omitted, since they are all similar to the corresponding curve in Fig. 3.23. The PAPR can be further reduced by employing time windowing. A gain of 0.1 dB is achieved by smoothing the transitions between SC-FDMA symbols with a Bartlett window (18 coefficients), as shown in Fig. 3.24 for 5 allocated RBs.

It is difficult to establish at what clipping probability it is pertinent to read the curves in Fig. 3.23 and Fig. 3.24. When working with normalized HPA models parameter γ^2 may be interpreted as the IBO, and the OBO(IBO) characteristics can be plotted for different types of signals. In order to correctly interpret the CCDF of PAPR or INP, we need to know the necessary amount of OBO for the system's operating point. In these conditions, the amount of gain read on the CCDF curves indicates a maximum potential gain that might be obtained if an ideal clipper HPA was employed [CiBu06]. As discussed in 3.1.3, CCDF curves give a measure of the signal's dynamic range, but do not explicitly take into account the presence of the nonlinearity.

3.6.2. Spectral analysis

To obtain a more realistic evaluation of the system's performance, let us analyze the effects introduced by an HPA. The Rapp and Saleh models will be employed here. As discussed in 3.1, three main limitations are imposed to a system in realistic scenarios: Comply with the spectrum mask requirements, comply with the Out-Of-Band (OOB) radiation limits, and preserve good system performance. Spectrum masks are defined by regulatory standards bodies, based on system-dependent prerequisites. OOB radiation limits are given under the form of maximum ACLR values. System performance directly depends on the degree of in-band distortion suffered by the signal, which is specified under the form of maximum EVM accepted levels.

Fig. 3.25 shows the spectrum of a SC-FDMA signal with 1 distributed RBs allocated to one user, with QPSK signal mapping. The Rapp HPA is employed. Since less than 8 RBs are allocated, [TS36101] imposes that measurements be conducted for a maximum radiated power of

24 dBm. An OBO of 7.9 dB (corresponding to an IBO of 7.8 dB) is needed in order to comply with the spectrum mask requirements. The mask constraint is in this case stronger than the ACLR and EVM constraint, which are largely complied with for values of 36.1 dB and 1.9% respectively. Similar considerations show that OFDMA / SS-MC-MA would require an OBO of 9.6 dB (which corresponds to IBO=9.5 dB, 35.9 dB of ACLR and an EVM of 2.4%) in order to comply with the mask. Thus, employing SC-FDMA brings a gain of 1.7 dB in terms of OBO.

Let us now consider the case of localized subcarrier mapping, depicted in Fig. 3.26. The worst-case scenario of spectral allocation is when the RBs are allocated at the edge of the band, causing a maximum of OOB radiation. Spectrum mask still remains the hardest constraint, but the EVM value becomes critical: At $\text{OBO} = 4.5\text{dB}$, OFDMA with 1 localized RB exhibits an EVM of 17.1%. Employing SC-FDMA brings an OBO gain of 1.4 dB. This gain is brought to 2 dB when 5 localized RBs are employed.

Even if the PAPR of distributed and localized MC systems described here are roughly the same, a more important back-off is required in the distributed case. This effect is due to the different spectral repartition of the subcarriers, which give rise to different profiles of the third-order intermodulation product (IMP) after passing through the HPA. Mathematically, this is represented by the term $G_3 v_{\text{IN}}^3$ in (3.12). The HPA nonlinearity can be regarded as a question of the regeneration of new spectral components and/or modifications in the fundamental signal with increasing power level. A signal containing spectral components on a set of fundamental frequencies f_i with $i = 0 \ldots M-1$ for example, will grow, after passing through the HPA, IMP on all frequencies $\sum k_i f_i$ where k_i are integers. The IMP's order is given by $\sum |k_i|$. In practical applications, odd-order IMP is of most interest, as it falls within the vicinity of the original frequency components, and may therefore interfere with the desired behavior. Third order IMP is the main cause of OOB. In a localized scenario the IMP will mainly affect the spectrum in the very vicinity of the occupied subcarriers, leading to a spectral "enlargement" noticeable in Fig. 3.26. On the other hand, in a distributed scenario, due to the regular repartition of the occupied subcarriers throughout the transmission bandwidth, the third-order IMP will create the comb-shaped OOB profile in Fig. 3.25. The spectral spikes generated in the third order harmonic zone need to respect the spectral mask, which leads to more severe spectral limitations than in the localized case. This effect cannot be anticipated from CM measurements: Indeed, it is not the power of the third order harmonics which differs between the localized and distributed cases, but their spectral repartitioning. One can alleviate this regrowth by employing stronger filtering in the oversampling process. Steeper filters would of course reduce the OOB but would introduce more in-band distortion due to the ripple effects and would also complicate the filtering task with respect to localized scenarios. Thus, localized subcarrier mapping turns out to be more convenient from the point of view of spectral constraints.

Table 3.4 summarizes the behavior of OFDMA and SC-FDMA under spectrum constraints with a Rapp HPA. In all the presented scenarios, the spectrum mask is the hardest constraint. We notice that the CM gain of SC-FDMA over OFDMA, which is in the order of 2.4-2.7 dB, overestimates the OBO gain (1.4-2 dB) in this particular case when a Rapp amplifier is used.

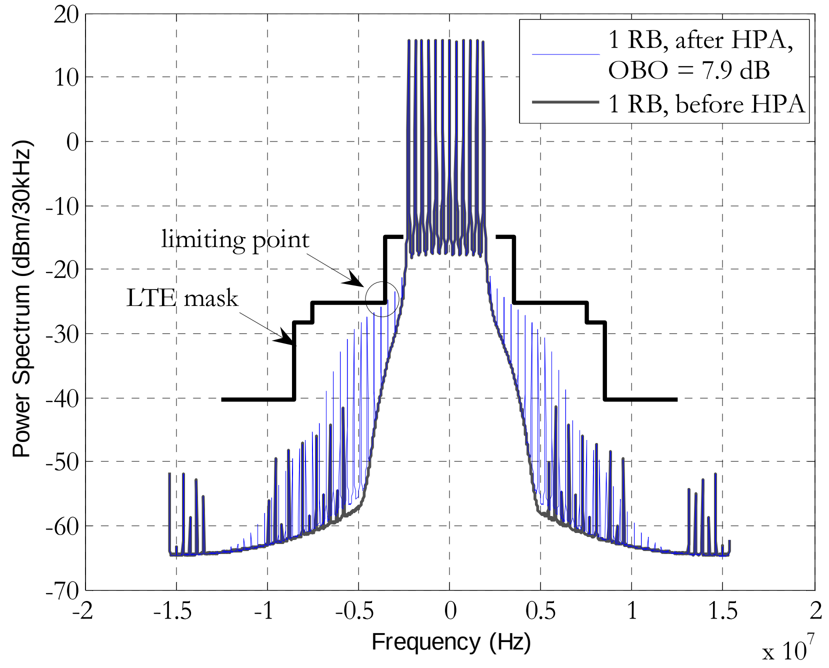

Fig. 3.25 Spectrum of distributed SC-FDMA @ Pout=24 dBm, QPSK, 1 RB, Rapp HPA.

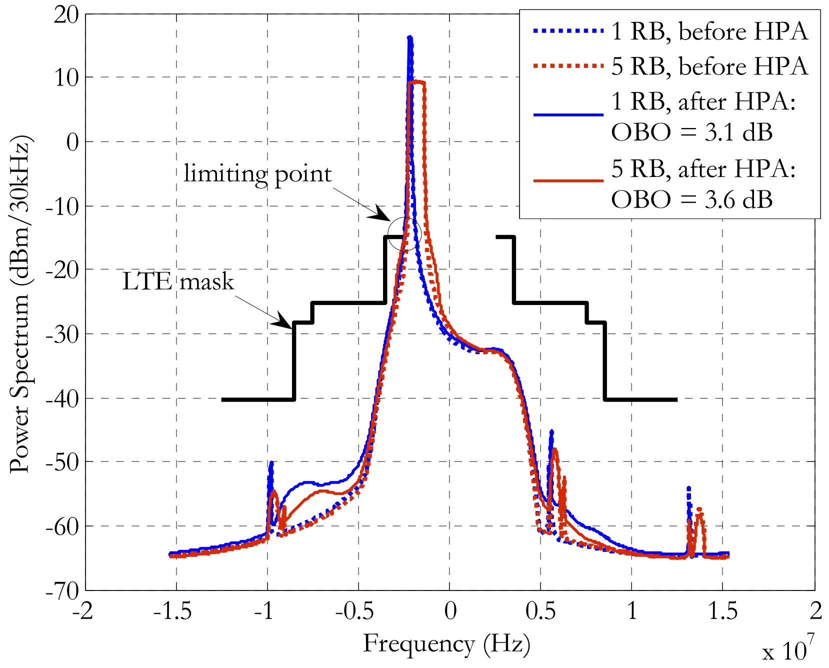

Fig. 3.26 Spectrum of localized SC-FDMA @ Pout=24 dBm, QPSK, 1 or 5 RBs, Rapp HPA.

Table 3.4 Comparative performance of OFDMA and SC-FDMA with QPSK constellation mapping under spectrum constraints, Rapp HPA.

Rapp HPA, $p_{\mathrm{Rapp}}=2$		SC-FDMA 1 RB	SC-FDMA 5 RBs	OFDMA 1 RB	OFDMA 5 RBs
localized	OBO (dB)	3.1	3.6	4.5	5.6
	IBO (dB)	2	2.8	3.3	4.8
	CM (dB)	1.97	1.96	4.4	4.7
	EVM (%)	14.6	11.6	17.1	12.2
	ACLR (dB)	30.9	31.7	31.8	32.7
distributed	OBO (dB)	7.9	6.1	9.6	7.8
	IBO (dB)	7.8	5.8	9.5	7.5
	CM (dB)	1.96	1.99	4.4	4.7
	EVM	1.9	4.3	2.4	5.4
	ACLR (dB)	36.1	34.5	35.9	33.8

When one single localized RB is used, the effect of spectral regrowth due to the presence of IMP is less important than in the case of a larger localized allocation (5 RBs), which explains larger OBO values in the latter case in order to comply with mask requirements. In the distributed case, the situation is reversed: Using more subcarriers means spreading the 3rd order IMP energy onto a finer frequency grid, which reduces the amplitude of the spikes and alleviates the mask constraints.

The Rapp amplifier model introduces amplitude distortion, but no phase distortion (see subsection 3.1.1). The in-band distortion (measured by EVM levels) is less significant than in the case of HPAs introducing phase distortions as the Saleh HPA, as it could be seen in Fig. 3.5. Table 3.5 describes the operating points of SC-FDMA and OFDMA systems with 1 or 5 localized RBs in the presence of a Saleh HPA model. With respect to the situation summarized in Table 3.4, here the EVM is the strongest constraint. Operating points lie at much more important back-offs when the Saleh model is employed, due to the more pronounced nonlinear HPA characteristic. The OBO gain of SC-FDMA over OFDMA is estimated to 1.7-1.8 dB, slightly higher than the case depicted in Table 3.4. Some preliminary results considering other types of amplifiers were obtained in [CiMo06], [Mit06], and are confirmed by the present analysis.

Note that all numerical results in this subsection strongly depend on the HPA type and on the spectral allocation. In a practice, conducting an extensive analysis based on OBO values would mean testing all possible configurations of subcarrier allocation, and still the results would be valid only for a given amplifier. From this point of view, when comparing two systems, INP evaluations turn out to be an useful tool, since they give a rather good approximation of the OBO difference to be expected in function of the operating point.

Table 3.5 Comparative performance of localized OFDMA and SC-FDMA with QPSK constellation mapping under EVM constraints, Saleh HPA

Saleh HPA, $\alpha=1, \beta=1/4, \alpha_p=\beta_p=1$		SC-FDMA		OFDMA	
		1 RB	5 RBs	1 RB	5 RBs
localized	OBO (dB)	8.9	8.9	10.6	10.7
	IBO (dB)	11.5	11.6	13.3	13.5
	CM (dB)	1.97	1.96	4.4	4.7
	EVM (%)	17.4	17.3	17.4	17.4
	ACLR (dB)	31.6	31.9	31.9	32.8

3.6.3. Overall system degradation

We have so far analyzed the spectral behavior of the system taking into account mask, ACLR and EVM constraints. Let us now investigate if the operating points previously indicated are acceptable from a performance point of view. The analysis in subsection 3.6.2 is completely independent of interleaving, coding or any other operation performed before constellation mapping. In order to separate the FER degradation due to nonlinear effects from the effects of the frequency selective channels seen in subsection 3.5, let us consider in a first step that transmission is being performed on AWGN channel. The impact of the HPA on the FER performance is depicted in Fig. 3.27, for SC-FDMA, QPSK TC3/4 with 5 localized RBs.

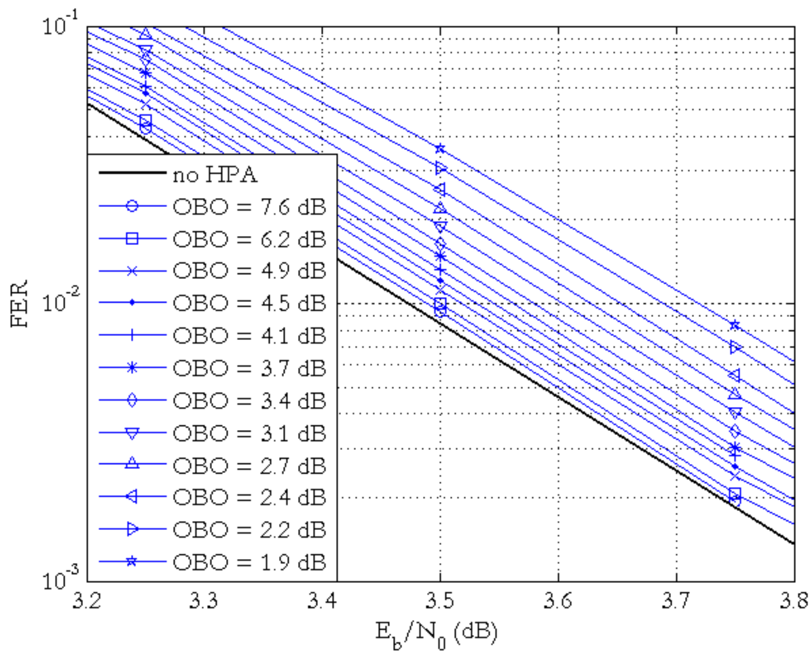

Fig. 3.27 FER performance, SC-FDMA, QPSK TC3/4, 5 localized RBs, Rapp HPA, AWGN channel, detail around target FER of 1%.

The FEC manages to alleviate the distortion introduced by the HPA. As expected, the lower the OBO, the higher the loss in E_b/N_0. However, even at strong distortion levels of OBO, unacceptable from a spectral point of view (see Table 3.4), the loss in E_b/N_0 is hardly superior to 0.2 dB. Stronger codes would lead to even better protection (and thus inferior loss), while uncoded or low-coded systems would suffer more from the effects of this distortion. To support this statement, let us examine Fig. 3.28 and the AWGN part of Fig. 3.29 and Fig. 3.30.

We marked by blue, red and green dots respectively the operating points of SC-FDMA OFDMA and SS-MC-MA systems resulting from the analysis in subsection 3.6.2. These figures represent the total system degradation against OBO as defined in (3.14). We use E_b/N_0 to illustrate the SNR loss. In Fig. 3.28 we represent the case when no coding is employed, while in Fig. 3.29 and Fig. 3.30 turbo codes of rate 3/4 and 1/2 are employed, respectively. We notice that the operating points determined by the spectral constraints lie in the linear region of the total degradation curves, rather far from the optimal operating point. This effect is even more accentuated in the coded case, where employing FEC partly masks the impact of the nonlinearity on the system performance and optimal operating points are unacceptable from a spectral point of view.

The advantage of SC-FDMA over OFDMA in terms of total degradation (approximately 2.1 dB in the coded case) mainly comes from the OBO gain (2 dB, see Table 3.4). On an AWGN channel, SS-MC-MA behaves like OFDMA, as it has similar PAPR properties.

Let us now see how these results evolve when taking into account the fact that on a frequency selective channel they have different diversity-recovering capabilities. To have a fair comparison, we have computed in Fig. 3.29 and Fig. 3.30 the total degradation of each system with respect to a same reference value for all the curves present in a same figure. This reference was considered to be the necessary E_b/N_0 to attain a target FER of 1% for a SC-FDMA system on AWGN channel in the absence of the HPA, when TC3/4 and TC1/2, respectively, are employed as FEC.

When TC3/4 is employed, the situation is favorable to SC-FDMA which outperforms OFDMA both in FER performance (0.8 dB) and in OBO performance (2.1 dB). The combined effects of these two criteria lead to an overall gain of 2.9 dB. At a stronger coding rate of 1/2, SC-FDMA is outperformed by OFDMA in terms of FER performance (0.5 dB), which reduces its 2.1 dB OBO advantage to 1.5 dB. When QPSK is employed, using SC-FDMA instead of ODFMA brings thus a performance improvement of at least 1.5 dB in the most unfavorable case. SS-MC-MA performs a trade-off between SC-FDMA-like behavior on frequency-selective channels and OFDMA-like behavior in the presence of nonlinearities. At high OBO, the system evolves in the linear region of the HPA with basically no nonlinear distortion: SS-MC-MA approaches SC-FDMA performance. At low OBO, the high PAPR exhibited by SS-MC-MA leads to strong distortion levels and SS-MC-MA performance degrades with respect to SC-FDMA. Using SS-MC-MA does not bring any real gain with respect to its competitors, as it achieves neither the good PAPR properties of SC-FDMA nor the FER performance of OFDMA.

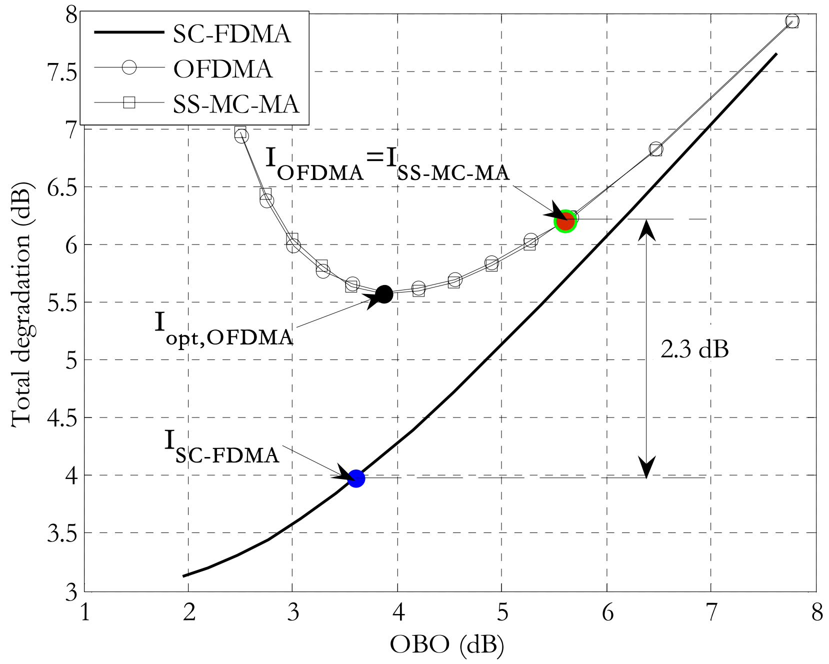

Fig. 3.28 Total system degradation of SC-FDMA, OFDMA and SS-MC-MA, QPSK uncoded, 5 localized RBs, Rapp HPA, AWGN channel, target FER 1%.

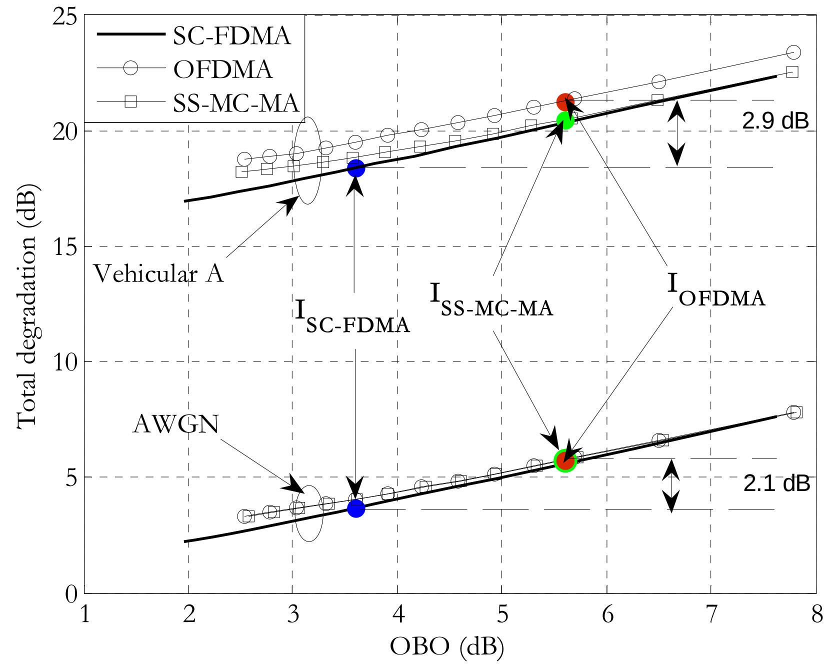

Fig. 3.29 Total system degradation of SC-FDMA and OFDMA, QPSK TC3/4, 5 localized RBs, Rapp HPA, AWGN and frequency selective channel, target FER 1%.

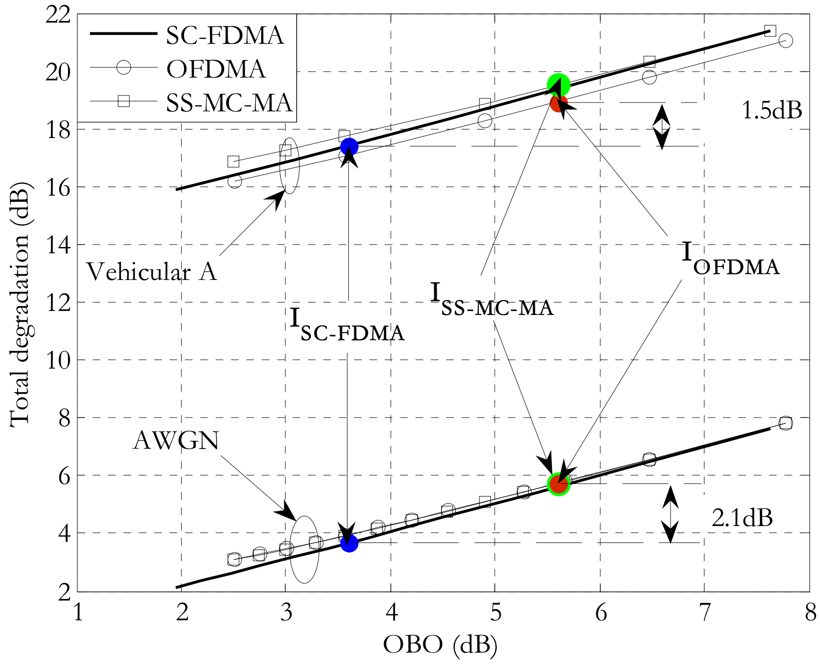

Fig. 3.30 Total system degradation of SC-FDMA, OFDMA and SS-MC-MA, QPSK TC1/2, 5 localized RBs, Rapp HPA, AWGN transmission, target FER 1%.

When the modulation order increases, OFDMA becomes more and more attractive. Indeed, the potential OBO gain of SC-FDMA over OFDMA decreases when the modulation order increases, as it can be seen in Fig. 3.23. Consequently, a gain of less than 2 dB is achieved in terms of OBO by employing SC-FDMA, which is largely outperformed by OFDMA (up to 4.4 dB for 64QAM as shown in Table 3.2).

Let us stress out the importance of channel estimation in the presence of nonlinearities. If the receiver was to have perfect CSI of the physical transmission channel, it would manage to perfectly compensate for the channel effects but performance would still be strongly impacted by the nonlinearity. Take for instance the case of Saleh HPA: even with perfect equalization, the constellation points suffer phase distortions that render detection difficult or even impossible for high modulation orders at acceptable levels of OBO. Yet, the presence of a channel estimation module "absorbs" in some sort the effect of the nonlinearity, since the equivalent channel (HPA plus physical channel) is estimated. In the equalization process, nonlinear distortion is partly corrected. On the other hand, we experience the same effects at high SNR as in the FH case. Particular precautions need to be taken when estimating the SNR at the receiver, so as to correctly take into account the estimation noise.

3.7. Summary and conclusions

We have presented and compared three multiple access schemes suitable for the uplink air interface of future mobile systems: SC-FDMA, OFDMA and SS-MC-MA. Details on the transmitter and receiver implementation are given.

We have described the specific constraints a mobile terminal needs to comply with in a real system, where strict levels of in-band distortions and out-of-band radiations are imposed. We have clarified and evaluated the impact of a nonlinear HPA on the three multiple access schemes performing in realistic scenarios and complying with regulated requirements.

While OFDMA has no built-in diversity, and has thus poor performance in the low-coded or uncoded cases, SC-FDMA (resp. SS-MC-MA) benefit from the diversity achieved by DFT (resp. Walsh) precoding, but tend to degrade due to the intercode interference at high modulation orders. A trade-off between diversity, coding gain and intercode interference exists.

Distributed subcarrier mapping benefits from higher diversity than localized subcarrier mapping, but distributed structures render channel estimation techniques less effective. Also, from a spectral point of view, distributed subcarrier mapping leads to an OOB radiation profile which is more likely to infringe spectral mask regulations than localized frequency mapping, especially when few RBs are allocated to a same user. Frequency hopping techniques show good performance at low velocities, but their performance rapidly degrades in high mobility scenarios, as the channel estimation module is unable to track the time-domain variations of the channel with a low number of pilots. It seems convenient to use FH techniques at low velocities and localized carrier mapping in high mobility scenarios.

SC-FDMA has the advantage of a lower PAPR than its competitors, which leads to a signal more robust to nonlinear distortions. An overall analysis shows that SC-FDMA outperforms OFDMA when QPSK is employed but might be over-performed when higher modulation orders are employed. This leads to the conclusion that SC-FDMA is a good choice for MS at cell edge, emitting at full power with low modulation orders. If the mobile station is close to the base station, MS can reduce its emission power which would alleviate the PAPR problem and/or use higher modulation orders. In this latter case, OFDMA is a good choice.

SS-MC-MA brings a compromise between these two techniques, but keeps the drawbacks of both: It has high OFDMA-like PAPR and suffers from intercode interference for high modulation orders as SC-FDMA.

The OBO is the determining factor to clarify the impact of a nonlinear amplification on a given transmission scheme. However, OBO is dependent on many parameters, such as the amplifier type or the spectral allocation. In order not to render our analysis too dependent on the used amplifier or on a specific configuration, in the following chapters we will mainly rely on CCDF of INP, which turns out to be a more reliable tool than CCDF of PAPR and which gives a good approximation of the OBO difference to be expected when comparing two systems.

Chapter 4

Transmit diversity in SC-FDMA systems with two transmit antennas

MIMO techniques have become an indispensable part of wireless communications systems in order to satisfy the ever increasing demands in throughput and performance. The use of multiple antennas both at the base station and at the terminal can improve the BER/FER performance by providing spatial diversity, increase the transmitted data rate through spatial multiplexing, reduce interference from other users, or make some trade-off among the above. MIMO techniques have been incorporated in all recent wireless communications standards (*e.g.*, IEEE 802.11n for wireless local area networks - WLAN, IEEE 802.16e-2005 for WiMAX, 3GPP LTE) and are actually under discussion at the 3GPP LTE-Advanced.

4.1. MIMO techniques

In subsection 2.3 we have discussed the physical properties of the MIMO channel and we have shown that, in MIMO systems, besides frequency and time there is a third available dimension which is space. In order to exploit the space dimension introduced by the presence of multiple transmit and/or receive antennas, different techniques have been developed to take advantage either of the supplementary degrees of freedom, or of the space diversity, or make some compromise between the two.

4.1.1. Diversity – multiplexing tradeoff

In any digital communication system, two key parameters describe the performance of the system: transmission rate and FER. The transmission rate describes how much information is being transferred in a certain interval of time, while FER is a measure of the quality of the transmission (as we have seen in the previous chapter, it represents the probability that a transmitted frame is erroneously decoded at the receiver). Intuitively, one cannot transmit an unlimited quantity of data through a limited resource without suffering any loss. At a fixed transmission rate, an increase in the link quality (increase in SNR) enables reduced FER. At a target FER, increased SNR enables increased data rates. In other words, a fundamental tradeoff exists between FER and transmission rate.

In MIMO systems, this tradeoff is usually expressed as a diversity-multiplexing tradeoff [ZhTs03], [TsVi05], as anticipated in subsection 2.5. Indeed, the transmission rate in a MIMO system essentially depends of the multiplexing gain R_{Mux}, given by the number of independent streams simultaneously sent through the system. The maximum multiplexing gain is given by the number of degrees of freedom of the MIMO channel, $\min(N_{\mathrm{Tx}}, N_{\mathrm{Rx}})$. On the other hand, the BER/FER decays like (2.36), its asymptotic slope being the system's diversity gain. The maximum order of diversity attainable by the system is given by the number of branches of diversity, $N_{\mathrm{Tx}}N_{\mathrm{Rx}}$. Diversity gain d is thus related to FER performance. The fundamental trade-off FER - transmission rate tradeoff translates into the diversity – multiplexing tradeoff $d(R_{\mathrm{Mux}})$, which is a central concept in MIMO systems.

For example, a 2x2 uncorrelated narrowband MIMO channel disposes of 2 degrees of freedom for a 4-fold available diversity. A repetition coding scheme sending the same symbol successively from the two antennas recovers all the spatial diversity, but uses only one half degree of freedom (one symbol sent over two periods of time). The Alamouti scheme also recovers all the available space diversity, and uses one degree of freedom (two symbols sent over two periods of time). Some systems attempt to use all the available degrees of freedom in a MIMO system as, *e.g.*, the BLAST (Bell Labs Layered Space-Time Architecture) scheme. Others make the best use of the available diversity, like the Alamouti scheme. Some compromise between the two is also possible, like in the double Alamouti scheme for example [Jaf05]. A flexible tradeoff can be achieved. The optimal tradeoff for Rayleygh iid channels is a piecewise linear curve [TsVi05] depicted in Fig. 4.1, connecting plots with coordinates (R_{Mux}, $d(R_{\mathrm{Mux}})$), where $R_{\mathrm{Mux}} = 0 \ldots \min(N_{\mathrm{Tx}}, N_{\mathrm{Rx}})$ and:

$$d(R_{\mathrm{Mux}}) = (N_{\mathrm{Tx}} - R_{\mathrm{Mux}})(N_{\mathrm{Rx}} - R_{\mathrm{Mux}}) \,. \tag{4.1}$$

In this chapter we will focus on a system using SC-FDMA multiple access in the uplink. Both MS and BS are equipped with at least 2 antennas each. We have seen in Chapter 3 that SC-FDMA is of interest especially for MS emitting at full power and using low-order modulation, which is typically the case at cell-edge, in bad propagation conditions or at high velocities. In such scenarios with users in poor conditions, it is reasonable to assume that MS has limited or unreliable channel knowledge and cannot efficiently use closed-loop methods to improve its multiplexing capabilities or implement transmission methods based on a priori CSI. This motivates us to concentrate on methods susceptible of maximizing the spatial diversity gain in order to take advantage of the presence of multiple transmit antennas at the MS. It should be understood that the same MS, at a different time, may be much closer to the base station with better propagation conditions so as to allow the use alternative MIMO solutions in order to exploit the potential multiplexing gain. As a result, the selection of the MIMO scheme becomes part of the link adaptation process in order to make the most of the actual user conditions.

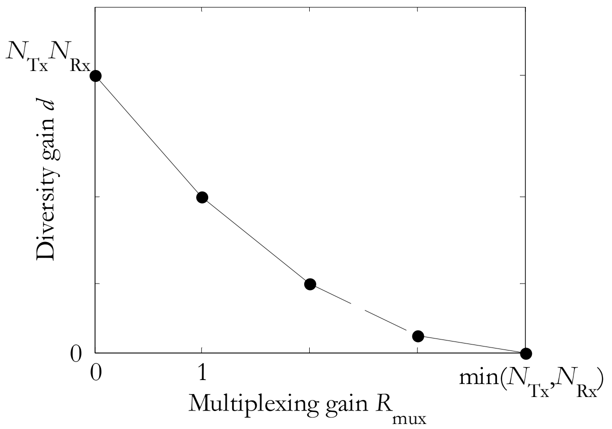

Fig. 4.1 Diversity – multiplexing tradeoff.

4.1.2. Transmit diversity

Transmit diversity is a form of spatial diversity which makes use of the presence of multiple transmit antennas to combat the detrimental effects of the fading channel. With respect to receive diversity, which is simply recovered by employing adequate detection techniques, exploiting transmit diversity needs using more sophisticated transmission techniques. Two main classes of techniques can be identified: When the transmitter does not have any information about the channel, the system is "open-loop"; when the receiver sends CSI information to the transmitter through a feedback channel, the system is "closed-loop".

In closed-loop systems, the transmitter uses channel knowledge to perform some precoding which is best fit to the actual channel state and sends a maximum of information. This is the case in beamforming techniques [LiLo96], for example. In most practical cases however, the transmitter disposes of imperfect or limited channel knowledge. Either the CSI is partial, and this knowledge can be used to perform some simplified channel-dependent precoding, or there is no available CSI, like in open-loop systems for example, and the best strategy is to employ transmit diversity techniques.

Open-loop systems allow the recovery of spatial diversity either in a direct or in an indirect manner, transforming space diversity into time or frequency diversity. Delay diversity (DD) or cyclic delay diversity (CDD) schemes transform space diversity into frequency diversity by emitting time delayed copies of the same signal onto different transmit antennas, as it will be explained later in this chapter. Intentional frequency offset diversity [HiAd92] transforms space diversity into time diversity, by emitting frequency shifted copies of the same signal onto different transmit antennas. Directly exploiting the available spatial transmit diversity can be done by means of space-time trellis coded modulation (STTCM) [TaSe98] or space-time block codes (STBC)/space-frequency block codes (SFBC) for example.

4.1.3. Alamouti orthogonal space - time block codes

Due to their simplicity and performance, STBCs are very attractive solutions for systems needing to take advantage from transmit diversity. Design criterions that give guidelines for designing "good codes" have been established [Jaf05]: The "Rank criterion" determines whether a code attains or not maximum diversity, the "determinant criterion" and the "trace criterion" give guidelines for obtaining high coding gains, and the "maximum mutual information criterion" gives guideline to obtain high throughput.

One of the most elegant, simple and well known transmit diversity schemes for $N_{\mathrm{Tx}} = 2$ transmit antennas was introduced by Alamouti [Ala98]. It is an orthogonal code providing full diversity at a rate of one symbol per channel use, while keeping a very simple optimum decoder. Let us consider the precoding matrix:

$$\mathbf{A}_{01} = \begin{array}{cl} \begin{pmatrix} a_0 & a_1 \\ -a_1^* & a_0^* \end{pmatrix} & \begin{array}{l} \leftarrow i_0 \\ \leftarrow i_1 \end{array} \\ \begin{array}{cc} \uparrow & \uparrow \\ \mathrm{Tx}_0 & \mathrm{Tx}_1 \end{array} & \end{array} . \tag{4.2}$$

The symbol on the m-th row (m=0,1) and n-th column (n=0,1) of the matrix (4.2) is sent on the n-th transmit antenna Tx_n during the m-th time interval i_m. Let us consider a narrowband 2×1 MISO channel with channel matrix $[h_{0,0}^{(i)} \quad h_{0,1}^{(i)}]^{\mathrm{T}}$ at time t_i. The signal $r_{\mathrm{A}}^{(i)}$ received at time i can be written as:

$$\begin{cases} r_{\mathrm{A}}^{(0)} = \quad h_{0,0}^{(0)} a_0 + h_{0,1}^{(0)} a_1 + n^{(0)} \\ r_{\mathrm{A}}^{(1)} = -h_{0,0}^{(1)} a_1^* + h_{0,1}^{(1)} a_0^* + n^{(1)} \end{cases} , \tag{4.3}$$

where we use the same notation conventions as in subsection 2.3.1. We will denote by $\mathbf{r}_{\mathrm{A}} = \left[r_{\mathrm{A}}^{(0)} \quad r_{\mathrm{A}}^{(1)*} \right]^{\mathrm{T}}$, $\mathbf{a} = \left[a_0 \quad a_1^* \right]^{\mathrm{T}}$, $\mathbf{n} = \left[n_0 \quad n_1^* \right]^{\mathrm{T}}$ and by:

$$\mathbf{H}_{\mathrm{A}} = \begin{bmatrix} h_{0,0}^{(0)} & h_{0,1}^{(0)} \\ h_{0,1}^{(1)*} & -h_{0,0}^{(1)*} \end{bmatrix} . \tag{4.4}$$

Transmission can be written in matrix form:

$$\mathbf{r}_{\mathrm{A}} = \mathbf{H}_{\mathrm{A}} \mathbf{a} + \mathbf{n} . \tag{4.5}$$

If we suppose the channel to be time-invariant during the transmission of the Alamouti code, then superscripts (i) can be ignored. The equivalent channel matrix $\mathbf{H}_{\mathrm{A}}$ becomes orthogonal:

$$\mathbf{H}_{\mathrm{A}} = \begin{bmatrix} h_{0,0} & h_{0,1} \\ h_{0,1}^* & -h_{0,0}^* \end{bmatrix} . \tag{4.6}$$

With perfect CSI at the receiver, the signal is easily estimated in an optimal manner as:

$$\hat{\mathbf{a}} = \mathbf{H}_{\mathrm{A}}^{\mathrm{H}}\mathbf{r} = \begin{bmatrix} |h_{0,0}|^2 + |h_{0,1}|^2 & 0 \\ 0 & |h_{0,0}|^2 + |h_{0,1}|^2 \end{bmatrix} \mathbf{a} + \mathbf{H}_{\mathrm{A}}^{\mathrm{H}}\mathbf{n} \,. \tag{4.7}$$

The Alamouti technique thus recovers the same diversity as a SIMO 1×2 system with maximum ratio combining (MRC) detector, but with a 3 dB SNR loss due to emission on 2 transmit antennas. When several receive antennas are used, MRC decoding allows to recover the full diversity offered by the channel, which is $2N_{\mathrm{Rx}}$. This can be confirmed by applying the rank criterion, stating that the error matrix defined as the difference $\mathbf{D}$ between two codewords, $\mathbf{D} = \mathbf{A}_{01} - \mathbf{A}_{01}^{'}$, has to be full rank in order to obtain full spatial diversity $N_{\mathrm{Tx}}N_{\mathrm{Rx}}$.

The Alamouti code uses one degree of freedom (it sends two symbols over two time intervals, which is equivalent to one symbol per channel use). Consequently, in MISO 2×1 channels, where a single degree of freedom is available, the Alamouti scheme reaches the optimal diversity-multiplexing tradeoff. In MIMO $2\times N_{\mathrm{Rx}}$ channels, where 2 degrees of freedom are available, the Alamouti scheme is suboptimal, even if it keeps the full diversity. Alternatively, this can be explained using the maximum mutual information criterion, which states that the mutual information between the transmitted and received signals has to be large to obtain high throughput. It can be verified that the maximum mutual information is attained with one receive antennas, but this is no longer valid for multiple receive antennas [HaHo02], [SaPa00].

4.2. Classical open-loop transmit diversity schemes for SC-FDMA

In this section, we show how the main open-loop transmit diversity techniques can be implemented in a SC-FDMA system. Transmitters having multiple transmit antennas can be equipped with a single RF chain or with multiple RF chains. In the first case, a single SC-FDMA signal can be generated (one single IDFT module available). Processed versions of this signal are sent onto different transmit antennas. This is the case for CDD or OL-TAS (open-loop transmit antenna selection) techniques. If the transmitter is equipped with N_{Tx} RF chains, it can separately produce N_{Tx} SC-FDMA-type signals, as in frequency switched transmit diversity (FSTD) or Alamouti-based techniques.

4.2.1. Cyclic delay diversity

CDD [DaKa01a], [DaKa01b] emerged as an extension, suitable for OFDMA systems, of the simpler DD scheme proposed in [Wit93]. The goal of these techniques is to increase the frequency selectivity of the channel, and therefore, to decrease the coherence bandwidth. Let us consider a system with N_{Tx} transmit antennas, like in Fig. 4.2. We keep the same notation conventions as in subsection 3.3.1.

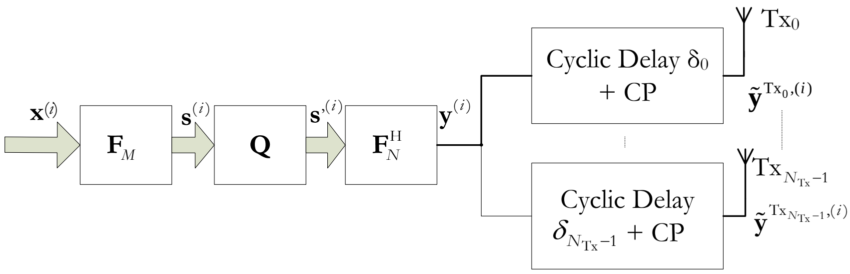

Fig. 4.2 Block diagram of an SC-FDMA transmitter employing CDD.

The SC-FDMA signal after the N-point IDFT is split between N_{Tx} antenna branches and a cyclic shift of $\delta_{n_{\mathrm{Tx}}}$ $\left(0 \leq \delta_{n_{\mathrm{Tx}}} \leq N-1\right)$ samples is applied to each n_{Tx}-th copy of the signal to be sent on the n_{Tx}-th transmit antenna, prior to CP insertion:

$$y_k^{\mathrm{Tx}_{n_{\mathrm{Tx}}},(i)} = y_{\left(k-\delta_{n_{\mathrm{Tx}}}\right) \bmod N}^{(i)}, \quad k = 0 \ldots N-1,\ n_{\mathrm{Tx}} = 0 \ldots N_{\mathrm{Tx}}-1. \tag{4.8}$$

As long as the CP length is superior to the maximum delay spread, there is no inter-symbol interference. The minimum length of the cyclic prefix for CDD equals the maximum delay spread and does not depend on the cyclic delays $\delta_{n_{\mathrm{Tx}}}$. This allows shorter CP than in the case of DD techniques, where the minimum value of CP must be incremented by $\max_{n_{\mathrm{Tx}}}\left(\delta_{n_{\mathrm{Tx}}}\right)$ with respect to the CDD case.

At the receiver, each cyclically delayed copy is transparently received as an additional echo of the same transmitted SC-FDMA symbol. Equivalently, this can be seen as the transmission of the SC-FDMA symbol over an equivalent SIMO channel with modified transfer function. The cyclic delay (4.8) corresponds in the frequency domain to a multiplication with an antenna dependent phase ramp $\mathbf{\Phi}^{n_{\mathrm{Tx}}}$ with elements:

$$\phi_k^{n_{\mathrm{Tx}}} = \exp\left(-j2\pi \frac{k\delta_{n_{\mathrm{Tx}}}}{N}\right), \quad k = 0 \ldots N-1,\ n_{\mathrm{Tx}} = 0 \ldots N_{\mathrm{Tx}}-1, \tag{4.9}$$

which can be transferred to the appropriate channel coefficient. Let us denote by $H_{k,n_{\mathrm{Rx}},n_{\mathrm{Tx}}}^{(i)}$ the complex valued channel coefficient on subcarrier k from transmit antenna n_{Tx} to receive antenna n_{Rx} (obtained by DFT transform with respect to the delay variable applied onto the discrete-time representation of $h_{n_{\mathrm{Rx}},n_{\mathrm{Tx}}}(\tau,t)$ presented in (2.26). In the case of static fading during the transmission of the i-th SC-FDMA symbol, the equivalent SIMO channel transfer function has a simple closed form, since at the receive antenna n_{Rx} the superposition of the original signal and the virtual echo results in a transformed channel coefficient:

$$H_{k,n_{\mathrm{Rx}}}^{\mathrm{CDD},(i)} = \sum_{n_{\mathrm{Tx}}=0}^{N_{\mathrm{Tx}}-1} H_{k,n_{\mathrm{Rx}},n_{\mathrm{Tx}}}^{(i)} \exp\left(-j2\pi \frac{k\delta_{n_{\mathrm{Tx}}}}{N}\right), \quad k = 0 \ldots N-1. \tag{4.10}$$

CDD transforms a system with multiple transmit antennas into an equivalent single transmit antenna system. The transformed SIMO channel finds its frequency selectivity increased as a result of the virtual echoes produced by the CDD technique. Without any generality loss, it is usually considered that $\delta_0 = 0$: The original SC-FDMA symbol is sent onto the first transmit antenna Tx_0. When used for open-loop systems to increase frequency diversity gain, large-delay CDD is preferred. Also, since simple cyclic delays do not impact on the amplitude distribution, CDD conserves the good PAPR properties of SC-FDMA.

The advantage of CDD is its simplicity and its standard compatibility. Indeed, a receiver can decode the CDD signal without being aware of the number of transmit antennas employed at the transmitter side. The receiver estimates the transformed channel coefficients and proceed to classical SIMO detection. This also means that CDD employs same pilot grid whatever the number of transmit antennas N_{Tx}, *i.e.*, using the full available pilot energy to estimate every antenna channel. In contrast, a conventional MIMO system requires splitting the pilot energy according to the number of transmit antennas N_{Tx} in order to estimate the different channels coming from the N_{Tx} transmit antennas. As a result, one one hand, CDD increases the channel selectivity which may limit the smoothing gain due to channel estimation; on the other hand, the channel estimation benefits from a larger SNR thanks to additional pilot power available.

4.2.2. Open-loop transmit antenna selection

The principle relying behind the concept of TAS is a basic one: diversity is gained by switching between multiple transmit antennas during the transmission of a coded data block. We consider here only the simple case of Open-Loop TAS (OL-TAS), when no channel knowledge is available at the transmitter. For example, if a block of KN_{Tx} SC-FDMA symbols coded together (and forming thus a codeword) is to be transmitted, blocks of K SC-FDMA successive symbols will be successively transmitted onto each transmit antenna, regardless of the state of the channel. This is depicted in Fig. 4.3, where the switch commutes every K SC-FDMA symbols. At all times, SC-FDMA symbols with good PAPR properties are sent.

Closed-Loop TAS, which consists in choosing at each moment the antenna with the highest channel gain, would give better performance. However, it would need a feedback path from the receiver in order to get the channel state information. Besides, reliability of feedback information may be drastically reduced in case of fast moving terminals. OL-TAS transforms spatial diversity into frequency diversity, just as CDD. Since only one antenna is active at a time, OL-TAS transmission can be seen as a SIMO transmission through a modified channel:

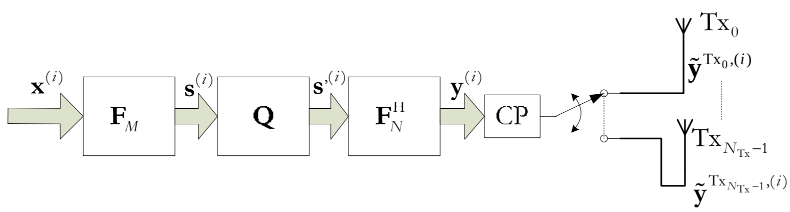

Fig. 4.3 Block diagram of an SC-FDMA transmitter employing OL-TAS.

$$H_{k,n_{\mathrm{Rx}}}^{\text{OL-TAS},(i)} = H_{k,n_{\mathrm{Rx}},n_{\mathrm{Tx}}(i)}^{(i)}, \quad k = 0...N-1 \tag{4.11}$$

where $n_{\mathrm{Tx}}(i)$ denotes the active transmit antenna at time (i). But channel estimation task is more difficult than in the CDD case, for reasons which will be detailed in subsection 4.4.

The advantage of OL-TAS is its simplicity since only one transmit RF chain is needed at the transmitter side. This is the reason why OL-TAS has been selected in 3GPP-LTE as the only transmit diversity scheme in uplink.

4.2.3. Frequency switched transmit diversity

While OL-TAS accomplishes a form of time switched transmit diversity, by sending different portions of a codeword in the whole allocated band during several time intervals over different transmit antennas, FSTD applies the same principle in the frequency domain. Indeed, an FSTD transmitter sends different portions of the same codeword onto different subcarriers on each transmit antenna.

This is depicted in Fig. 4.4. Modulation symbols forming data block $\mathbf{x}^{(i)}$ are split into N_{Tx} parallel streams $\mathbf{x}^{',\mathrm{Tx}_{n_{\mathrm{Tx}}},(i)}$ by the serial to parallel S/P module. Each stream undergoes SC-FDMA modulation. Since at time (i) data blocks $\mathbf{x}^{',\mathrm{Tx}_{n_{\mathrm{Tx}}},(i)}$ of size M / N_{Tx} are present at the input of each n_{Tx}-th SC-FDMA modulator, the size of the DFT precoder is adjusted accordingly. The M subcarriers allocated to the FSTD transmission are split between the N_{Tx} streams in a non-overlapping manner, each n_{Tx}-th SC-FDMA modulator using M / N_{Tx} subcarriers according to the corresponding mapping matrix $\mathbf{Q}_{n_{\mathrm{Tx}}}$. Note that the S/P multiplexing needs to be performed before DFT, such that each $\tilde{\mathbf{y}}^{\mathrm{Tx}_{n_{\mathrm{Tx}}},(i)}$ is a low-PAPR SC-FDMA symbol corresponding to the transmission of the modulation symbols $\mathbf{x}^{',\mathrm{Tx}_{n_{\mathrm{Tx}}},(i)}$. Thus, N_{Tx} DFTs, each of size M / N_{Tx}, must be performed instead of a single M-sized DFT. Performing DFT before S/P multiplexing would be equivalent to performing manipulations over the spectrum of $\mathbf{x}^{(i)}$ which would result in PAPR degradation.

The accumulation $\mathbf{Q}$ of these mapping matrices, defined as:

$$\mathbf{Q} = \begin{bmatrix} \mathbf{Q}_0 & \cdots & \mathbf{Q}_{N_{\mathrm{Tx}}-1} \end{bmatrix}, \tag{4.12}$$

is a $N \times M$ mapping matrix (with M non-null elements equal to 1) describing the position of the carriers used during the FSTD MIMO transmission. The N_{Tx} SC-FDMA signals formed after IDFT and CP insertion are simultaneously sent by the N_{Tx} antennas.

FSTD can be implemented in an either localized or distributed manner. Here, localized or distributed refers to the form of the mapping matrices $\mathbf{Q}_{n_{\mathrm{Tx}}}$, independently of the overall mapping $\mathbf{Q}$. In localized FSTD, SC-FDMA signals onto each antenna use contiguous subcarrier allocation. For example, a system implementing localized FSTD with M used subcarriers and two transmit antennas will allocate the first M/2 available subcarriers for transmission over Tx_0 and the last half for Tx_1. In distributed FSTD, the same system would allocate even subcarriers to transmission on Tx_0 and odd subcarriers to transmission on Tx_1. The first approach eases the

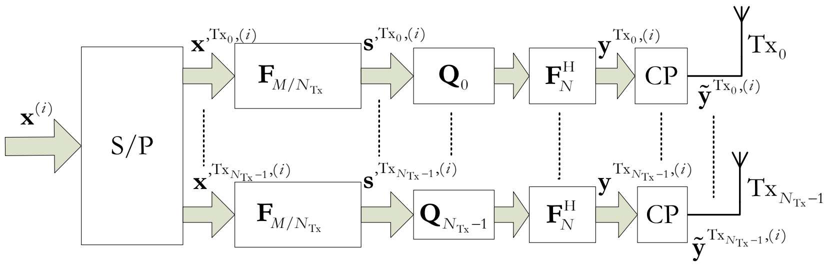

Fig. 4.4 Block diagram of an SC-FDMA transmitter employing FSTD.

channel estimation task, due to the stronger correlation between antennas, while the second one gains in diversity. Even when $\mathbf{Q}$ (eventually after some simple column permutations) corresponds to a localized overall mapping similar to (3.18) for example, we can choose $\mathbf{Q}_{n_{\mathrm{Tx}}}$ to correspond to distributed FSTD.

4.2.4. Alamouti-based orthogonal block codes

Future mobile terminals will be equipped with typically 2 or even 4 transmit antennas and several RF chains. Therefore, employing STBC/SFBC can be considered as an attractive solution due to their simplicity and performance. Special precautions need to be taken for the implementation of block codes to be compatible with SC-FDMA. As discussed in subsection 3.4.1, (3.33) proves that after DFT precoding the system experiences an equivalent diagonal channel. Therefore, it is at this point that a precoding module must be inserted to perform either space-time (ST), space-frequency (SF), space-time-frequency, or some other type of precoding.

On one hand, this ensures that classical ST/SF codes, originally designed for the narrowband case, are correctly applied and transmission can be described by a multiplicative relationship with channel coefficients (*e.g.*, like in (4.3)). Indeed, as discussed in subsection 3.3.2, in OFDMA-like systems IDFT operation is equivalent to splitting the information transmitted through a wideband channel into parallel data streams, each one being transmitted by modulating distinct subcarriers in a narrowband-like manner. This property allows us to use codes designed for the narrowband case in OFDMA-like systems, by applying them at subcarrier level. Applying such a code at block level (before DFT precoding or after IDFT operation) would not lead to constructions capable of exploiting the properties that the narrowband code was designed for. On the other hand, the diagonal structure of the equivalent channel renders such codes, if correctly applied, easy to decode.

Fig. 4.5 shows the general structure of an SC-FDMA transmitter implementing ST/SF precoding. For systems with 2 transmit antennas, the Alamouti code is a natural choice for the ST/SF precoder, due to its good performance and simple optimum decoding.

Note that this frequency-domain implementation is the most straightforward, but time-domain implementations are also possible. Any frequency manipulation performed in the ST/SF precoding block can be easily translated into the time domain. For any transmit antenna $\mathrm{Tx}_{n_{\mathrm{Tx}}}$ $n_{\mathrm{Tx}} = 0 \ldots N_{\mathrm{Tx}} - 1$, let us denote by:

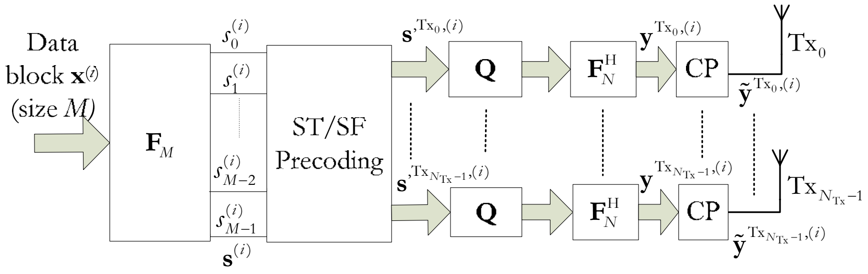

Fig. 4.5 Block diagram of an SC-FDMA transmitter employing STBC / SFBC: frequency-domain implementation.

$$\mathbf{x}_{\mathrm{equiv}}^{\mathrm{Tx}_{n_{\mathrm{Tx}}},(i)} = \mathbf{F}_M^{-1}\mathbf{s}'^{\mathrm{Tx}_{n_{\mathrm{Tx}}},(i)} \tag{4.13}$$

the equivalent time-domain virtual constellation (depending on the original constellation $\mathbf{x}^{(i)}$) that would produce $\mathbf{y}^{\mathrm{Tx}_{n_{\mathrm{Tx}}},(i)}$ when undergoing SC-FDMA modulation, that is:

$$\mathbf{y}^{\mathrm{Tx}_{n_{\mathrm{Tx}}},(i)} = \mathbf{F}_N^{-1}\mathbf{Q}\mathbf{F}_M\mathbf{x}_{\mathrm{equiv}}^{\mathrm{Tx}_{n_{\mathrm{Tx}}},(i)}. \tag{4.14}$$

This interpretation leads to the equivalent transmitter representation in Fig. 4.6. This model, which is generally not suitable for a practical implementation of an ST/SF frequency-domain precoded SC-FDMA, will be used as an equivalent representation in the following subsections to give some intuitive insight on the signal structure. It also provides a powerful means of converting the ST/SF precoding family presented in this paper to systems where we have no physical access to the subcarriers (*e.g.*, IFDMA with time-domain implementation).

Besides the original precoding matrix $\mathbf{A}_{01}$ given in (4.2), let us also consider an equivalent version $\mathbf{A}_{01}^{(I)}$ defined by:

$$\mathbf{A}_{01}^{(I)} = \begin{array}{c} \begin{pmatrix} a_0 & -a_1^* \\ a_1 & a_0^* \end{pmatrix} \begin{array}{l} \leftarrow i_0 \\ \leftarrow i_1 \end{array} \\ \begin{array}{cc} \uparrow & \uparrow \\ \mathrm{Tx}_0 & \mathrm{Tx}_1 \end{array} \end{array}. \tag{4.15}$$

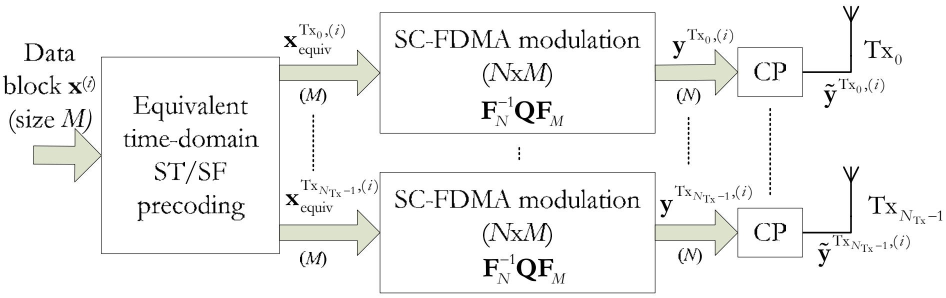

Fig. 4.6 Block diagram of an SC-FDMA transmitter employing STBC / SFBC: time-domain equivalent implementation.

We will also use the following notations and conventions:

- $\mathbf{J} = \begin{bmatrix} 0 & 1 \\ -1 & 0 \end{bmatrix}$, skew symmetric antidiagonal matrix;
- $\mathbf{P}_M^{(\mathbf{J})}$, a M-sized block-diagonal matrix containing $M/2$ copies of $\mathbf{J}$ on its main diagonal, and $\overline{\mathbf{P}}_M^{(\mathbf{J})}$ is the M-sized block-antidiagonal matrix containing $M/2$ copies of $\mathbf{J}$ on its secondary diagonal:

$$\mathbf{P}_M^{(\mathbf{J})} = \begin{bmatrix} \begin{bmatrix} 0 & 1 \\ -1 & 0 \end{bmatrix} & \mathbf{0}_2 & \cdots & \mathbf{0}_2 \\ \mathbf{0}_2 & \begin{bmatrix} 0 & 1 \\ -1 & 0 \end{bmatrix} & \cdots & \mathbf{0}_2 \\ \vdots & \vdots & \ddots & \vdots \\ \mathbf{0}_2 & \mathbf{0}_2 & \cdots & \begin{bmatrix} 0 & 1 \\ -1 & 0 \end{bmatrix} \end{bmatrix}, \tag{4.16}$$

$$\overline{\mathbf{P}}_M^{(\mathbf{J})} = \begin{bmatrix} \mathbf{0}_2 & \cdots & \mathbf{0}_2 & \begin{bmatrix} 0 & 1 \\ -1 & 0 \end{bmatrix} \\ \mathbf{0}_2 & \cdots & \begin{bmatrix} 0 & 1 \\ -1 & 0 \end{bmatrix} & \mathbf{0}_2 \\ \vdots & ⋰ & \vdots & \vdots \\ \begin{bmatrix} 0 & 1 \\ -1 & 0 \end{bmatrix} & \cdots & \mathbf{0}_2 & \mathbf{0}_2 \end{bmatrix}; \tag{4.17}$$

- $\mathbf{S}_M^p$ is an operator which cyclically shifts the rows of an M-sized matrix down p positions:

$$\mathbf{S}_M^p = \begin{bmatrix} 0 & \cdots & \cdots & 0 & 1 \\ 1 & 0 & & 0 & 0 \\ 0 & 1 & \ddots & \vdots & \vdots \\ \vdots & \ddots & \ddots & 0 & \vdots \\ 0 & \cdots & 0 & 1 & 0 \end{bmatrix}^p .$$

For any complex vector $\mathbf{x} = \left[x_0, x_1, x_2, ..., x_{M-1}\right]^{\mathrm{T}}$ the following property stands:

(P1): $$\overline{\mathbf{x}} = \mathbf{F}_M^{\mathrm{H}} \mathbf{F}_M^{\mathrm{H}} \mathbf{x} = \left[x_0, x_{M-1}, x_{M-2}, ..., x_1\right]^{\mathrm{T}} \tag{4.18}$$

is the time reversed version of vector $\mathbf{x}$:

$$\overline{x}_k = x_{(-k) \bmod M}, \tag{4.19}$$

where mod is the modulo operator and k=0…M-1) [WaGi00].

Throughout the paper, we will use the following known inequalities [Har34]:

(I1): $$\left|\sum_{k=0}^{M-1} x_k y_k\right|^2 \le \left(\sum_{k=0}^{M-1}|x_k|^2\right)\left(\sum_{k=0}^{M-1}|y_k|^2\right), \tag{4.20}$$

where $x_k, y_k \in \mathbb{C}$ (the Cauchy-Schwarz inequality). Equality holds if and only if $\mathbf{x}$ and $\mathbf{y}$ are linearly dependent, *i.e.*, one is a scalar multiple of the other.

(I2): $$\left|\sum_{k=0}^{M-1} x_k\right| \le \sum_{k=0}^{M-1}|x_k|, \tag{4.21}$$

where $x_k \in \mathbb{C}$. The equality holds if and only if all x_k have the same argument, that is, $\exists\varphi_0 \in [0, 2\pi)$ such that $x_k = |x_k|\exp(j\varphi_0)$, $\forall k = 0...M-1$.

To describe ST/SF codes, we will proceed as follows: describe the ST/SF precoding matrix, deduce the signal representation in the frequency domain - $\mathbf{s}^{\mathrm{Tx}_{0,1},(i)}$ - onto each antenna, deduce the equivalent constellations $\mathbf{x}_{\mathrm{equiv}}^{\mathrm{Tx}_{0,1},(i)}$ to be sent onto each antenna after SC-FDMA modulation, and comment on the PAPR properties of SC-FDMA signals based on these constellations.

Space-time block codes

To construct an Alamouti STBC in a SC-FDMA context, we choose as ST precoder any of the matrices in (4.2) or (4.15) with the convention:

$$a_m = s_k^{(i_m)}, \ \left(\forall k = 0,...M-1,\ m = 0,1\right). \tag{4.22}$$

Consequently, onto each of the M occupied subcarriers $k = 0,...M-1$, Alamouti precoding is performed between the corresponding frequency samples $s_k^{(i_0=2i)}$ and $s_k^{(i_1=2i+1)}$ belonging to two successive time blocks that are likely to experience similar channel fading. This allows the receiver to use a simple STBC decoder. An example of precoding with matrix $\mathbf{A}_{01}^{(I)}$ is given in Table 4.1. For simplicity, we will always send on the first transmit antenna Tx_0 an SC-FDMA signal corresponding to the original constellation $\mathbf{x}^{(i)}$, *i.e.*, $\mathbf{s}^{\mathrm{Tx}_0,(i)} = \mathbf{s}^{(i)}$. This ensures us to always have a low-PAPR SC-FDMA signal on the first antenna, independently of the type of ST/SF precoding.

Table 4.1 Example of STBC precoding with matrix $\mathbf{A}_{01}^{(I)}$

	On k-th subcarrier		**At block level**	
	Time i_0=2i	Time i_1=2i+1	Time i_0=2i	Time i_1=2i+1
Tx_0	$s_k^{\mathrm{Tx}_0,(i_0)} = s_k^{(i_0)}$	$s_k^{\mathrm{Tx}_0,(i_1)} = s_k^{(i_1)}$	$\mathbf{s}^{\mathrm{Tx}_0,(i_0)} = \mathbf{s}^{(i_0)}$	$\mathbf{s}^{\mathrm{Tx}_0,(i_1)} = \mathbf{s}^{(i_1)}$
Tx_1	$s_k^{\mathrm{Tx}_1,(i_0)} = -\left(s_k^{(i_1)}\right)^*$	$s_k^{\mathrm{Tx}_1,(i_1)} = \left(s_k^{(i_0)}\right)^*$	$\mathbf{s}^{\mathrm{Tx}_1,(i_0)} = -\left(\mathbf{s}^{(i_1)}\right)^*$	$\mathbf{s}^{\mathrm{Tx}_1,(i_1)} = \left(\mathbf{s}^{(i_0)}\right)^*$

Matrix $\mathbf{A}_{01}^{(I)}$ is therefore privileged over matrix $\mathbf{A}_{01}$. Let us revisit the equivalent representation given in Fig. 4.6. From Table 4.1 and (4.13) we have:

$$\begin{cases} \mathbf{x}_{\text{equiv}}^{\text{Tx}_0,(i_m)} = \mathbf{x}^{(i_m)},\ m = 0,1 \\ \mathbf{x}_{\text{equiv}}^{\text{Tx}_1,(i_0)} = \mathbf{F}_M^{-1} \cdot \left(-\mathbf{s}^{(i_1)}\right)^* = -\mathbf{F}_M^{\text{H}}\mathbf{F}_M^{\text{H}} \left(\mathbf{x}^{(i_1)}\right)^* = -\left(\overline{\mathbf{x}}^{(i_1)}\right)^* \\ \mathbf{x}_{\text{equiv}}^{\text{Tx}_1,(i_1)} = \mathbf{F}_M^{-1} \cdot \left(\mathbf{s}^{(i_0)}\right)^* = \mathbf{F}_M^{\text{H}}\mathbf{F}_M^{\text{H}} \left(\mathbf{x}^{(i_0)}\right)^* = \left(\overline{\mathbf{x}}^{(i_0)}\right)^* \end{cases}. \tag{4.23}$$

If the elements of $\mathbf{x}^{(i_{0,1})}$ belong to a QAM constellation, then their complex conjugate time-reversed versions $\pm\left(\overline{\mathbf{x}}^{(i_{0,1})}\right)^*$ are also sets of QAM symbols. Thus, on both transmit antennas, we always send SC-FDMA modulated signals corresponding to a QAM constellation. Consequently, these signals have strictly the same PAPR as the original signal.

Directly applying (4.23) in the time domain for an IFDMA transmitter provides a very simple alternative to the formalism developed in [FrKl06], where the proposed combination of STBC and IFDMA results in the same system model as the one described above.

Since STBC precoding is performed for each occupied subcarrier independently, the frequency structure of the signal is not impacted and we can consider that Alamouti-type precoding is performed at data block level in the frequency domain, as if we were precoding between $\mathbf{s}^{(i_0)}$ and $\mathbf{s}^{(i_1)}$. As a result, SC-FDMA symbols must be precoded by pairs. From a practical point of view, this imposes that all uplink bursts contain an even number of SC-FDMA symbols. When pilot and dynamic control signals are present within the burst, it may be hard or even impossible to ensure that an even number of SC-FDMA symbols be allocated to each data burst. This type of restriction also prevents the use of some algorithms relying onto the flexibility of the data allocation, such as [MoBr06]. As another drawback, STBC is also reported to be sensitive to high vehicular speeds [Alc05].

Space-frequency block codes

The idea of using an STBC in the frequency domain as SFBC is not new. ST codes were originally intended to achieve full spatial diversity for narrow-band single-carrier systems where only spatial diversity was available. In broadband MC systems, both spatial diversity and frequency diversity are available. The analysis of the pairwise error probability conducted in [BöPa00] proved that STBC applied as SFBC in OFDM-type systems fail to achieve full space-frequency diversity. Alamouti-type SFBC is considered to be inappropriate in combination with uncoded OFDMA since uncoded OFDMA has no built-in diversity. Still, the conclusions in [BöPa00] are not pertinent for our case. On one hand, SC-FDMA benefits to some extent from built-in frequency diversity thanks to the DFT-precoding operation, especially in distributed subcarrier allocation scenarios. On the other hand, wireless communication systems employ FEC coding, *e.g.*, turbo or convolutional coding. Frequency diversity is thus recovered by the outer error-correcting code and the role of the SFBC is mainly to recover the spatial diversity. Moreover, since SFBC in OFDMA systems classically precodes data across adjacent subcarriers which are highly correlated, there is virtually no frequency diversity available for the SFBC to exploit anyway. Finally, it is shown in [Bau03] that there is no capacity loss by applying the Alamouti scheme as SF code with respect to the case where it is applied as ST code.

In order to describe the implementation of an Alamouti-type SFBC, let us consider that the symbols on different rows of any of the matrices (4.2) or (4.15) no longer correspond to transmission over different intervals of time $i_{0,1}$, but to transmission over different subcarrier $k_{0,1}$. (4.22) becomes:

$$a_m = s_{k_m}^{(i)}, \ \left(\forall i, \ m = 0,1\right). \tag{4.24}$$

As stated above, Alamouti precoding classically involves adjacent frequency samples to be mapped onto contiguous subcarriers, *i.e.*, $k_0 = 2k$ and $k_1 = 2k+1$, in a localized allocation scenario or subcarriers as close as possible in a distributed allocation scenario so as to allow simple decoding strategies. In contrast to STBC, SFBC does not require data bursts to be composed of an even number of SC-FDMA symbols. SFBC only implies the number of allocated subcarriers M to be even, which is much easier to achieve in the design of today's MC systems with high bandwidth capabilities. In 3GPP LTE for example, M will be a multiple of 12, which is compatible with SFBC-type precoding.

Table 4.2 provides an implementation example using matrix $\mathbf{A}_{01}^{(I)}$. When SFBC is performed as described in Table 4.2, we send on the Tx_0 a SC-FDMA signal corresponding to the original constellation $\mathbf{x}^{(i)}$, *i.e.*, represented as $\mathbf{s}^{\mathrm{Tx}_0,(i)} = \mathbf{s}^{(i)}$ after SF precoding. The signal sent on Tx_1 corresponds to:

$$\mathbf{s}^{\mathrm{Tx}_1,(i)} = \left[-s_1^{(i)*}, s_0^{(i)*}, -s_3^{(i)*}, s_2^{(i)*} \ldots, -s_{M-1}^{(i)*}, -s_{M-2}^{(i)*}\right]^{\mathrm{T}} = \mathbf{P}_M^{(\mathbf{J})}\left(\mathbf{s}^{(i)}\right)^*. \tag{4.25}$$

Note that a comparison of implementations similar to using matrices $\mathbf{A}_{01}$ and $\mathbf{A}_{01}^{(I)}$ described here is given in [LiLe07], both for STBC and SFBC. Using $\mathbf{A}_{01}$ instead of $\mathbf{A}_{01}^{(I)}$ degrades the PAPR on both transmit antennas, causing a loss in the order of 1 dB over the single antenna transmission. Using $\mathbf{A}_{01}^{(I)}$ turns out to be more convenient, since signal on Tx_0 is undistorted. The PAPR loss on the second transmit antenna will be evaluated later in this chapter.

In order to understand the impact of SFBC precoding with $\mathbf{A}_{01}^{(I)}$ on the time-domain SC-FDMA signal sent on Tx_1, let us consider the equivalent-constellation representation. Since all

Table 4.2 Example of SFBC precoding with matrix $\mathbf{A}_{01}^{(I)}$

At time i	**At subcarrier level** Subcarrier $k_0=2k$	Subcarrier $k_1=2k+1$	**At block level**
Tx_0	$s_{k_0}^{\mathrm{Tx}_0,(i)} = s_{k_0}^{(i)}$	$s_{k_1}^{\mathrm{Tx}_0,(i)} = s_{k_1}^{(i)}$	$\mathbf{s}^{\mathrm{Tx}_0,(i)} = \mathbf{s}^{(i)}$
Tx_1	$s_{k_0}^{\mathrm{Tx}_1,(i)} = -\left(s_{k_1}^{(i)}\right)^*$	$s_{k_1}^{\mathrm{Tx}_1,(i)} = \left(s_{k_0}^{(i)}\right)^*$	$\mathbf{s}^{\mathrm{Tx}_1,(i)} = \mathbf{P}_M^{(\mathbf{J})}\left(\mathbf{s}^{(i)}\right)^*$

operations are performed within the same SC-FDMA symbol, we will omit the superscript (i) in the following. From (4.13), the equivalent-constellation representation is thus given by:

$$\begin{cases} \mathbf{x}_{\text{equiv}}^{\text{Tx}_0} = \mathbf{x} \\ \mathbf{x}_{\text{equiv}}^{\text{Tx}_1} = \mathbf{F}_M^{-1} \cdot \mathbf{P}_M^{(\mathbf{J})} \mathbf{s}^* = \mathbf{F}_M^{-1} \mathbf{P}_M^{(\mathbf{J})} \mathbf{F}_M^{-1} \cdot \mathbf{x}^* \end{cases} \tag{4.26}$$

where $\mathbf{P}_M^{(\mathbf{J})} \mathbf{s}^*$ models the effect of SFBC precoding with matrix $\mathbf{A}_{01}^{(I)}$ on Tx_1, as explained in (4.25).

Yet, the (m,n)-th element of matrix $\mathbf{F}_M^{-1} \mathbf{P}_M^{(\mathbf{J})} \mathbf{F}_M^{-1} \triangleq \mathbf{\Pi}^{(\mathbf{J})}$ (m, n=0…M-1) can be computed in a straightforward manner as:

$$\Pi_{m,n}^{(\mathbf{J})} = \sum_{k=0}^{M-1} F_{m,k}^* \left(\sum_{\ell=0}^{M-1} P_{k,\ell}^{(\mathbf{J})} F_{\ell,n}^* \right) = \frac{1}{M} \sum_{k=0}^{M-1} \sum_{\ell=0}^{M-1} P_{k,\ell}^{(\mathbf{J})} \omega^{-(km+\ell n)} \tag{4.27}$$

But since $\mathbf{P}_M^{(\mathbf{J})}$ given in (4.16) is a sparse block diagonal matrix containing $M/2$ repetitions of matrix $\mathbf{J}$, we can isolate $M/2$ groups of two non-null elements and rewrite (4.27) as:

$$\begin{aligned} \Pi_{m,n}^{(\mathbf{J})} &= \frac{1}{M} \sum_{q=0}^{M/2-1} \left(-\omega_M^{-(2qm+(2q+1)n)} + \omega_M^{-((2q+1)m+2qn)} \right) = \frac{\omega_M^{-m} - \omega_M^{-n}}{M} \sum_{q=0}^{M/2-1} \left(\omega_M^{-2(m+n)} \right)^q \\ &= \begin{cases} \frac{1}{2}(\omega_M^{-m} - \omega_M^{-n}), \text{ if } \left[2(m+n) \right] \operatorname{mod} M = 0 \\ 0, \text{ otherwise} \end{cases} \end{aligned} \tag{4.28}$$

In conjunction with (4.26), this gives us the elements of the equivalent constellation $\mathbf{x}_{\text{equiv}}^{\text{Tx}_1}$ as a function of the original constellation elements:

$$\begin{aligned} x_{m,\text{equiv}}^{\text{Tx}_1} &= \sum_{n=0}^{M-1} \Pi_{m,n}^{(\mathbf{J})} x_n^* = \sum_{n \in \{M-m, M/2-m\}} \Pi_{m,n}^{(\mathbf{J})} x_n^* \\ &= \cos\left(2\pi \frac{m}{M} \right) x_{(M/2-m) \operatorname{mod} M}^* + j \sin\left(2\pi \frac{m}{M} \right) x_{M-m}^* \end{aligned} \tag{4.29}$$

By applying inequality (4.20) to relation (4.29), it can easily be seen that the maximum attainable peak power of the equivalent constellation $\mathbf{x}_{\text{equiv}}^{\text{Tx}_1}$ is doubled with respect to $\mathbf{x}$, since:

$$\max\left(\left| \mathbf{x}_{\text{equiv}}^{\text{Tx}_1} \right|^2 \right) = \max_m \left(\left| x_{m,\text{equiv}}^{\text{Tx}_1} \right|^2 \right) \leq \max_m \left(\left| x_{M-m} \right|^2 + \left| x_{M/2-m} \right|^2 \right) = 2 \max\left(\left| \mathbf{x} \right|^2 \right). \tag{4.30}$$

Equality is attained when $\arg\left(x_{M/2-m} / x_{M-m} \right) = \pi / 2$ and $m = M / 8$. The mean power is not affected, since in (4.26) all applied operations preserve the mean power. The PAPR of the equivalent constellation is higher on Tx_1, which imply that the resulting SC-FDMA signal will also have a higher PAPR. Indeed, if SC-FDMA follows perfectly distributed subcarrier mapping, we have seen in subsection 3.3.3 that $\mathbf{y}$ consists of the compression and repetition of samples $\mathbf{x}$.

If the maximum peak of the equivalent constellation $\mathbf{x}_{\text{equiv}}^{\text{Tx}_1}$ is doubled with respect to **x**, so will be the maximum peak of the resulting signal. In localized scenarios, the SC-FDMA modulation operation $\mathbf{F}_N^{-1}\mathbf{Q}\mathbf{F}_M$ with, *e.g.,* $\mathbf{Q} = [\mathbf{I}_M \ \mathbf{0}_{M\times(N-M)}]^{\mathrm{T}}$, is completely equivalent to a resampling operation with factor N/M. The signal on antenna Tx_1 is thus expected to have a PAPR superior to the one on antenna Tx_0, since it is the result of oversampling of a signal with higher dynamic range. Numerical evaluation of the PAPR of SFBC by means of simulation will be presented later in this chapter.

4.3. Single-Carrier space-frequency block codes for SC-FDMA

We have shown in the previous section that the use of STBC is limited to data bursts composed of an even number of SC-FDMA symbols and that classical SFBC performs frequency shuffling $\mathbf{P}_M^{(\mathrm{J})}$ which results in increasing the PAPR of the equivalent constellation $\mathbf{x}_{\text{equiv}}^{\text{Tx}_1}$, and thus of the resulting SC-FDMA signal transmitted on antenna Tx_1. Our purpose is to build a modified SFBC where we replace $\mathbf{P}_M^{(\mathrm{J})}$ by a matrix $\mathbf{P}_M$ such that the resulting signal has good PAPR properties. As in the case of SFBC, superscripts (i) are ignored since precoding is always performed within the same data block.

We will proceed as following:

- Find a matrix $\mathbf{P}_M$ corresponding to an Alamouti-type SFBC such that the PAPR of the equivalent constellation $\mathbf{x}_{\text{equiv}}^{\text{Tx}_1}$ is the same as the PAPR of the original constellation **x**;
- Interpret the physical meaning of the SFBC precoding $\mathbf{s}^{\text{Tx}_1} = \mathbf{P}_M \mathbf{s}^{\text{Tx}_0 *}$ in the time domain (at the level of the equivalent constellation $\mathbf{x}_{\text{equiv}}^{\text{Tx}_1}$), and in the frequency domain (at the level of frequency samples $\mathbf{s}^{\text{Tx}_1}$);
- Prove that the found matrix leads to signals $\mathbf{y}^{\text{Tx}_{0,1}}$ exhibiting the same PAPR on both transmit antennas; we will investigate both localized and distributed subcarrier allocation scenarios.

We will search therefore a matrix $\mathbf{P}_M$ such as $\mathbf{x}_{\text{equiv}}^{\text{Tx}_1} = \mathbf{F}_M^{-1}\mathbf{P}_M\mathbf{F}_M^{-1} \cdot \mathbf{x}^* \triangleq \mathbf{\Pi}\mathbf{x}^*$ has the same signal distribution as **x**, *i.e.,* the following three sets have the same elements:

$$\left\{ \left| x_{m,\text{equiv}}^{\text{Tx}_1} \right|_{m=0\ldots M-1} \right\} = \left\{ \left| x_{m,\text{equiv}}^{\text{Tx}_0} \right|_{m=0\ldots M-1} \right\} = \left\{ \left| x_m \right|_{m=0\ldots M-1} \right\}. \tag{4.31}$$

In addition, $\mathbf{P}_M$ must be chosen such that an Alamouti-type SFBC correspondence based on matrix $\mathbf{A}_{01}^{(I)}$ exists between the elements of vectors $\mathbf{s}^{\text{Tx}_0}$ and $\mathbf{s}^{\text{Tx}_1} = \mathbf{P}_M \mathbf{s}^{\text{Tx}_0 *}$. $\mathbf{P}_M$ must be a skew symmetric matrix ($\mathbf{P}_M = -\mathbf{P}_M^{\mathrm{T}}$) with only one non-null element per row and per column.

It is proven in Appendix D that:

$$\mathbf{P}_M = -\mathbf{S}_M^{p}\overline{\mathbf{P}}_M^{(\mathrm{J})}, \tag{4.32}$$

where p is an even integer parameter, corresponds to an Alamouti-type precoding in the frequency domain satisfying (4.31).

At sample level in the frequency domain, this gives:

$$s_k^{\mathrm{Tx}_1} = (-1)^{k+1} s^*_{(p-1-k) \bmod M}, \quad (k = 0 \ldots M-1). \tag{4.33}$$

We will call this space-frequency precoding "single-carrier SFBC" (SC-SFBC). In the sequel, we will denote by SC_M^p the operation transforming $\mathbf{s}^{\mathrm{Tx}_0} = \mathbf{s}$ into:

$$\mathbf{s}^{\mathrm{Tx}_1} = \mathbf{P}_M \mathbf{s}^* \triangleq \mathrm{SC}_M^p(\mathbf{s}). \tag{4.34}$$

The SC_M^p operation consists thus in taking the complex conjugates of a vector $\mathbf{s}$ in reversed order, applying alternative sign changes and then cyclically shifting down its elements by p positions. This is depicted in Fig. 4.7. As it can be easily seen, Alamouti-precoded pairs not only appear onto adjacent frequency samples but also onto non-adjacent frequency samples $\left(k_0, k_1 = \mathrm{f}(k_0)\right)$, with k_0 even and:

$$\mathrm{f}(k) = (p - 1 - k) \bmod M. \tag{4.35}$$

Indeed, for the example presented in Fig. 4.7, Alamouti precoding with matrix $\mathbf{A}_{01}^{(I)}$ is performed between the following pairs $\left(k_0, k_1\right)$ of frequency samples: (0,5), (2,3), (4,1), (6,11), (8,9), (10,7). Eq. (4.24) still stands, but k_0 and $k_1 = \mathrm{f}(k_0)$ are no longer necessarily consecutive. Precoding is performed between non-adjacent subcarriers situated at variable distances, and thus susceptible of suffering different fadings, which results in increased interference and consequently in performance loss. The maximum distance between two subcarriers precoded together is $\max(p, M-p)$. To minimize the maximum distance between coded subcarriers, which aims at minimizing the performance loss due to precoding onto different subcarriers, we need to choose $p = M/2$. The pertinence of this choice will be proven in subsection 4.4.2.

Table 4.3 summarizes the SC-SFBC precoding operation in the frequency domain.

Let us now investigate the properties of the equivalent constellation generated by SC-SFBC precoding. The equivalent constellation $\mathbf{x}_{\mathrm{equiv}}^{\mathrm{Tx}_1}$ is deduced by applying IDFT transform to (4.33), or by directly applying (D.12):

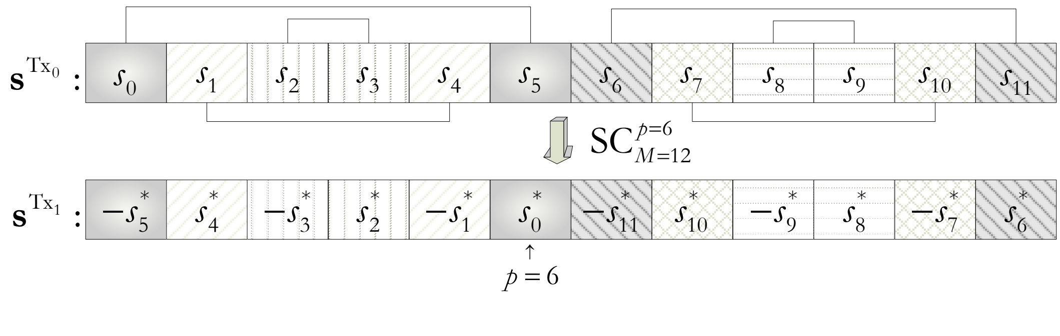

Fig. 4.7 SC-SFBC precoding; example for M=12, p=6.

Table 4.3 Example of SC-SFBC precoding with matrix $\mathbf{A}_{01}^{(I)}$

At time i	At subcarrier level: Subcarrier $k_0=2k$	At subcarrier level: Subcarrier $k_1=\left(p-1-k_0\right)\mathrm{mod}M$	At block level
Tx_0	$s_{k_0}^{\mathrm{Tx}_0,(i)}=s_{k_0}^{(i)}$	$s_{k_1}^{\mathrm{Tx}_0,(i)}=s_{k_1}^{(i)}$	$\mathbf{s}^{\mathrm{Tx}_0,(i)}=\mathbf{s}^{(i)}$
Tx_1	$s_{k_0}^{\mathrm{Tx}_1,(i)}=-\left(s_{k_1}^{(i)}\right)^*$	$s_{k_1}^{\mathrm{Tx}_1,(i)}=\left(s_{k_0}^{(i)}\right)^*$	$\mathbf{s}^{\mathrm{Tx}_1,(i)}=\underbrace{-\mathbf{S}_M^p\overline{\mathbf{P}}_M^{(\mathrm{J})}}_{\mathbf{P}_M}\left(\mathbf{s}^{(i)}\right)^*$

$$
\begin{aligned}
x_{m,\mathrm{equiv}}^{\mathrm{Tx}_1} &= \frac{1}{\sqrt{M}}\sum_{k=0}^{M-1} s_k^{\mathrm{Tx}_1}\omega_M^{-km} = \frac{1}{\sqrt{M}}\sum_{k=0}^{M-1}\underbrace{(-1)^{k+1}}_{\omega_M^{M/2(k+1)}} s_{(p-1-k)\bmod M}^{*}\,\omega_M^{-km} \\
&\overset{k\to p-1-k}{\underset{p\ \mathrm{even}}{=}} \frac{1}{\sqrt{M}}\sum_{k=0}^{M-1} s_k^{*}\omega_M^{-(p-1)m+k(m+M/2)} \\
&= \omega_M^{-(p-1)m} x_{(m+M/2)\bmod M}^{*}
\end{aligned}
\qquad . \tag{4.36}
$$

From (4.36), we can notice that the equivalent constellation $\mathbf{x}_{\mathrm{equiv}}^{\mathrm{Tx}_1}$ is obtained via complex conjugation and phase shifts $\omega_M^{-(p-1)m}$ applied to the original constellation points, but no amplitude modification is performed: Design criterion (4.31) is obviously satisfied. Let us assume that $\mathbf{x}$ is composed of Quadrature Phase-Shift Keying (QPSK) symbols, for example. In this case, antenna Tx_1 transmits an SC-FDMA signal based on a M'-PSK (Phase Shift Keying) constellation where $M'=M/\gcd(M,p\text{-}1)$ (we have denoted by $\gcd(a,b)$ the greatest common divisor of the integers a and b). Equivalent constellations for QPSK and 16QAM signal mapping for SFBC and SC-SFBC transmission are represented in Fig. 4.8, where we considered M=24, and confirm the analysis in [CiMo07b], [CiMo07c]. The original constellation $\mathbf{x}$ generating the SC-FDMA signal to be sent on the first transmit antenna Tx_0 is plotted in red, as a reference. All constellations are considered normalized to unitary mean power. The points of the equivalent constellation $\mathbf{x}_{\mathrm{equiv}}^{\mathrm{Tx}_1}$ generating the SC-FDMA signal to be sent on the second transmit antenna Tx_1 are plotted in blue. While SFBC precoding results in distorting the original constellation in a manner that leads to peak growth, SC-SFBC only performs some phase rotation without impacting the amplitude of any of the constellation points. Let us also note that the Parseval's theorem together with the fact that vectors $\mathbf{s}^{\mathrm{Tx}_0}$ and $\mathbf{s}^{\mathrm{Tx}_1}$ have the same norm, ensures that the mean power of the original and equivalent constellations are equal, for both SFBC and SC-SFBC.

Let us now analyze how SC-SFBC and the constellation rotation introduced by it impact the PAPR of the sent signals. Let us at first treat the case of perfectly distributed subcarrier allocation, where $\mathbf{y}^{\mathrm{Tx}_{0,1}}$ appears as the repetition of contracted $\mathbf{x}_{\mathrm{equiv}}^{\mathrm{Tx}_{0,1}}$ sequence. By expressing any $n=0\ldots N-1$ with respect to its integer quotient k and remainder r with respect to division by M, we can state:

$$
\left|y_{n=km+r}^{\mathrm{Tx}_1}\right| = \left|x_{r,\mathrm{equiv}}^{\mathrm{Tx}_1}\right| = \left|\omega_M^{-(p-1)m} x_{(r+M/2)\bmod M}^{*}\right| = \left|x_{(r+M/2)\bmod M}\right| = \left|y_{km+(r+M/2)\bmod M}^{\mathrm{Tx}_0}\right| . \tag{4.37}
$$

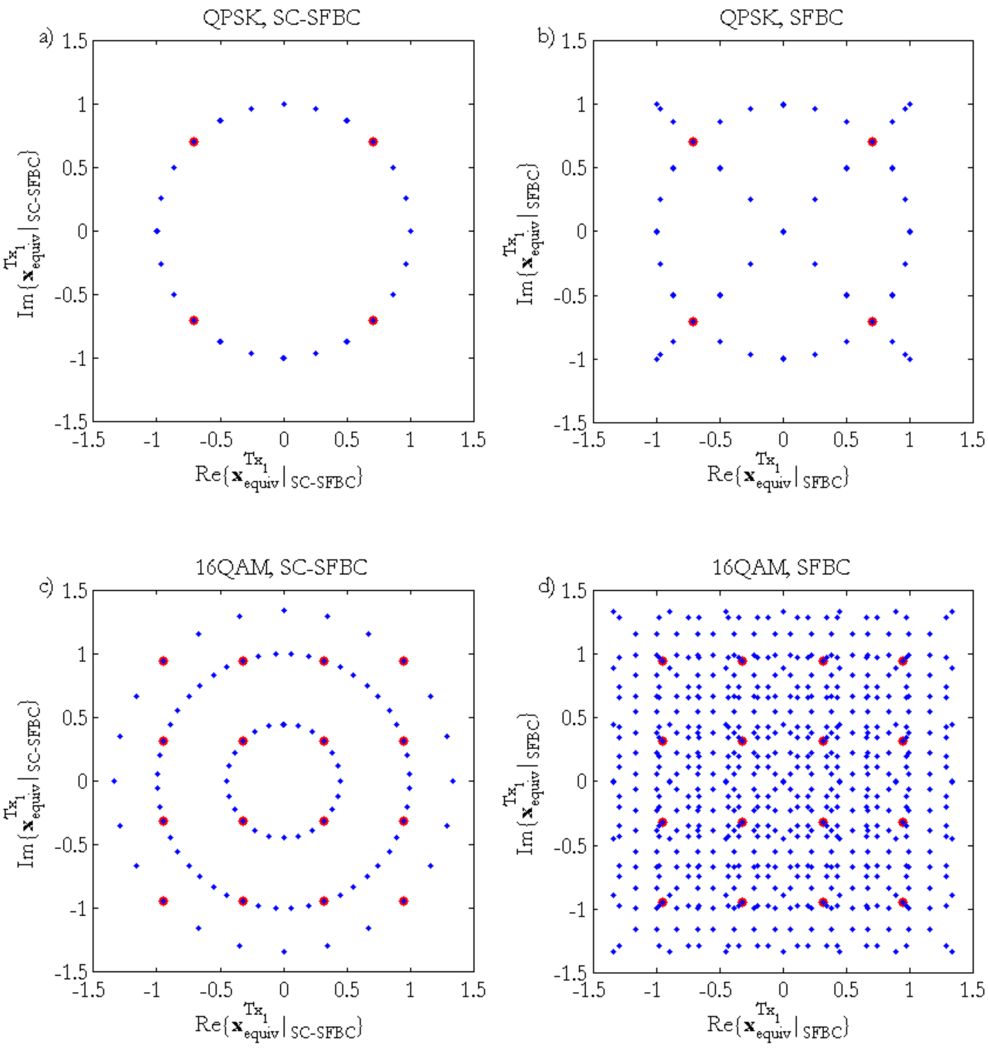

Fig. 4.8 Equivalent constellation representation for SFBC and SC-SFBC transmission with QPSK and 16QAM, example for $M=24$.

If the system follows localized subcarrier allocation with, *e.g.*, $\mathbf{Q}=[\mathbf{I}_M \;\; \mathbf{0}_{M\times(N-M)}]^{\mathrm{T}}$, then:

$$\begin{aligned}\left|y_n^{\mathrm{Tx}_1}\right| &= \left|\frac{1}{\sqrt{N}}\sum_{k=0}^{M-1}(-1)^k s^*_{(p-1-k)\bmod M}\,\omega_N^{-kn}\right| \overset{k\to(p-1-\ell)\bmod M}{=} \left|\frac{1}{\sqrt{N}}\sum_{\ell=0}^{M-1}\omega_N^{-(p-1)n}\underbrace{(-1)^{\ell}}_{\omega_N^{\ell N/2}} s^*_{\ell}\,\omega_N^{\ell n}\right| \\ &= \left|\left(\frac{1}{\sqrt{N}}\sum_{\ell=0}^{M-1}s_{\ell}\,\omega_N^{-\ell(n+N/2)}\right)^*\right| = \left|y_{n+N/2}^{\mathrm{Tx}_0 *}\right| = \left|y_{n+N/2}^{\mathrm{Tx}_0}\right|\end{aligned}. \qquad (4.38)$$

In both (4.37) and (4.38), we see that the samples to be sent on Tx_1 are a reordering of the samples to be sent on Tx_0. $\mathbf{y}^{\mathrm{Tx}_{0,1}}$ have thus strictly the same amplitude distribution and therefore the same PAPR and INP distribution. This is confirmed by the results in Fig. 4.9, giving the CCDF of INP for SC-SFBC/QPSK transmission with STBC, SFBC and SC-SFBC precoding.

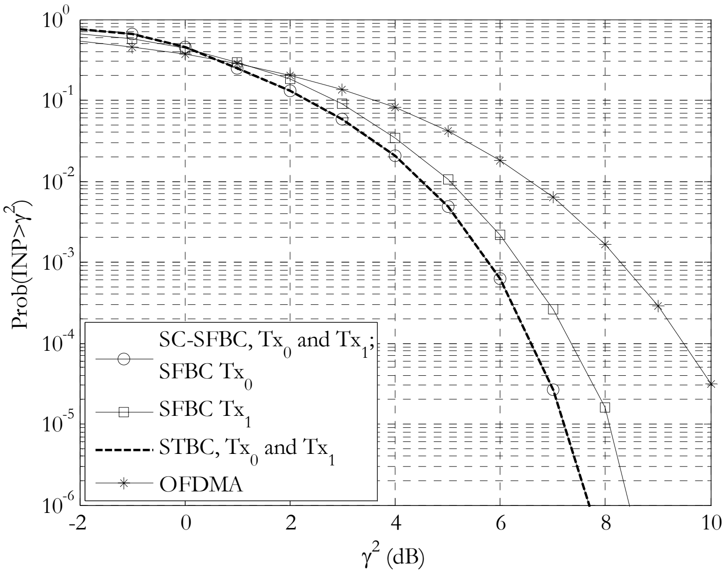

Fig. 4.9 CCDF of INP, QPSK transmission, M=60, N=512, oversampling to L=4.

For all precoding types, on the transmit antenna Tx_0 we send the original SC-FDMA signal, as we employ matrix $\mathbf{A}_{01}^{(1)}$. As expected, we can see that the proposed SC-SFBC has very good PAPR performance and preserve the SC nature of the SC-FDMA signal, just as STBC. On the other hand, as explained in section 4.2.4, the frequency manipulations involved by SFBC lead to an increased PAPR. The obtained waveform is a hybrid signal with a PAPR higher than that of SC-FDMA but lower than that of OFDMA. At a clipping probability of 10^{-4} for example, we lose 0.8 dB in terms of CCDF of INP when using classical SFBC, with respect to a PAPR-invariant precoding scheme. The degradation is numerically evaluated to 1.1 dB in terms of CCDF of PAPR at clipping probability 10^{-4}. Cubic metric is evaluated to 2.7 dB for SFBC and 1.9 dB for SC-SFBC/STBC, which gives a difference of 0.8 dB.

4.4. Comparative performance of different transmit diversity techniques

4.4.1. Particularities of the MIMO receiver

The Alamouti code was designed for narrowband transmission with the assumption that the channel does not vary between the two transmission periods. Applying Alamouti-based codes into the frequency domain causes some degradation: Different (even adjacent) subcarriers suffer slightly different fadings, which causes self-interference within the Alamouti pair. STBCs suffer from the same phenomenon in the case of high mobility users, with important Doppler shifts. A good strategy in both cases is to minimize the intercode interference by using an MMSE receiver instead of the MRC proposed by Alamouti. The small complexity increase due to using MMSE instead of MRC detector is acceptable at the base station, since we are in an uplink context.

Let us detail the SC-SFBC detector. SFBC and STBC are decoded following the same principles and can easily be deduced by simplifying the SC-SFBC detector described here. Pairs of Alamouti precoded symbols are present onto used data subcarriers with index k_0 and k_1, thus we need to proceed to a joint Alamouti decoding and equalization on a "per-subcarrier" basis. The relationship between the index pair $\left(k_0, k_1 = \mathrm{f}(k_0)\right)$, with k_0 even, is given by (4.35) in the SC-FDMA case. At the receiver side, after CP removal and IDFT on each Rx antenna, let us select the received samples onto used data carriers k_0 and k_1, under the form of a $2N_{\mathrm{Rx}}$-sized column vector $\mathbf{r}''_{(k_0,k_1)}$ corresponding to the Alamouti encoded transmission of $\mathbf{s}_{(k_0,k_1)} = [s_{k_0} \;\; s_{k_1}]^{\mathrm{T}}$:

$$\breve{\mathbf{r}}_{(k_0,k_1)} = \begin{bmatrix} \mathbf{r}''_{k_0} \\ -\mathbf{r}''^{*}_{k_1} \end{bmatrix}, \text{ with } \mathbf{r}''_{k_i} = \begin{bmatrix} r''^{\mathrm{Rx}_0}_{k_i} \\ r''^{\mathrm{Rx}_1}_{k_i} \\ \vdots \\ r''^{\mathrm{Rx}_{N_{\mathrm{Rx}}-1}}_{k_i} \end{bmatrix},\; i = 0,1, \tag{4.39}$$

where $r''^{\mathrm{Rx}_{n_{\mathrm{Rx}}}}_{k_i}$ is the sample received on the k_i-th used subcarrier on receive antenna n_{Rx}, after IDFT and subcarrier selection. We followed the notations in Fig. 3.13.

Let us denote by $H_{n_{\mathrm{Rx}},n_{\mathrm{Tx}},k}$ the channel coefficient (in the frequency domain) corresponding to a transmission from the $n_{\mathrm{Tx}}-$th transmit antenna $n_{\mathrm{Tx}} = 0,1$ to the $n_{\mathrm{Rx}}-$th receive antenna $n_{\mathrm{Rx}} = 0 \ldots N_{\mathrm{Rx}} - 1$ on the k-th used subcarrier. Let us also define:

$$\mathbf{H}_k = \begin{bmatrix} H_{0,0,k} & H_{0,1,k} \\ H_{1,0,k} & H_{1,1,k} \\ \vdots & \vdots \\ \underbrace{H_{N_{\mathrm{Rx}}-1,0,k}}_{n_{\mathrm{Tx}}=0} & \underbrace{H_{N_{\mathrm{Rx}}-1,1,k}}_{n_{\mathrm{Tx}}=1} \end{bmatrix}. \tag{4.40}$$

In order to model the transmission under a linear form similar to (4.5), we need to define:

$$\breve{\mathbf{s}}_{(k_0,k_1)} = \begin{bmatrix} s_{k_0} \\ -s^{*}_{k_1} \end{bmatrix} \text{ and } \mathbf{H}_{(k_0,k_1)} = \begin{bmatrix} \mathbf{H}_{k_0} \\ \mathbf{H}^{*}_{k_1} \begin{bmatrix} 0 & -1 \\ 1 & 0 \end{bmatrix} \end{bmatrix}. \tag{4.41}$$

This allows us to linearize the equation of the transmission under the form:

$$\breve{\mathbf{r}}_{(k_0,k_1)} = \mathbf{H}_{(k_0,k_1)} \breve{\mathbf{s}}_{(k_0,k_1)} + \breve{\mathbf{n}}_{(k_0,k_1)}, \tag{4.42}$$

where $\breve{\mathbf{n}}_{(k_0,k_1)}$ is an additive white Gaussian noise of variance σ^2. Note that the convention of using precoding of type $\mathbf{A}_{01}^{(I)}$ instead of the classical $\mathbf{A}_{01}$ in order to keep the good PAPR properties on Tx_0 makes appear in (4.42) a modified version $\breve{\mathbf{s}}_{(k_0,k_1)}$ of the transmitted symbols

$\mathbf{s}_{(k_0,k_1)}$, which keeps us from directly modeling the transmission under a compact form similar to (3.31) with modified channel matrix (4.4), as it is conventionally done in Alamouti SFBC-type coding for OFDMA. Note also that, since precoding is performed onto distinct subcarriers, $\mathbf{H}_{(k_0,k_1)}$ is not orthogonal like in the classical case (4.6) and MRC decoding is no longer optimal. Nevertheless, since pairs of subcarriers can be isolated and decoded together, simple decoding strategies can be applied, such as MRC or MMSE, to avoid complex ML decoding. For example, we can equalize (4.42) by applying:

$$\begin{aligned}\mathbf{E}^{\mathrm{MRC}}_{(k_0)} &= \mathrm{diag}^{-1}\left(\mathbf{H}^{\mathrm{H}}_{(k_0,k_1)}\mathbf{H}_{(k_0,k_1)}\right)\mathbf{H}^{\mathrm{H}}_{(k_0,k_1)} \quad \text{or} \\ \mathbf{E}^{\mathrm{MMSE}}_{(k_0)} &= \left(\mathbf{H}^{\mathrm{H}}_{(k_0,k_1)}\mathbf{H}_{(k_0,k_1)} + \sigma^2\mathbf{I}_2\right)^{-1}\mathbf{H}^{\mathrm{H}}_{(k_0,k_1)}\end{aligned}. \tag{4.43}$$

Index k_1 can be omitted, since $k_1 = \mathrm{f}(k_0)$. Implementations corresponding to (4.43) have low computational complexity, since decoding only involves inverting $M/2$ matrices of order 2 (one for every couple of subcarriers precoded together. We can therefore detect:

$$\begin{bmatrix}\hat{s}_{k_0} \\ -\hat{s}^*_{k_1}\end{bmatrix} = \underbrace{\mathbf{E}_{(k_0)}\mathbf{H}_{(k_0,k_1)}}_{\triangleq\mathbf{A}^{(k_0)}}\begin{bmatrix}s_{k_0} \\ -s^*_{k_1}\end{bmatrix} + \mathbf{E}_{(k_0)}\breve{\mathbf{n}}_{(k_0,k_1)}. \tag{4.44}$$

We can further write:

$$\begin{cases}\hat{s}_{k_0} = A^{(k_0)}_{00}s_{k_0} - A^{(k_0)}_{01}s^*_{k_1} + \breve{n}'_{k_0} \\ \hat{s}_{k_1} = A^{(k_0)}_{11}s_{k_1} - A^{(k_0)*}_{10}s^*_{k_0} + \breve{n}'_{k_1}\end{cases}, \tag{4.45}$$

with:

$$\boldsymbol{\sigma}^2_{\breve{\mathbf{n}}'_{(k_0,k_1)}} = \sigma^2\,\mathrm{diag}(\mathbf{E}_{(k_0)}\mathbf{E}^{\mathrm{H}}_{(k_0)}). \tag{4.46}$$

But (4.45) can now be brought to a compact form:

$$\hat{\mathbf{s}} = \mathrm{diag}\underbrace{\begin{bmatrix}A^{(0)}_{00} \\ A^{\mathrm{f}^{-1}(1)}_{11} \\ A^{(2)}_{00} \\ A^{\mathrm{f}^{-1}(3)}_{11} \\ \vdots \\ A^{(M/2-2)}_{00} \\ A^{\mathrm{f}^{-1}(M/2-1)}_{11}\end{bmatrix}}_{\triangleq\tilde{\mathbf{A}}}\mathbf{s} + \mathrm{diag}\underbrace{\begin{bmatrix}A^{(0)}_{01} \\ -A^{\mathrm{f}^{-1}(1)*}_{10} \\ A^{(2)}_{01} \\ -A^{\mathrm{f}^{-1}(3)*}_{10} \\ \vdots \\ A^{(M/2-2)}_{01} \\ -A^{\mathrm{f}^{-1}(M/2-1)*}_{10}\end{bmatrix}}_{\triangleq\mathbf{B}}\cdot\mathbf{P}_M\mathbf{s}^* + \breve{\mathbf{n}}'. \tag{4.47}$$

Here, f^{-1} stands for the inverse of function f. Following the same reasoning as in subsection 3.4.1, we can first deduce a rough (un-normalized) estimate for the modulation symbols as:

$$\hat{\mathbf{x}}' = \underbrace{\mathrm{diag}\left(\overbrace{\mathbf{F}_M^{\mathrm{H}}\,\mathrm{diag}(\tilde{\mathbf{A}})\mathbf{F}_M}^{\triangleq\mathbf{A}}\right)\mathbf{x}}_{\text{useful signal}} + \underbrace{\overbrace{\left(\mathbf{A}-\mathrm{diag}(\mathbf{A})\right)\mathbf{x}}^{\text{intercode interference}} + \overbrace{\mathbf{F}_M^{\mathrm{H}}\,\mathrm{diag}(\mathbf{B})\mathbf{P}_M\mathbf{F}_M^{\mathrm{H}}\mathbf{x}^*}^{\text{self-interference within Alamouti pairs}}}_{\text{interference}} + \underbrace{\mathbf{F}_M^{\mathrm{H}}\breve{\mathbf{n}}'}_{\text{noise}}. \quad (4.48)$$

As in (3.40), $\mathrm{diag}(\mathbf{A}) = \tilde{\alpha}\mathbf{I}_M$ with $\tilde{\alpha}$ being the arithmetical mean value of $\tilde{\mathbf{A}}$:

$$\tilde{\alpha} = \mathrm{mean}(\tilde{\mathbf{A}}) = \frac{1}{M}\sum_{k_0\in\{0,2,\ldots,M-2\}} \mathrm{trace}\left(\mathbf{A}^{(k_0)}\right). \quad (4.49)$$

Estimates $\hat{\mathbf{x}}$ are obtained after post-equalization with $\tilde{\alpha}^{-1}$:

$$\hat{\mathbf{x}} = \mathbf{x} + \underbrace{\tilde{\alpha}^{-1}\left[\left(\mathbf{A}-\tilde{\alpha}\mathbf{I}_M\right)\mathbf{x} + \mathbf{F}_M^{\mathrm{H}}\,\mathrm{diag}(\mathbf{B})\mathbf{P}_M\mathbf{F}_M^{\mathrm{H}}\mathbf{x}^* + \mathbf{F}_M^{\mathrm{H}}\breve{\mathbf{n}}'\right]}_{\text{interference+noise}\triangleq\mathbf{C}}. \quad (4.50)$$

The power of the interference and noise affecting the useful signal can be computed as:

$$\begin{aligned}
\mathrm{diag}(P_{\text{interference+noise}}) &= \mathrm{E}\left\{\mathrm{diag}(\mathbf{C}\mathbf{C}^{\mathrm{H}})\right\} \\
&= \frac{1}{\tilde{\alpha}^2}\mathrm{diag}\left(\underbrace{\mathbf{A}\mathbf{A}^{\mathrm{H}}}_{=\mathbf{F}_M^{\mathrm{H}}\mathrm{diag}(\tilde{\mathbf{A}})\mathrm{diag}(\tilde{\mathbf{A}}^{\mathrm{H}})\mathbf{F}_M} - \tilde{\alpha}^2\mathbf{I}_M\right) \\
&\quad + \frac{1}{\tilde{\alpha}^2}\mathrm{diag}\left(\mathbf{F}_M^{\mathrm{H}}\,\mathrm{diag}(\mathbf{B})\overbrace{\mathbf{P}_M\mathbf{P}_M^{\mathrm{H}}}^{\mathbf{I}_M}\mathrm{diag}(\mathbf{B}^{\mathrm{H}})\mathbf{F}_M\right) \\
&\quad + \frac{\sigma^2}{\tilde{\alpha}^2}\frac{1}{M}\mathrm{diag}\left(\mathbf{F}_M^{\mathrm{H}}\underbrace{\mathbf{E}}_{\underset{k_0\in\{0,2,\ldots,M-2\}}{\mathrm{blkdiag}}\left(\mathbf{E}_{(k_0)}\right)}\mathbf{E}_{(k_0)}^{\mathrm{H}}\mathbf{F}_M\right) \\
&= \frac{1}{\tilde{\alpha}^2}\left(\frac{\tilde{\mathbf{A}}^{\mathrm{H}}\tilde{\mathbf{A}}}{M} + \frac{\mathbf{B}^{\mathrm{H}}\mathbf{B}}{M} - \tilde{\alpha}^2\right)\mathbf{1}_{M\times1} + \frac{\sigma^2}{\tilde{\alpha}^2 M}\mathrm{diag}\left(\mathbf{F}_M^{\mathrm{H}}\mathbf{E}\mathbf{E}_{(k_0)}^{\mathrm{H}}\mathbf{F}_M\right) \\
&= \frac{1}{M\tilde{\alpha}^2}\left(\sum_{k_0\in\{0,2,\ldots,M-2\}}\left(\sum_{i=0}^{1}\sum_{j=0}^{1}\left|A_{ij}^{(k_0)}\right|^2 - M\tilde{\alpha}^2\right)\right)\mathbf{1}_{M\times1} + \frac{\sigma^2}{\tilde{\alpha}^2 M}\underbrace{\mathrm{diag}\left(\mathbf{F}_M^{\mathrm{H}}\mathbf{E}\mathbf{E}_{(k_0)}^{\mathrm{H}}\mathbf{F}_M\right)}_{\triangleq\tilde{\mathbf{E}}}
\end{aligned} \quad (4.51)$$

The SINR present at the input of the soft bit detector corresponding to a bit corresponding from the n-th modulation symbol x_n, n=0…M-1, from the analyzed SC-FDMA symbol is:

$$\mathrm{SINR}_n = \frac{\left| \sum_{k_0 \in \{0,2,\ldots,M-2\}} \sum_{i=0}^{1} A_{ii}^{(k_0)} \right|^2}{M \sum_{k_0 \in \{0,2,\ldots,M-2\}} \left(\sum_{i=0}^{1} \sum_{j=0}^{1} \left| A_{ij}^{(k_0)} \right|^2 + \sigma^2 \tilde{E}_n \right) - \left| \sum_{k_0 \in \{0,2,\ldots,M-2\}} \sum_{i=0}^{1} A_{ii}^{(k_0)} \right|^2} . \qquad (4.52)$$

The soft bit estimates in the form of LLR are normalized to take into account (4.52) and sent to the, *e.g.*, turbo or Viterbi decoder.

Let us comment on the role of interference in SC-SFBC with Alamouti-type precoding. In (4.48), interference composed of two terms is identified. It is clear that MRC is not suitable in this case, since it completely ignores this term, while an MMSE strategy aims at minimizing it.

Let us separately analyze the two interference components. $(\mathbf{A} - \mathrm{diag}(\mathbf{A}))\mathbf{x}$ is the term corresponding to the intercode interference within an SC-FDMA symbol: If DFT precoding is removed (OFDMA), this term is null. The second term $\mathbf{F}_M^{\mathrm{H}} \mathrm{diag}(\mathbf{B}) \mathbf{P}_M \mathbf{F}_M^{\mathrm{H}} \mathbf{x}^*$ corresponds to the self-interference within an Alamouti-precoded pair, and is due to precoding onto different subcarriers in SFBC-type schemes (or at different time instants for STBC in mobility scenarios), as it can be seen in (4.45). Matrix $\mathbf{B}$ is composed of terms $A_{ij}^{(k)}$, $i \neq j$, that depend on the cross-correlation between the channel realizations corresponding to subcarriers involved in the coding. For SC-SFBC in a frequency selective channel, let us take the simple case where transmit antennas are decorrelated and only one receive antenna is present. If we assume that the channel is normalized to unitary mean power, the mean power of interference terms can be expressed in function of the channel cross-correlations:

$$E\left\{ \left| A_{ij}^{(k_0)} \right|^2 \right\} = 1 - \rho_{(H_{0,0,k_0}, H_{0,0,k_1})} \rho_{(H_{0,1,k_0}, H_{0,1,k_1})} . \qquad (4.53)$$

If precoding is performed between distant subcarriers suffering low-correlated or independent fading, the power of these interference terms is high, which results in decreasing the SINR, as it can be seen from (4.52). The term in (4.53) is null for SFBC/SC-SFBC on a perfectly flat channel (and for STBC if the channel does not present any time selectivity, respectively).

4.4.2. FER Performance

Let us numerically analyze the relative performance of the schemes presented in this chapter. Simulation conditions remain the ones given in Table 3.1. We first analyze the influence of parameter p on the performance of SC-SFBC. Let us consider that $M = 120$ localized subcarriers are allocated to a user travelling at 3kmph, and benefiting from perfect channel estimation and MMSE decoding. Fig. 4.10 analyzes how the choice of parameter p influences the performance of SC-SFBC. $p = 60$ and $p = 30$, corresponding to $p = M/2$ and $p = M/4$ respectively, have similar performance. Employing $p = 16$ and $p = 0$ leads to a degradation of 0.2 dB and 0.4 dB respectively. The reason of this behavior is explained in Fig. 4.11, where subcarriers carrying Alamouti pairs are linked together, and the pairs of subcarriers likely to exhibit channel

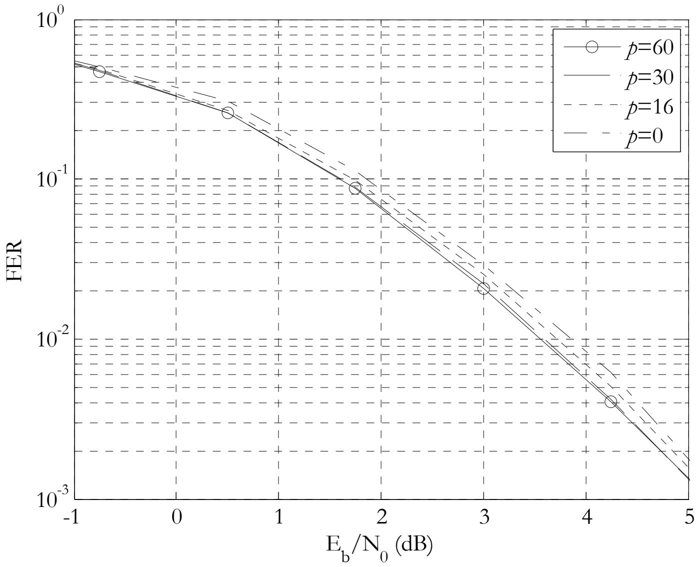

Fig. 4.10 2x2 SC-SFBC with variable p: 3kmph, 120 localized subcarriers, QPSK 1/2, MMSE decoding with ideal channel estimation.

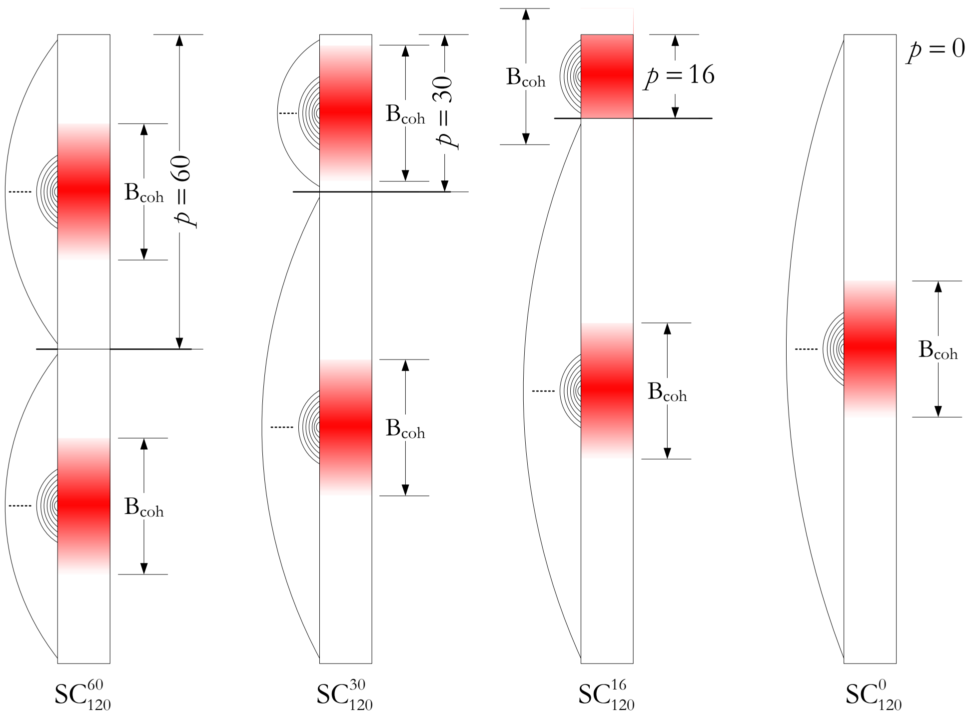

Fig. 4.11 Influence of channel correlation properties on the choice of parameter p.

realizations highly correlated are highlighted. We have already established in Chapter 3 that, for the Vehicular A channel and for the present simulation parameters, the correlation bandwidth B_{coh} corresponds to approximately 26 subcarriers. In these conditions, when employing $p = 60$ and $p = 30$, about 43% of the Alamouti pairs (26 out of 60 pairs) are situated on subcarriers suffering highly correlated fadings. This percentage drops to 35% and 21% when choosing $p = 16$ and $p = 0$ respectively. It is sufficient to choose p in the order of the number of subcarriers corresponding to the correlation bandwidth in order to ensure good performance. The best strategy is nevertheless to choose $p = M/2$, which ensures a good compromise without prior channel knowledge.

Tx diversity is of particular interest in the uplink for users at cell-edge, with no reliable CSI and bad propagation conditions, which will typically be allocated a rather small number of subcarriers (maximum 60) at low modulation rate (typically QPSK) and strong coding (1/2 or even stronger). We will place ourselves in this realistic case. Fig. 4.12 compares the performance of Alamouti-based transmit diversity schemes in terms of FER for the case of two transmit antennas and 60 allocated subcarriers. SFBC has similar performance with STBC, since there is no significant channel variation between two adjacent subcarriers of a same SC-FDMA symbol as for the same subcarrier of two successive SC-FDMA symbols. Compared to SFBC, SC-SFBC has a performance loss on the order of 0.3 dB at a target FER of 1%, due to Alamouti precoding between non-adjacent frequency samples. But since SFBC loses up to 0.9 dB in terms of PAPR with respect to SC-SFBC or STBC, we can conclude that SC-SFBC has better overall performance than classical SFBC. Indeed, as discussed in Chapter 3, the overall system loss can be defined as the sum of the necessary HPA OBO and the $\Delta E_b/N_0$ performance degradation at a target FER. In practical cases (coded systems with back-offs high enough to respect regulated spectrum masks), the $\Delta E_b/N_0$ performance degradation due to clipping is completely negligible (under 0.1 dB in our case), and thus the system degradation is mainly given by the necessary back-off. Note that this back-off is directly related to the signal dynamic range. For clipper-type amplifiers, the difference in back-off for two systems to satisfy the same spectrum mask roughly equals the CCDF of INP difference between the two corresponding signals [CiBu06], [CiMo06].

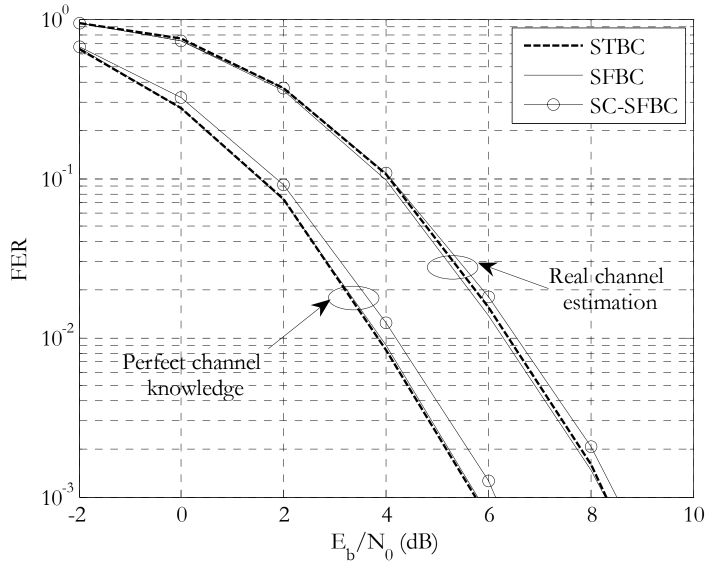

Fig. 4.12 Influence of channel estimation: 3 km/h, 60 localized subcarriers, QPSK 1/2, MMSE decoding, 2 transmit antennas and 2 receive antennas.

The same relative behavior is reported for any vehicular speed. Employing actual channel estimation causes a loss for all schemes around 2.4 dB, due to the estimation errors and to the energy spent by pilots. Note however that with channel estimation errors, the additional degradation brought by SC-SFBC is slightly masked and thus reduced as compared to SFBC and STBC (0.15 dB).

In Fig. 4.13 we analyze the system performance at high vehicular speeds (120 km/h) with real channel estimation and 1 allocated RB (12 subcarriers). STBC, which is more sensitive to Doppler shifts than the SFBC-based techniques, is outperformed by SFBC (0.2 dB). SC-SFBC and SFBC exhibit similar performance. Since SC-SFBC combines the advantages of SFBC (high flexibility, robustness at high vehicular speeds) and STBC (low PAPR), we conclude that it is a very suitable technique when combined with SC-FDMA. We also compare here these two techniques with other simple well-known transmit diversity techniques: CDD, OL-TAS and FSTD. We use a CDD with δ=128 samples, which is preferred in practice due to its reduced implementing complexity: since $\delta = N/4$ the cyclic delay operation can be implemented in the frequency domain by simple multiplications with ± 1 and $\pm j$, eliminating the necessity of a buffer or other complex operations.

Even if all transmit diversity techniques show performance benefits as compared to single antenna transmission (referred to as Single Input Multiple Output – SIMO 1x2 in the legend), we can see that CDD and OL-TAS are outperformed by the Alamouti-based techniques, by 0.6 dB and 2 dB respectively. FSTD and CDD have sensibly similar performance. OL-TAS is more vulnerable to high vehicular speeds than its other counterparts: Because of the antenna switching, each pilot will be used to estimate the channel onto one slot, and no time interpolation can consequently be employed between the two slots of the same frame. Also note that since the

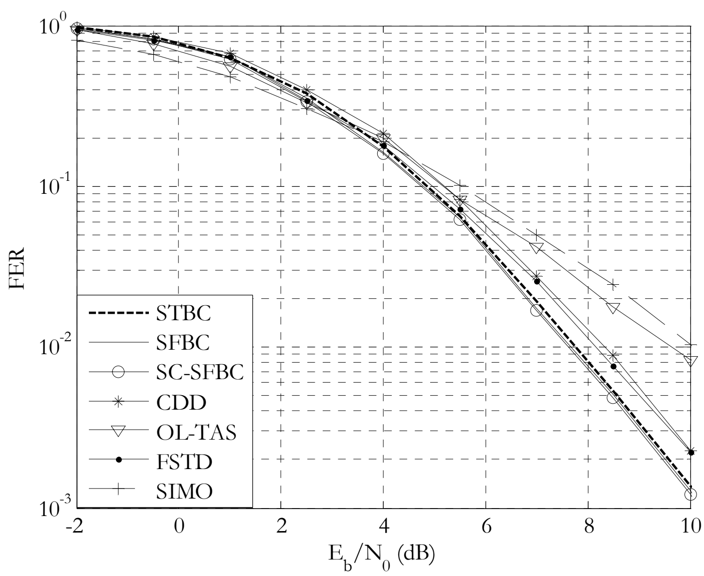

Fig. 4.13 Comparison with other open-loop diversity schemes: 120 km/h, 12 localized subcarriers, QPSK 1/2, MMSE decoding with real channel estimation, 2x2 MIMO.

mobile terminal in future systems will be equipped with at least 2 RF chains to allow spatial multiplexing, the lower complexity of CDD and OL-TAS due to the fact that they need one single RF chain is not necessarily an argument for the choice of a Tx diversity technique for SC-FDMA. The thorough comparative performance analysis conducted in [Mit08b]-[Mit08d] and [Mit09a]-[Mit09c], including simulations with different coding rates, and/or taking into account channel correlation profiles on the more selective 3GPP TU channel confirm the results obtained here. SC-SFBC suffers more due to increased channel selectivity, but it still outperforms SFBC.

In order to completely assess the performance of SC-SFBC, let us look into some unfavorable cases. First, we consider the case where a large number of subcarriers is allocated to a user, which has little probability in practice. In such a case, SC-SFBC is likely to suffer more degradation, since precoding is performed between rather distant subcarriers. Fig. 4.14 presents the case when 10 RBs (120 subcarriers) are allocated to a user. This leads to some 0.4 dB degradation with respect to STBC/SFBC at a target FER of 1%.

In Fig. 4.15, we treat the worst case scenario where 12 distributed subcarriers are allocated to a user in a static scenario, which favors STBC. This leads to a maximal separation of $N/2-1$ subcarriers between two data subcarriers carrying Alamouti-precoded pairs in the case of SC-SFBC. In the case of SFBC, two subcarriers precoded together are not adjacent any longer, but separated by $N/M-1$ null subcarriers. Both SFBC and SC-SFBC thus suffer some performance degradation, estimated at 0.5 dB and 0.7 dB, respectively, at FER 1% when two receive antennas are used. This performance loss can be reduced to 0.2 dB and 0.3 dB, respectively, by using 4 receive antennas, which is a reasonable assumption at the base station. Note that these results are presented only to point out a theoretical worst case scenario, and that we used perfect channel estimation. Indeed, in MIMO systems with distributed carrier allocation,

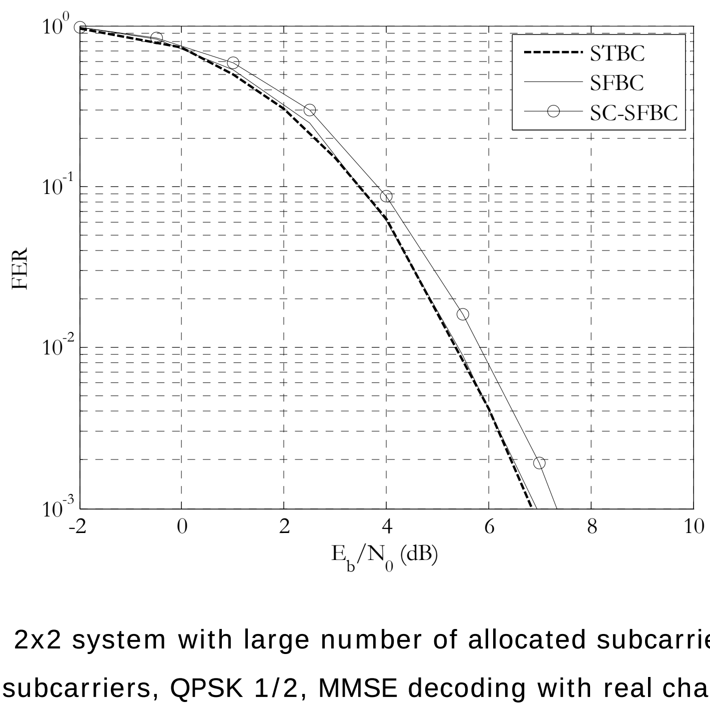

Fig. 4.14 2x2 system with large number of allocated subcarriers: 3kmph, 120 localized subcarriers, QPSK 1/2, MMSE decoding with real channel estimation.

conventional channel estimation methods fail as already anticipated in section3.4.2. The channel coefficients that we are trying to estimate are no longer correlated and the channel estimation module can no longer take advantage of the channel correlation profile: We are trying to estimate $N_{Rx}N_{Tx}$ independent coefficients based on N_{Rx} observations. The difficulty of building an efficient low-complexity channel estimation module for the MIMO case was the main reason for the choice of localized versus distributed SC-FDMA.

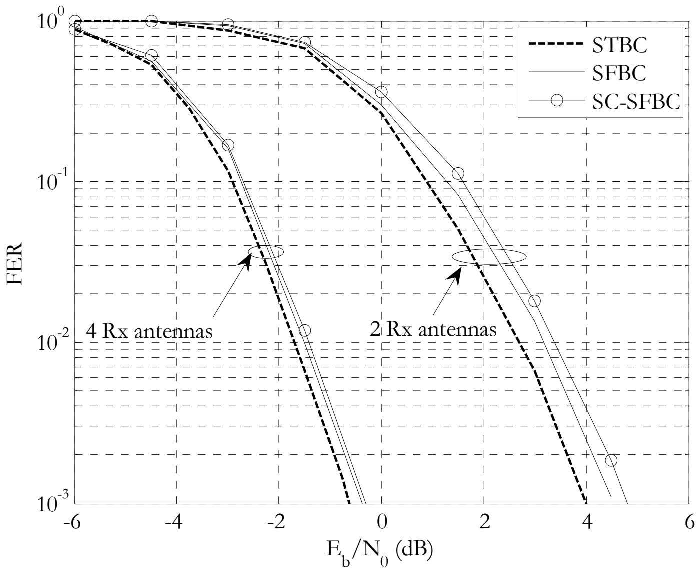

Fig. 4.15 12 distributed subcarriers, 1/2 QPSK with perfect channel estimation.

4.5. Summary and conclusions

In this chapter, we discussed the problem of combining MIMO techniques with SC-FDMA. The results of chapter 3 led us to the conclusion that it is interesting to use SC-FDMA instead of OFDMA for users employing low modulation orders, typically power-limited terminals located at the cell-edge and suffering from bad link quality and unreliable CSI. The priority of these users is to extend coverage via Tx diversity without degrading the PAPR, since they are already emitting at full power and supplementary back-off would further reduce the coverage. We have reviewed some drawbacks of classical Tx diversity schemes used in OFDMA-type systems. First, conventional STBC lacks framing flexibility. Next, conventional SFBC is not suitable to be combined with SC-SFBC since it leads to PAPR degradation. To overcome these problems, we have proposed an innovative mapping that allows Alamouti-based SFBC-type precoding without degrading the PAPR properties of SC-FDMA. This scheme, coined SC-SFBC, shows good performance in realistic simulation scenarios: It outperforms CDD, FSTD and OL-TAS; it is more flexible than STBC, and it has better PAPR than classical SFBC for almost equivalent performance.

Chapter 5

Transmit diversity in SC-FDMA systems with more than two transmit antenna

Since the introduction of orthogonal STBC by Alamouti [Ala98] many efforts were concentrated on developing robust STBCs and finding generalized designs for more than two transmit antennas. The Alamouti code achieves full diversity with rate 1 symbol per channel use as it transmits two symbols in two time intervals. It was shown in [TaJa99] that an orthogonal full-rate design, offering full diversity for complex symbol constellations, does not exist for more than two transmit antennas. Several approaches exist to design codes suitable for more than two Tx antennas and arbitrary complex constellations. Either transmission rate or diversity needs to be sacrificed to obtain a robust design. For example, [TaJa99] proposes a generalization of the theory of orthogonal code design leading to full diversity codes for any number of transmit antennas, but achieving 1/2 of the full transmission rate. For the particular case of four Tx antennas, the transmission rate can go up to 3/4 while keeping full diversity. Another approach is to design non-orthogonal, so-called quasi-orthogonal, rate 1 codes providing only part of the maximum possible diversity, as, *e.g.*, [Jaf01].

The difficulty here consists in finding codes suitable for SC-FDMA. Tx diversity precoding must be applied after DFT precoding, onto the signal's frequency samples. But if we do not want to change the dynamic range of the resulting signal, the ST/SF code must be chosen with much caution, verifying that it does not modify the amplitude distribution of the resulting signal. We will present in this chapter several approaches implementing quasi-orthogonal space-time, space-frequency, and space-time-frequency codes suitable for SC-FDMA systems with 4 Tx antennas, as well as an extension of a code devised for 2 transmit antennas. All codes presented here have rate 1 symbol per channel use and provide half of the full available space diversity.

5.1. Extended Alamouti schemes

Let us review an extension of the Alamouti code and comment on its performance. We will then present the advantages and the drawbacks of using such a code with SC-FDMA.

5.1.1. Jafarkhani-type quasi-orthogonal space-time block codes

Based on the Alamouti generator matrix $\mathbf{A}_{01}$ given in (4.2), Jafarkhani proposed in [Jaf01] a family of quasi-orthogonal (QO) codes with generator matrices:

$$\begin{pmatrix} \mathbf{A}_{01} & \mathbf{A}_{23} \\ -\mathbf{A}_{23}^{*} & \mathbf{A}_{01}^{*} \end{pmatrix}, \begin{pmatrix} \mathbf{A}_{01} & \mathbf{A}_{23} \\ \mathbf{A}_{23}^{*} & -\mathbf{A}_{01}^{*} \end{pmatrix}, \begin{pmatrix} \mathbf{A}_{01} & \mathbf{A}_{23} \\ -\mathbf{A}_{23} & \mathbf{A}_{01} \end{pmatrix}, \begin{pmatrix} \mathbf{A}_{01} & \mathbf{A}_{23} \\ \mathbf{A}_{23} & -\mathbf{A}_{01} \end{pmatrix}. \tag{5.1}$$

These codes achieve a diversity of $2N_{\mathrm{Rx}}$ (half of the full diversity) for a rate of 1 symbol per channel use. Full diversity $N_{\mathrm{Tx}}N_{\mathrm{Rx}}$ is impossible to achieve in this case. The code matrix is no longer orthogonal, but quasi-orthogonal: Each column of matrices in (5.1) is orthogonal to 2 out of the other 3 columns.

As shown in subsections 4.2.4 and 4.3, in an SC-FDMA system it is more convenient to proceed in such a manner that the signal remains undistorted (no sign change, complex conjugation or index permutation) on the first transmit antenna. It is therefore more interesting to work with transpose versions of the generator matrices (5.1). Let us present here a modified version of (5.1) and prove that it exhibits similar properties. The reason of this choice will be clarified in subsection 5.2. We define the following code:

$$\mathcal{A}^{(I)} = \begin{pmatrix} \mathbf{A}_{01}^{(I)} & \mathbf{A}_{23}^{(I)} \\ \mathbf{A}_{23}^{(I)} & \mathbf{A}_{01}^{(I)} \end{pmatrix} = \begin{array}{cl} \begin{pmatrix} a_0 & -a_1^{*} & a_2 & -a_3^{*} \\ a_1 & a_0^{*} & a_3 & a_2^{*} \\ a_2 & -a_3^{*} & a_0 & -a_1^{*} \\ a_3 & a_2^{*} & a_1 & a_0^{*} \end{pmatrix} & \begin{matrix} \leftarrow i_0 \\ \leftarrow i_1 \\ \leftarrow i_2 \\ \leftarrow i_3 \end{matrix} \\ \begin{matrix} \uparrow & \uparrow & \uparrow & \uparrow \\ \mathrm{Tx}_0 & \mathrm{Tx}_1 & \mathrm{Tx}_2 & \mathrm{Tx}_3 \end{matrix} & \end{array} . \tag{5.2}$$

This is a rate-one code, since it transmits 4 symbols over 4 time intervals. It is also a quasi-orthogonal code. Quasi-orthogonality here means that for a given row (resp. column) vector of the generator matrix (5.2), there exists only one other row (resp. column) non-orthogonal vector in the generator matrix (5.2). Indeed, if we denote by v_i the *i*–th row (or column) of the generator matrix (5.2) and by $\langle .,. \rangle$ the scalar product operation, the following quasi-orthogonality relationship stands:

$$\langle v_0, v_1 \rangle = \langle v_0, v_3 \rangle = \langle v_1, v_2 \rangle = \langle v_2, v_3 \rangle = 0 . \tag{5.3}$$

Also, it exhibits the same diversity as the codes in (5.1). To determine the diversity order, we need to determine the minimum rank of the codeword difference matrix $\mathbf{D} = \mathcal{A}^{(I)}\left(a_0 - a_0^{'}, a_1 - a_1^{'}, a_2 - a_2^{'}, a_3 - a_3^{'}\right) = \mathcal{A}^{(I)}\left(d_0, d_1, d_2, d_3\right)$, where all d_i $(i = 0 \ldots 3)$ cannot be simultaneously null. This is equivalent to finding the number of non-null eigenvalues of this matrix, which equals the number of non-null eigenvalues of the Grammian:

$$\mathbf{D}^{\mathrm{H}}\mathbf{D}=\begin{pmatrix} \left(\sum_{i=0}^{3}|d_i|^2\right)\mathbf{I}_2 & 2\,\mathrm{Re}(d_0d_2^*+d_1d_3^*)\cdot\mathbf{I}_2 \\ 2\,\mathrm{Re}(d_0d_2^*+d_1d_3^*)\cdot\mathbf{I}_2 & \left(\sum_{i=0}^{3}|d_i|^2\right)\mathbf{I}_2 \end{pmatrix}. \tag{5.4}$$

These eigenvalues can be computed by solving the characteristic Cayley-Hamilton equation $\det\left(\mathbf{D}^{\mathrm{H}}\mathbf{D}-\lambda I_4\right)=0$, which yields:

$$\lambda_0=\lambda_1=\left(\sum_{i=0}^{3}|d_i|^2\right)+2\,\mathrm{Re}(d_0d_2^*+d_1d_3^*),\quad \lambda_2=\lambda_3=\left(\sum_{i=0}^{3}|d_i|^2\right)-2\,\mathrm{Re}(d_0d_2^*+d_1d_3^*). \tag{5.5}$$

A maximum of 2 eigenvalues can be null: Indeed, if all 4 were null, we would have $\lambda_0+\lambda_2=0$ and consequently all d_i would be null, which is impossible. The minimum rank of **D** is 2, and (5.2) therefore achieves a diversity of $2N_{\mathrm{Rx}}$ [TaSe98].

5.1.2. Quasi-orthogonal STBC and SFBC in SC-FDMA

When implementing QOSTBC/QOSFBC in an SC-FDMA system, the same precautions need to be taken as in the case of STBC/SFBC described in subsection 4.2.4. The system model in Fig. 4.4 remains valid, and we consider $N_{\mathrm{Tx}}=4$. The same notations as in the previous chapter are employed.

Quasi-orthogonal space-time block codes

Employing a Jafarkhani-type code in the time-dimension (QOSTBC) implies choosing in (5.2):

$$a_m=s_k^{(i_m)},\ \left(\forall k=0,\dots M-1,\ m=0\dots3\right). \tag{5.6}$$

To interpret the PAPR properties of the resulting signal, we can rely on the equivalent constellation representation. From (5.2), it follows:

$$\begin{cases} \mathbf{x}_{\mathrm{equiv}}^{\mathrm{Tx}_0,(i_m)}=\mathbf{x}^{(i_m)} \\ \mathbf{x}_{\mathrm{equiv}}^{\mathrm{Tx}_1,(i_m)}=\mathbf{F}_M^{-1}\cdot\left((-1)^{m+1}\mathbf{s}^{(i_{(1-m)\bmod 4})}\right)^*=(-1)^{m+1}\mathbf{F}_M^{\mathrm{H}}\mathbf{F}_M^{\mathrm{H}}\left(\mathbf{x}^{(i_{(1-m)\bmod 4})}\right)^* \\ \qquad\qquad\qquad=(-1)^{m+1}\left(\overline{\mathbf{x}}^{(i_{(1-m)\bmod 4})}\right)^* \\ \mathbf{x}_{\mathrm{equiv}}^{\mathrm{Tx}_2,(i_m)}=\mathbf{F}_M^{-1}\cdot\mathbf{s}^{(i_{(m+2)\bmod m})}=\mathbf{F}_M^{\mathrm{H}}\mathbf{F}_M^{\mathrm{H}}\mathbf{x}^{(i_{(m+2)\bmod m})}=\overline{\mathbf{x}}^{(i_{(m+2)\bmod m})} \\ \mathbf{x}_{\mathrm{equiv}}^{\mathrm{Tx}_3,(i_m)}=\mathbf{F}_M^{-1}\cdot\left((-1)^{m+1}\mathbf{s}^{(i_{(3-m)\bmod 4})}\right)^*=(-1)^{m+1}\mathbf{F}_M^{\mathrm{H}}\mathbf{F}_M^{\mathrm{H}}\left(\mathbf{x}^{(i_{(3-m)\bmod 4})}\right)^* \\ \qquad\qquad\qquad=(-1)^{m+1}\left(\overline{\mathbf{x}}^{(i_{(3-m)\bmod 4})}\right)^* \end{cases},\ m=0\dots3. \tag{5.7}$$

If the elements of $\mathbf{x}^{(i_{0...3})}$ belong to a QAM constellation, then their complex conjugate time-reversed versions $\pm\left(\overline{\mathbf{x}}^{(i_{0...3})}\right)^*$ are also sets of QAM symbols. Thus, on both transmit antennas, we always send SC-FDMA modulated signals corresponding to a QAM constellation. Consequently, these signals have strictly the same PAPR as the original signal.

From (5.2) and (5.6), we also notice that QOSTBC results in precoding between frequency samples on the same *k*-th subcarrier but coming from 4 time-consecutive data blocks (*e.g.*, $s_k^{(4i)} s_k^{(4i+1)} s_k^{(4i+2)} s_k^{(4i+3)}$). This assumes that all uplink bursts contain a multiple of 4 SC-FDMA symbols, which is a strong constraint, difficult or even impossible to meet in practice.

Quasi-orthogonal space-frequency block codes

As in the two-antenna case, (5.2) may be employed in the frequency domain, as QOSFBC:

$$\begin{array}{c} \mathcal{A}^{(I)} = \begin{pmatrix} \mathbf{A}_{01}^{(I)} & \mathbf{A}_{23}^{(I)} \\ \mathbf{A}_{23}^{(I)} & \mathbf{A}_{01}^{(I)} \end{pmatrix} = \begin{pmatrix} a_0 & -a_1^* & a_2 & -a_3^* \\ a_1 & a_0^* & a_3 & a_2^* \\ a_2 & -a_3^* & a_0 & -a_1^* \\ a_3 & a_2^* & a_1 & a_0^* \end{pmatrix} \begin{matrix} \leftarrow f_{k_0} \\ \leftarrow f_{k_1} \\ \leftarrow f_{k_2} \\ \leftarrow f_{k_3} \end{matrix} \\ \begin{matrix} \uparrow & \uparrow & \uparrow & \uparrow \\ \mathrm{Tx}_0 & \mathrm{Tx}_1 & \mathrm{Tx}_2 & \mathrm{Tx}_3 \end{matrix} \end{array} \tag{5.8}$$

QOSTBC can thus be applied as QOSFBC with virtually no additional loss of capacity (with respect to their use as QOSTBC codes). The available frequency and time diversity can be picked up by an outer FEC decoder. We can thus alleviate the restrictions of QOSTBC by using a more flexible frequency-domain code.

In a SC-FDMA system, this can be applied by precoding together frequency samples from the same data bloc but lying on different subcarriers:

$$a_m = s_{k_m}^{(i)}, \ \left(\forall i, \ m = 0...3\right) \tag{5.9}$$

Precoding is classically applied to 4 adjacent frequency samples $s_{4k} s_{4k+1} s_{4k+2} s_{4k+3}$, resulting in some spectrum permutations which, as in the case of SFBC with two transmit antennas, are likely to break the low-PAPR property of the signal and can cause important PAPR. This is exemplified in Fig. 5.1. To investigate the properties of the equivalent constellations thus generated, let us first define the permutation $\mathbf{P}_M^{(\mathbf{I})}$ under the form of a block diagonal matrix:

$$\mathbf{P}_M^{(\mathbf{I})} = \begin{bmatrix} \mathbf{0}_2 & \mathbf{I}_2 & & & \\ \mathbf{I}_2 & \mathbf{0}_2 & & \mathbf{0} & \\ & & \ddots & & \\ & \mathbf{0} & & \mathbf{0}_2 & \mathbf{I}_2 \\ & & & \mathbf{I}_2 & \mathbf{0}_2 \end{bmatrix}. \tag{5.10}$$

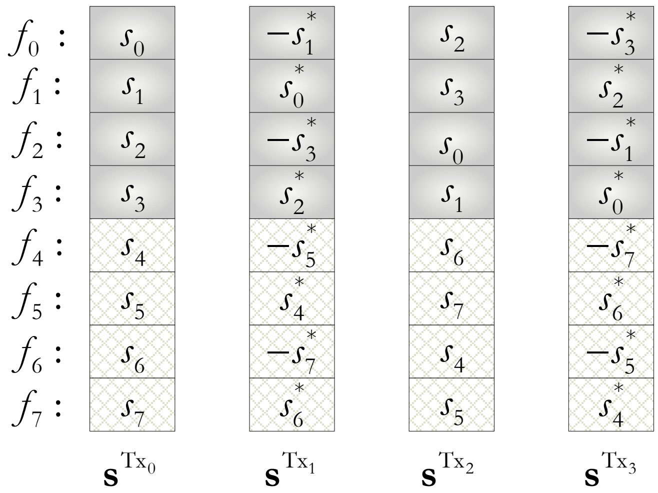

Fig. 5.1 QOSFBC precoding; example for $M=8$;
$(k_0,\ k_1,\ k_2,\ k_3)=\{(0,\ 1,\ 2,\ 3),\ (4,\ 5,\ 6,\ 7)\}$.

By also using $\mathbf{P}_M^{(\mathbf{J})}$, as defined in (4.16), this allows us to express, at block level in the frequency and in the time domains:

$$\begin{cases} \mathbf{s}^{\mathrm{Tx}_0,(i)} = \mathbf{s}^{(i)} \\ \mathbf{s}^{\mathrm{Tx}_1,(i)} = \mathbf{P}_M^{(\mathbf{J})}\left(\mathbf{s}^{(i)}\right)^* \\ \mathbf{s}^{\mathrm{Tx}_2,(i)} = \mathbf{P}_M^{(\mathbf{I})}\mathbf{s}^{(i)} \\ \mathbf{s}^{\mathrm{Tx}_1,(i)} = \mathbf{P}_M^{(\mathbf{J})}\mathbf{P}_M^{(\mathbf{I})}\left(\mathbf{s}^{(i)}\right)^* \end{cases} \Rightarrow \begin{cases} \mathbf{x}_{\mathrm{equiv}}^{\mathrm{Tx}_0} = \mathbf{F}_M^{-1}\mathbf{s}^{(i)} = \mathbf{x} \\ \mathbf{x}_{\mathrm{equiv}}^{\mathrm{Tx}_1} = \mathbf{F}_M^{-1}\mathbf{P}_M^{(\mathbf{J})}\mathbf{F}_M^{-1}\cdot\mathbf{x}^* \\ \mathbf{x}_{\mathrm{equiv}}^{\mathrm{Tx}_2} = \mathbf{F}_M^{-1}\mathbf{P}_M^{(\mathbf{I})}\mathbf{F}_M\cdot\mathbf{x} \\ \mathbf{x}_{\mathrm{equiv}}^{\mathrm{Tx}_3} = \mathbf{F}_M^{-1}\mathbf{P}_M^{(\mathbf{J})}\mathbf{P}_M^{(\mathbf{I})}\mathbf{F}_M^{-1}\cdot\mathbf{x}^* \end{cases}. \tag{5.11}$$

In the following, we will omit superscript (i) for all QOSFBC-type codes. The equivalent constellation on Tx_1 is the same as the one computed in (4.29) for the two-antenna classical SFBC:

$$x_{m,\mathrm{equiv}}^{\mathrm{Tx}_1} = \cos\left(2\pi\frac{m}{M}\right)x^*_{(M/2-m)\bmod M} + j\sin\left(2\pi\frac{m}{M}\right)x^*_{M-m}. \tag{5.12}$$

The peak power of $\mathbf{x}_{\mathrm{equiv}}^{\mathrm{Tx}_1}$ is increased with respect to $\mathbf{x}$ (at most doubled), as it has been discussed in subsection 4.2.4 and proven by simulation in 4.3. To deduce the equivalent constellation on Tx_2, we will proceed as in (4.27)-(4.28) and compute:

$$\begin{aligned} \Pi_{m,n}^{(\mathbf{I})} &= \left(\mathbf{F}_M^{-1}\mathbf{P}_M^{(\mathbf{I})}\mathbf{F}_M\right)_{m,n} = \frac{1}{M}\sum_{k=0}^{M-1}\sum_{\ell=0}^{M-1}P_{k,\ell}^{(\mathbf{I})}\omega_M^{-km+\ell n} = \frac{\omega_M^{2n}+\omega_M^{-m+3n}+\omega_M^{-2m}+\omega_M^{-3m+n}}{M}\sum_{q=0}^{M/4-1}\left(\omega_M^{4(n-m)}\right)^q \\ &= \begin{cases} \frac{1}{4}(\omega_M^{2n}+\omega_M^{-m+3n}+\omega_M^{-2m}+\omega_M^{-3m+n}), \text{ if } \left[4\left(m+n\right)\right]\bmod M = 0 \\ 0, \text{ otherwise} \end{cases} \end{aligned} . \tag{5.13}$$

This gives:

$$\begin{aligned} x_{m,\mathrm{equiv}}^{\mathrm{Tx}_2} &= \sum_{n=0}^{M-1} \Pi_{m,n}^{(\mathbf{I})} x_n = \sum_{n \in \left\{m, \frac{M}{4}+m, \frac{M}{2}+m, \frac{3M}{4}+m\right\} \bmod M} \Pi_{m,n}^{(\mathrm{J})} x_n \\ &= \cos\left(2\pi \frac{2m}{M}\right) x_m + \frac{1-j}{2} \sin\left(2\pi \frac{2m}{M}\right) x_{(M/4+m) \bmod M} \\ &\qquad + \frac{-1-j}{2} \sin\left(2\pi \frac{2m}{M}\right) x_{(3M/4+m) \bmod M} \end{aligned} \tag{5.14}$$

Let us compare the peak power of $\mathbf{x}_{\mathrm{equiv}}^{\mathrm{Tx}_2}$ with the peak power of the original constellation. Indexes will be considered mod$M$. By applying inequality (1.20), it can be seen that the maximum attainable peak power of the equivalent constellation $\mathbf{x}_{\mathrm{equiv}}^{\mathrm{Tx}_2}$ is tripled with respect to $\mathbf{x}$, since:

$$\begin{aligned} \left|x_{m,\mathrm{equiv}}^{\mathrm{Tx}_2}\right|^2 &\le \left(\cos^2\left(2\pi \frac{2m}{M}\right) + 2 \cdot \frac{1}{2} \sin^2\left(2\pi \frac{2m}{M}\right)\right) \cdot \left(\left|x_m\right|^2 + \left|x_{M/4+m}\right|^2 + \left|x_{3M/4+m}\right|^2\right) \\ &\le 3 \max_m \left(\left|x_m\right|^2\right) = 3 \max\left(\left|\mathbf{x}\right|^2\right) \end{aligned} \tag{5.15}$$

Equality is attained when $\arg\left(x_m\right) = \arg\left(x_{M/4+m}\right) + \pi/8 = \arg\left(x_{3M/4+m}\right) + 3\pi/8$. Consequently, (5.15) is not attainable for any type of constellation. For QAM type constellations, this maximum is not attained but we can prove that peak power of $\mathbf{x}_{\mathrm{equiv}}^{\mathrm{Tx}_2}$ can be at least twice the peak power of the original constellation, by a convenient choice of constellation points in (5.14), *e.g.*, when $x_{M/4+m}$ and $x_{3M/4+m}$ are corner points of maximum amplitude and with $\arg\left(x_{M/4+m}\right) = -\arg\left(x_{3M/4+m}\right) = \pi/8$. For $m = M/4$, this gives:

$$x_{M/4,\mathrm{equiv}}^{\mathrm{Tx}_2} = \frac{1}{\sqrt{2}}\left(\left|x_0\right| + \left|x_{M/2}\right|\right) \Rightarrow \left|x_{M/4,\mathrm{equiv}}^{\mathrm{Tx}_2}\right|^2 = 2\max\left(\left|\mathbf{x}\right|^2\right). \tag{5.16}$$

The signal on Tx_2 is consequently expected to have a higher PAPR than signals on both Tx_0 and Tx_1, but this needs to be confirmed numerically, which will be done further in this chapter.

As for the signal on Tx_3, by analyzing (5.8) we notice that $\mathbf{x}_{\mathrm{equiv}}^{\mathrm{Tx}_3}$ can be deduced from $\mathbf{x}_{\mathrm{equiv}}^{\mathrm{Tx}_2}$ in the same manner as $\mathbf{x}_{\mathrm{equiv}}^{\mathrm{Tx}_1}$ was deduced from $\mathbf{x}$. Indeed,

$$\begin{aligned} &\mathbf{x}_{\mathrm{equiv}}^{\mathrm{Tx}_1} = \mathbf{F}_M^{-1} \mathbf{P}_M^{(\mathrm{J})} \mathbf{F}_M^{-1} \cdot \mathbf{x}^* \quad \text{and} \\ &\mathbf{x}_{\mathrm{equiv}}^{\mathrm{Tx}_3} = \mathbf{F}_M^{-1} \mathbf{P}_M^{(\mathrm{J})} \mathbf{F}_M^{-1} \mathbf{F}_M \mathbf{P}_M^{(\mathbf{I})} \mathbf{F}_M^{-1} \cdot \mathbf{x}^* = \mathbf{F}_M^{-1} \mathbf{P}_M^{(\mathrm{J})} \mathbf{F}_M^{-1} \cdot \left(\mathbf{F}_M^{-1} \mathbf{P}_M^{(\mathbf{I})} \mathbf{F}_M \cdot \mathbf{x}\right)^* = \\ &\qquad = \mathbf{F}_M^{-1} \mathbf{P}_M^{(\mathrm{J})} \mathbf{F}_M^{-1} \cdot \mathbf{x}_{\mathrm{equiv}}^{\mathrm{Tx}_2 *} \end{aligned} \tag{5.17}$$

It is consequently expected to have higher PAPR than $\mathbf{x}_{\mathrm{equiv}}^{\mathrm{Tx}_2}$, which, in turn, has larger peaks than $\mathbf{x}$.

5.2. Quasi-orthogonal SC-SFBC

5.2.1. A code for four transmit antennas

To preserve the framing flexibility of SF-type coding without causing any PAPR degradation, let us extend the SC-SFBC precoding principle to the case of four transmit antennas. First, in order to obtain a QO code, we need to satisfy the following QO condition: For each $\mathbf{s}^{\mathrm{Tx}_i}$, two out of the three precoded vectors $\mathbf{s}^{\mathrm{Tx}_j}$ ($j\neq i$, $i,j=0\ldots3$) should be obtained via an orthogonal operation applied to $\mathbf{s}^{\mathrm{Tx}_i}$. Furthermore, in order not to degrade the PAPR, this orthogonal operation must be PAPR-invariant.

Since the SC_M^p operation defined in (4.34) is both orthogonal and PAPR-invariant, we will impose the following condition: For each $\mathbf{s}^{\mathrm{Tx}_i}$, two out of the three precoded vectors $\mathbf{s}^{\mathrm{Tx}_j}$ ($j\neq i$, $i,j=0\ldots3$) should be SC-orthogonal to $\mathbf{s}^{\mathrm{Tx}_i}$, *e.g.*, $\mathbf{s}^{\mathrm{Tx}_0}$ and $\mathbf{s}^{\mathrm{Tx}_2}$ are both SC-orthogonal to $\mathbf{s}^{\mathrm{Tx}_1}$ and to $\mathbf{s}^{\mathrm{Tx}_3}$. This may be further written as:

$$\mathbf{s}^{\mathrm{Tx}_1} = \mathrm{SC}_M^{p}(\mathbf{s}^{\mathrm{Tx}_0}) = \mathrm{SC}_M^{p'}(\mathbf{s}^{\mathrm{Tx}_2}) \text{ and } \mathbf{s}^{\mathrm{Tx}_3} = \mathrm{SC}_M^{p''}(\mathbf{s}^{\mathrm{Tx}_0}) = \mathrm{SC}_M^{p'''}(\mathbf{s}^{\mathrm{Tx}_2}). \quad (5.18)$$

But (5.18) cannot be satisfied by any set of parameters p. It is proven in Appendix E that, in order to satisfy (5.18), we need to choose:

$$\begin{cases} p' = p'' = p - M/2 \\ p''' = p \end{cases}. \quad (5.19)$$

This results in precoding between non-adjacent frequency samples $s_{k_{0\ldots3}}$ where $k_{0\ldots3}$ are given below. It is sufficient to restrict k_0 to even values lower than $M/2$ in order for (k_0, k_1, k_2, k_3) to sweep the entire range $0\ldots M-1$ without index superposition:

$$\begin{cases} k_1 = (p-1-k_0) \bmod M \\ k_2 = (k_0 - M/2) \bmod M \\ k_3 = (p - M/2 - 1 - k_0) \bmod M \end{cases}, \text{ with } k_0 < \frac{M}{2} \text{ even}. \quad (5.20)$$

As in the case of SC-SFBC, p is an even parameter. The solution is detailed in Fig. 5.2, and a concise representation is also given in Fig. 5.3. Note that indexes of subcarriers containing frequency samples precoded together are not adjacent any longer, as it was the case in QOSFBC. By giving an explicit form of (5.20) for, *e.g.*, $M = 12$ and $p = 4$, we find that groups (k_0, k_1, k_2, k_3) belong to the set {(0, 3, 6, 9), (2, 1, 8, 7), (4, 11, 10, 5)}, as described in Fig. 5.2.

Let us isolate the data carried by a group of subcarriers precoded together, $(f_{k_0}, f_{k_1}, f_{k_2}, f_{k_3})$. This corresponds to precoding with a code with generator matrix (5.8), where, in the case of SC-FDMA, we made the choice (5.9). Therefore, by trying to extend the Alamouti-based SC-SFBC from two to four transmit antennas, we found the Jafarkhani-like QO code (5.8). It is obvious that this Single-Carrier QOSFBC (SC-QOSFBC) ensures by construction an SC-like PAPR onto

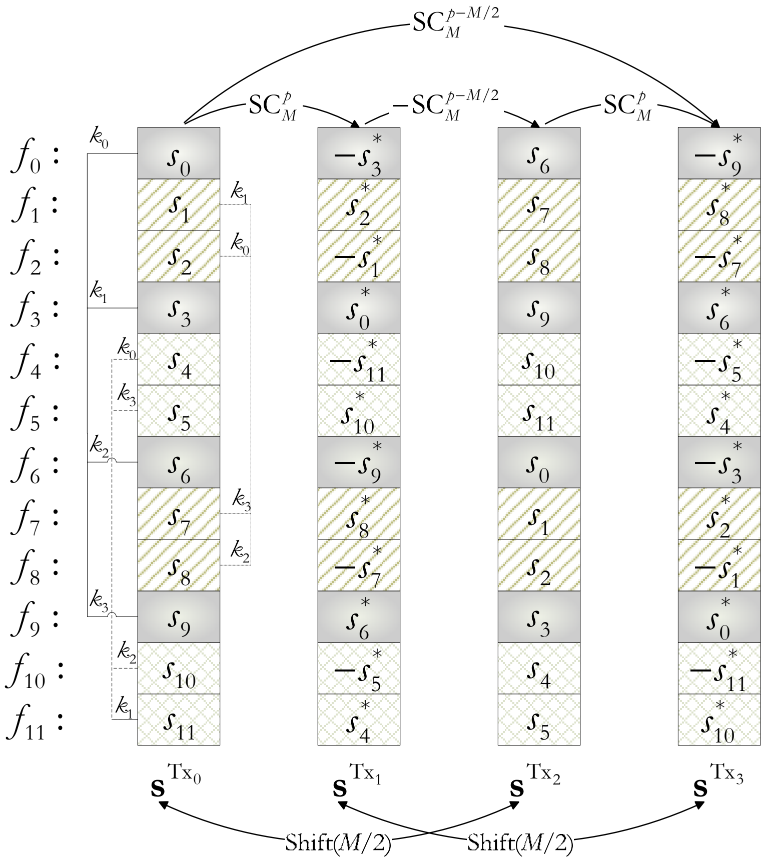

Fig. 5.2 SC-QOSFBC precoding, example for M=12, p=4;
(k_0, k_1, k_2, k_3)={(0, 3, 6, 9), (2, 1, 8, 7), (4, 11, 10, 5)}.

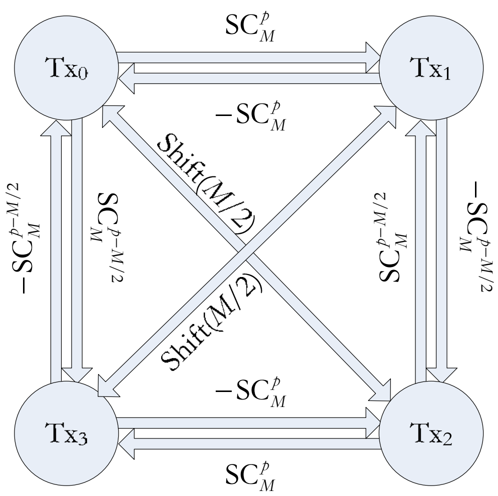

Fig. 5.3 SC-QOSFBC precoding: relationships between the antennas in the frequency domain.

all transmit antennas: All signals undergo, two by two, SC-type operations that were proven to conserve the PAPR. This can be confirmed by computing the equivalent constellations onto the four transmit antennas. Using (4.36) and (5.18)-(5.19), we have:

$$\begin{cases} x_{m,\mathrm{equiv}}^{\mathrm{Tx}_0} = x_m \\ x_{m,\mathrm{equiv}}^{\mathrm{Tx}_1} = \omega_M^{-(p-1)m} x_{(m+M/2)\bmod M}^{*} \\ x_{m,\mathrm{equiv}}^{\mathrm{Tx}_2} = -\omega_M^{-(p-M/2-1)m} x_{(m+M/2)\bmod M,\mathrm{equiv}}^{\mathrm{Tx}_1 *} = (-1)^m x_m \\ x_{m,\mathrm{equiv}}^{\mathrm{Tx}_3} = \omega_M^{-(p-M/2-1)m} x_{(m+M/2)\bmod M}^{*} \end{cases}. \tag{5.21}$$

If $\mathbf{x}_{\mathrm{equiv}}^{\mathrm{Tx}_0} = \mathbf{x}$ is a QAM constellation, then $\mathbf{x}_{\mathrm{equiv}}^{\mathrm{Tx}_2}$ is also QAM; $\mathbf{x}_{\mathrm{equiv}}^{\mathrm{Tx}_1}$ and $\mathbf{x}_{\mathrm{equiv}}^{\mathrm{Tx}_3}$ are rotated QAM constellations like the ones depicted in Fig. 4.8 - a and c.

The good PAPR properties of the resulting code can be confirmed by means of simulation. Fig. 5.4 depicts the PAPR performance of QOSTBC, QOSFBC and SC-QOSFBC for every transmit antenna. The PAPR of an equivalent OFDMA transmission is given as reference. As expected, we can see that the proposed SC-QOSFBC has very good PAPR performance and preserves the SC nature of the SC-FDMA signal, just as QOSTBC. As in the case of SFBC and as expected from the analysis in subsection 5.1.2, the frequency manipulations involved in QOSFBC lead to an increased PAPR. The amount of degradation depends on the considered transmit antenna because of the different spectrum manipulations performed. No degradation is present on the first transmit antenna, because this antenna sends the original SC-FDMA signal. But at a clipping probability of 10^{-4} for example, we can lose up to 0.9 dB/1.1 dB/1.3 dB on antennas $\mathrm{Tx}_{1,2,3}$ when using classical QOSFBC with respect to a PAPR-invariant precoding scheme.

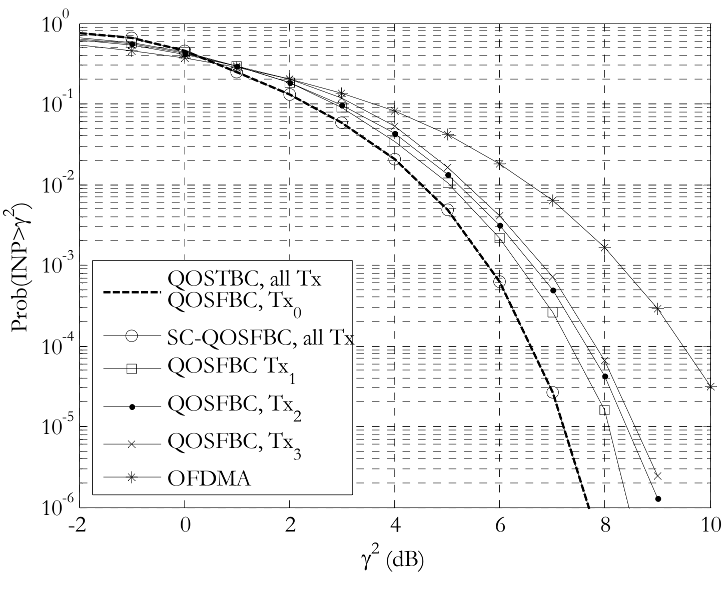

Fig. 5.4 CCDF of INP, QPSK transmission, M=60, N=512, oversampling to L=4.

The properties of the QO codes were thoroughly investigated in [RuMe02], [MeRu04], [PaFo01]. We would consequently expect SC-QOSFBC to have similar performance, with a small penalty with respect to conventional QOSFBC, which is due to precoding samples to be transmitted onto non-adjacent subcarriers. This penalty will be evaluated in section 5.5. The best strategy for minimizing this loss is to minimize the maximum distance between subcarriers precoded together, which means to find:

$$\min_{p}\left(\max_{i,j\in\{0\ldots3\}}\left(\left|k_i-k_j\right|\right)\right). \tag{5.22}$$

Suppose $p<M/2$. The maximum precoding distance between k_0 and k_1, corresponding to an SC_M^p operation, is $\max\left(p,M-p\right)=M-p$. The same holds for k_2 and k_3. Note that (k_0,k_2) and (k_1,k_3) are always at equal distance, $M/2$. The maximum precoding distance between k_2 and k_3 obtained by an $\mathrm{SC}_M^{p-M/2}=\mathrm{SC}_M^{p+M/2}$ operation is $\max\left(p+M/2,M/2-p\right)=p+M/2$. Again, the same holds for k_0 and k_3. We need to determine:

$$\min_{p}\left(\max\left(p+M/2,M-p\right)\right), \tag{5.23}$$

The minimum equals $3M/4$ when $p=M/4$. Accepting $p\geq M/2$ leads to the symmetric solution $p=3M/4$, yielding the same minimum distance and a completely equivalent solution (*e.g.*, taking $p=8$ in Fig. 5.2 leads to the same construction, but the roles of Tx_1 and Tx_3 are inverted). The optimum strategy is consequently to choose $p=M/4$.

5.2.2. Extension to more than four transmit antennas

The solution in 5.2.1 can be generalized for higher number of antennas. We briefly present a solution for eight transmit antennas. This is done to show that these extensions are theoretically possible. Nevertheless, they have limited interest in practice, since user terminals are likely to be equipped with a maximum of four transmit antennas.

SC-QOSFBC is derived from SC-SFBC as follows: the four antennas are split into two groups of two antennas. Onto each group of two antennas, signals are precoded in an SC-SFBC manner, and a shift of $M/2$ is applied between the two groups of antennas. To extend SC-QOSFBC to 8 transmit antennas, we will split the antennas into two groups of 4 antennas. Inside each group, signals are precoded in an SC-QOSFBC manner, and a shift of $M/4$ is applied between the two groups of signals. This processing results in the solution presented in Fig. 5.5, and can be further generalized.

It can be easily verified that this corresponds to precoding with matrix:

$$\begin{pmatrix} \mathcal{A}_{0123}^{(I)} & \mathcal{A}_{4567}^{(I)} \\ \mathcal{A}_{4567}^{(I)} & \mathcal{A}_{0123}^{(I)} \end{pmatrix}, \tag{5.24}$$

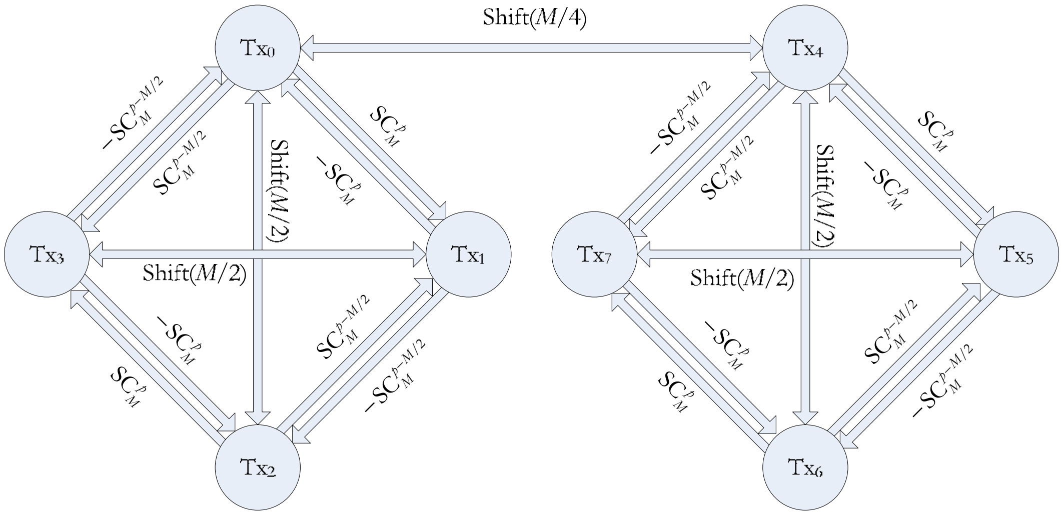

Fig. 5.5 Example of SC-QOSFBC precoding with 8 transmit antennas.

and choosing

$$a_m = s_{k_m}^{(i)}, \ (\forall i, \ m = 0 \ldots 7) \tag{5.25}$$

onto a set of indices $k_{0\ldots7}$ linked by:

$$\begin{cases} k_0 \\ k_1 = (p-1-k_0) \bmod M \\ k_2 = (k_0 - M/2) \bmod M \\ k_3 = (p - M/2 - 1 - k_0) \bmod M \\ k_4 = (k_0 + M/4) \bmod M \\ k_5 = (p-1-k_0 - M/4) \bmod M \\ k_6 = (k_0 - M/4) \bmod M \\ k_7 = (p-1-k_0 + M/4) \bmod M \end{cases}, \text{ with } k_0 < \frac{M}{4} \text{ even}. \tag{5.26}$$

5.3. Quasi-orthogonal space-time-frequency schemes

When M is not a multiple of 4 or when we are sure to have an even number of SC-FDMA symbols in the frame, frequency-domain coding can be replaced with space-time-frequency block code (STFBC) as, for example:

$$\mathcal{A}^{(I)} = \begin{array}{l} \begin{pmatrix} a_0 & -a_1^* & a_2 & -a_3^* \\ a_1 & a_0^* & a_3 & a_2^* \\ a_2 & -a_3^* & a_0 & -a_1^* \\ a_3 & a_2^* & a_1 & a_0^* \end{pmatrix} \begin{array}{l} \left.\begin{array}{l} \leftarrow f_{k_0} \\ \leftarrow f_{k_1} \end{array}\right\} \text{time } i_0 \\ \left.\begin{array}{l} \leftarrow f_{k_0} \\ \leftarrow f_{k_1} \end{array}\right\} \text{time } i_1 \end{array} \\ \begin{array}{cccc} \uparrow & \uparrow & \uparrow & \uparrow \\ \mathrm{Tx}_0 & \mathrm{Tx}_1 & \mathrm{Tx}_2 & \mathrm{Tx}_3 \end{array} \end{array} \tag{5.27}$$

To insure low PAPR, (k_0, k_1) must be related by an SC_M^p operation. This scheme relies basically on the SC-SFBC construction (only two subcarriers are involved in the precoding). This principle can be also applied to classical Jafarkhani constructions of type:

$$\begin{pmatrix} \mathbf{A}_{01}^{(I)} & -\mathbf{A}_{23}^{(I)} \\ \mathbf{A}_{23}^{(I)} & \mathbf{A}_{01}^{(I)} \end{pmatrix}, \quad \begin{pmatrix} \mathbf{A}_{01}^{(I)} & \mathbf{A}_{23}^{(I)} \\ \mathbf{A}_{23}^{(I)} & -\mathbf{A}_{01}^{(I)} \end{pmatrix}. \tag{5.28}$$

Indeed, sign changes would affect all frequency samples sent on an antenna at a certain time, and no PAPR degradation is expected. Applying such a sign change in (5.8) for SC-QOSFBC would only affect a part of the frequency samples (spectrum) of the signal to be sent on an antenna, which would degrade the PAPR. An example of explicit implementation of precoding with (5.27) is given in Fig. 5.6. To give a more concise representation of this scheme, coined SC-STFBC, let us remind that the SC_M^p operation transforms an M-sized vector $\mathbf{s}$ into an M-sized vector $\mathbf{s}' = \mathrm{SC}_M^p(\mathbf{s})$ containing the complex conjugate elements of vector $\mathbf{s}$ in reversed order, with alternative sign changes and cyclically shifted down by p positions:

$$s'_k = (-1)^{k+1} s^*_{(p-1-k) \bmod M}, \quad (k = 0 \ldots M-1). \tag{5.29}$$

We will decompose the SC_M^p operation into two separate operations: The first one, named Flip_p, consists of inverting the order of a vector's elements and then cyclically shift them down by p positions:

$$\mathrm{Flip}_p(\mathbf{s}) = \mathbf{S}_M^p \mathbf{F}_M^{\mathrm{H}} \mathbf{F}_M^{\mathrm{H}} \mathbf{s}\,. \tag{5.30}$$

The second one, that we will call $\mathrm{Altconj}$, consists in complex conjugation and sign alternations of the vector it is applied to. If we denote by $\mathbf{P}_M^{\mathrm{Alt}}$ the diagonal matrix:

$$\mathbf{P}_M^{\mathrm{Alt}} = \mathrm{diag}\Big((-1)^k \big|_{k=0\ldots M-1} \Big), \tag{5.31}$$

we can write:

$$\mathrm{Altconj}(\mathbf{s}) = \mathbf{P}_M^{\mathrm{Alt}} \mathbf{s}^*. \tag{5.32}$$

and we notice that:

$$\begin{aligned}\mathrm{Flip}_p \circ \mathrm{Altconj} &= \mathrm{SC}_M^p \\ \mathrm{Altconj} \circ \mathrm{Flip}_p &= \text{-}\,\mathrm{SC}_M^p\end{aligned}. \tag{5.33}$$

With these notations, we can summarize SC-QOSTFBC as in Fig. 5.7, and deduce:

$$\begin{cases} \mathbf{s}^{\mathrm{Tx}_0,(i_0)} = \mathbf{s}^{(i_0)} \\ \mathbf{s}^{\mathrm{Tx}_0,(i_1)} = \mathbf{s}^{(i_1)} \\ \mathbf{s}^{\mathrm{Tx}_1,(i_0)} = \mathbf{P}_M^{(\mathrm{J})}\left(\mathbf{s}^{(i_0)}\right)^* \\ \mathbf{s}^{\mathrm{Tx}_1,(i_1)} = -\mathbf{P}_M^{(\mathrm{J})}\left(\mathbf{s}^{(i_1)}\right)^* \\ \mathbf{s}^{\mathrm{Tx}_2,(i_0)} = \mathrm{Flip}_p\left(\mathbf{s}^{(i_1)}\right) \\ \mathbf{s}^{\mathrm{Tx}_2,(i_1)} = \mathrm{Flip}_p\left(\mathbf{s}^{(i_0)}\right) \\ \mathbf{s}^{\mathrm{Tx}_3,(i_0)} = -\,\mathrm{Altconj}\left(\mathbf{s}^{(i_1)}\right)^* \\ \mathbf{s}^{\mathrm{Tx}_3,(i_1)} = \mathrm{Altconj}\left(\mathbf{s}^{(i_0)}\right)^* \end{cases} \Rightarrow \begin{cases} \mathbf{x}_{\mathrm{equiv}}^{\mathrm{Tx}_0,(i_0)} = \mathbf{F}_M^{-1}\mathbf{s}^{(i_0)} = \mathbf{x}^{(i_0)} \\ \mathbf{x}_{\mathrm{equiv}}^{\mathrm{Tx}_0,(i_1)} = \mathbf{F}_M^{-1}\mathbf{s}^{(i_1)} = \\ \mathbf{x}_{\mathrm{equiv}}^{\mathrm{Tx}_1,(i_0)} = \mathbf{F}_M^{-1}\mathbf{P}_M^{(\mathrm{J})}\mathbf{F}_M^{-1}\cdot\left(\mathbf{x}^{(i_0)}\right)^* \\ \mathbf{x}_{\mathrm{equiv}}^{\mathrm{Tx}_1,(i_1)} = -\mathbf{F}_M^{-1}\mathbf{P}_M^{(\mathrm{J})}\mathbf{F}_M^{-1}\cdot\left(\mathbf{x}^{(i_1)}\right)^* \\ \mathbf{x}_{\mathrm{equiv}}^{\mathrm{Tx}_2,(i_0)} = \mathbf{F}_M^{-1}\,\mathrm{Flip}_p\left(\mathbf{s}^{(i_1)}\right) \\ \mathbf{x}_{\mathrm{equiv}}^{\mathrm{Tx}_2,(i_1)} = \mathbf{F}_M^{-1}\,\mathrm{Flip}_p\left(\mathbf{s}^{(i_0)}\right) \\ \mathbf{x}_{\mathrm{equiv}}^{\mathrm{Tx}_3,(i_0)} = -\mathbf{F}_M^{-1}\,\mathrm{Altconj}\left(\mathbf{s}^{(i_1)}\right)^* \\ \mathbf{x}_{\mathrm{equiv}}^{\mathrm{Tx}_3,(i_1)} = -\mathbf{F}_M^{-1}\,\mathrm{Altconj}\left(\mathbf{s}^{(i_0)}\right)^* \end{cases} \tag{5.34}$$

We already know that SC_M^p operations do not modify the PAPR. In order to thoroughly prove that SC-QOSTFBC is PAPR invariant, we need to show that Flip_p operations do not modify the PAPR. To prove this, we rely onto a known property of the DFT transform: Cyclic shift in the frequency domain corresponds to a phase ramp in the time domain, which in matrix form becomes:

$$\mathbf{F}_M^{\mathrm{H}}\mathbf{S}_M^p \cdot \mathbf{s} = \mathrm{diag}(1, \omega_M^p, ..., \omega_M^{(M-1)p}) \cdot \mathbf{F}_M^{\mathrm{H}}\mathbf{s}\,. \tag{5.35}$$

This means that the equivalent constellation generated by Flip_p operation in the frequency domain is given by:

$$\begin{aligned}\mathbf{x}_{\mathrm{equiv}}^{(\mathrm{Flip}_p)} &= \mathbf{F}_M^{\mathrm{H}}\mathrm{Flip}_p(\mathbf{s}) = \mathbf{F}_M^{\mathrm{H}}\mathbf{S}_M^p\mathbf{F}_M^{\mathrm{H}}\mathbf{F}_M^{\mathrm{H}}\mathbf{s} = \mathbf{F}_M^{\mathrm{H}}\mathbf{S}_M^p\mathbf{F}_M^{\mathrm{H}}\mathbf{x} = \\ &= \mathrm{diag}(1, \omega_M^p, ..., \omega_M^{(M-1)p})\mathbf{F}_M^{\mathrm{H}}\mathbf{F}_M^{\mathrm{H}}\mathbf{x} = \\ &= \mathrm{diag}(1, \omega_M^p, ..., \omega_M^{(M-1)p})\overline{\mathbf{x}}\end{aligned} \tag{5.36}$$

Since time reversal and phase rotations do not change the PAPR of the original constellation, we can conclude that signals sent onto antennas Tx_2 and Tx_3 preserve the low-PAPR properties. Since SC_M^p-type structures appear, the optimum value of p is $M/2$.

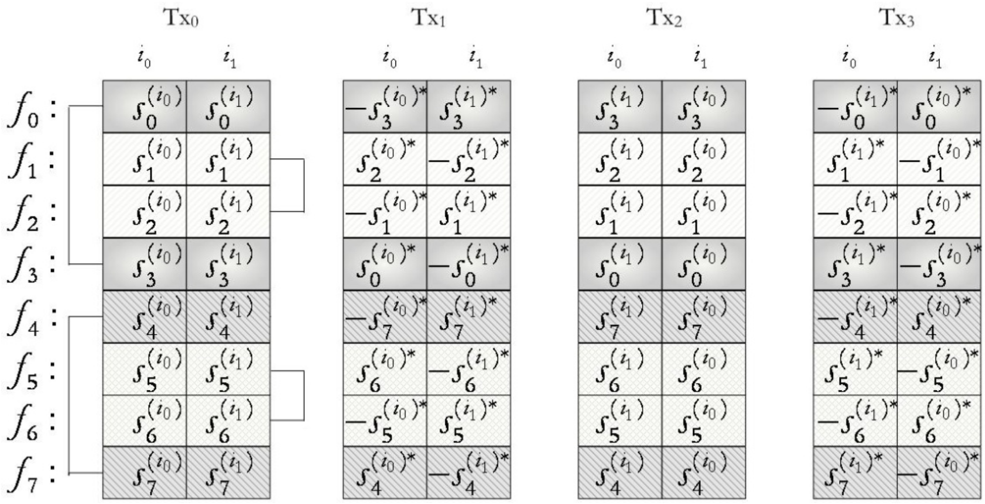

Fig. 5.6 SC-QOSTFBC precoding for $M=8$, $p=4$.

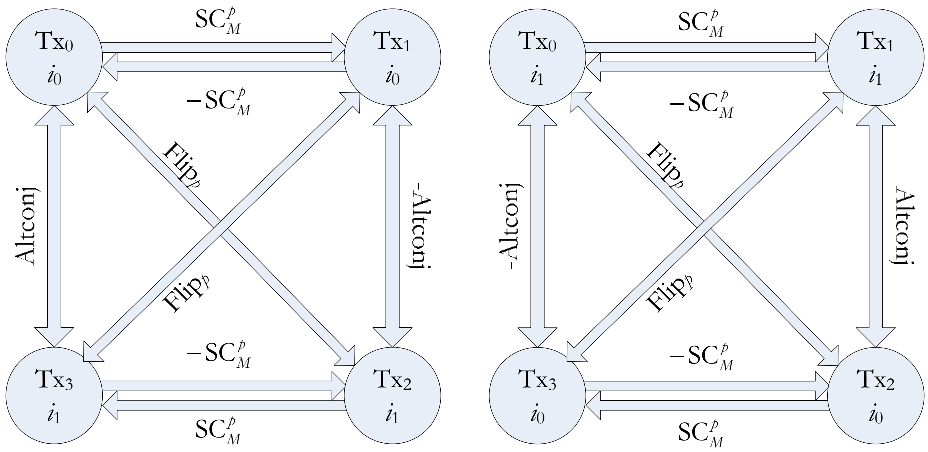

Fig. 5.7 SC-QOSTFBC precoding: relationships between the antennas in the frequency domain.

5.4. SC-SFBC with frequency-domain switching

Another means of extending SC-SFBC to a system with 4 transmit antennas is to combine it with FSTD. The occupied spectrum (M subcarriers) is split into two groups of $M/2$ non-overlapping subcarriers. Each group of $M/2$ subcarriers is encoded together in an SC-SFBC manner. This principle, also presented in [Hua08], is depicted in Fig. 5.8.

Modulation symbols forming data block $\mathbf{x}^{(i)}$ of size M are split into 2 parallel streams, $\mathbf{x}'^{(i)}$ and $\mathbf{x}''^{(i)}$, by the serial to parallel (S/P) module. Each stream is processed as in a SC-FDMA systems with 2 transmit antennas employing SFBC-type precoding and using $M/2$ data subcarriers. Here, we present the case of SC-SFBC to keep good PAPR characteristics, but classical SFBC could be employed instead. Groups of antennas (Tx_0, Tx_1) and (Tx_2, Tx_3) are

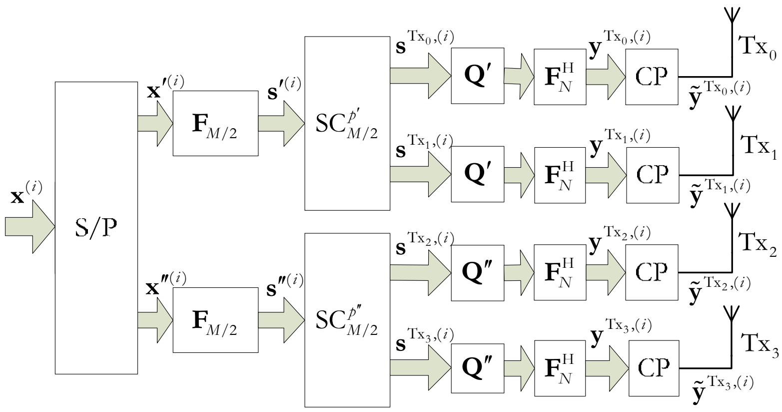

Fig. 5.8 Block diagram of an SC-FDMA transmitter employing SC-SFBC with FSTD.

completely decoupled, since they use different groups of non-overlapping subcarriers selected by the $N \times M/2$ subcarrier mapping matrices $\mathbf{Q}'$ and $\mathbf{Q}''$.

The generator matrix of this code can be written as:

$$\mathcal{A}^{(\text{SC-SFBC/FSTD})} = \begin{pmatrix} \mathbf{A}_{01}^{(I)} & \mathbf{0}_{2\times2} \\ \mathbf{0}_{2\times2} & \mathbf{A}_{23}^{(I)} \end{pmatrix} = \begin{array}{c} \begin{pmatrix} a_0 & -a_1^* & 0 & 0 \\ a_1 & a_0^* & 0 & 0 \\ 0 & 0 & a_2 & -a_3^* \\ 0 & 0 & a_3 & a_2^* \end{pmatrix} \begin{matrix} \leftarrow f'_{k_0} \\ \leftarrow f'_{k_1} \\ \leftarrow f''_{k_2} \\ \leftarrow f''_{k_3} \end{matrix} \\ \begin{matrix} \uparrow & \uparrow & \uparrow & \uparrow \\ \mathrm{Tx}_0 & \mathrm{Tx}_1 & \mathrm{Tx}_2 & \mathrm{Tx}_3 \end{matrix} \end{array}, \tag{5.37}$$

where:

$$a_m = \begin{cases} s_{k_m}'^{(i)}, \text{ if } m = 0,1 \\ s_{k_m}''^{(i)}, \text{ if } m = 2,3 \end{cases} \quad \forall i, \tag{5.38}$$

f' and f'' are chosen from distinct non-overlapping groups of $M/2$ subcarriers, k_0 and k_2 are even integers and:

$$\begin{cases} k_1 = (p' - 1 - k_0) \bmod M/2 \\ k_3 = (p'' - 1 - k_2) \bmod M/2 \end{cases}. \tag{5.39}$$

With such a construction, the two Alamouti-type codes $\mathbf{A}_{01}^{(I)}$ and $\mathbf{A}_{23}^{(I)}$ are mapped onto different portions of the used spectrum, and there is no intercode interference between the two Alamouti pairs due to the construction of the code. Also, let us note that all signals on the 4 transmit antennas preserve the low PAPR properties: signals on Tx_0 and Tx_2 are SC-FDMA signals based on the original constellation $\mathbf{x}$, and signals on Tx_1 and Tx_3 are obtained through

PAPR-invariant operations of type SC. If SFBC was used instead of SC-SFBC, signals on antennas Tx_1 and Tx_3 would have increased PAPR as shown in subsection 4.2.4.

5.5. Comparative performance

Let us give some comparative performance of the various transmit diversity schemes presented in this chapter. In the schemes based on SC-SFBC with frequency switching, the two groups of subcarriers are easily separated at the receiver and the decoding process can be carried out for each group of subcarriers as in 4.4.1.

When QO coding is employed, the main idea consists in separating at the receiver groups of 4 subcarriers encoded together and perform decoding as in the narrowband case. For the narrowband case, the properties of ML and linear detectors (MMSE, ZF) have been thoroughly studied in [RuMe02], [MeRu04], [PaFo01]. Here, we will use MMSE decoding. We place ourselves in a simulation scenario similar to the one in subsection 4.4.2.

In Fig. 5.9, we present the performance of a 4 Tx antenna system with real channel estimation assuming that 60 localized subcarriers are allocated to a user. We use QPSK signal mapping and rate 1/2 turbo FEC. At a target FER of 1%, SC-QOSFBC loses 0.4 dB with respect to QOSTBC and QOSFBC if two Rx antennas are employed at the base station. The scheme combining FSTD with SFBC/SC-SFBC outperforms QOSTBC by 0.2 dB. Adding more receive antennas diminishes the relative performance difference between the studied schemes: QOSTBC and QOSFBC outperform SC-QOSFBC by 0.1 dB and are outperformed by FSTD with SFBC/SC-SFBC by 0.15 dB.

Let us remind that, in terms of PAPR, QOSTBC, SC-QOSFBC and SC-SFBC with frequency switching have SC-like performance, while SFBC with frequency switching and QOSFBC lose up to 0.9 dB and 1.3 dB, respectively. Thus, as a whole, SC-like schemes outperform the others.

The good performance of FSTD-based schemes is explained by the fact that, due to the separation in the frequency domain of the four transmit antennas in two groups of two transmit antennas, channel estimation has better performance than in the case of QO codes. Indeed, in FSTD-based schemes we need to estimate two orthogonal 2×2 (2×4) MIMO channels, while in the QO case we need to estimate one 4×2 (4×4) MIMO channel. When estimating the coefficients of a channel from one transmit antenna, the role of the Wiener filter is to reduce not only the transmission noise but also the jammer signal consisting in the pilots of the other Tx antennas. This is a more difficult task in the latter case, since 3 jammer signals need to be eliminated. Indeed, by analyzing the results in Fig. 5.10, we notice that FSTD-based schemes are outperformed by QO schemes when perfect channel knowledge is assumed at the receiver: QOSTBC/QOSFBC outperform SFBC with frequency switching, SC-SFBC with frequency switching and SC-QOSFBC by 0.3 dB, 0.4 dB and 0.5 dB, respectively, when we assume 2 receive antennas.

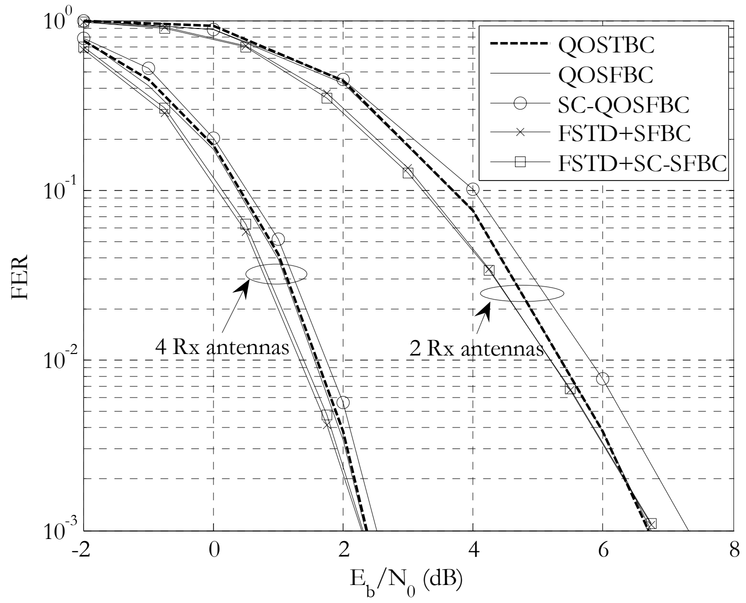

Fig. 5.9 Performance of transmit diversity schemes with 4 Tx antennas: 3 km/h, 60 localized subcarriers, QPSK 1/2, MMSE decoding, 2 and 4 receive antennas, real channel estimation.

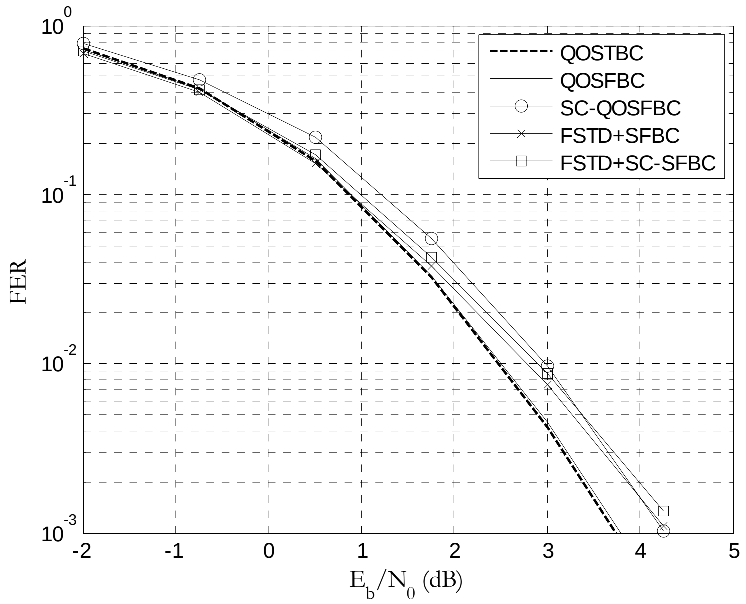

Fig. 5.10 Performance of transmit diversity schemes with 4 Tx antennas: 3 km/h, 60 localized subcarriers, QPSK 1/2, MMSE decoding, 2 receive antennas, perfect channel knowledge.

5.6. Summary and conclusions

In this chapter we have discussed transmit diversity techniques for SC-FDMA with four transmit antennas. Orthogonal designs do not exist in this case. We considered two approaches: extending the SC-SFBC codes presented in chapter 4 in a quasi-orthogonal manner, and combining SC-SFBC with some frequency switching techniques. Classical quasi-orthogonal designs such as the Jafarkhani codes have some drawbacks when combined with SC-FDMA. First, QOSTBC lacks framing flexibility, imposing frames composed of multiple of 4 symbols. Next, QOSFBC is not suitable to be combined with SC-SFBC since it leads to PAPR degradation. Extending SC-SFBC to the 4-antenna case, we proposed a QO code conserving the good PAPR properties of SC-FDMA. We thus developed SC-QOSFBC or SC-QOSTFBC type solutions. We generalized the QO approach to numbers of transmit antennas larger than 4. Taking into account actual channel estimation constraints, combining SC-SFBC with FSTD makes the most of transmit diversity with 4 transmit antennas.

Chapter 6

Combined spatial multiplexing / space-frequency block coding schemes

So far, we concentrated on rate-one transmit-diversity schemes. Space-time block codes, like the Alamouti orthogonal design for example, were conceived to ensure full spatial diversity, $N_{\mathrm{Tx}} \times N_{\mathrm{Rx}}$, with very low complexity separate decoding. In this case, the multiple antennas are used to improve the performance at a given throughput, making use of the diversity gain. The drawback of such schemes is their low maximum transmission rate: to achieve full spatial diversity without relying on an outer FEC, the maximum transmission rate for a code with symbols drawn from a complex constellation is one symbol per channel use, for any number of transmit antennas [Jaf05]. This is the same throughput as a SISO system. The code rate can be eventually increased by choosing symbols drawn from different (usually rotated) complex constellations, or using FEC and space-time codes jointly optimized.

On another hand, the use of multiple antennas can be translated in increasing the capacity of MIMO channels. The aim is to increase the throughput with respect to SISO channels for the same target performance, measured, *e.g.*, by means of FER. As already introduced in subsection 2.5, the maximum transmission rate which is possible to be achieved is of $\min(N_{\mathrm{Tx}},N_{\mathrm{Rx}})$ symbols per channel use. Assuming in uplink a number of antennas larger at the base station than at the terminal, this means a maximum transmission rate N_{Tx} times higher than the SISO data rate. The simplest approach to achieve this maximum throughput is to demultiplex the data stream into N_{Tx} parallel streams, and transmit one independent stream per transmit antenna. This technique is called spatial multiplexing. Many space-time architectures based on this idea were developed, as for example V-BLAST (Vertical BLAST), D-BLAST (Diagonal BLAST) or Turbo-BLAST. Obviously, as it can be seen from the diversity-multiplexing tradeoff in Fig. 4.1, this extra throughput is obtained at the expense of sacrificing some diversity. Generally, these types of systems achieve a diversity gain in the order of N_{Rx}.

Moreover, good detectors capable of decoding spatially multiplexed streams are extremely complex. In future communications systems, with the development of, *e.g.*, femtocell solutions conceived for use in residential or small business environments, the complexity and cost of the base station also becomes a limiting factor. Thus, in the sequel we will consider MMSE receivers.

Spatial multiplexing is a good solution for increasing the throughput of users, already in good transmission conditions, *e.g.*, at high SNR, while transmit diversity is appropriate for improving the performance of users in severe situations, *e.g.*, at low SNR. We will focus in the following on hybrid solutions, achieving a trade-off between data rate and diversity by combining STBC/SFBC with spatial multiplexing. This is a solution of interest, since in practice it will allow the users to increase their throughput when the channel conditions are acceptable, while keeping the complexity of the detector rather low.

6.1. SC-SFBC for single-user MIMO

To combine transmit diversity techniques with spatial multiplexing, the main idea consists in splitting the N_{Tx} transmit antennas into K groups. The input data stream will be divided into K parallel data sub-streams, each sub-stream being encoded according to a transmit diversity technique (*e.g.*, STBC) in order to achieve the maximum diversity for each group of antennas. The transmission of the K transmit-diversity codes is done simultaneously, each code representing therefore interference for the other K-1 codes. The receiver should be able to decode each sub-stream, while minimizing the effects of the other interfering sub-streams. If the sub-streams are FEC coded separately (*e.g.*, multi-user (MU)-MIMO), or uncoded, the detection is equivalent to that of multi-user systems. Sphere decoders or sequential interference cancelling (SIC) techniques are known to be effective, although rather complex. When the sub-streams are FEC coded together (single-user (SU)-MIMO), linear low complexity techniques like MMSE receivers also give rather good results, since the residual interference is also managed by the error correcting code.

We will treat here a case where an MS is equipped with $N_{\mathrm{Tx}} = 4$ transmit antennas, split in $K = 2$ groups of 2 antennas each. The transmit diversity technique employed by each group of 2 antennas is an orthogonal block code, as, for example, Alamouti-based STBC or SFBC. The generator matrix of this code can be expressed as:

$$\mathcal{A}^{\mathrm{dA}} = \begin{array}{c} \begin{pmatrix} a_0 & -a_1^* & a_2 & -a_3^* \\ a_1 & a_0^* & a_3 & a_2^* \end{pmatrix} \begin{array}{l} \leftarrow i_0 \text{ or } f_{k_0} \\ \leftarrow i_1 \text{ or } f_{k_1} \end{array} \\ \begin{array}{cccc} \uparrow & \uparrow & \uparrow & \uparrow \\ \mathrm{Tx}_0 & \mathrm{Tx}_1 & \mathrm{Tx}_2 & \mathrm{Tx}_3 \end{array} \end{array} . \tag{6.1}$$

This type of code is sometimes called double-STTD (space-time transmit diversity) [Hot03], or product STBC [TaNa99], when applied in the time domain. Since we also treat here of codes implemented in the frequency domain, we will employ the generic term of double Alamouti, which can take the form of double STBC, double SFBC or double SC-SFBC respectively.

When employed in an SC-FDMA transmitter, the double Alamouti scheme is implemented as in Fig. 6.1. We maintained the same notations as in Chapter 4. In a SU-MIMO context, coded bits belonging to the same FEC codeword are mapped onto constellation symbols forming the data stream $\mathbf{x}_{\text{global}}^{(i)}$, split in two parallel sub-streams $\mathbf{x}^{(i)}$ and $\mathbf{x}'^{(i)}$. In a MU-MIMO context, sub-streams $\mathbf{x}^{(i)}$ and $\mathbf{x}'^{(i)}$ would contain modulation symbols generated from separate FEC codewords. Implementing double Alamouti in the time domain (STBC) implies choosing in (6.1):

$$a_m = \begin{cases} s_k^{(i_m)}, \text{ if } m = 0,1 \\ s_k'^{(i_{m \bmod 2})}, \text{ if } m = 2,3 \end{cases}, \quad \forall k = 0,\ldots M-1\,. \tag{6.2}$$

For a frequency-domain approach, the choice is:

$$a_m = \begin{cases} s_{k_m}^{(i)}, \text{ if } m = 0,1 \\ s_{k_{m \bmod 2}}'^{(i)}, \text{ if } m = 2,3 \end{cases}, \quad \forall i\,, \tag{6.3}$$

(k_0, k_1) being chosen as discussed in chapter 4 to correspond to SFBC or to SC-SFBC transmit diversity schemes. The PAPR considerations, as well as the advantages and drawbacks of STBC/SFBC/SC-SFBC approach were discussed in the previous chapters and will not be repeated here. We briefly treat here the practical case of an MS using SC-FDMA and disposing of 4 transmit antennas, attempting to optimize its performance without increasing the complexity of the detector. MMSE decoding is similar to the one presented in subsection 4.4.1. For double SC-SFBC, we ignore the time superscript (i). We consider $\mathbf{H}_k = \left[H_{n_{\text{Rx}}, n_{\text{Tx}}, k} \right]$, with $n_{\text{Rx}} = 0\ldots N_{\text{Rx}} - 1$ and $n_{\text{Tx}} = 0\ldots3$, and:

$$\mathbf{H}_{(k_0,k_1)} = \begin{bmatrix} \mathbf{H}_{k_0} \\ \mathbf{H}_{k_1}^* \begin{bmatrix} \begin{matrix} 0 & -1 \\ 1 & 0 \end{matrix} & \mathbf{0}_2 \\ \mathbf{0}_2 & \begin{matrix} 0 & -1 \\ 1 & 0 \end{matrix} \end{bmatrix} \end{bmatrix}. \tag{6.4}$$

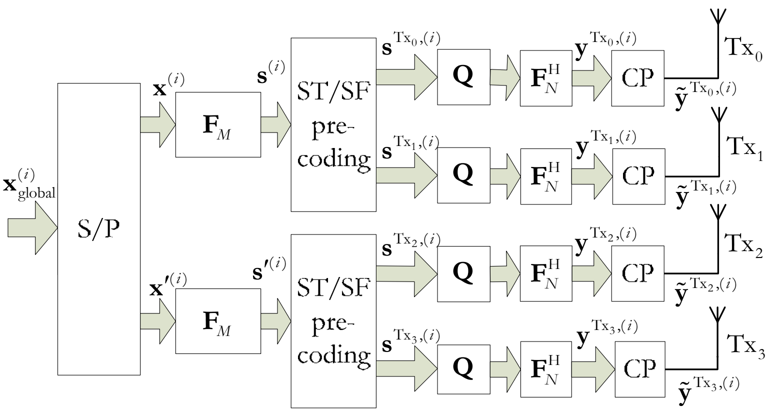

Fig. 6.1 Block diagram of an SU-MIMO SC-FDMA transmitter employing combined spatial multiplexing and ST/SF block coding.

(4.44) becomes:

$$\begin{aligned}\begin{bmatrix}\hat{s}_{k_0}\\ -\hat{s}^*_{k_1}\\ \hat{s}'_{k_0}\\ -\hat{s}'^*_{k_1}\end{bmatrix} &= \underbrace{\mathbf{E}_{(k_0)}\mathbf{H}_{(k_0,k_1)}}_{\triangleq \mathbf{A}^{(k_0)}}\begin{bmatrix}s_{k_0}\\ -s^*_{k_1}\\ s'_{k_0}\\ -s'^*_{k_1}\end{bmatrix} + \mathbf{E}_{(k_0)}\breve{\mathbf{n}}_{(k_0,k_1)}\\ &= \begin{bmatrix}A^{(k_0)}_{0,0} & A^{(k_0)}_{0,1} & A^{(k_0)}_{0,2} & A^{(k_0)}_{0,3}\\ A^{(k_0)}_{1,0} & A^{(k_0)}_{1,1} & A^{(k_0)}_{1,2} & A^{(k_0)}_{1,3}\\ A^{(k_0)}_{2,0} & A^{(k_0)}_{2,1} & A^{(k_0)}_{2,2} & A^{(k_0)}_{2,3}\\ A^{(k_0)}_{3,0} & A^{(k_0)}_{3,1} & A^{(k_0)}_{3,2} & A^{(k_0)}_{3,3}\end{bmatrix}\begin{bmatrix}s_{k_0}\\ -s^*_{k_1}\\ s'_{k_0}\\ -s'^*_{k_1}\end{bmatrix} + \underbrace{\mathbf{E}_{(k_0)}\breve{\mathbf{n}}_{(k_0,k_1)}}_{\text{coloured noise}}\end{aligned} \tag{6.5}$$

Self-interference within an Alamouti pair (null on flat channels)

Inter-stream interference

Useful part (+intercode interference)

After splitting the two Alamouti streams, the decoding process can continue as in subsection 4.4.1. The diagonal (blue) term in (6.5) gives rise to the useful signal and (after per-subcarrier equalization and size-M IDFT deprecoding) to an intercode interference term, as explained in subsection 4.4.1. A self-interference term due to precoding onto different subcarriers (yellow) also appears, which becomes null on flat channels (or for STBC with stationary channel). But, with respect to (4.48), a third term appears (red), representing the inter-stream interference between the two Alamouti pairs sent in parallel. This term has the most important part in the interference balance, since each Alamouti stream represents for the other an interference with the same power as the useful signal. To compare the interference profile, we also give here the equivalent of (6.5) for QO codes:

$$\begin{bmatrix}\hat{s}_{k_0}\\ \hat{s}^*_{k_1}\\ \hat{s}_{k_2}\\ \hat{s}^*_{k_3}\end{bmatrix} = \begin{bmatrix}A^{(k_0)}_{0,0} & A^{(k_0)}_{0,1} & A^{(k_0)}_{0,2} & A^{(k_0)}_{0,3}\\ A^{(k_0)}_{1,0} & A^{(k_0)}_{1,1} & A^{(k_0)}_{1,2} & A^{(k_0)}_{1,3}\\ A^{(k_0)}_{2,0} & A^{(k_0)}_{2,1} & A^{(k_0)}_{2,2} & A^{(k_0)}_{2,3}\\ A^{(k_0)}_{3,0} & A^{(k_0)}_{3,1} & A^{(k_0)}_{3,2} & A^{(k_0)}_{3,3}\end{bmatrix}\begin{bmatrix}s_{k_0}\\ s^*_{k_1}\\ s_{k_2}\\ s^*_{k_3}\end{bmatrix} + \text{coloured noise} \tag{6.6}$$

Self-interference (null on flat channels)

Self-interference (QO part)

Useful part (+intercode interference)

For the same spectral efficiency and using detectors with comparable complexity, we evaluate the different methods proposed throughout this work in order to determine which one would produce better performance. We consider two scenarios. First, we suppose that the user is situated at cell edge and is subject to poor propagation conditions operating thus at low SNR. It typically uses low modulation orders and low spectral occupancy, and employs MIMO techniques to improve its link quality. A second possibility is that of a high mobility user, rather close to the base station and thus subject to good propagation conditions, but unable to dispose of reliable channel feedback due to its high velocity. This user might try to increase its throughput by using higher modulation orders.

Fig. 6.2 presents results comparing different methods employed by a low-velocity mobile station equipped with 4 transmit antennas for 1RB allocation. For a spectral efficiency of 1 bit/s/Hz, this user can employ either rate one transmit diversity techniques (QOST/SFBC, SC-QOSFBC, FTSD+ST/SFBC, FSTD+SC-SFBC) with QPSK 1/2 coding, or for example double Alamouti techniques (double STBC, double SC-SFBC) and QPSK with rate-1/4 coding in order to trade-off diversity and multiplexing gain. In this case, double Alamouti techniques are outperformed by about 1 dB at the FER of 10%, when low-complexity MMSE detection is used. This is due to the fact that double Alamouti schemes suffer from stronger intercode interference than QO schemes: QO schemes have low self-interference [TiBo00], while in double Alamouti schemes, each Alamouti layer suffers not only from self-interference within an Alamouti pair, but also from inter-stream interference from a second Alamouti stream, having the same power, as pointed out in (6.5)-(6.6). Double STBC and double SC-SFBC have similar performance, with the advantage of a higher flexibility for the latter. In the following we will omit double STBC, as well as the combined schemes studied in Chapter 5.

In Fig. 6.3, a high mobility user moving at 120 kmph is also allocated 1RB. For a higher spectral efficiency (2.66 bit/s/Hz), we considered several scenarios: rate one transmit diversity with 16QAM rate-2/3 code, and double Alamouti with either 16QAM rate-1/3 or QPSK rate-2/3. V-BLAST with QPSK rate-1/3 is also presented, to show the impact of strong inter-stream interference on the sub-optimal MMSE receiver. In this case, double Alamouti outperforms QO techniques. This can be explained by the fact that the outer turbo code of rate 2/3 is not strong

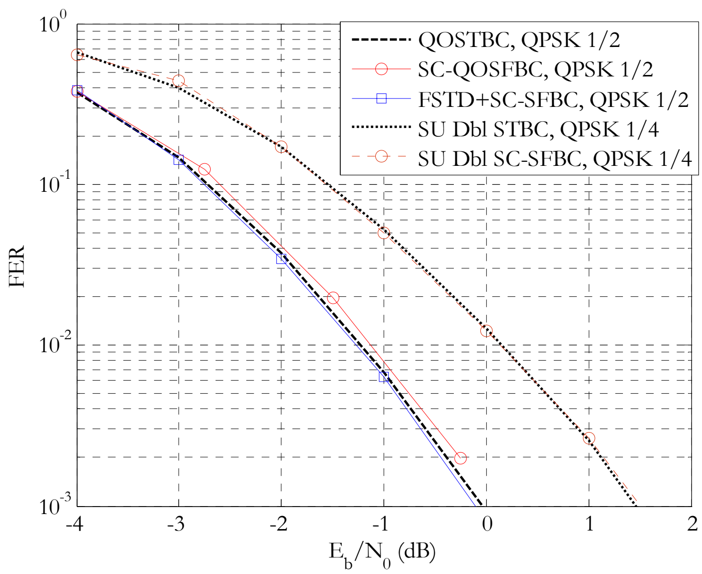

Fig. 6.2 Different 4x4 schemes at spectral efficiency 1 bit/s/Hz; 1RB, 3kmph, perfect CSI.

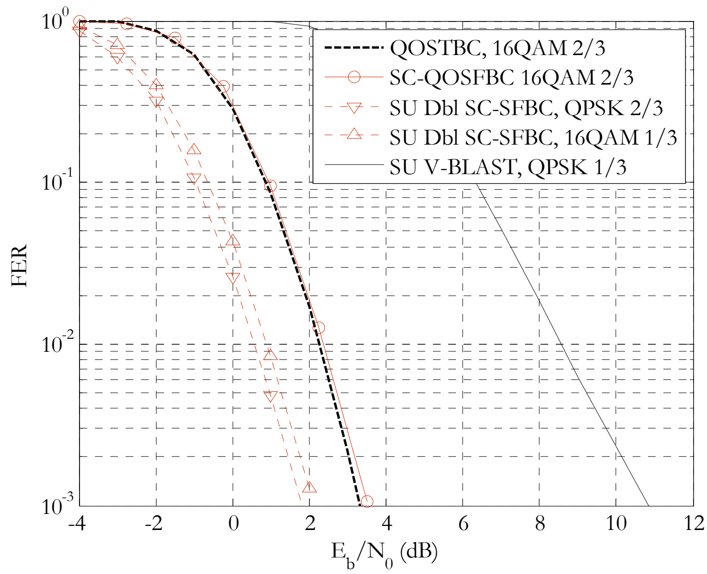

Fig. 6.3 Different 4x4 schemes at spectral efficiency 2.66 bit/s/Hz; 1RB, 120kmph, perfect CSI.

enough to manage the impact of interference of QO codes on the sensitive 16QAM constellation. Using a stronger code (1/3) or a more robust constellation (QPSK) brings important performance improvement, which explains the better performance of the double Alamouti code.

Also note in Fig. 6.3 that double Alamouti with QPSK 2/3 outperforms double Alamouti with 16QAM 1/3 by about 0.3 dB. This can be explained by the fact that 16QAM is more sensitive to interference than QPSK, as we have shown in Chapter 3.

6.2. SC-SFBC for multi-user MIMO

Let us now consider that several users, disposing of at least 2 transmit antennas each, are managed by the same BS. The BS tries to map the uplink signals of these users in a given limited bandwidth in an optimal manner. Each such user implements SC-SFBC as a transmit diversity scheme. According to the desired throughput, to the capabilities of each mobile station and to the corresponding channel quality, the scheduler at the BS will decide the spectral allocation and the modulation and coding scheme (MCS) of each user. To optimize the spectral occupancy and increment the throughput, it is interesting to allow some spectral superposition between users using the same MCS, but having either the same or different spectral allocations (different number of allocated RBs).

6.2.1. Double SC-SFBC with the same spectral allocation

If two users with the same spectral allocation wish to share the same band, using SC-SFBC each, this can be simply done as schematically shown in Fig. 6.4. The only restriction is for them to use the same p parameter, which results in a MU double SC-SFBC scheme, as in Fig. 6.4.

A simple MMSE detector is still able to decode the double Alamouti stream, but the MU case experiences performance degradation with respect to the SU case, as shown in Fig. 6.5. MMSE detection is suboptimal in reducing the interference between the two Alamouti streams. While in the SU case the outer turbo code manages to significantly reduce the residual interference after MMSE detection, the MU scheme does not benefit from any joint coding. To improve the MU performance, more complex detectors are needed.

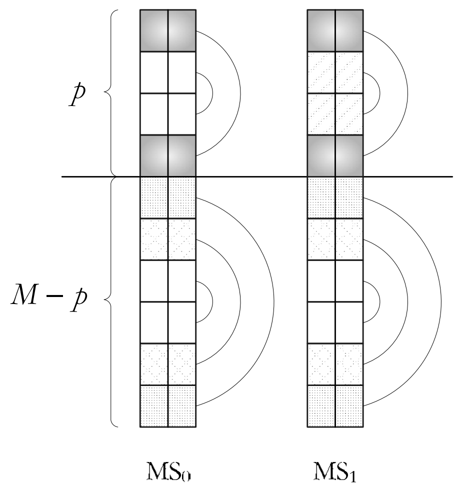

Fig. 6.4 MU Double SC-SFBC with the same spectral allocation.

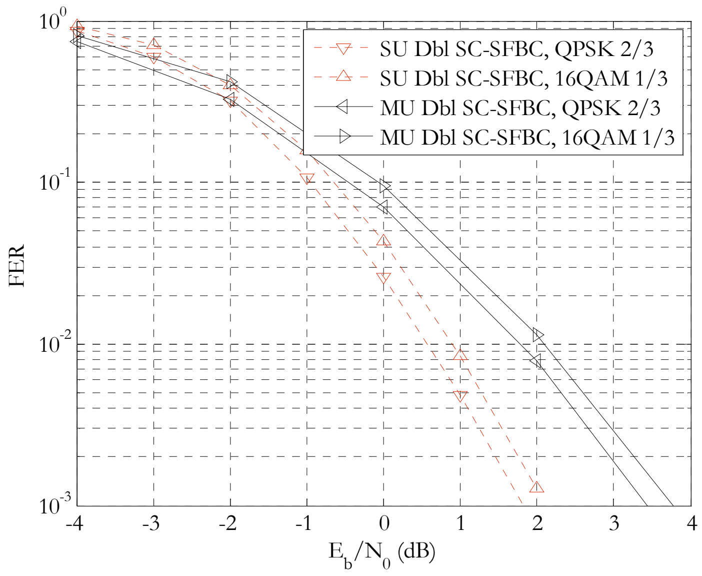

Fig. 6.5 SU and MU double SC-SFBC, 4x4; 1RB, 120kmph, perfect CSI.

6.2.2. Double SC-SFBC with different spectral allocations

Let us assume that the scheduler allows at most two users (MS_0 and MS_1) to share simultaneously groups of subcarriers corresponding to all or to part of the subcarriers allocated to each user. Each user is employing transmit diversity techniques, *e.g.* SC-SFBC, independently from the other users. For the part of the spectrum where the two users transmit simultaneously, this is equivalent to applying a MIMO scheme that combines spatial multiplexing and SC-SFBC in a MU context. The MU-MIMO channel has N_{Tx} transmit antennas, split into $K=2$ non-collocated groups, $N_{\mathrm{Tx}} = N_{\mathrm{Tx}_0} + N_{\mathrm{Tx}_1}$.

The spectral allocation decided by the scheduler consists in computing the number of subcarriers M_i, as well as the starting position n_i of the portion of spectrum allocated to each MS_i. When SC-SFBC is used, the discussion in Chapter 4 showed that, to minimize the maximum distance between subcarriers coded together, the best strategy is to employ $\mathrm{SC}_M^{p=M/2}$. But in a MU-MIMO context, double SC-SFBC might have some pairing incompatibility problems. Indeed, let us analyze the situation depicted in Fig. 6.6, where MS_0 is allocated M_0=8 subcarriers and MS_1 is allocated M_1=12 subcarriers. The portions of spectrum occupied by the 2 MSs are aligned, $n_0 = n_1 = 0$, which means that the first occupied subcarrier by each MS is the one with index 0, denoted f_0 in Fig. 6.6.

Therefore, MS_0 uses SC_8^4 and MS_1 uses SC_{12}^6. Subcarriers with indexes (k_0, k_1) obtained by applying (4.35) contain Alamouti pairs. On the 5-th occupied subcarrier f_4 for example, MS_0 transmits frequency samples s_4 and $-s_7^*$ onto its two transmit antennas respectively. Next, f_4 is paired with f_7, onto which MS_0 transmits frequency samples s_7 and s_4^*, respectively. On the same subcarrier f_4, MS_1 transmits frequency samples s'_4 and $-s_1'^*$, respectively, onto its two transmit antennas. Since MS_1 uses SC_{12}^6, f_4 is paired with f_1. As a result, the pairing of subcarriers is not compatible between MS_0 and MS_1. Because of this incompatibility, this structure does not correspond to a double SC-SFBC construction and the conventional MMSE detector cannot be employed anymore. A joint MMSE detection over all the bandwidth containing cross-codes subcarriers is necessary. For the example in Fig. 6.6, this would involve inverting a matrix of order $M_0 + M_1 = 20$ instead of 2 matrices of order 4 and 2 matrices of order 2, as it would have been the case if the two MSs were correctly aligned to form double Alamouti pairs on the overlapping subcarriers, and simple Alamouti pairs on the remaining subcarriers. The problem becomes even more complex when 3 or more users have overlapping subcarriers.

To show how this incompatibility problem can be avoided, let us state here a property of the SC_M^p operation:

Property: Any SC_M^p operation can be decomposed into the juxtaposition of SC_p^0 and SC_{M-p}^0 operations.

Proof: Let us analyze the structure of matrix $\mathbf{P}_M$ in (D.10) as a function of parameter p. $\mathbf{P}_M(p)$ is a block diagonal matrix, containing on its main diagonal matrices $-\overline{\mathbf{P}}_p^{(\mathrm{J})} = -\mathbf{S}_p^0 \overline{\mathbf{P}}_p^{(\mathrm{J})} = \mathbf{P}_p(0)$ corresponding to a SC_p^0 operation, and $-\overline{\mathbf{P}}_{M-p}^{(\mathrm{J})} = -\mathbf{S}_{M-p}^0 \overline{\mathbf{P}}_{M-p}^{(\mathrm{J})} = \mathbf{P}_{M-p}(0)$ corresponding to a SC_{M-p}^0 operation, respectively. This property can be verified by investigating the structure of an SC-SFBC frame as, *e.g.*, Fig. 4.7.

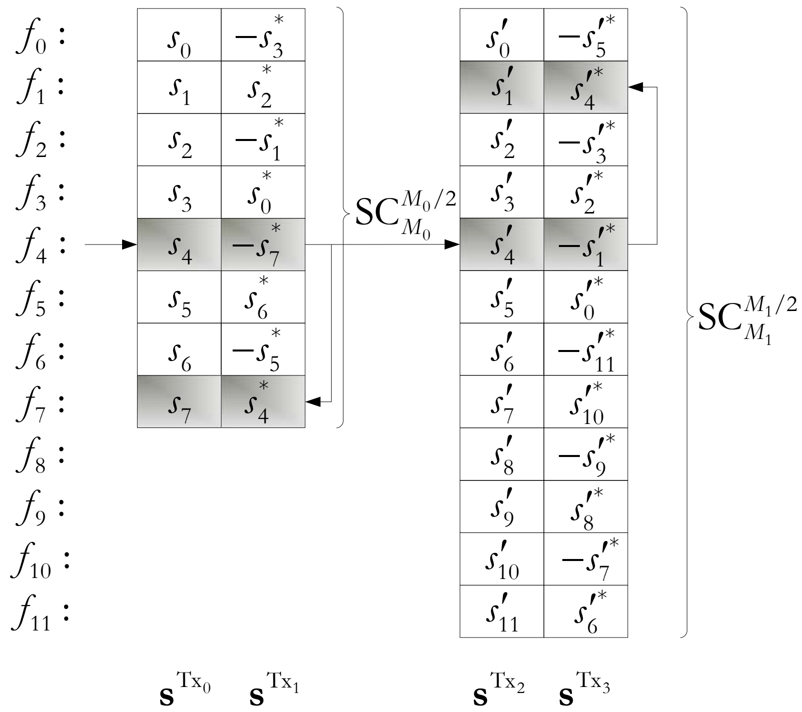

Fig. 6.6 MU Double SC-SFBC with incompatible pairing of subcarriers.

Let us denote the number of subcarriers simultaneously used by two MSs by M_{overlap}. To avoid any pairing incompatibility, the 2 MSs need to transmit the same symbol structure over the overlapping spectral portion. Based on the property stated above, when the two MSs have strictly different (or misaligned) spectral allocations, the only valid option is to chose p parameters p_i and spectrum positions n_i such that the overlapping portion has a structure based on $\mathrm{SC}_{M_{\text{overlap}}}^{0}$. While an optimization of parameter p has no direct impact on the allocated set of subcarriers, an optimization of the spectrum positions n_i limits the flexibility of the frequency scheduler. We will give some examples in the following section.

Optimization of parameter *p*

Two mobile stations with different spectral allocations

In this section, we aim at allowing the use of SC-SFBC by two terminals MS_0 and MS_1 having overlapping spectrum allocation with low-complexity MMSE receiver at the base station. From the receiver side, we implicitly assume that the portions of the spectrum that are not shared by both MS_0 and MS_1 are not shared with any other user.

In the trivial case where the scheduler imposes the same bandwidth for the two MSs $(M_0 = M_1 = M)$ and the two MSs are aligned $(n_0 = n_1)$, they can use the same default allocation $p_1 = p_2 = p$ (*e.g.*, p=$M/2$, the default optimal value), as this case reduces to the one in Fig. 6.4. Thus, double SC-SFBC can be employed onto all pairs of subcarriers.

If the two MSs have strictly different bandwidths, $M_0 < M_1$, a solution is given in Fig. 6.7. We need to impose MS_0 to use $\mathrm{SC}_{M_0}^{p_0=0}$ and MS_1 to use $\mathrm{SC}_{M_1}^{p_1=M_0}$. The $\mathrm{SC}_{M_1}^{p_1=M_0}$ can be seen as the juxtaposition of two SC-like operations:

- $\mathrm{SC}_{M_0}^{0}$ to match the configuration of MS_0; on this part of the spectrum, double SC-SFBC transmission can thus be employed;
- the remaining $\mathrm{SC}_{M_1-M_0}^{0}$ corresponds to a simple SC-SFBC transmission and keeps an overall SC-type signal to be transmitted by MS_1.

Hence, it is no longer possible to use one single predefined p for all the system but double SC-SFBC potential is kept at the expense of a modification of the p parameter, *i.e.*, some performance degradation as the maximum distance between subcarriers that are jointly precoded is increased. But only two matrices of order 4 and two matrices of order 2 need to be inverted during MMSE decoding. It should also be noted that additional signaling is necessary to indicate the values of p to be used by each MS in this case.

An alternative solution where the two MSs are misaligned is to decompose $\mathrm{SC}_{M_1}^{p_1}$ into $\mathrm{SC}_{p_1}^{0}$ and $\mathrm{SC}_{M_1-p_1}^{0}$, and to allocate MS_0 in the middle of the bandwidth occupied by $\mathrm{SC}_{p_1}^{0}$ if $p_1 > M_0$ or in the middle of the bandwidth occupied by $\mathrm{SC}_{M_1-p_1}^{0}$ otherwise. An example is depicted in Fig. 6.8. Nevertheless, this might lead to a modified double SC-SFBC (there is a sign inversion within the double SC-FDMA pair on antenna Tx_3) which needs to be taken into account at the receiver, without any performance loss.

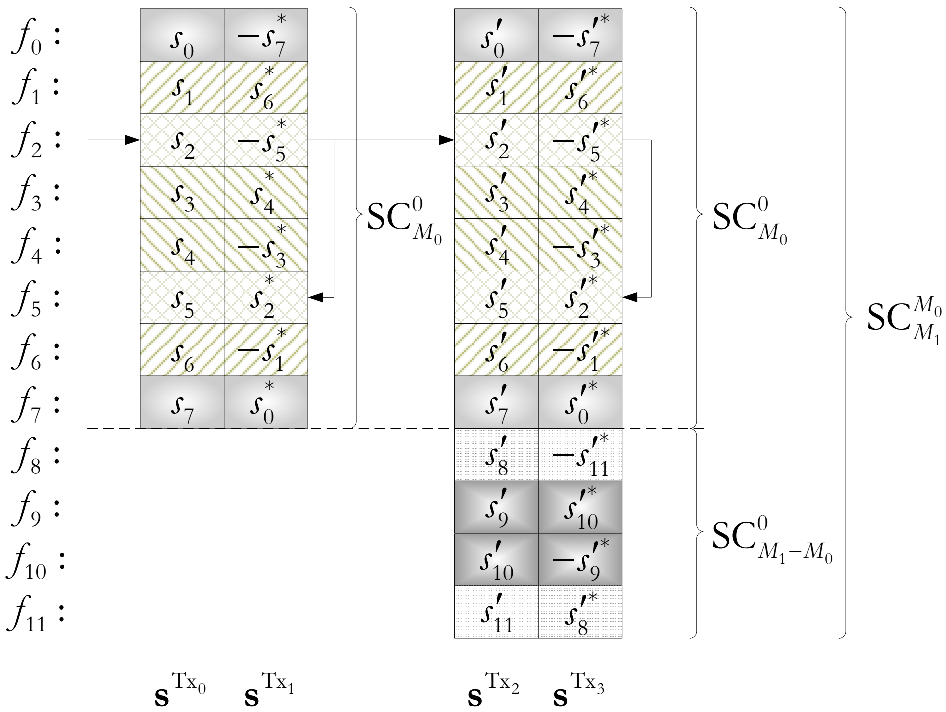

Fig. 6.7 Double SC-SFBC with aligned MSs, $M_0 \leq M_1$, an example for $M_0=8$, $M_1=12$, $p_0=0$, $p_1=8$, $n_0=n_1$.

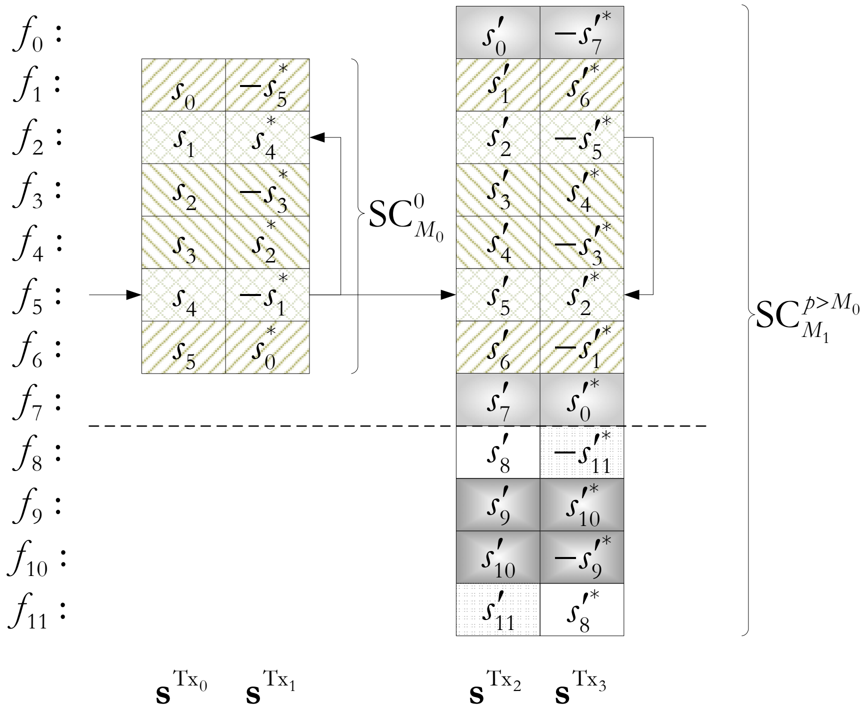

Fig. 6.8 Double SC-SFBC with misaligned MSs, $M_0 \leq M_1$, an example for $M_0=6$, $M_1=12$, $p_0=0$, $p_1=8$, $n_0>n_1$.

In both cases depicted in Fig. 6.7 and Fig. 6.8 it is possible to allow double SC-SFBC thanks to an optimization of parameter p only. No constraint is introduced in the frequency scheduler to optimize n_0 and n_1.

Three or four mobile stations with various spectral allocations

Let us now consider that 3 MSs need to be scheduled in an optimal manner. We can consider without any loss of generality that MS_2 has the largest spectral allocation, *i.e.*, $M_0, M_1 < M_2$. When $M_0+M_1=M_2$, the three MSs can be scheduled together by using a decomposition of $\mathrm{SC}_{M_2=M_0+M_1}^{p_2=M_2}$ into $\mathrm{SC}_{M_0}^{0}$ and $\mathrm{SC}_{M_1}^{0}$. The solution is presented in Fig. 6.9.

When equality is not satisfied, we have two cases:

- if $M_0+M_1<M_2$, we schedule MS_1 in the middle of second sub-band of MS_3;
- if $M_0+M_1>M_2$, we target a decomposition for MS_1 in $\mathrm{SC}_{M_2-M_0}^{0}$ and $\mathrm{SC}_{M_1-M_2+M_0}^{0}$.

It is easy now to extend this structure to the case where 4 MSs need to be scheduled, as in Fig. 6.10. The case $M_0+M_1=M_2+M_3$ is treated here, the other cases being easily reduced to one of the previously treated cases.

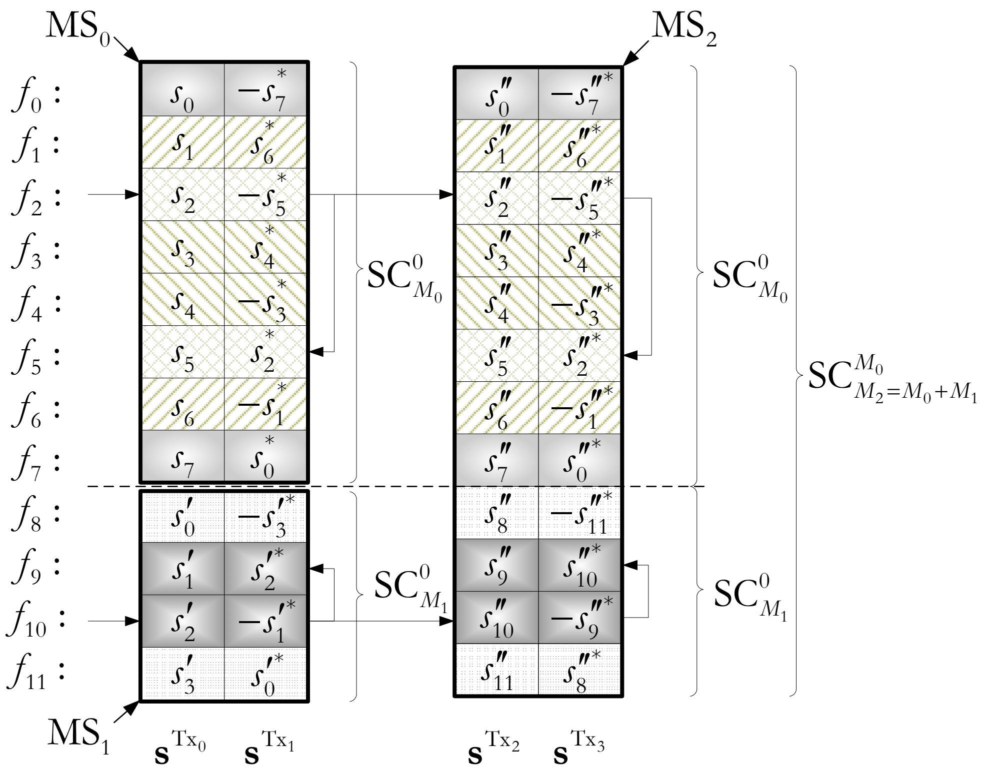

Fig. 6.9 Double SC-SFBC with M_0+M_1=M_2, an example for M_0=8, M_1=4, M_2=12, p_0=0, p_1=0, p_2=8

Optimization of spectral occupancy

Let us now extend the particular cases treated in the previous subsection to a general framework where a BS manages several MSs, let their number be N_{users}. We propose here to optimize not only the parameter p but also the spectrum positions n_i so as to allow using double SC-SFBC by several terminals having overlapping spectrum allocations.

Depending on the needs and capabilities of uplink communication of each MS, the BS determines the number of subcarriers M_i allocated to each MS$_i$, $i = 0 \ldots N_{\text{users}} - 1$. Each MS is equipped of at least 2 transmit antennas and uses SC-FDMA with SC-SFBC transmit diversity for its uplink communication. Our purpose is to schedule these N_{users} MSs, in such a manner that the occupied bandwidth is minimized and the overall throughput is optimized. The couple (p_i, n_i), representing the p parameter and the first occupied subcarrier, need to be determined for each MS$_i$.

The main idea behind the solution is to determine 2 groups of users, A and B. Users' allocated bands do not overlap inside of each group, but each user of each group can have overlapping subcarriers with a maximum of 2 users from the other group, such as onto the overlapping subcarriers double Alamouti pairs are formed.

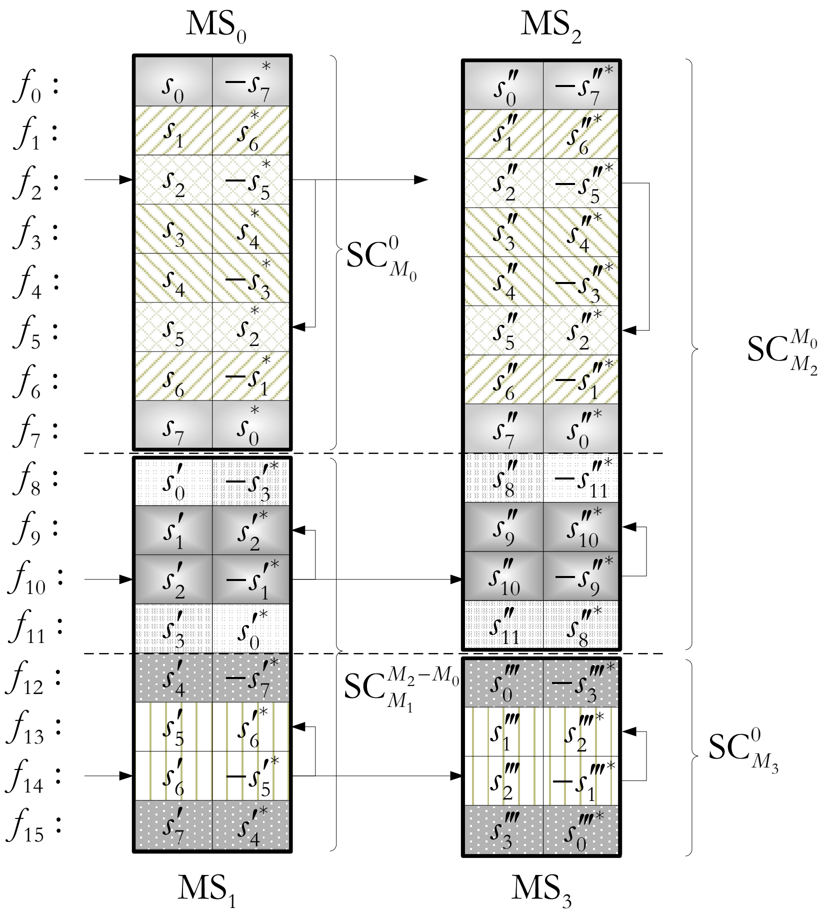

Fig. 6.10 Double SC-SFBC with $M_0+M_1=M_2+M_3$, an example for $M_0=8$, $M_1=8$, $M_2=12$, $M_3=4$, $p_0=0$, $p_1=4$, $p_2=8$, $p_3=0$.

We suppose subcarrier numbering starting at $n_0^{\mathrm{A}}=0$; n_0^{B} can be either null or take another positive value. n^{A}, n^{B} are auxiliary parameters indicating the index of the first available subcarrier in groups A and B, respectively. We suppose that BS tries to map N_{users} MSs in a bandwidth that is as compact as possible (alternatively, it could have one given available bandwidth and would try to map as many users as possible; algorithm still stands but the STOP condition needs to be modified). The algorithm presented in Appendix F tries to minimize the number of subcarriers allocated to only one single MS in order to improve the overall spectral efficiency, while forming double SC-SFBC pairs on the subcarriers simultaneously allocated to 2 MSs in order to ensure low-complexity decoding. All the cases depicted in Fig. 6.7 - Fig. 6.10 can be deduced based on this algorithm.

This scheduling strategy of course directly constrains the frequency scheduler. However, it should be understood that transmit diversity is mainly intended for terminals that cannot benefit from any close-loop processing as CSI-based frequency scheduling. In other words, no frequency scheduling gain can be achieved in this case and the constraint imposed on the frequency scheduler is only a specific ordering of each allocated spectrum given predetermined spectrum sizes M_i.

6.3. Summary and conclusions

This chapter addressed the case of combined spatial multiplexing / space-frequency block coding schemes in an SC-FDMA context. Double Alamouti schemes based on the techniques developed so far were introduced and evaluated in comparison with rate one transmit diversity techniques, for the same spectral efficiency. Due to the different amount of the intercode interference (depending on the structure of the code) and to the suboptimal nature of the MMSE detector, performance of different investigated scenarios is strongly dependent of the capacity of the outer FEC in coping with the residual interference of the MMSE receiver. For power-limited transmission scenario, using SC-SFBC technology (SC-QOSFBC or SC-SFBC+FSTD) provides the best performance taking into account the PAPR constraints. We also investigated the feasibility of implementing double SC-SFBC-based techniques in MU-MIMO SC-FDMA systems, where different users are likely to have different spectral allocations. On one hand, we proposed a specific optimization of SC-SFBC specific parameters to make the most of low-complexity MMSE receiver. On the other hand, an algorithm jointly optimizing the parameters of SC-SFBC and the frequency scheduler was given. This algorithm yields an improvement of the system's overall spectral efficiency.

Chapter 7

Conclusions and future work

In this thesis, we proposed and investigated new transmission strategies employing MIMO techniques at the mobile station for the uplink of an SC-FDMA system.

After a tremendous evolution in the past few decades, the 3rd generation of mobile telecommunications systems arrived at maturity. Research efforts are now concentrated on the development of B3G/4G systems. The suitability of SC-FDMA for the air interface of future generation systems is now an acknowledged fact, 3GPP having already adopted it for the uplink of LTE and LTE-advanced systems. Also, in order to fulfill the requirements of future communications systems, the use of MIMO technologies is mandatory.

SC-FDMA was not the only viable competitor for next-generation mobile systems. OFDMA or precoded-OFDMA schemes such as SS-MC-MA were strong candidates. A major issue in comparing the above-mentioned schemes is the trade-off between diversity, coding gain and intercode interference. While OFDMA has no built-in diversity and therefore poor performance in the uncoded case or in the presence of low code rates, SC-FDMA and SS-MC-MA benefit from the diversity achieved by spreading but tend to degrade at high modulation orders due to the intercode interference arising from channel frequency selectivity. But the main advantage of SC-FDMA is its low PAPR property, leading to a signal more robust to nonlinear distortions. An overall analysis, taking into account the presence of nonlinearities and realistic constraints (signal quality, in-band and out-of-band radiation limits, regulatory spectrum masks, *etc.*), points out the strengths and weaknesses of each technique. SC-FDMA outperforms OFDMA at low modulation orders, but might be over-performed when higher modulation orders are employed. This makes OFDMA a good solution for improving the performance of users in good transmission conditions, *i.e.*, power non-limited terminals which are already capable to be allocated high modulation orders. Nevertheless, SC-FDMA has a supplementary gain in terms of output back-off, which is important especially for users in severe transmission conditions, *e.g.*, when the terminal is power limited, as a terminal located at the cell-edge. SS-MC-MA is a compromise solution, not having any clear advantage over OFDMA and SC-FDMA.

An analysis of SC-FDMA was also conducted, showing the impact of different carrier mapping techniques, frequency hopping or channel estimation. Localized subcarrier mapping is preferred for spectral reasons and makes the most of the channel estimation effort. Frequency hopping techniques bring some improvement in low velocity scenarios.

Combining MIMO techniques with SC-FDMA in order to improve uplink performance turns out to be a real design challenge. Indeed, the interest of using SC-FDMA relies on its good PAPR properties, which gives it a significant advantage over its competitors. But most of the classical MIMO techniques result either in PAPR degradation or in strong constraints when applied to SC-FDMA. We have proposed an innovative mapping that allows Alamouti-based SFBC-type precoding for two transmit antennas without degrading the PAPR properties of SC-FDMA. This scheme, coined SC-SFBC, shows good performance in realistic simulation scenarios: It outperforms CDD, FSTD and OL-TAS, it is more flexible than STBC, and it has better PAPR than classical SFBC for almost equivalent performance.

As future user terminals will be equipped with higher number of antennas, typically 4 or higher, we extended the SC-SFBC concept to numbers of antennas larger than 2 so as to allow terminals to benefit from further performance improvement thanks to transmit diversity. Orthogonal transmit diversity designs do not exist in this case, so we considered two approaches: extending the SC-SFBC codes in a quasi-orthogonal manner, or combining SC-SFBC with some frequency switching techniques. Both approaches result in robust performance, but with different needs in terms of channel estimation effort, due to structural differences.

To not only improve the uplink performance but also the uplink throughput , we studied combined spatial multiplexing / space-frequency block coding schemes in an SC-FDMA context. Double Alamouti schemes based on the techniques developed so far were introduced and evaluated in comparison with rate one transmit diversity techniques, for the same spectral efficiency. Due to the different amount of the intercode, inter-stream or self- interference (depending on the structure of the code) and to the suboptimal nature of the MMSE detector, we showed the great impact of the outer FEC, which has to deal with residual interference after MMSE receiver.

We also investigated the possibilities of implementing double SC-SFBC-based techniques in MU-MIMO SC-FDMA systems, where different users are likely to have different spectral allocations. We proposed specific optimizations of SC-SFBC as well as frequency scheduling approaches to allow these different users to benefit from transmit diversity while keeping low PAPR.

In the actual context of mobile communications, we have proposed different open-loop solutions for the uplink of a MIMO SC-FDMA system. The evaluation was performed at link level. As a future investigation direction, an analysis of these techniques at system level would be useful in order to validate the performance improvement for cell-edge users using SC-SFBC-based techniques. Also, the principles described in this thesis can be extended and optimized, so as to render SC-SFBC-based techniques compatible with the more flexible clustered SC-FDMA in an LTE-Advanced context, for example. A closer analysis of the MU-MIMO case can be conducted, aiming at evaluating the impact of the proposed methods on the flexibility and performance of the frequency scheduling module.

In the actual context, low-complexity receivers are needed to allow, *e.g.*, low-cost base-stations for residential use such as femto-cell. MMSE detection is exhibiting good performance in a large number of scenarios, but also has limitations in important interference conditions. A theoretical study of the diversity of SC-FDMA with suboptimal MMSE detection would allow us to have a better understanding of the system's behavior and of the possibilities of optimizing the detector. Another direction of study is finding low-complexity receivers that improve the performance of hybrid techniques combining transmit diversity and spatial multiplexing.

Appendix A.
3GPP channel models

Table A.1 SCM Vehicular A channel parameters

No° of paths: 6		Path Power (dB)	Delay (ns)
Channel power profile		0 -1.0 -9.0 -10.0 -15.0 -20.0	0 310 710 1090 1730 2510
Speed (km/h)		3, 30, 120	
Mobile station	Antenna spacing	0.5λ	
	Power Azimuth Spectrum (PAS)	RMS angle spread of 35° per path with a Laplacian distribution, or 360° uniform PAS.	
	DoT (degrees)	22.5°	
	DoA (degrees)	67.5°	
Base station	Antenna spacing	0.5λ or 4λ or 10λ	
	PAS	Laplacian distribution with RMS angle spread of 2° or 5° per path, depending on AoA/AoD	
	AoD/AoA (degrees)	50° for 2° RMS angle spread per path 20° for 5° RMS angle spread per path	

Table A.2 3GPP TU reduced setting (6 taps) channel parameters

No° of paths: 6	Path Power (dB)	Delay (ns)
Channel power profile	-3.0 0 -2.0 -6.0 -8.0 -10.0	0 20 50 160 230 500

Appendix B.

E-UTRA user equipment specifications

Table B.1 Spectrum Emission Mask 3GPP LTE requirements

Δf_{OOB} (MHz)	1.4 MHz	3.0 MHz	5 MHz	10 MHz	15 MHz	20 MHz	Measurement bandwidth
± 0-1	[TBD]*	[TBD]	-15	-18	-20	-21	30 kHz
± 1-2.5	[-10]	[-10]	-10	-10	-10	-10	1 MHz
± 2.5-5	[-25]	[-10]	-10	-10	-10	-10	1 MHz
± 5-6		[-25]	-13	-13	-13	-13	1 MHz
± 6-10			-25	-13	-13	-13	1 MHz
± 10-15				-25	-13	-13	1 MHz
± 15-20					-25	-13	1 MHz
± 20-25						-25	1 MHz

*: To be defined

Table B.2 General requirements for E-UTRA ACLR

	Channel bandwidth / E-UTRA ACLR/ measurement bandwidth					
	1.4 MHz	3.0 MHz	5 MHz	10 MHz	15 MHz	20 MHz
E-UTRA ACLR	30 dB	30 dB	30 dB	30 dB	30 dB	30 dB
E-UTRA channel measurement bandwidth			4.5 MHz	9.0 MHz	13.5 MHz	18 MHz

Appendix C.
Hadamard matrices

In mathematics, a Hadamard matrix is defined as a square matrix with entries either +1 or −1 and whose columns are mutually orthogonal. Every two different columns have matching entries in exactly half of their columns and mismatched entries in the remaining columns. Corresponding properties holding for columns equally hold for rows. This property ensures the orthogonality, which can be expressed under matrix form as:

$$\mathbf{WH}_M \mathbf{WH}_M^{\mathrm{T}} = M\mathbf{I}_M \tag{C.1}$$

Examples of Hadamard matrices were first constructed by Sylvester in 1867 [Syl67]. Let $\mathbf{WH}_M$ be a Hadamard matrix of order *M*. Then the partitioned matrix

$$\mathbf{WH}_{2M} = \begin{bmatrix} \mathbf{WH}_M & \mathbf{WH}_M \\ \mathbf{WH}_M & -\mathbf{WH}_M \end{bmatrix} \tag{C.2}$$

is also a Hadamard matrix. Repeated application of the Sylvester construction (C.2) allows the construction of all Hadamard matrices of rank $M = 2^m$, also called Walsh matrices:

$$\mathbf{WH}_0 = 1;\ \mathbf{WH}_2 = \begin{bmatrix} 1 & 1 \\ 1 & -1 \end{bmatrix};\ \mathbf{WH}_{2^m} = \mathbf{WH}_2 \otimes \mathbf{WH}_{2^{m-1}} \tag{C.3}$$

It has been proven that in order for the Hadamard matrices to exist, their rank *M* must be a multiple of 4 [LiWi93]. An important open question in the theory of Hadamard matrices is that of existence.

Hadamard matrices of orders 12 and 20 were constructed by Hadamard in 1893 [Had93]. Paley discovered in 1933 a method using finite fields [Pal33] that generates Hadamard matrices of order q+1 when q is any prime power that is congruent to 3 modulo 4 and that produces a Hadamard matrix of order 2(q+1) when q is a prime power that is congruent to 1 modulo 4. The smallest order that cannot be constructed by a combination of Sylvester's and Paley's methods is 92, which was firstly presented in [BaGo62]. Other methods exist for generating a large number of Hadamard matrices. After the discovery in 2004 of a Hadamard matrix of order 428, the smallest order for which no Hadamard matrix is presently known is 668.

In the present thesis, it is of interest to present the Hadamard matrix of order 12, since multiple of 12 subcarriers are allocated to users in the investigated scenarios:

$$\mathbf{WH}_{12} = \begin{bmatrix} 1 & 1 & 1 & 1 & 1 & 1 & 1 & 1 & 1 & 1 & 1 & 1 \\ 1 & -1 & 1 & -1 & 1 & 1 & 1 & -1 & -1 & -1 & 1 & -1 \\ 1 & -1 & -1 & 1 & -1 & 1 & 1 & 1 & -1 & -1 & -1 & 1 \\ 1 & 1 & -1 & -1 & 1 & -1 & 1 & 1 & 1 & -1 & -1 & -1 \\ 1 & -1 & 1 & -1 & -1 & 1 & -1 & 1 & 1 & 1 & -1 & -1 \\ 1 & -1 & -1 & 1 & -1 & -1 & 1 & -1 & 1 & 1 & 1 & -1 \\ 1 & -1 & -1 & -1 & 1 & -1 & -1 & 1 & -1 & 1 & 1 & 1 \\ 1 & 1 & -1 & -1 & -1 & 1 & -1 & -1 & 1 & -1 & 1 & 1 \\ 1 & 1 & 1 & -1 & -1 & -1 & 1 & -1 & -1 & 1 & -1 & 1 \\ 1 & 1 & 1 & 1 & -1 & -1 & -1 & 1 & -1 & -1 & 1 & -1 \\ 1 & -1 & 1 & 1 & 1 & -1 & -1 & -1 & 1 & -1 & -1 & 1 \\ 1 & 1 & -1 & 1 & 1 & 1 & -1 & -1 & -1 & 1 & -1 & -1 \end{bmatrix}. \tag{C.4}$$

Appendix D.
SC-SFBC: computing $\mathbf{P}_M$

In the context described in section 4.1.3, we are searching for a matrix $\mathbf{P}_M$ such as $\mathbf{x}_{\text{equiv}}^{\text{Tx}_1} = \mathbf{F}_M^{-1}\mathbf{P}_M\mathbf{F}_M^{-1}\cdot\mathbf{x}^* \triangleq \mathbf{\Pi}\mathbf{x}^*$ has the same signal distribution as $\mathbf{x}$, *i.e.,* the following three sets have the same elements:

$$\left\{\left|x_{m,\text{equiv}}^{\text{Tx}_1}\right|_{m=0\ldots M-1}\right\} = \left\{\left|x_{m,\text{equiv}}^{\text{Tx}_0}\right|_{m=0\ldots M-1}\right\} = \left\{\left|x_m\right|_{m=0\ldots M-1}\right\} \tag{D.1}$$

In addition, $\mathbf{P}_M$ must be chosen such that an Alamouti-type SFBC correspondance based on matrix $\mathbf{A}_{01}^{(I)}$ exists between the elements of vectors $\mathbf{s}^{\text{Tx}_0}$ and $\mathbf{s}^{\text{Tx}_1} = \mathbf{P}_M\mathbf{s}^{\text{Tx}_0 *}$. $\mathbf{P}_M$ must be a skew symmetric matrix ($\mathbf{P}_M = -\mathbf{P}_M^{\text{T}}$) with only one non-null element per row and per column.

Let us denote by $\mathcal{P}$ the class of skew symmetric matrices ($\mathbf{P}_M^{\text{T}} = -\mathbf{P}_M$) with elements $p_{m,n}$ (m,n=0…M-1) in $\{1,0,-1\}$, containing one single non-null element per column and per row in position (k, f(k)). M must be even. Since $\mathbf{P}_M$ has one single non-null element per row and per column, it results that f is a one-to-one transformation of the set $\{0\ldots M\text{-}1\}$. If $\mathbf{P}_M \in \mathcal{P}$, than $-\mathbf{P}_M = \mathbf{P}_M^{\text{T}} \in \mathcal{P}$ because it remains skew-symmetric with only one non-null element ± 1 per row and per column.

Let us define K_0 (resp. K_1) as the $M/2$ sized set of elements k for which $P_{k,\text{f}(k)}$=-1 (resp. 1). Thus, if $k \in K_0$ then f(k)$\in K_1$ because $P_{\text{f}(k),k} = -P_{k,\text{f}(k)} = 1$; also, f(f($k$))=$k$ because of the symmetry condition, and it will suffice to define f onto the set K_0. We can choose without loss of generality K_0 such as $0 \in K_0$.

Besides, from (D.1) and the properties of $\mathbf{P}_M$, we deduce that $\mathbf{\Pi} = \mathbf{F}_M^{-1}\mathbf{P}_M\mathbf{F}_M^{-1}$ should perform a permutation of the elements in $\mathbf{x}$, possibly accompanied by some phase rotation. $\mathbf{\Pi}$ should consequently belong to the class $\mathcal{T}$ of matrices having only one non-null element of type $e^{j\xi}$ per row and per column, $\xi \in [0, 2\pi)$. $\mathbf{\Pi}$ is also skew symmetric and thus all the elements on its main diagonal are null. We are consequently searching for:

$$\mathbf{P}_M \in \mathcal{P} \text{ such as } \mathbf{\Pi}=\mathbf{F}_M^{-1}\mathbf{P}_M\mathbf{F}_M^{-1} \in \mathcal{T} \tag{D.2}$$

For classical SFBC for example we can easily see from (4.28) that $\mathbf{F}_M^{-1}\mathbf{P}_M^{(\text{J})}\mathbf{F}_M^{-1}$ is not in $\mathcal{T}$ even if $\mathbf{P}_M^{(\text{J})}$ is in $\mathcal{P}$. Let us show that (D.2) has solutions. We can compute:

$$
\begin{aligned}
\Pi_{m,n} &= \sum_{k=0}^{M-1} \frac{\omega_M^{-mk}}{\sqrt{M}} \left(\sum_{\ell=0}^{M-1} P_{k,\ell} \frac{\omega_M^{-\ell n}}{\sqrt{M}} \right) = \frac{1}{M} \sum_{k=0}^{M-1} \omega_M^{-mk} \left(P_{k,\mathrm{f}(k)} \omega_M^{-n\,\mathrm{f}(k)} \right) \\
&= \frac{1}{M} \sum_{k \in K_0} \left(P_{k,\mathrm{f}(k)} \omega_M^{-mk-n\,\mathrm{f}(k)} + P_{\mathrm{f}(k),k} \omega_M^{-m\,\mathrm{f}(k)-nk} \right) \\
&= \frac{1}{M} \sum_{k \in K_0} \left(-\omega_M^{-(mk+n\,\mathrm{f}(k))} + \omega_M^{-(m\,\mathrm{f}(k)+nk)} \right) \\
&= \frac{1}{M} \sum_{k \in K_0} \left(\omega_M^{-(mk+n\,\mathrm{f}(k)+M/2)} + \omega_M^{-(m\,\mathrm{f}(k)+nk)} \right), \quad m,n = 0 \ldots M-1
\end{aligned}
\tag{D.3}
$$

Let $\Pi_{0,n_0} = \mathrm{e}^{j\xi_0}$ ($n_0 \neq 0$) be the only non-null element on the first row. Since:

$$
\Pi_{0,M-n_0} = \frac{1}{M} \sum_{k \in K_0} \left(-\omega_M^{-n_0\,\mathrm{f}(k)} + \omega_M^{-n_0 k} \right) = \Pi_{0,n_0}^{*} \neq 0 \,, \tag{D.4}
$$

we deduce $n_0 = \left(M - n_0\right) \bmod M$. But n_0 cannot be null, because $\Pi_{0,0} = 0$. Consequently, $n_0=M/2$. But

$$
\Pi_{0,M/2} = \frac{1}{M} \sum_{k \in K_0} \left[(-1)^k - (-1)^{\mathrm{f}(k)} \right] = \mathrm{e}^{j\xi_0} \tag{D.5}
$$

is real, thus it can take as values either 1 or -1: either all elements in K_0 are even and all elements in $K_1=\mathrm{f}(K_0)$ are odd, or vice versa. As we have chosen $0 \in K_0$ by convention, we conclude that $\Pi_{0,n_0} = 1$ and $K_0 = \{0, 2, \ldots, M-2\}$ contains only even integers. Choosing $0 \in K_1$ instead would simply lead to changing the sign of $\mathbf{P}_M$. and trying to find solution -$\mathbf{P}_M$ instead of $\mathbf{P}_M$.

Let us apply inequality (4.21) to (D.3). This leads to $\left|\Pi_{m,n}\right| \leq 1$. But since $\mathbf{\Pi} \in \mathcal{P}$ already implies that $\left|\Pi_{m,n}\right| \in \{0,1\}$, we deduce that for all the non-null elements of $\mathbf{\Pi}$ the equality conditions of (4.21) must be satisfied and thus all elements in the right-hand part of (D.3) must have the same argument. For any $m = 0 \ldots M-1$, uniquely exists $n \neq m$ such that for any k even all elements in the right-hand part of (D.3) have the same argument, which must be constant with respect to m, let us denote it λ_m. Mathematically, this can be expressed as:

$$
\begin{aligned}
&\forall m, \exists! n \neq m \text{ such that, } \forall k \in K_0, \\
&\left(mk + n\,\mathrm{f}(k) + M/2 \right) \bmod M = \left(m\,\mathrm{f}(k) + nk \right) \bmod M \triangleq \lambda_m
\end{aligned}
\tag{D.6}
$$

This leads directly to $\left[(k - \mathrm{f}(k))(m-n) \right] \bmod M = M/2$ and thus:

$$
(k - \mathrm{f}(k))(m-n) = M/2 + q_k M = (2q_k + 1) M/2 \,, \tag{D.7}
$$

where q_k is an integer depending on k. Let us concentrate on the particular case where M is a power of 2. Given that k-f(k) is always odd ($k \in K_0$ and $\mathrm{f}(k) \in K_1$), $\left(m-n\right)$mod$M$ must equal

$M/2$. On each line m the non-null element in $\mathbf{\Pi}$ must be on the column $n=(m+M/2)\mathrm{mod}M$. Taking $m=1$ (and implicitly $n=M/2+1$) in (D.6), we find that:

$$\forall k \in K_0,\ \left(\mathrm{f}(k)+k+Mk/2\right)\mathrm{mod}\,M \overset{k \text{ even}}{=} \left(\mathrm{f}(k)+k\right)\mathrm{mod}\,M = \lambda_1\,. \tag{D.8}$$

Consequently, $k+\mathrm{f}(k)$, independent from m, is a constant odd integer (modulo M) for any k, let it be $\lambda_1=p-1$ with p even integer. We can thus write:

$$\mathrm{f}(k) = \left(p-1-k\right)\mathrm{mod}\,M,\ k \text{ even}\,. \tag{D.9}$$

From (D.9) we can deduce matrix $\mathbf{P}_M$ with elements -1 in position $(k,\mathrm{f}(k))$ and 1 in position $(\mathrm{f}(k),k)$ with k even:

$$\mathbf{P}_M = \left[\begin{array}{cc} \overbrace{\begin{matrix} 0 & \cdots & 0 & -1 \\ & & 1 & 0 \\ \vdots & & \iddots & \\ & \iddots & & \vdots \\ 0 & -1 & & \\ 1 & 0 & \cdots & 0 \end{matrix}}^{p} & \mathbf{0}_{p\times(M-p)} \\ \mathbf{0}_{(M-p)\times p} & \underbrace{\begin{matrix} 0 & \cdots & 0 & -1 \\ & & 1 & 0 \\ \vdots & & \iddots & \\ & \iddots & & \vdots \\ 0 & -1 & & \\ 1 & 0 & \cdots & 0 \end{matrix}}_{M-p} \end{array}\right] = -\mathbf{S}_M^p\overline{\mathbf{P}}_M^{(\mathbf{J})} \tag{D.10}$$

With this choice, we can compute the elements of $\mathbf{\Pi}$:

$$\begin{aligned} \Pi_{m,n} &= \frac{1}{M}\sum_{k=0}^{M/2-1}\left(\omega_M^{-(2mk+n(p-1-2k))-M/2} + \omega_M^{-m(p-1-2k)+2nk}\right) = \\ &= \frac{1}{M}\omega_M^{-n(p-1)-M/2}\sum_{k=0}^{M/2-1}\omega_M^{-2(m-n)k} + \frac{1}{M}\omega_M^{-m(p-1)}\sum_{k=0}^{M/2-1}\omega_M^{2(m-n)k} \end{aligned} \tag{D.11}$$

Or, both geometric series in (D.11) sum to M/2 when $2(m-n)\equiv 0\,\mathrm{mod}\,M$, and to 0 otherwise. Since $\Pi_{m,n}=0$ for any $m=n$, we can only obtain non-null elements when $(m-n)\equiv M/2\,\mathrm{mod}\,M$, which gives:

$$\Pi_{m,n} = \begin{cases} \omega_M^{-(p-1)m}, & n = (m + M/2) \bmod M \\ 0, & \text{otherwise} \end{cases} \tag{D.12}$$

The design criterion (D.2) is consequently satisfied and $\mathbf{P}_M = \pm\mathbf{S}_M^p \overline{\mathbf{P}}_M^{(\mathrm{J})}$ leads to an operation conserving the amplitude distribution of the original constellation. Let us note that (D.10) verifies the design criterion (D.2) for any even value of *M*, since (D.11) and (D.12) remain valid when *M* is not a power of 2. This is not sufficient to state that (D.10) is the only solution when *M* is not a power of 2, and other solutions might exist. Nevertheless, in the case *M*=12 which is typical in LTE, we have verified that no other solutions exist.

Appendix E.
SC-QOSFBC: computing *p* parameters

The QO condition for constructing SC-QOSFBC codes can be written as:

$$\mathbf{s}^{\mathrm{Tx}_1} = \mathrm{SC}_M^{p}(\mathbf{s}^{\mathrm{Tx}_0}) = \mathrm{SC}_M^{p'}(\mathbf{s}^{\mathrm{Tx}_2}) \text{ and } \mathbf{s}^{\mathrm{Tx}_3} = \mathrm{SC}_M^{p''}(\mathbf{s}^{\mathrm{Tx}_0}) = \mathrm{SC}_M^{p'''}(\mathbf{s}^{\mathrm{Tx}_2}) \tag{E.1}$$

Let us prove that, in order to satisfy (5.18), we need to choose:

$$\begin{cases} p' = p'' = p - M/2 \\ p''' = p \end{cases} \tag{E.2}$$

Proof: Let (k_0, k_1, k_2, k_3) be a set of four indices k_i denoting subcarriers encoded together. We will concentrate here only on the index of the used subcarriers (and thus of the frequency samples). We define the following notation: $f_{k_i} : (k_i, k_j, k_m, k_n)$, with *i*, *j*, *m*, *n* drawn from 0…3, means that on the k_i-th used subcarrier f_{k_i}, onto antennas $\mathrm{Tx}_{0\ldots3}$ we will send a version (with eventual sign change and/or complex conjugation) of s_{k_i}, s_{k_j}, s_{k_m} and respectively s_{k_n}. For example, for the implementation in Fig. 5.1, we can state $f_2 : (2,3,0,1)$ $f_3 : (3,2,1,0)$ etc. In order for our construction to lead to a valid SFBC-type code, when isolating the symbols lying onto groups of 4 frequencies $f_{k_{0\ldots3}}$ precoded together, we need to find combinations containing only the same indices (k_0, k_1, k_2, k_3). For example, in Fig. 5.1, onto frequencies $f_{0..3}$ we find different combinations of frequency samples $s_{0..3}$, and onto frequencies $f_{4..7}$ we find different combinations of frequency samples $s_{4..7}$. Since we made the convention of sending the original SC-FDMA signal on Tx_0, all series of indices corresponding to f_{k_i} starts with k_i. Each symbol s_{k_i} appears only one time per antenna and per subcarrier. We can conveniently choose the order of $f_{k_{0\ldots3}}$ in order to have by default $f_{k_0} : (k_0, k_1, k_2, k_3)$.

SC operations, defined for the two antennas case, are symmetric with respect to indices, *i.e.*, if $f_{k_i} : (k_i, k_j)$, then $f_{k_j} : (k_j, k_i)$, in order to form an Alamouti pair. By isolating the four subcarriers participating in SFBC-type precoding, we deduce:

- Since SC_M^{p} and $\mathrm{SC}_M^{p'''}$, relying the signals on $\mathrm{Tx}_0 \leftrightarrow \mathrm{Tx}_1$ and on $\mathrm{Tx}_2 \leftrightarrow \mathrm{Tx}_3$, are symmetric and since $f_{k_0} : (k_0, k_1, k_2, k_3)$, then $f_{k_1} : (k_1, k_0, k_3, k_2)$;
- On f_{k_2}, k_2 comes in first position. Neither k_0 nor k_1 cannot be in second position (corresponding to Tx_1), since they already appear on Tx_1 on frequencies f_{k_1} and respectively f_{k_0}. Since $\mathrm{SC}_M^{p'}$, relying the signals on $\mathrm{Tx}_1 \leftrightarrow \mathrm{Tx}_2$ is symmetric, and since $f_{k_1} : (k_1, k_0, k_3, k_2)$, then $f_{k_2} : (k_2, k_3, k_0, k_1)$;
- Since SC_M^{p} and $\mathrm{SC}_M^{p'''}$, relying the signals on $\mathrm{Tx}_0 \leftrightarrow$Tx1 and on $\mathrm{Tx}_2 \leftrightarrow \mathrm{Tx}_3$, are symmetric and since $f_{k_2} : (k_2, k_3, k_0, k_1)$, then $f_{k_3} : (k_3, k_2, k_1, k_0)$.

It follows that $\left(k_2,k_3\right)$ are relied by both SC_M^{p} and $\mathrm{SC}_M^{p'''}$, and explicating the SC-type dependence between the indexes we obtain:

$$k_2=(p-1-k_3)\operatorname{mod}M=(p'''-1-k_3)\operatorname{mod}M \tag{E.3}$$

and thus $p'''=p$. A similar reasoning for $\left(k_0,k_1\right)$ leads to $p'=p''$.

For a valid precoding we need that $p\neq p'$: If $p=p'$, from (5.18) we would have $\mathbf{s}^{\mathrm{Tx}_0}=\mathbf{s}^{\mathrm{Tx}_2}$, which is not compatible with the code design. In $f_{k_0}:\left(k_0,k_1,k_2,k_3\right)$, we can express k_2 in a double manner: via its $\mathrm{SC}_M^{p'}$ relation with k_1 and respectively via its $\mathrm{SC}_M^{p'''=p}$ relation with k_3:

$$\begin{aligned}&k_2=(p'-1-\underbrace{k_1}_{=(p-1-k_0)\operatorname{mod}M})\operatorname{mod}M=(p-1-\underbrace{k_3}_{=(p'-1-k_0)\operatorname{mod}M})\operatorname{mod}M\Rightarrow\\&\Rightarrow p-(p'-1-k_0)\operatorname{mod}M=p'-(p-1-k_0)\operatorname{mod}M+nM,\\&\qquad\qquad n\in\mathbb{Z},\forall k_0\in 0...M-1\end{aligned} \tag{E.4}$$

n can only take values 0 and ±1, since the left-hand term of (E.4) is bounded by $\pm(M-1)$. We can suppose without loss of generality that $p>p'$. Let us choose $k_0=p'-1$.

$$p-p'+(\overbrace{p-p'}^{\in\{2,4,...,M-2\}})\operatorname{mod}M=nM\Rightarrow p-p'=n\frac{M}{2} \tag{E.5}$$

Since $p>p'$, n can only equal 1 and thus $p=p'+M/2$. Accepting $p<p'$ leads to $p'=p+M/2$. These solutions verify (E.4) for any k_0.

Appendix F. Optimization of spectrum occupancy for MU-SC-SFBC

We determine 2 groups of users, A and B. Users' allocated bands do not overlap inside of each group, but each user of each group can have overlapping subcarriers with a maximum of 2 users from the other group, such as onto the overlapping subcarriers double Alamouti pairs are formed.

We proceed as following:

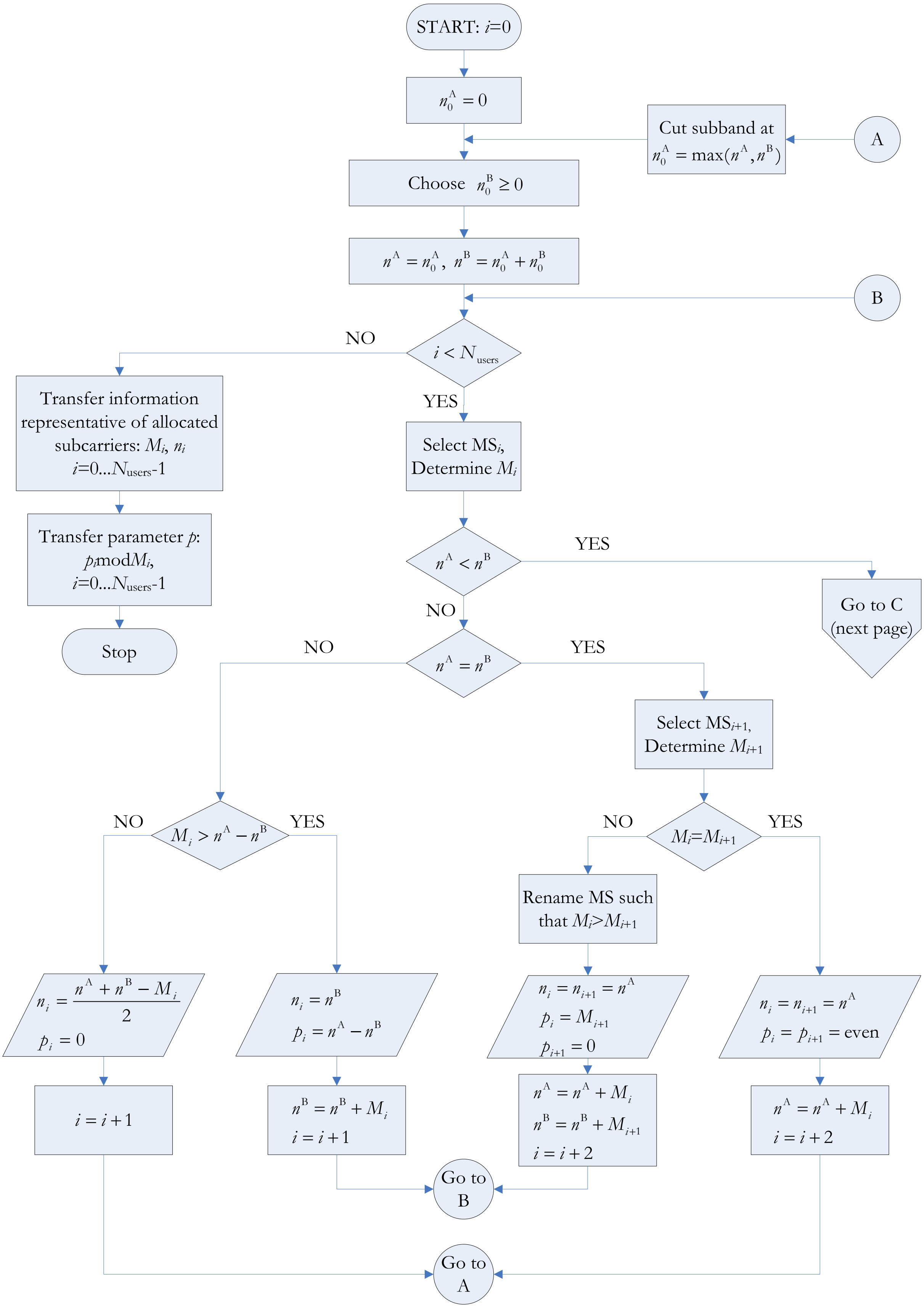
START: i=0
$n_0^A = 0$
Cut subband at $n_0^A = \max(n^A, n^B)$
A
Choose $n_0^B \geq 0$
$n^A = n_0^A$, $n^B = n_0^A + n_0^B$
B
NO
$i < N_{users}$
YES
Transfer information representative of allocated subcarriers: M_i, n_i i=0...N_{users}-1
Select MS$_i$, Determine M_i
Transfer parameter p: $p_i$modM_i, i=0...N_{users}-1
$n^A < n^B$
YES
Go to C (next page)
NO
Stop
NO
$n^A = n^B$
YES
Select MS$_{i+1}$, Determine M_{i+1}
NO
$M_i > n^A - n^B$
YES
NO
M_i=M_{i+1}
YES
Rename MS such that M_i>M_{i+1}
$n_i = \frac{n^A + n^B - M_i}{2}$
$p_i = 0$
$n_i = n^B$
$p_i = n^A - n^B$
$n_i = n_{i+1} = n^A$
$p_i = M_{i+1}$
$p_{i+1} = 0$
$n_i = n_{i+1} = n^A$
$p_i = p_{i+1} =$ even
$i = i + 1$
$n^B = n^B + M_i$
$i = i + 1$
$n^A = n^A + M_i$
$n^B = n^B + M_{i+1}$
$i = i + 2$
$n^A = n^A + M_i$
$i = i + 2$
Go to B
Go to A

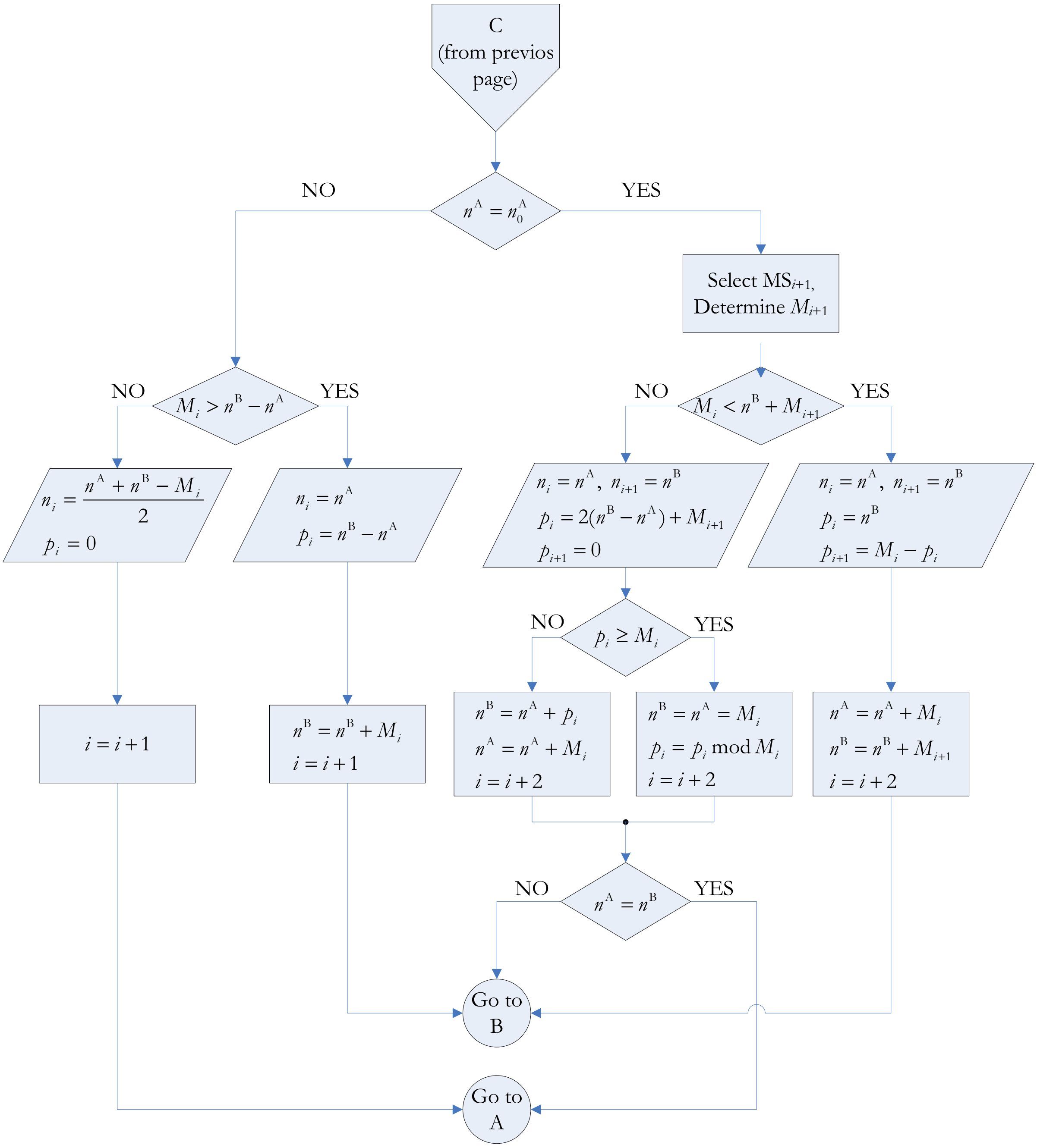
C
(from previos page)
NO
YES
$n^A = n_0^A$
Select MS_{i+1},
Determine M_{i+1}
NO
$M_i > n^B - n^A$
YES
NO
$M_i < n^B + M_{i+1}$
YES
$n_i = \frac{n^A + n^B - M_i}{2}$
$p_i = 0$
$n_i = n^A$
$p_i = n^B - n^A$
$n_i = n^A,\ n_{i+1} = n^B$
$p_i = 2(n^B - n^A) + M_{i+1}$
$p_{i+1} = 0$
$n_i = n^A,\ n_{i+1} = n^B$
$p_i = n^B$
$p_{i+1} = M_i - p_i$
NO
$p_i \geq M_i$
YES
$i = i + 1$
$n^B = n^B + M_i$
$i = i + 1$
$n^B = n^A + p_i$
$n^A = n^A + M_i$
$i = i + 2$
$n^B = n^A = M_i$
$p_i = p_i \bmod M_i$
$i = i + 2$
$n^A = n^A + M_i$
$n^B = n^B + M_{i+1}$
$i = i + 2$
NO
$n^A = n^B$
YES
Go to B
Go to A

List of symbols and functions

$(.)^*$, $[.]^*$	Complex conjugate of a scalar, vector or matrix.
$[.]^T$	Transpose of a vector or matrix.
$[.]^H$	Hermitian (transpose and complex conjugate) of a vector or matrix.
$[.]^{1/2}$	Matrix square root.
$[.]^\dagger$	Pseudoinverse of a matrix.
$\otimes$	Kronecker product.
$\odot$	Schur-Hadamard (element-wise) matrix product.
$\tilde{*}$	Circular convolution product.
$\langle .,. \rangle$	Scalar product.
$\mathrm{blkdiag}(\mathbf{X}^{(i)})$	Builds a block diagonal matrix with $\mathbf{X}^{(i)}$ on the main diagonal.
$\mathrm{circ}(\mathbf{h})$	Circulant matrix having as first column vector **h**.
diag(**X**)	Extracts the main diagonal of **X** when **X** is a matrix. Transforms **X** into a matrix with **X** on its main diagonal and all zeros elsewhere when **X** is a vector.
$E\{.\}$	Statistical expectation function
$\Pr\{X\}$	Probability of the event X.
sinc(x)	Cardinal sinus function, sin(x)/x.
$\mathrm{trace}\{.\}$	Trace of a matrix: sum of the elements on the main diagonal.
$\mathrm{unvec}(.)$	Inverse of the $\mathrm{vec}(.)$ function.
$\mathrm{vec}(.)$	Stacks up the columns of a $M \times N$ matrix, transforming it into a $MN \times 1$ vector.
$\mathbf{0}_{M \times N}$	All-zero matrix of size $M \times N$
$\mathbf{A}$, $\mathbf{A}^{(i)}$	Equivalent system transfer function (overall and respectively at block level) for a coded modulation system employing block-based transmission.
$\tilde{\mathbf{A}}^{(i)}$	Modified equivalent system transfer function.
$\mathcal{A}^{(I)}$	Generator matrix of a modified Jafarkhani STBC/SFBC.
$\mathbf{A}_{ij}$	Generator matrix of an Alamouti STBC/SFBC with indeterminates $a_{i,j}$.
$\mathbf{A}_{ij}^{(I)}$	Generator matrix of a modified Alamouti STBC/SFBC with indeterminates $a_{i,j}$.
B_{coh}	Coherence bandwidth.
d	Diversity gain.
F_{c}	Carrier frequency.
$\mathbf{F}_N$, $\mathbf{F}_N^{\mathrm{H}}$	N-point DFT and IDFT under matrix form.
F_{s}	Sampling frequency.

G_1, G_2	Linear/nonlinear HPA gain factor.
h	Channel representation in the time domain.
$H(f,t)$	Time variant frequency selective channel transfer function.
$\mathbf{H}_A$	Modified channel matrix for Alamouti-type transmission.
$H_N[k,i]$, $H[k,i]$	Discrete-time discrete-frequency version of the channel transfer function, corresponding to all/used subcarriers.
$H^{(i)}_{k,n_{Rx},n_{Tx}}$	Complex valued MIMO channel transfer function coefficient on subcarrier k from transmit antenna n_{Tx} to receive antenna n_{Rx} at time (i).
$H^{'}[k_P,i_P]$	Noisy channel observation in position (k_P,i_P).
$\hat{H}[k,i]$	Channel estimate in position (k,i).
$\mathbf{I}_M$	$M \times M$ identity matrix.
$\mathbf{J}$	Antidiagonal skew matrix of order 2, defined in 4.2.4.
L	Number of taps in a tapped delay line channel model.
L_{ovs}	Oversampling factor.
M	Number of subcarriers allocated to one user.
$\mathbf{M}$	Precoding matrix of generalized MC transmitters.
N	Total number of subcarriers in an OFDMA-like system (IDFT size)
$\mathbf{N}$, $\mathbf{N}^{(i)}$	Colored noise (overall and respectively at block level) seen by the MC receiver after demapping, equalization and despreading.
N_{CP}	Cyclic prefix length, in samples.
N_s	Number of discrete samples in a block $\mathbf{v}$.
N_{Sym}	Number of MC symbols coded together.
N_{Taps}	Number of coefficients of a Wiener filter.
N_{ZC}	Length of Zadoff-Chu sequences.
p	Parameter of the SC-SFBC mapping scheme.
P_{IN}, P_{OUT}	Signal power at the input/output of an HPA.
$P_{IN/OUT,Avg}$	Signal average power level before/after passing through an HPA.
$P_{IN,Sat}$, $P_{OUT,Sat}$	Input/output saturation power level of an HPA.
$\mathbf{P}_M^{(J)}$, $\overline{\mathbf{P}}_M^{(J)}$, $\mathbf{P}_M$	Matrices defined in 4.24, corresponding to SFBC-type operations.
p_{Rapp}	Knee factor of the Rapp HPA model.
$\mathbf{Q}$, $\mathbf{Q}^{\dagger}$	Subcarrier mapping/demapping matrix.
R_{Mux}	Multiplexing gain.
$\mathbf{r}$	Received signal, in vector form.
$\mathbf{s}^{(i)}$, $s_k^{(i)}$	Discrete spectrum of the i-th block of M modulation symbols $\mathbf{x}^{(i)}$, and its k-th sample, respectively.
$\mathbf{s}^{'(i)}$, $s_k^{'(i)}$	MC-type symbol represented in the frequency domain, prior to IDFT and after subcarrier mapping.
$\mathbf{S}_M^p$	Operator which cyclically shifts the rows of an M-sized matrix down p positions
$S_{P(k,i)}$	Set of positions in the pilot grid where the observations are correlated to the sample in position (k,i) to be estimated.

T	Duration of an OFDM-like symbol.
T_c	T/N.
T_{coh}	Coherence time.
T_{CP}	Cyclic prefix duration.
T_s	Duration of a constellation symbol, T/M in an OFDMA-like system.
$\mathcal{T}$	Period of measurement for estimating PAPR.
$\mathbf{v}$	Block of discrete samples of signal v.
$v(t)$, $v[n]$	Continuous- and discrete-time domain signal.
v_{IN}, v_{OUT}	Signal at the input/output of an HPA.
$v_{\mathrm{IN,Sat}}$, $v_{\mathrm{OUT,Sat}}$	Input/output saturation level of an HPA.
v_{norm}	Signal normalized to unitary rms value.
v_{Ref}	Reference signal for computing CM.
w_{k,i,k_P,i_P}	Coefficients of a 2D Wiener filter.
$\mathbf{w}_k$	Set of 1D Wiener tap weights for estimation of the k-th channel coefficient.
W	System's bandwidth.
$\mathbf{WH}^{(M)}$	$M \times M$ Walsh Hadamard orthogonal matrix.
$\mathbf{WH}_k$	$M \times 1$ vector containing a WH sequence, k-th column of $\mathbf{WH}^{(M)}$.
$\mathbf{x}$	Vector of modulation symbols drawn from a modulation constellation (*e.g.* QAM), after eventual coding, scrambling or interleaving.
$\overline{\mathbf{x}}$	Time reversed version of any vector $\mathbf{x}$.
$\mathbf{x}^{(i)}$, $x_k^{(i)}$	i-th block of M modulation symbols composing $\mathbf{x}$ and its k-th sample, respectively.
$\mathbf{x}_{\mathrm{equiv}}^{\mathrm{Tx}_{n_{\mathrm{Tx}}},(i)}$	Equivalent constellation to be sent after SC-FDMA modulation on the n_{Tx}-th transmit antenna at time (i).
$\mathbf{y}^{(i)}$ / $\mathbf{y}^{\mathrm{Tx}_{n_{\mathrm{Tx}}},(i)}$	MC-type data symbol corresponding to $\mathbf{x}^{(i)}$ / $\mathbf{x}_{\mathrm{equiv}}^{\mathrm{Tx}_{n_{\mathrm{Tx}}},(i)}$, before CP insertion.
$\tilde{\mathbf{y}}^{(i)}$	MC-type data symbol corresponding to $\mathbf{x}^{(i)}$, after CP insertion.
$z_q[n]$	n-th position of the q-th root Zadoff-Chu sequence.
α, α_p	Amplitude and phase parameters for the Saleh model, respectively.
$\tilde{\alpha}^{(i)}$	Mean value of $\mathrm{diag}(\tilde{\mathbf{A}}^{(i)})$.
β, β_p	Amplitude and phase parameters for the Saleh model, respectively.
$\delta_{n_{\mathrm{Tx}}}$	Cyclic delay shift (in samples) on the n_{Tx}-th Tx antenna for CDD.
$\delta[.]$	Discrete Dirac function.
$\mathbf{\Phi}^{n_{\mathrm{Tx}}}$, $\phi_k^{n_{\mathrm{Tx}}}$	Antenna dependent phase ramp generated in the frequency domain by the CDD delays: vector and its elements.
η_P	Channel estimation noise.
$\mathbf{\Pi}^{(\mathrm{J})}$, $\mathbf{\Pi}$	Auxiliary matrices defined as $\mathbf{F}_M^{-1}\mathbf{P}_M^{(\mathrm{J})}\mathbf{F}_M^{-1}$, $\mathbf{F}_M^{-1}\mathbf{P}_M\mathbf{F}_M^{-1}$.
ω_N	N-th order primitive unity root.

Abbreviations

3G/B3G/4G	Third / Beyond Third/ Fourth Generation
3GPP	Third Generation Partnership Project
ACLR	Adjacent Channel Leakage power Ratio
AFD	Average Fade Duration
AM/AM	Amplitude/amplitude HPA characteristic
AM/PM	Amplitude/phase HPA characteristic
AMPS	Advanced Mobile Phone Service
AWGN	Additive White Gaussian Noise
BER	Bit Error Rate
BLAST	Bell Labs Layered Space-Time Architecture
BRAN	Broadband Radio Access Network
BS	Base Station
CAZAC	Constant Amplitude Zero Autocorrelation sequence
COST	European Cooperation in the field of Scientific and Technical research project
CCDF	Complementary Cumulative Distribution Function
CDD	Cyclic Delay Diversity
CDF	Cumulative Distribution Function
CDMA	Code Division Multiple Access
CM	Cubic Metric
CP	Cyclic Prefix
CSI	Channel State Information
D/A	Digital to Analog conversion
D-BLAST	Diagonal Bell Labs Layered Space-Time architecture
DD	Delay Diversity
DECT	Digital Enhanced Cordless Telecommunications
DFT	Discrete Fourier Transform
DL	Downlink
DoA/DoD	Direction of Arrival/Departure
DS-CDMA	Direct Sequence Code Division Multiple Access
EDGE	Enhanced Data rates for GSM Evolution
ETSI	European Telecommunications Standards Institute
E-UTRA	Evolved Universal Terrestrial Radio Access
EVM	Error Vector Magnitude

FDD	Frequency Division Duplexing
FDE	Frequency-Domain Equalization
FDOSS	Frequency-Domain Orthogonal Signature Sequences
FDMA	Frequency Division Multiple Access
FEC	Forward Error Correction
FER	Frame Error Rate
FH	Frequency Hopping
FSK	Frequency Shift Keying
GPRS	General Packet Radio Service
GSM	Global System for Mobile Communications
HARQ	Hybrid Automatic Repeat Request
HPA	High Power Amplifier
HSDPA	High Speed Downlink Packet Access
HSPA	High Speed Packet Access
HSUPA	High Speed Uplink Packet Access
IDFT	Inverse Discrete Fourier Transform
IFDMA	Interleaved Frequency Division Multiple Access
i.i.d.	independent identically distributed
IMP	Intermodulation product
INP	Instantaneous Normalized Power
IS-95	Interim Standard 95
ITU	International Telecommunication Union
LCR	Level Crossing Rate
LLR	Log Likelihood Ratio
LOS	Line of Sight
LTE	Long Term Evolution
MC	Multicarrier
MC-CDMA	Multicarrier Code Division Multiple Access
MIMO	Multiple Input Multiple Output
MISO	Multiple Input Single Output
ML	Maximum Likelihood
MMSE	Minimum Mean Square Error
MRC	Maximum Ratio Combining
MS	Mobile Station
MU	Multi-user
NLOS	Non Line of Sight
OFDM	Orthogonal Frequency Division Multiplexing
OFDMA	Orthogonal Frequency Division Multiple Access

OL-TAS	Open-Loop Transmit Antenna Selection
PAPR	Peak to Average Power Ratio
PAS	Power Azimuth Spectrum
PDP	Power Delay Profile
QAM	Quadrature Amplitude Modulation
QO	Quasi-orthogonal
QPSK	Quadrature Phase Shift Keying
RB	Resource Block
RF	Radio Frequency
RMS	Root Mean Square
Rx	Receiver
SNR	Signal to Noise Ratio
TAS	Transmit Antenna Selection
TC	Turbo Code
TDD	Time Division Duplexing
TDMA	Time Division Multiple Access
Tx	Transmitter
S/P	Serial to Parallel
SC	Single Carrier
SC-FDMA	Single Carrier Frequency Domain Multiple Access
SDMA	Space Division Multiple Access
SIMO	Single Input Multiple Output
SISO	Single Input Single Output
SON	Self-Organizing Network
SS-MC-MA	Spread Spectrum Multicarrier Multiple Access
STBC	Space-Time Block Codes
STTCM	Space-Time Trellis Coded Modulation
SU	Single-user
UL	Uplink
UMTS	Universal Mobile Telecommunications System
V-BLAST	Vertical Bell Labs Layered Space-Time architecture
W-CDMA	Wideband Code Division Multiple Access
WLAN	Wireless Local Area Networks
WH	Walsh Hadamard
WiFi	Wireless Fidelity
WiMAX	Worldwide Interoperability for Microwave Access
WSSUS	Wide Sense Stationary with Uncorrelated Sources
ZF	Zero Forcing

References

[AbSt72] M. Abramowitz and I. A. Stegun, (editors), *Handbook of Mathematical Functions with Formulas, Graphs, and Mathematical Tables*, 9th printing, New York, Dover, 1972.

[Ala98] S. Alamouti, "A simple transmit diversity technique for wireless communications," *IEEE Journal on Selected Areas in Communications*, vol. 16, pp. 1451-1458, 1998.

[Alc06] Alcatel, "Performance evaluations of STBC/SFBC schemes in E-UTRA uplink," contribution R1-063179, *3GPP RAN WG1 #47 meeting*, Riga, Latvia, Nov. 2006.

[And02] J. B. Andersen, "Power distributions revisited," *COST 273*, TD(02)004, 2002.

[BaGo62] L.D. Baumert; S.W. Golomb, and M. Hall Jr, "Discovery of an Hadamard matrix of order 92," *Bull. Amer. Math. Soc.* no. 68, pp. 237-238, 1962.

[BaFu79] F. G. Bass and I. M. Fuks, *Wave Scattering from Statistically Rough Surfaces*, Pergamon, 1979.

[Bau03] G. Bauch, "Space-time-frequency transmit diversity in broadband wireless OFDM systems," *Proceedings of 8th International OFDM Workshop*, Hamburg, Germany, Sept. 2003.

[Bel63] P. A. Bello, "Characterization of randomly time-variant linear channels," *IEEE Transactions on Communications*, 11, pp. 360-393, 1966.

[BoÖz03] E. Bonek, H. Özcelik, M. Herdin, W. Weichselberger, and J. Wallace, "Deficiencies of a popular stochastic MIMO radio channel model," *International Symposium on Wireless Personal Multimedia Communications*, *WPMC'03*, Yokosuka, Japan, Oct. 2003.

[BöPa00] H. Bölcskei and A. Paulraj, "Space-Frequency coded broadband OFDM systems," *IEEE Wireless Commun. and Networking Conference, WCNC 2000*, Chicago, Illinois, Sept. 2000.

[Bow58] F. Bowman, *Introduction to Bessel Functions*, Dover, New York, 1958.

[Bul47] K. Bullington, "Radio propagation at frequencies above 30 MC," *Proceedings of. IRE*, vol. 35, no. 10, pp. 1122-1136, 1947.

[CCIR82] "Method and statistics for estimating field strength values in the land mobile services using the frequency range 30 MHz to 1 GHz," *CCIR XV Plenary Assembly*, Geneva, 1982.

[CiBu06] C. Ciochina, F. Buda and H. Sari, "An Analysis of OFDM Peak Power Reduction Techniques for WiMAX Systems," *IEEE International Conference on Communications, ICC'06*, Istanbul, Turkey, June 2006.

[CiMo06] C. Ciochina, D. Mottier and H. Sari, "Multiple Access Techniques for the Uplink in Future Wireless Communications Systems," *Third COST 289 Workshop*, Aveiro, Portugal, July 2006.

[CiMo07a] C. Ciochina, D. Mottier and H. Sari, "An Analysis of OFDMA, Precoded OFDMA and IFDMA for the Uplink in Cellular Systems," *6th International Workshop on Multi-Carrier Spread Spectrum (MC-SS) 2007*, Herrsching, Germany, May 07-09, 2007.

[CiMo07b] C. Ciochina, D. Castelain, D. Mottier and H. Sari, "A Novel Space-Frequency Coding Scheme for Single-Carrier Modulations," *18th Annual IEEE International Symposium on Personal, Indoor and Mobile Communications (PIMRC'07)*, Athens, Greece, September 2007.

[CiMo07c] C. Ciochina, D. Castelain, D. Mottier and H. Sari, "Single-Carrier Space-Frequency Block Coding: Performance Evaluation," *IEEE 66th Vehicular Technologies Conference (VTC 2007 Fall)*, Baltimore, USA, September 29 - October 3 2007.

[CiMo08a] C. Ciochina, D. Mottier and H. Sari, "An analysis of three multiple access techniques for the uplink of future cellular mobile systems," *European Transactions on Telecommunications ETT*, no. 19, pp. 581-588, 2008.

[CiMo08b] C. Ciochina, D. Castelain, D. Mottier and H. Sari, "Space-Frequency Block Code for Single-Carrier FDMA," *Electronics Letters*, vol. 44, no. 11, pp. 690-691, May 2008.

[CiMo08c] C. Ciochina, D. Castelain, D. Mottier and H. Sari, "A Novel Quasi-Orthogonal Space-Frequency Block Code for Single-Carrier FDMA," *IEEE 67th Vehicular Technologies Conference (VTC 2008 Spring)*, Singapore, May 2008.

[ChKa98] C. N. Chuah, J. M. Kahn, and D. Tse, "Capacity of multi-antenna array systems in indoor wireless environment," in *Proc. of IEEE Global Telecommunications Conference GLOBECOM'88*, vol. 4, pp. 1894-1899, Sydney, Australia, Dec. 1988.

[DaKa01a] A. Dammann and S. Kaiser, "Performance of low complex antenna diversity techniques for mobile OFDM systems," *International Workshop on Multi-Carrier Spread Spectrum*, *MC-SS 2001*, Oberpfaffenhofen, Germany, Sept. 2001, pp. 53–64, ISBN 0-7923-7653-6.

[DaKa01b] A. Dammann and S. Kaiser, "Standard conformable antenna diversity techniques for OFDM and its application to the DVBT system," *Proceedings IEEE Global Telecommunications Conference*, *GLOBECOM 2001*, San Antonio, Texas, November 2001, pp. 3100–3105.

[Dav79] P. J. Davis, *Circulant Matrices*, Wiley-Interscience, New York, 1979.

[Dey66] J. Deygout, "Multiple knife edge diffraction of microwaves," *IEEE Transactions on Antennas Propagation*, 14, pp. 480-489, 1966.

[Den93] *P*. Dent, G. E. Bottomley and T. Croft, "Jakes Fading Model Revisited," *Electronics Letters*, vol. 29, no. 13, pp. 1162–1163, 1993.

[Ede92] *A. Eden, The Search for Christian Doppler, Springer-Verlag, 1992.*

[EpPe53] J. Epstein and D. W. Peterson, "An experimental study of wave propagation at 850 MC," *Proceedings of the IEEE*, 41, pp. 595-611, 1953.

[Fle00] B. H. Fleury, "First- and second-order characterization of directional dispersion and space selectivity in the radio channel," *IEEE Transactions on Information Theory*, vol. 46, no. 6, pp. 2027-2044, 2000.

[FrKl05] T. Frank, A. Klein, E. Costa and E. Schultz, "Robustness of IDFMA as Air Interface Candidate for Future High Rate Mobile Radio Systems," *Advances in Radio Science*, vol. 3, pp. 265-270, 2005.

[FrKl06] T. Frank, A. Klein, and E. Costa, "Low Complexity and Power Efficient Space-Time-Frequency Coding for OFDMA," in *Proceedings of 15th Mobile & Wireless Communications Summit*, Mykonos, Greece, June 2006.

[GaAd05] D. Garg and F. Adachi, "Diversity-Coding-Orthogonality Trade-off for Coded MC-CDMA with High Level Modulation," *IEICE Transactions* 88-B(1), pp. 76-83, 2005.

[GeBo02] D. Gesbert, H. Boelcskei, and A. Paulraj, "Outdoor MIMO wireless channels: Models and performance prediction," *IEEE Transactions on Communications*, vol. 50, no. 12, pp. 1926-1935, 2002.

[Hay96] S. Haykin, *Adaptive filter theory*, Prentice Hall International Editions, 1996.

[Had93] J. Hadamard, "Résolution d'une question relative aux determinants," *Bulletin des Sciences Mathématiques*, vol. 17, pp. 240-246, 1893.

[HaHo02] B. Hassibi and B. Hochwald, "High rate codes that are linear in space and in time," *IEEE Transactions on Information Theory*, vol. 48, no. 7, pp. 1804-1824, 2002.

[Hal63] P. Halmos, "What Does the Spectral Theorem Say?," *American Mathematical Monthly*, vol. 70, no. 3, pp. 241-247, 1963.

[Har34] G.H. Hardy, J.E. Littlewood and G. Pólya, *Inequalities*, Cambridge Univ. Press 1934.

[Hat80] M. Hata, "Empirical formula for propagation loss in land mobile radio services," *IEEE Transactions on Vehicular Technologies*, 29, pp. 317-325, 1980.

[HeGi99] R.W. Heath and G.B. Giannakis, "Exploiting input cyclostationarity for blind channel identification in ODFM systems," *IEEE Transactions on Signal Processing*, vol. 47, no. 3, pp. 848-856, 1999.

[HeGr04] M. Herdin, G. Gritsch, B. Badic and E. Bonek, "The influence of channel models on simulated MIMO performance," *IEEE Vehicular Technologies Conference*, *VTC'04 Spring*, Milan, Italy, May 2004.

[HiAd92] A. Hiroike, F. Adachi and N. Nakajima, "Combined effects of phase sweeping transmitter diversity and channel coding," *IEEE Transactions on Vehicular Technologies,* vol. 41, pp. 170-176, 1992.

[HoKa97] P. Hoeher, S. Kaiser and P. Robertson, "Two-dimensional pilot-symbol-aided channel estimation by Wiener filtering," *IEEE International Conference on Acoustics, Speech, and Signal Processing ICASSP'97*, Munich, Germany, April 1997.

[Hot03] A. Hottinen, "Multiuser scheduling with matrix approximation," *IEEE International Symposium on Signal Processing and Information Technology ISSPIT 2003*, Darmstadt, Germany, 14-17 Dec. 2003.

[Hua08] Huawei, "Uplink 4 transmit antennas transmit diversity for LTE-Advanced," contribution R1-083021, *3GPP RAN WG1 #54 meeting*, Jeju, South Coreea, August 2008.

[Ike84] F. Ikegami et al, "Propagation factors controlling mean field strength on urban streets," *IEEE Transactions on Antennas Propagation*, pp. 822-829, 1984.

[Jaf01] H. Jafarkhani, "A Quasi-Orthogonal Space-Time Block Code," *IEEE Transactions on Communications*, vol. 49, no. 1, January 2001.

[Jaf05] H. Jafarkhani, *Space-Time Coding: Theory and Practice*, Cambridge University Press, 2005.

[Jak94] C. J. Jakes, *Microwave Mobile Communications*, IEEE Press, New Jersey, 1994.

[Kai01] T. Kaitz, "Channel and interference model for 802.16b Physical Layer," contribution to the IEEE 802.16b standard, 2001.

[KaFa97] S. Kaiser and K. Fazel, "A flexible spread-spectrum multi-carrier multiple-access system for multi-media applications," *IEEE International Symposium on Personal, Indoor and Mobile Radio Communications PIMRC'97*, Helsinki, Finland, Sept. 1997.

[KaKr99] S. Kaiser and W.A. Krzymien, "An asynchronous spread spectrum multi-carrier multiple access system," *IEEE Global Telecommunications Conference GLOBECOM'99*, vol. 1, pp. 314-319, Dec. 1999.

[KeSc02] J.P. Kermoal, L. Schumacher, K.I. Pedersen, P.E. Mogensen, and F. Frederiksen, "A Stochastic MIMO Radio Channel Model with Experimental Validation," *IEEE Journal on Selected Areas in Communications*, vol. 20, no. 6, pp. 1211-1226, 2002.

[Lan69] P. Lancaster, *Theory of Matrices*, Academic Press, New York, 1969.

[LiLe07] D. Li, P. Lei and X. Zhu, "Novel space-time coding and mapping scheme in single-carrier FDMA systems," *IEEE International Symposium on Personal, Indoor and Mobile Radio Communications PIMRC'07*, Athens, Greece, Sept. 2007.

[LiLo96] J. Litva and T. Lo, *Digital beamforming in wireless communications*, Artech House Publishers, 1996.

[LiWi93] J.H. vanLint, and R.M. Wilson, *A Course in Combinatorics*, Cambridge University Press, 1993.

[Lge05] LG Electronics, "PAPR comparison of uplink MA schemes," contribution R1-0504753, *3GPP TSG RAN WG1 Meeting #41*, Athens, Greece, 2005.

[MATRICE] European IST MATRICE project, "MC-CDMA Transmission Techniques for Integrated Broadband Cellular Systems," www.ist-matrice.org.

[MeRu04] C. F. Mecklenbräuker and M. Rupp, "Generalized Alamouti Codes for Trading Quality of Service against Data Rate in MIMO UMTS," *EURASIP Journal on Applied Signal Processing*, no. 5, pp. 662-675, May 2004

[MeSc98] J. Medbo, P. Schramm, "Channel Models for HIPERLAN/2 in Different Indoor Scenarios," ETSI BRAN 3ERI085B, 1998.

[Mit06] Mitsubishi Electric, "Number of occupied sub-carriers in the LTE 5MHz bandwidth," contribution R4-060902, *3GPP TSG RAN WG4 Meeting #40*, Tallinn, Estonia, Aug. 2006.

[Mit08a] Mitsubishi Electric, "Uplink transmit diversity schemes for LTE Advanced," contribution R1-082522, *3GPP TSG RAN WG1 Meeting #53bis*, Warsaw, Poland, June 2008.

[Mit08b] Mitsubishi Electric, "Uplink transmit diversity schemes with low cubic metric for LTE-Advanced," contribution R1-083198, *3GPP TSG RAN WG1 Meeting #54*, Jeju, Korea, Aug. 2008.

[Mit08c] Mitsubishi Electric, "Uplink transmit diversity schemes with low CM for LTE-Advanced," contribution R1-083763, *3GPP TSG RAN WG1 Meeting #54bis*, Prague, Czech Republic, Sept. 2008.

[Mit08d] Mitsubishi Electric, "Comparison of uplink transmit diversity schemes for LTE-Advanced," contribution R1-084355, *3GPP TSG RAN WG1 Meeting #55*, Prague, Czech Republic, Oct. 2008.

[Mit09a] Mitsubishi Electric, "Comparison of uplink transmit diversity schemes for LTE-Advanced," contribution R1-090391, *3GPP TSG RAN WG1 Meeting #55bis*, Ljubljana, Slovenia, Jan. 2009.

[Mit09b] Mitsubishi Electric, "Comparison of uplink transmit diversity schemes for LTE-Advanced," contribution R1-090739, *3GPP TSG RAN WG1 Meeting #56*, Athens, Greece, Jan. 2009.

[Mit09c] Mitsubishi Electric, "Comparison of uplink 2-Tx transmit diversity schemes for LTE-Advanced," contribution R1-091582, *3GPP TSG RAN WG1 Meeting #56bis*, Seoul, Korea, March 2009.

[MoBr06] "Idle period shortening for TDD communications in large cells," *IEEE Vehicular Technologies Conference*, *VTC Spring'06*, Melbourne, Australia, May 2006.

[Mol05] A. F. Molisch, *Wireless Communications*, John Wiley & Sons, 2005.

[Mot04] Motorola, "Comparison of PAR and Cubic Metric for Power De-rating," contribution R1-040642, *3GPP TSG RAN WG1 Meeting #37*, Montreal, Canada, 2004.

[Mot06] Motorola, "Cubic Metric in 3GPP-LTE," contribution R1-060385, *3GPP RAN WG1 #44 meeting*, Denver, USA, 2006.

[MuCo02] B. Muquet, M. de Courville and P. Duhamel, "Subspace-based blind and semi-blind channel estimation for OFDM systems," *IEEE Transactions on Signal Processing*, vol.50, no. 7, pp. 1699-1712, 2002.

[Nak60] M. Nakagami, "The *m*-Distribution, a general formula of intensity of rapid fading," in W. G. Hoffman, (editor), *Statistical Methods in Radio Wave Propagation: Proceedings of a Symposium held at the University of California*, pp 3-36, Permagon Press, 1960.

[OcIm01] H. Ochiai and H. Imai, "On the distribution of the Peak to Average Power Ratio in OFDM signals," *IEEE Transactions on Communications*, vol. 49, 2001.

[Oku68] Y. Okumura et al, "Field strength and its variability in VHF and UHF land mobile services," *Review of the Electrical Communications Laboratory*, 16, pp. 825-873, 1968.

[ÖzHe03] H. Özcelik, M. Herdin, W. Weichselberger, J. Wallace, and E. Bonek., "Defciencies of the Kronecker MIMO radio channel model," *Electronics Letters*, vol. 39, no. 16, pp. 1209-1210, 2003.

[PaFo01] C. Papadias and G. Foschini, "A Space-Time Coding Approach for Systems Employing Four Transmit Antennas," *Proceedings of IEEE International Conference on Acoustics, Speech, and Signal Processing ICASSP'01*, Vol. 4, pp. 2481-2484, Salt Lake City, Utah, 2001.

[Pal33] C. Paley, "On orthogonal matrices," *Journal of Mathematics and Physics*, vol. 12, pp. 311–320, 1933.

[Par01] J. D. Parsons, *The Mobile Radio Channel*, 2nd edition, John Wiley & Sons Ltd, 2001.

[Rap02] T. S. Rappaport, *Wireless Communications: Principles & Practice*, 2nd edition, Prentice Hall, 2002.

[Rapp91] C. Rapp, "Effects of the HPA-nonlinearity on a 4-DPSK/OFDM signal for a digital sound broadcasting system," *European Conference on Sattelite Communications ECSC'91*, Liège, Belgium, Oct. 1991.

[RuMe02] M. Rupp and C. F. Mecklenbräuker, "On Extended Alamouti Schemes for Space-Time Coding," *Wireless Personal Multimedia Communications Symposium WPMC'02*, Honolulu, Hawaii, October 2002.

[Sal81] A. Saleh, "Frequency independent and frequency dependent nonlinear models of TWT amplifiers," *IEEE Transactions on Communications*, vol. 29, pp. 1715-1720, 1981.

[Säl04] T. Sälzer, *Transmission strategies employing multiple antennas for the downlink of MC-CDMA systems*, PhD thesis, Institut National des Sciences Appliquées de Rennes, 2004.

[SaKa98] H. Sari and G. Karam, "Orthogonal Frequency-Division Multiple Access and its Application to CATV Networks," *European Transactions on Telecommunications (ETT)*, vol. 9, no. 6, pp. 507-516, November - December 1998.

[SaLe96a] H. Sari, Y. Levy, and G. Karam, "Orthogonal Frequency-Division Multiple Access for the Return Channel on CATV Networks," *International Conference on Telecommunications, ICT '96*, vol. 1, pp. 52-57, April 1996, Istanbul, Turkey.

[SaLe96b] H. Sari, Y. Levy, and G. Karam, "OFDMA — A New Multiple Access Technique and its Application to Interactive CATV Networks," *Proc. ECMAST '96*, vol. 1, pp. 117-127, May 1996, Louvain-la-Neuve, Belgium.

[SaLe97] H. Sari, Y. Levy, and G. Karam, "An Analysis of Orthogonal Frequency-Division Multiple Access," *GLOBECOM '97 Proc.*, vol. 3, pp. 1635-1639, November 1997, Phoenix, Arizona.

[SaPa00] S. Sandhu and A. Paulraj, "Space-time block codes: A capacity perspective," *IEEE Communications Letters*, no. 4, pp. 384-386, Dec. 2000.

[Sar97] H. Sari, "Orthogonal Frequency-Division Multiple Access with Frequency Hopping and Diversity" (invited paper), *in Multi-Carrier Spread Spectrum, K. Fazel & G. P. Fettweis* (*Editors*), pp. 57-68, Kluwer Academic Publishers, The Netherlands, 1997.

[Say02] A. M. Sayeed, "Deconstructin multiantenna fading channels," *IEEE Transactions on Signal Processing*, vol. 50, 2002.

[SoBr98] U. Sorger, I. De Broeck and M. Schnell, "Interleaved FDMA – A new spread-spectrum multiple-access scheme," *IEEE International Conference on Communications, ICC'98*, Atlanta, Georgia, USA, June 1998.

[StMo98] H. Steendam, M. Moeneclaey, and H. Sari, "The Effect of Carrier Phase Jitter on the Performance of Orthogonal Frequency-Division Multiple Access Systems," *IEEE Transactions on Communications*, vol. 46, pp. 456-459, April 1998.

[Suz77] H. Suzuki, "A statistical model for urban radio propagation," *IEEE Transactions on Communications*, vol. COM-25, no. 4, pp. 673-680, 1977.

[Syl67] J. J. Sylvester, "Thoughts on inverse orthogonal matrices, simultaneous sign successions, and tessellated pavements in two or more colours, with applications to Newton's rule, ornamental tile-work, and the theory of numbers," *Philosophical Magazine*, no. 34, pp. 461-475, 1867.

[Taf06] Wireless World Research Forum, *Technologies for the Wireless Future*, vol. 2, John Wiley & Sons, Ltd, 2006.

[TaJa99] V. Tarokh, H. Jafarkhani, and A.R. Calderbank, "Space-Time Block Codes from Orthogonal Design," *IEEE Transactions on Information Theory*, vol. 45, pp. 1456-1467, July 1999.

[TaSe98] V. Tarokh, N. Seshadri and A. Calderbank, Space-time codes for high data rate wireless communications: performance criterion and code construction," *IEEE Transactions on Information Theory*, vol. 44, no. 2, pp. 774-764, 1998.

[Tel99] J. Tellado, *Peak to Average Power Reduction for Multicarrier Modulations*, PhD thesis, Stanford University, 1999.

[TiBo00] O. Tirkkonen, A. Boariu, and A. Hottinen, "Minimal non-orthogonality rate one space–time block code for 3+ transmit antennas," in *Proc. IEEE ISSSTA 2000*, vol. 2, pp. 429–432, Portland, Oregon, Aug. 2000.

[TS25814] 3rd Generation Partnership Project; Technical Specification Group Radio Access Network;"Physical Layer Aspects for Evolved Universal Terrestrial Radio Access (UTRA)," 3GPP TR 25.814 V7.1.0 (2009-09).

[TS36101] 3rd Generation Partnership Project; Technical Specification Group Radio Access Network; "Evolved Universal Terrestrial Radio Access (E-UTRA); User Equipment (UE) radio transmission and reception" (Release 8), 3GPP TS 36.101 v8.3.0 (2008-09).

[TS36211] 3rd Generation Partnership Project; Technical Specification Group Radio Access Network; "Evolved Universal Terrestrial Radio Access (E-UTRA); Physical Channels and Modulation" (Release 8), 3GPP TS 36.211 v8.2.0 (2008-03).

[TS36212] 3rd Generation Partnership Project; Technical Specification Group Radio Access Network; "Evolved Universal Terrestrial Radio Access (E-UTRA); Multiplexing and Channel Coding" (Release 8), 3GPP TS 36.212 V8.4.0 (2008-09).

[TS45005] 3rd Generation Partnership Project; Technical Specification Group GSM/EDGE Radio Access Network; Radio transmission and reception, 3GPP TS 45.005 v8.2.0 (2008-08).

[TsVi05] D. Tse and P. Viswanath, *Fundamentals of Wireless Communications*, Cambridge University Press, 2005.

[TR25996] 3rd Generation Partnership Project; Technical Specification Group Radio Access Network; Spatial channel model for Multiple Input Multiple Output (MIMO) simulations, 3GPP TR 25.996 v7.0.0 (2007-06).

[VaAn03] R. Vaughan and J. B. Andersen, *Channels, Propagation and Antennas for Mobile Communications*, IEEE Press, 2003.

[WaBe88] J. Walfish and H. L. Beroni, "A theoretical model of UHF propagation in urban environments," *IEEE Transactions on Antennas Propagation*, pp. 822-829, 1988.

[WaGi00] Z. Wang and G. B. Giannakis, "Wireless multicarrier communications: Where Fourier meets Shannon," *IEEE Signal Processing Magazine*, vol. 17, pp. 29–48, May 2000.

[Wei03] W. Weichselberger, *Spatial Structure of Multiple Antenna Radio Channels: A Signal Processing Viewpoint*, PhD thesis, Technical University of Wien, 2003.

[WeÖz03] W. Weichselberger, H. Özcelik, M. Herdin, and E. Bonek, "A novel stochastic MIMO channel model and its physical interpretation," *International Symposium on Wireless Personal Multimedia Communications*, *WPMC'03*, Yokosuka, Japan, Oct. 2003.

[WeÖz06] W. Weichselberger, M. Herdin, H. Özcelik, and E. Bonek, "A stochastic MIMO channel model with joint correlation of both link ends", *IEEE Transactions on Wireless Communications* vol. 5, no. 1, pp. 90-100, 2006.

[Wie49] N. Wiener, Norbert, *Extrapolation, Interpolation, and Smoothing of Stationary Time Series*, Wiley, New York, 1949.

[Wit93] A. Wittneben, "A new bandwidth efficient transmit antenna modulation diversity scheme for linear digital modulation," *Proceedings of IEEE International Conference on Communications*, *ICC 1993*, Geneva, Switzerland, May 1993, pp. 1630–1634.

[WWRF08] K. David (Editor), *Technologies for the Wireless Future -Wireless World Research Forum (WWRF) Volume 3*, John Wiley & Sons, Ltd, 2008.

[ZhTs03] L. Zheng and D. Tse, "Diversity and multiplexing: a fundamental trade-off in multiple-antenna channels," *IEEE Transactions on Information Theory*, vol. 49, no. 5, pp. 1073-1096, May 2003.

Author's publications

Journal Papers

- C. Ciochina, D. Mottier and H. Sari, "An analysis of three multiple access techniques for the uplink of future cellular mobile systems," *European Transactions on Telecommunications ETT*, no. 19, pp. 581-588, 2008.
- C. Ciochina, D. Castelain, D. Mottier and H. Sari, "Space-Frequency Block Code for Single-Carrier FDMA," *Electronics Letters*, vol. 44, no. 11, pp. 690-691, May 2008.
- C. Ciochina, D. Castelain, D. Mottier and H. Sari, "New PAPR-Preserving Mapping Methods for Single-Carrier FDMA with Space-Frequency Block Codes," submitted to *IEEE Transactions on Wireless Communications*, under second revision.

Conference Papers

- C. Ciochina, D. Mottier and H. Sari, "Multiple Access Techniques for the Uplink in Future Wireless Communications Systems," *Third COST 289 Workshop*, Aveiro, Portugal, July 2006.
- C. Ciochina, D. Mottier and H. Sari, "An Analysis of OFDMA, Precoded OFDMA and IFDMA for the Uplink in Cellular Systems," *6th International Workshop on Multi-Carrier Spread Spectrum (MC-SS) 2007*, Herrsching, Germany, May 07-09, 2007.
- C. Ciochina, D. Castelain, D. Mottier and H. Sari, "A Novel Space-Frequency Coding Scheme for Single-Carrier Modulations," *18th Annual IEEE International Symposium on Personal, Indoor and Mobile Communications (PIMRC'07)*, Athens, Greece, September 2007.
- C. Ciochina, D. Castelain, D. Mottier and H. Sari, "Single-Carrier Space-Frequency Block Coding: Performance Evaluation," *IEEE 66th Vehicular Technologies Conference (VTC 2007 Fall)*, Baltimore, USA, September 29 - October 3 2007.
- C. Ciochina, D. Castelain, D. Mottier and H. Sari, "A Novel Quasi-Orthogonal Space-Frequency Block Code for Single-Carrier FDMA," *IEEE 67th Vehicular Technologies Conference (VTC 2008 Spring)*, Singapore, May 2008.

Filed patents

- Method of ratio data emission, emitter and receiver using the method, EP 07 003191.9, filed on February 15, 2007. Authors: D. Castelain, C. Ciochina, D. Mottier.
- Method of multi-antenna wireless data emission, emitter and receiver using the method, EP 07 006681.6, filed on March 30, 2007. Authors: D. Castelain, C. Ciochina, D. Mottier.
- SC-QOSTFBC codes for MIMO transmitters, EP 08 000578, filed on January 25, 2008.
- Method and a device for determining shifting parameters to be used by at least a first and a second telecommunication devices, EP 08 171643.3, filed on December 15, 2008. Authors: C. Ciochina, D. Mottier, D. Castelain.
- Method and a device for determining shifting parameters to be used by a telecommunication device for transferring symbols, EP 09 155717.3, filed on March 20, 2009. Authors: C. Ciochina, D. Castelain, D. Mottier, L. Brunel.

Contributions to standardization

- Mitsubishi Electric, "Number of occupied sub-carriers in the LTE 5MHz bandwidth," contribution R4-060902, *3GPP TSG RAN WG4 Meeting #40*, Tallinn, Estonia, Aug. 2006.
- Mitsubishi Electric, "Uplink transmit diversity schemes for LTE Advanced," contribution R1-082522, *3GPP TSG RAN WG1 Meeting*#53, June 2008.
- Mitsubishi Electric, "Uplink transmit diversity schemes with low cubic metric for LTE-Advanced," contribution R1-083198, *3GPP TSG RAN WG1 Meeting #54*, Jeju, Korea, Aug. 2008.
- Mitsubishi Electric, "Uplink transmit diversity schemes with low CM for LTE-Advanced," contribution R1-083763, *3GPP TSG RAN WG1 Meeting #54bis*, Prague, Czech Republic, Sept. 2008.
- Mitsubishi Electric, "Comparison of uplink transmit diversity schemes for LTE-Advanced," contribution R1-084355, *3GPP TSG RAN WG1 Meeting #55*, Prague, Czech Republic, Oct. 2008.
- Mitsubishi Electric, "Comparison of uplink transmit diversity schemes for LTE-Advanced," contribution R1-090391, *3GPP TSG RAN WG1 Meeting #55bis*, Ljubljana, Slovenia, Jan. 2009.
- Mitsubishi Electric, "Comparison of uplink transmit diversity schemes for LTE-Advanced," contribution R1-090739, *3GPP TSG RAN WG1 Meeting #56*, Athens, Greece, Jan. 2009.
- Mitsubishi Electric, "Comparison of uplink 2-Tx transmit diversity schemes for LTE-Advanced," contribution R1-091582, *3GPP TSG RAN WG1 Meeting #56bis*, Seoul, Korea, March 2009.

Contribution to European project

- CODIV deliverable D3.2a, "Preliminary PHY layer algorithm selection for integration in the prototypes," co-author of section "MU-MIMO for LTE uplink," Oct. 2008.